

Annual Report

2013-2014

Annual Report 2013 – 2014



Saha Institute of Nuclear Physics
Kolkata

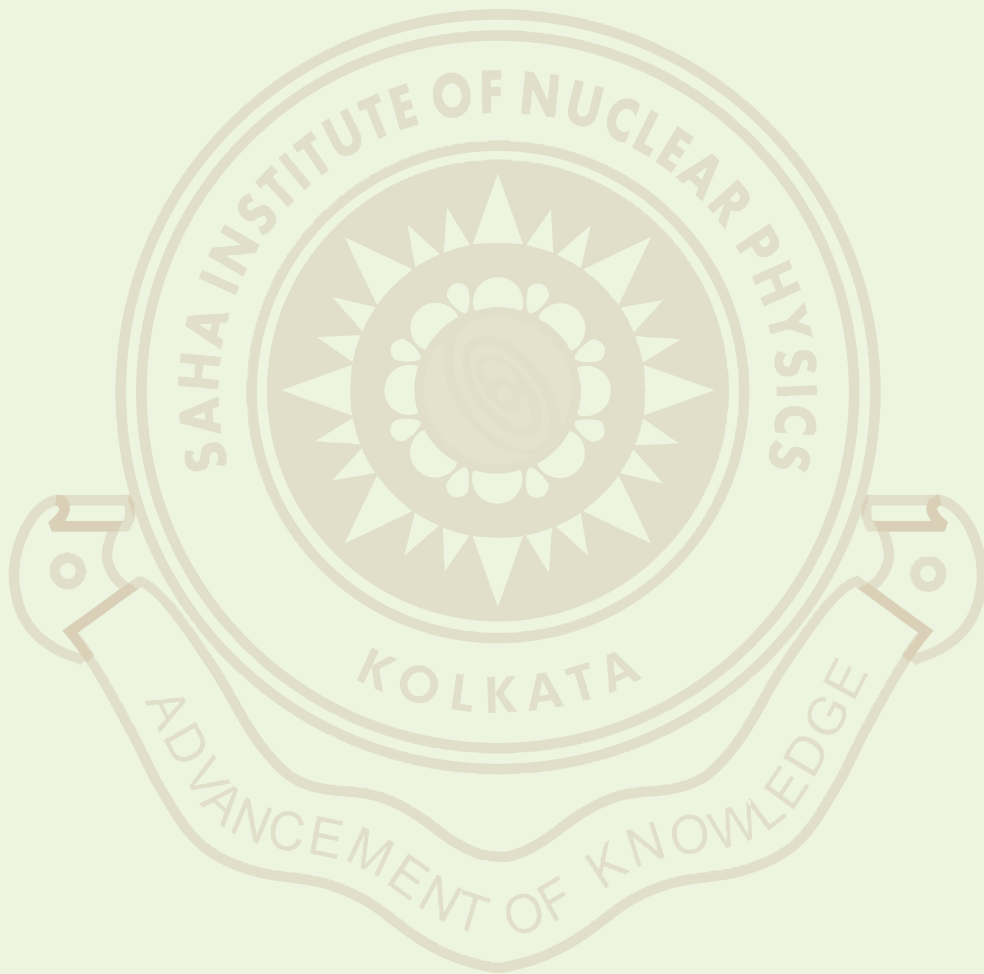
Please click
bookmark

S
I
N
P



Annual Report

2013-2014



Saha Institute of Nuclear Physics

1/AF, Bidhan Nagar, Kolkata 700 064, India

Editorial Team

Prof Milan Kumar Sanyal
Prof Palash Baran Pal
Prof Abhijit Chakrabarti
Prof Maitrayee Saha Sarkar
Prof Tapas Kumar Chini
Prof Munna Sarkar
Prof Suchandra Dutta
Shri Amit Kumar Saha
Shri Jeevan Shaw

Creation

Prof Abhijit Chakrabarti
Shri Amit Kumar Saha

Photographs

Shri Pradip Das

Cover Design & Printed at
Sailee Press Pvt Ltd

Published by

The Registrar, SINP
on behalf of
Centre for Advanced Research & Education
Saha Institute of Nuclear Physics
Tel: (33) 2337-5345-49 (5 lines) • Fax: (33)-2337-4637

<http://www.saha.ac.in>

October 1, 2014

Foreword



I am very happy to write this foreword for this 2013-2014 Annual Report of our Institute. Our members have continued to contribute significantly towards the development of research and teaching activities of our Institute. Apart from a few major developments of research facilities and organization of national/international conferences, seminars, etc, our faculty members and students have contributed more than three hundred and eighty publications in peer reviewed journals, including thirty five in journals having impact factor more than six.

Though many of our senior colleagues are leaving us due to retirements, etc, we have been extremely fortunate last few years to be able to attract very bright young researchers and add them to our faculty; in 2013-14, four young faculty members have joined our Institute.

I am sure, our Institute will continue to contribute even more successfully in the coming days.

October 1, 2014

Bikas K Chakrabarti
Director
Saha Institute of Nuclear Physics

Contents

Foreword	3
1 Biophysical Sciences including Chemistry	15
1.1 Summary of Research Activities of Divisions	15
1.1.1 Biophysics and Structural Genomics	15
1.1.2 C&MB	16
1.1.3 Chemical Sciences	17
1.1.4 Computational Science	17
1.2 Research Activities	20
1.2.1 Biophysics and Structural Genomics	20
1.2.2 C&MB	28
1.2.3 Chemical Sciences	33
1.2.4 Computational Science	43
1.3 Developmental Work	45
1.4 Publications	45
1.4.1 Publications in Books/Monographs & Edited Volumes	45
1.4.2 Publications in Journal	46
1.5 Ph D Awarded	51
1.6 Seminars/Lectures given in Conference/Symposium/Schools	52
1.7 Teaching elsewhere	55
1.8 Miscellany	56
2 Condensed Matter Physics including Surface Physics and NanoScience	57
2.1 Summary of Research Activities of Divisions	57
2.1.1 Condensed Matter Physics	57
2.1.2 Surface Physics and Material Science	58
2.2 Research Activities	60
2.2.1 Condensed Matter Physics	60
2.2.2 Surface Physics and Material Science	77
2.3 Developmental Work	98
2.3.1 Contact Angle Measurement System	98
2.4 Publications	99
2.4.1 Publications in Books/Monographs & Edited Volumes	99
2.4.2 Publications in Journal	99
2.5 Ph D Awarded	107
2.6 Seminars/Lectures given in Conference/Symposium/Schools	107
2.7 Teaching elsewhere	108

2.8	Miscellany	109
3	Experimental Nuclear and Particle Physics	111
3.1	Summary of Research Activities of Divisions	111
3.1.1	Applied Nuclear Physics	111
3.1.2	High Energy Nuclear and Particle Physics	112
3.1.3	Nuclear Physics	113
3.2	Research Activities	114
3.2.1	Applied Nuclear Physics	114
3.2.2	High Energy Nuclear and Particle Physics	120
3.2.3	Nuclear Physics	122
3.3	Developmental Work	125
3.3.1	125
3.4	Publications	127
3.4.1	Publications in Journal	127
3.5	Ph D Awarded	137
3.6	Seminars/Lectures given in Conference/Symposium/Schools	137
3.7	Teaching elsewhere	140
3.8	Miscellany	140
4	Plasma Physics	141
4.1	Summary of Research Activities of Divisions	141
4.1.1	Plasma Physics	141
4.2	Research Activities	142
4.2.1	Plasma Physics	142
4.3	Developmental Work	148
4.3.1	Plasma Physics	148
4.4	Publications	149
4.4.1	Publications in Journal	149
4.5	Ph D Awarded	150
4.6	Seminars/Lectures given in Conference/Symposium/Schools	150
4.7	Teaching elsewhere	151
5	Theoretical Physics & Astroparticle Physics	153
5.1	Summary of Research Activities of Divisions	153
5.1.1	Astroparticle Physics and Cosmology	153
5.1.2	Theory	155
5.2	Research Activities	157
5.2.1	Astroparticle Physics and Cosmology	157
5.2.2	Theory	165
5.3	Developmental Work	177
5.3.1	Astroparticle Physics and Cosmology	177
5.4	Publications	177
5.4.1	Publications in Books/Monographs & Volumes Edited	177
5.4.2	Publications in Journal	177
5.5	Ph D Awarded	182
5.6	Seminars/Lectures given in Conference/Symposium/Schools	182
5.7	Honours and Distinctions	185

5.8	Teaching elsewhere	186
5.9	Miscellany	186
6	Research Fellows/Visiting Fellows/Research Associates	189
6.1	Visiting Fellows/Research Associates and Research Fellows	189
6.1.1	Research Fellows	189
6.1.2	SRF(EX), PDF, RA, VS, VF	191
7	Facilities	193
7.1	Centre for Advanced Research & Education	193
7.1.1	The Post-M Sc Associateship Course	196
7.2	Library	203
8	Administration	207
8.1	Governing Council	207
8.2	Members of the Institute [As on March 31, 2014]	208
8.3	Audited Accounts	214
8.4	Balancesheet	214
8.5	Income & Expenditure Account	215
8.6	Receipts & Payments	216
9	External Collaborators	217
10	Index	223

Obituary



Our colleague **Professor Abhee Dutt-Mazumder** has passed away on December 15, 2013. The members of the whole institute is deeply shocked as it is a great loss to the institute as well as to the society. Abhee, in his research career in Physical Science, has published more than 50 papers in journals of international repute. He was also involved in ALICE experiment at CERN where he took great interest in shift duty for data taking and was also involved in the fabrication of the second station of muon spectrometer of ALICE. Apart from this, Professor Dutt-Mazumder was deeply involved in many social movements and wrote many articles regarding this in reputed daily for the general awareness among the common people. He also tried his level best to popularize science by writing many articles in science and organizing a number of science lectures in the institute as well as elsewhere.



R Holland Cheng, PIOMS Institutional Program, University of California,
Davis CA 95616, USA, July 2, 2013



Colloque Lecture delivered by John W Freeland Argonne National Laboratory,
USA, May 21, 2013



1st user's meeting of the Indian beamline at Photon Factory, KEK, Japan at SINP, Kolkata, October 7-8, 2013



Delegates of CMS Data Analysis School at SINP Auditorium, Saltlake City, Kolkata, November 7-11, 2013



Prof Palas Baran Pal delivering lecture at Vigyan-O-Prajukti Mela 2014 at Hedua Park, Kolkata, January 29–February 2, 2014



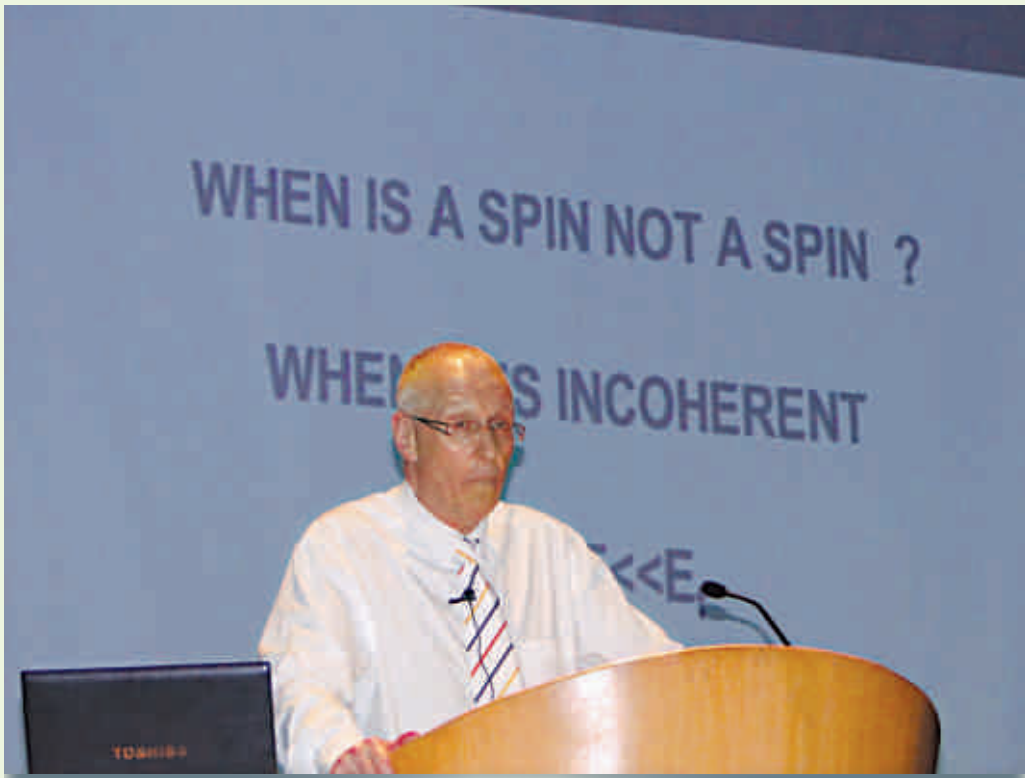
Science Gallery of SINP at 17th National Exhibition at Belur, Howrah, September 21-25, 2013



Prof Debasish Mukherjee delivering lecture during an Outreach Programme at Ramananda College, Bishnupur, Bankura, January 9, 2014



Lecture delivered by Prof Rupamanjari Ghosh, Dept of Physics, JNU and Dean, Shiv Nadar University, UP, CARE Science Education Meet held at SINP, August 20, 2013



Cockcroft-Walton Lecture 2013 delivered by Sir Prof Michael Pepper
held SINP, April 29, 2013



Amit Chattopadhyay of CCMB, Hyderabad delivering Institute Colloquie,
September 4, 2013

Chapter 1

Biophysical Sciences including Chemistry

1.1 Summary of Research Activities of Divisions

1.1.1 Biophysics and Structural Genomics

Experimental approaches to understand the biomolecular recognition process in different intracellular phenomena have been the major activities in Biophysics. The biomolecular recognition studies include mode of actions of flavones and flavonoids, chemical biology of the aureolic acid group of antibiotics, modulation of chromatin structure by small DNA binding molecules and self association of wild type and mutant lamins involved in laminopathy. In addition we have also studied the biophysical properties of lamins to understand their roles as intermediary filaments. Recognition of multiple stranded DNA (Quadruplex) and putative anticancer agents from plant source have shown that one such agent, ellipticine binds to DNA with 3:2 stoichiometry, with respect to ellipticine:DNA, also inhibiting telomerase activity. The widely prevalent disease of Eastern India, HbE-thalassemia, along with sickle cell anemia, hereditary spherocytosis and leukemia are being studied as model for hematological disorders while Alzheimers, Huntingtons, and the Prion diseases are being studied for the neurodegenerative diseases. Differential proteomics studies are being done in these diseases using clinical samples of cerebrospinal fluid, plasma, urine, red cells, cell extracts and platelets. Hundreds of proteins from these different tissue types are annotated and 10-15 proteins are identified to be differentially expressed in diseases. Classes of redox regulators and chaperone proteins have been found to be up-regulated in hemoglobinopathy. Studies in cell proliferation and differentiation have implicated the roles of self renewal pathways and cross talk between signaling pathways in chronic to blast transformation of CD34+ CML stem cells isolated from patients. Moreover, we have established that cytoplasmic sequestration of the cell cycle inhibitor, p27 led to its interaction with polycomb group of genes (Bmi1, EZH2) and activation of the Rho/Rac GTPase pathway resulting in actin depolymerization which, in turn, caused cellular egression/mobilization from the bone marrow. Currently this pathway is also being investigated to understand the process of metastasis in epithelial cancer. Among the various diseases that affect the nervous system, some of the most debilitating neurodegenerative disorders are Alzheimers, Huntingtons and Prion Diseases. These late onset but eventually fatal diseases are all caused by altered metabolism of individual proteins that interfere with normal cellular homeostasis. Several micro RNAs (miRNA), the negative regulator of protein coding gene expression, have been shown to target the Huntingtin (HTT) gene, whose mutation causes Huntingtons disease (HD). The expression of these miRNAs has been shown to decrease in cell and animal models of HD. Besides, it has been shown that

miR-150 target TP53 gene, explaining the over expression of TP53 in HD. HIPPI, a molecular partner of HTT interacting protein HIP1, has been shown to regulate many genes involved in HD pathogenesis. The normal life cycle of a protein, characterized by its biogenesis, trafficking and degradation, are compromised in these disorders resulting in misfolding, misprocessing or mislocalization of the proteins. Most likely, the aberrant protein can then engage in atypical interactions and ultimately lead to a series of unknown events culminating in cell death. The major focus of our research in Alzheimers disease (AD) is to study the downstream pathogenesis of the disease, mediated through AICD and its adaptor network. AICD possesses conserved motifs that are now known to interact with cytosolic adaptor proteins and these interactions in turn affect different signaling pathways. We have shown that Grb2, one such adaptor, interacted with AICD in late endosomal compartments. The excess protein, thus entrapped, could be degraded by autophagy. Currently, we are also trying to provide a comprehensive understanding of the disruption of the intracellular protein trafficking pathways in late-onset neurodegenerative disorders. With Prion disease as a model system, we plan to simultaneously pursue two broad facets: first, understanding the significance of the ESCRT machinery and the endo-lysosomal pathway in PrP-mediated (Prion protein) neurodegenerative diseases. This will aim to provide a molecular explanation for how the loss of function mutation of Mahogunin results in Prion disease like phenotype of spongiform neurodegeneration. Secondly, we also aim to explore how the various essential molecular components that are regulated during endoplasmic reticular stress (ER stress) and aging, both of which manifest in late onset neurodegenerative diseases. Studies on function and dynamics of transcription factors have been initiated to interpret the epigenetic language in Eucaryotic Cells. We aim to understand the critical interactions between histone posttranslational modifications and the 'readers' which regulate important cellular pathways and their dysfunctions leading to disease.

1.1.2 C&MB

The major goals of the Division are to understand the key biological processes using tools of X-ray crystallography, spectroscopy, cellular and molecular biology. 3D structures of various proteins like Psu from bacteriophage P4, involved in transcription termination in bacteria and thermostable mutant of pro-papain were determined. Psu exists as a knotted homodimer and is first of its kind in nature. Detailed structural elucidation of protease pro-papain explained the stepwise autocatalytic activation mechanism by limited proteolysis of the zymogen of papain. Cloning, expression, purification, crystallization and preliminary X-ray analysis of a fructokinase and two low-molecular-weight protein tyrosine phosphatases from *Vibrio cholerae* O395 have been reported. It has been shown that expression of recombinant human cathepsin K is increased by codon optimization. Computational algorithm has been developed to explain protein-protein interactions based on the electrostatic complementarity and surface (or shape) complementarity of interior residues. It was confirmed by site-directed mutagenesis that RXL-like cyclin-binding (Cy) motif dependent interaction of LdHAT1 with LdCyc1 is essential for its phosphorylation at a canonical Cdk target site by the kinase complex. Phosphorylation of LdHAT1 by the S-phase kinase inhibits its H4K10 acetylation activity, implicating a mechanism of periodic regulation of histone acetylation during cell cycle progression. The effect of post-translation modification on the activity of the homologous proteins in mammals during cell cycle progression is being studied. The regulation of gene expression at posttranscriptional level is also a major area of our research. Thirty six interacting partners of HYPK was identified. Various experimental and computation analysis of the interacting partners of HYPK reveal that HYPK together with its interacting partners involve in several biological processes like protein folding, response to unfolded protein, cell cycle regulation, apoptosis and regulation of transcription. Analysis of the validated targets of altered miRNAs in Huntingtons

disease reveals that they might be involved in apoptosis, differentiation and development, fatty acid, cholesterol, lipid, glucose, and carbohydrate metabolism, cell cycle and growth and transcription regulation. Besides, micro RNA 125b has been shown to involve in cell cycle regulation by targeting MDA1 protein. Clinical proteomics and lipidomics studies of various blood components from patients suffering from hemoglobin disorders e.g. thalassemia & sickle cell disease are underway. Spectroscopic, biochemical and biophysical studies of erythroid and non-erythroid spectrin with reference to hydrophobic ligand binding, lipid-protein interactions and chaperone activities are being done.

1.1.3 Chemical Sciences

Research in the Chemical Sciences Division is wide-ranging and interdisciplinary, and addresses fundamental aspects of science. Overarching goals of the research projects include understanding the excited state dynamics of complex phenomena using ultra fast spectroscopy and single molecule imaging, finding new functions for old drugs: Non Steroidal Anti-inflammatory Drugs (NSAIDs), different areas in Nuclear Chemistry, Radiochemistry and Green Chemistry, developing nanotechnology and novel advanced materials for a myriad of applications, unraveling problems associated with devising new, alternative sources of energy, neutron interaction, nano particle dosimetry and radiation safety. To explore the excited state dynamics, interaction of proteins like lysozyme, haemoglobin A etc. with a small therapeutically important drug molecule, Merocyanine 540, spectroscopic and crystallographic techniques have been used. Photo induced electron transfer coupled with magnetic field effect have been studied. Also, antioxidant efficacy of pyrrole and pyridine based Cu(II)-Schiff base complexes while binding with CT-DNA have been investigated. Copper complexes of Oxacam NSAIDs have been synthesized to study their biological applications. Increased membrane fusogenic efficacy, DNA-binding and apoptosis inducing properties have been found for these complexes. Au-Polyaniline based conducting nano-composite has been utilized for bio-sensing of glucose, DNA and protein, using different electrochemical techniques and also for detecting the positional effect of single base mismatch in oligonucleotides. PEDOT-MnO₂ and graphene based materials have been used to fabricate supercapacitors of high specific capacitance. A single molecule and ensemble spectroscopic study of protein folding, misfolding, aggregation and DNA-protein interaction have been carried on. Quantum chemical calculations have also been carried out to address some of the fundamental problems based on experimental findings. The Nanophotonics group is actively engaged in the field of sustainable nano-architecture addressing both their development and applications.

1.1.4 Computational Science

Computational Science Division maintains various IT infrastructure of the campus as central facilities. In addition members of the department carry out theoretical computational research on Bio-informatics. The central facilities are open to all the users of the Institute.

High Speed Local Area Network Wired and Wireless Infrastructure: SINP boasts to have a fully structured network environment in place for more than a decade now. The network is divided into security zones called MZ (Military zone) and DMZ (de-Militarized Zone); and connected to Internet via a Firewall/Router. All inward access is either via VPN or dual-hop inward secured shell access. All the internet facing servers are placed in the DMZ.

Presently there are 2 core switches and 12 distribution switches. All the distribution switches are fibre-connected to both of the core switches forming seamless HA (high available) infrastructure. The main backbone (Core-Distribution) is 1G and Distribution to Edge switches, about 32 in num-

bers are either 100Mbps or some cases 1G via copper.

There are about 42 Access Points connecting to Wireless LAN Controller via the wired network to provide wireless access cloud throughout the campus. Various SSIDs are broadcast to facilitate different categories of users. Users are authenticated with Radius servers in the backend which are running in virtual and physical infrastructures on High Availability mode. Segregation between guests and local users are ensured based on user credentials and hardware addresses of the respective devices to ensure wireless security.

Layer 3 IP Virtual LANs are configured and various access control lists (ACL) are employed to sanitize traffic and ensure better utilization of the network resources. The ACLs also help to restrict any malware activity. There are about 1500 end point connections laid for wired machines/devices and about 200+ active wireless end points/nodes connected to our network.

High Available (HA) Cluster running Internet Services: HA Cluster is running all the major Internet facing services namely Web, Proxy, Ftp, Mail, IMAP/POP, DNS, LDAP, secured dual hop inward access etc. All the services are authenticated from central LDAP services and user uses same credential to access all/most the services. A major project named Migration and Enhancement of HA Cluster is at its last phase of implementation. A new service user file store is in the process of testing and will be available to the users shortly. The purview of the project included a Disaster Recovery setup. So that in case of declared disaster that hamper the installation, the setup would provide continued service from a secondary site. To accommodate the data centre needs of DR site a modular data centre is procured and currently operational in Room no. 3401. The enhanced setup will ensure all round better availability, security and performance.

Presently the services run in a mix of Virtual and Physical instances, having high availability achieved between both the instances.

Modular Data Centre and Data Centre: New initiative was taken up for the project of implementation of a full-fledged Data Centre at the server room to house namely High performance Computing Facilities, CMS Grid Infrastructure, HA Cluster etc. To house the Disaster Recovery (DR) infrastructure, a Modular Data Centre (MDC) was procured and installed. The Modular Data Centre or MDC, i.e. a Data Centre in a box with all the functionality of a formal Data Centre (DC), e.g. Precision Air Conditioning, HA UPS, Proper design of rack for air-flow etc. MDC architecture is also chosen for its movability. In future if the Institute opens up another campus, we would be able to shift the MDC to that campus to achieve better disaster recovery (DR) functionality and meet the guidelines of a proper DR setup. Both the projects assume availability of appropriate backup power like DG sets. Purpose and some of the benefits of the Data Centre and MDC are given as under:

To house the Disaster Recovery Setup of HA Cluster

MDC is a one cabinet Data Centre with UPS, Precision Air Conditioning, Fire Suppression System. Scalable system, more resources can be added in the MDC

MDC can be relocated to location better suited for a DR scenario.

The DR setup would be able to provide much needed service continuity for all the central services like email, web, ftp, proxy and other applications.

Precision Air Conditioning

Appropriate Cooling for High Density Racks

High available AC, POWER

Remote Monitoring and Alerts

Handling cases of Fire, Water leakage etc.

Economical use of power

New Website for the Institute: The division along with members of New-Website committee worked hand in hand to address the need of a structured CMS (Content Management System) based web-

site for our Institute incorporating modern technology, standards, and UAT and security guidelines. Using the system departmental, personal, different application part of the website can be updated by the authorised persons in a de-centralized manner. Apart from that the scope includes implementation of some applications like Conferences, Colloquia/Seminar, Newsletter, Tender Management, Telephone Directory, Video and Image Gallery, Document Store, dashboard etc. The implementation includes a unique Class of User concept for authentication for various services/applications. The new website was inaugurated on the foundation day i.e. 11th Jan, 2014 by the Director. Apart from some applications the project is mostly complete.

Perimeter and End Point Security and other Security Measures: The Project of hardware Firewall/Unified Threat Management (UTM) system for perimeter and end points, the system was installed/configured was placed in the network replacing its software counterpart. Other than basic Firewalling/Intrusion Prevention System, the UTM also works as a gateway agent for malware and spam control. Some of the benefits of the Unified Threat Management (UTM) system are the following:

Hardware Gateway for high-speed Access (>1Gbps)

Authenticated Access and hardware proxy

Anti-malware Gateway

Hardware Firewall

High Availability of Firewall and Internet access

Network Access Control and endpoint security

The division also takes care of the various IT security needs of the above installations and that of the Institute at large. The recommendations and guidelines of the CISAG (Computer & Information Security Advisory Group), DAE are followed and periodic exercises and assessments are carried out. As instructed by the CISAG (Chief Information Security Audit Group, DAE), initiatives were taken to form a group of technical members to help CISO in the domain of work.



Bioinformatics, a subject of this millennium, tries to understand the rules of biology from the genomic and protein sequences of various organisms supplemented by chemical physics approaches.

These methods have been found to be very efficient in detecting genes from chromosomal sequences, in predicting structures of proteins from its sequence, in understanding their function and finally predicting structures of drug like molecules to control their malfunction. Researchers of Computational Science Division, addresses different aspects of bioinformatics using different computational techniques from sequence as well as three-dimensional structural data of proteins and nucleic acids. We developed an efficient Ant Colony Optimization method, namely Guided Ant Colony Optimization (GACO) technique for optimizing mathematical functions. The search process of the optimization approach is directed towards a region or a hypercube in a multidimensional space where the amount of pheromone deposited is maximum after a predefined number of iterations. The entire search area is initially divided into 2^n number of hypercubic quadrants where n is the dimension of the search space. Then the pheromone of each quadrant is measured. Now, the search jumps to the region (new search area) of maximum pheromone level and restarts the search process in the new region. However, the search area of the new region is reduced compared to the previous search area. Thus, the search advances and jumps to the new search space (with a reduced search area) in several stages until the algorithm is terminated. The GACO technique has been tested on a set of mathematical functions with number of dimension upto 100 and compared with several relevant optimizing approaches. It is observed that the GACO method performs better than or similar to the performance of other optimization techniques.

Bioinformatics, a subject of this millennium, tries to understand the rules of biology from the genomic and protein sequences of various organisms supplemented by chemical physics approaches. These methods have been found to be very efficient in detecting genes from chromosomal sequences, in predicting structures of proteins from its sequence, in understanding their function and finally predicting structures of drug like molecules to control their malfunction. Researchers of Computational Science Division, addresses different aspects of bioinformatics using different computational techniques from sequence as well as three-dimensional structural data of proteins and nucleic acids.

1.2 Research Activities

1.2.1 Biophysics and Structural Genomics

1.2.1.1 Mahogunin-mediated α -tubulin ubiquitination via noncanonical K6 linkage regulates microtubule stability and mitotic spindle orientation

Mahogunin ring finger-1 (MGRN1) is a cytosolic ubiquitin ligase whose disruption or interaction with some isoforms of cytosolically exposed prion protein leads to spongiform neurodegeneration and also lack of which results in reduced embryonic viability due to mispatterning of the left-right (LR) axis during development. Here we demonstrate an interaction between the cytoskeletal protein α -tubulin and MGRN1. In cultured cell systems, loss of the ubiquitin E3 ligase activity of MGRN1 results in spindle misorientation and decreased α -tubulin polymerization, an effect also seen in primary cells. α -Tubulin was posttranslationally modified by MGRN1 via noncanonical K6-linked polyubiquitination. This was significant because expression of catalytically inactive MGRN1 and/or ubiquitin mutant capable of only monoubiquitination resulted in similar mitotic spindle misorientation. The modulatory effect of MGRN1 was specific for α -tubulin and similar changes could not be detected in β - or γ -tubulin. However, catalytic inactivation of MGRN1 did not abrogate monoubiquitination of α -tubulin, thus unraveling a unique dual mode of ubiquitination by an unknown E3 ligase and MGRN1. MGRN1-mediated α -tubulin modification, and hence

its stability, may highlight a key event in the LR patterni ng during embryogenesis.

D Srivastava; O Chakrabarti

1.2.1.2 Fusion with Anticodon Binding Domain of GluRS is Not Sufficient to Alter the Substrate Specificity of a Chimeric Glu-Q-RS

Glutamyl-queuosine-tRNA(Asp) synthetase (Glu-Q-RS) is a paralog of glutamyl-tRNA synthetase (GluRS) and is found in more than forty species of proteobacteria, cyanobacteria, and actinobacteria. Glu-Q-RS shows striking structural similarity with N-terminal catalytic domain of GluRS (NGluRS) but it lacks the C-terminal anticodon binding domain (CGluRS). In spite of structural similarities, Glu-Q-RS and NGluRS differ in their functional properties. Glu-Q-RS glutamylates the Q34 nucleotide of the anticodon of tRNA(Asp) whereas NGluRS constitutes the catalytic domain of GluRS catalyzing the transfer of Glu on the acceptor end of tRNA(Glu). Since NGluRS is able to catalyze aminoacylation of only tRNA(Glu) the glutamylation capacity of tRNA(Asp) by Glu-Q-RS is surprising. To understand the substrate specificity of Glu-Q-RS we undertook a systemic approach by investigating the biophysical and biochemical properties of the NGluRS (1-301), CGluRS (314-471) and Glu-Q-RS-CGluRS, (1-298 of Glu-Q-RS fused to 314-471 from GluRS). Circular dichroism, fluorescence spectroscopy and differential scanning calorimetry analyses revealed absence of N-terminal domain (1-298 of Glu-Q-RS) and C-terminal domain (314-471 from GluRS) communication in chimera, in contrast to the native full length GluRS. The chimeric Glu-Q-RS is still able to aminoacylate tRNA(Asp) but has also the capacity to bind tRNA(Glu). However the chimeric protein is unable to aminoacylate tRNA(Glu) probably as a consequence of the lack of domain-domain communication.

Sutapa Ray; Mickael Blaise; Bappaditya Roy; Saptarni Ghosh; et al

1.2.1.3 Differential Expression of Neuroblastoma Cellular Proteome due to AICD Overexpression

Amyloid- β protein precursor intracellular domain (AICD), which exerts intracellular effects by interacting with proteins involved in a plethora of biological processes, is a key player behind the pathophysiology of Alzheimer's disease (AD). Keeping in mind that overwhelming presence of AICD would mimic AD-like conditions in neuroblastoma cell lines, we hypothesized alteration in the proteomic expression pattern in these cells in the presence of AICD compared to their normal proteome. The rationale behind the study was to distinguish between symptomatic pathophysiological effects as opposed to any artifactual consequence due to protein overload in the cell lines. Using 2D-DIGE analysis and MALDI-MS identifications in neuro2A (mouse) and SHSY5Y (human) cell lines, we have identified several proteins belonging to different functional classes and involved in several biological pathways including protein folding, cytoskeletal dynamics, metabolism, and stress. Many of these were being upregulated or downregulated due to AICD effects and could be correlated directly with AD phenotypes.

Arunabha Chakrabarti; Kasturi Roy; Debashis Mukhopadhyay

1.2.1.4 Growth Factor Receptor-Bound Protein 2 Promotes Autophagic Removal of Amyloid- β Protein Precursor Intracellular Domain Overload in Neuronal Cells

The ascertainment of elevated levels of amyloid- β protein precursor intracellular domain (AICD) in Alzheimer's disease (AD) brains and the fact that it contributes to AD-like pathology has geared the search toward a new paradigm. While studying endogenous as well as overexpressed Grb2-AICD interaction in AD cell models, it was found that Grb2 co-localized to compartments along with AICD. We report now that these vesicles form in a clathrin and dynamin independent manner. Both types of vesicles mature into autophagosomes, merge with lysosomes, and relieve the cells of AICD overload. Inhibiting autophagosome formation results in vesicle accumulation. AICD-level is reduced in Grb2 excess condition in Cycloheximide Chase setup. Reduced caspase activity and apoptosis point toward the fact that the cytotoxic effect of AICD is alleviated by its sequestration in autolysosomes. Hence we state that the entrapping of AICD in Grb2 vesicles and its clearance via autophagosomes is a survival contrivance on the part of the cell. This study unravels, for the first time, the roles of Grb2 in autophagy and in handling toxic protein overload in an AD-like scenario.

Kasturi Roy; Mithu Raychaudhuri; Oishee Chakrabarti; Debashis Mukhopadhyay

1.2.1.5 Molecular cross talk between Notch1, Shh and Akt pathways during erythroid differentiation of K562 and HEL cell lines

Erythropoiesis is a tightly regulated process dependent on extrinsic signals conveyed by the bone marrow niche. The signalling pathways thus activated or repressed do not act in isolation; rather an intricate cross talk among these pathways ensues homeostasis within the erythroid compartment. In this study, we describe the effects of two such signalling pathways namely the Notch1 and the Shh pathway on erythropoiesis in immortalised K562 and HEL cell lines as well as the cross talk that ensues between them. We show that while activation of the Notch1 pathway inhibits differentiation of erythroid lineage cell lines as well as in in-vitro primary erythroid cultures from the human CD34(+) cells; Shh pathway favours erythroid differentiation. Further, the Notch1 pathway activates the Akt pathway and constitutively active Akt partially mimics the effect of Notch1 activation on erythropoiesis. Moreover, the Notch1, Akt and Shh pathways were found to cross talk with each other. In this process, activation of Notch1 was found to down regulate the Shh pathway independent of Akt activation. Significantly, Notch1 not only down regulated the Shh pathway, but also inhibited recombinant Shh mediated erythropoiesis. Our study thus reveals an intricate crosstalk among the Notch1, Shh and Akt pathways wherein Notch1 emerges as a key regulator of erythropoiesis.

Anita Roy; Srijan Haldar; Nandini Pal Basak; Subrata Banerjee

1.2.1.6 Viscoelastic Behavior of Human Lamin A Proteins in the Context of Dilated Cardiomyopathy

Lamins are intermediate filament proteins of type V constituting a nuclear lamina or filamentous meshwork which lines the nucleoplasmic side of the inner nuclear membrane. This protein mesh provides a supporting scaffold for the nuclear envelope and tethers interphase chromosome to the

nuclear periphery. Mutations of mainly A-type lamins are found to be causative for at least 11 human diseases collectively termed as laminopathies majority of which are characterised by aberrant nuclei with altered structural rigidity, deformability and poor mechanotransduction behaviour. But the investigation of viscoelastic behavior of lamin A continues to elude the field. In order to address this problem, we hereby present the very first report on viscoelastic properties of wild type human lamin A and some of its mutants linked with Dilated cardiomyopathy (DCM) using quantitative rheological measurements. We observed a dramatic strain-softening effect on lamin A network as an outcome of the strain amplitude sweep measurements which could arise from the large compliance of the quasi-cross-links in the network or that of the lamin A rods. In addition, the drastic stiffening of the differential elastic modulus superposition of rotational and oscillatory shear stress reflect the increase in the stiffness of the laterally associated lamin A rods. These findings present a preliminary insight into distinct biomechanical properties of wild type lamin A protein and its mutants which in turn revealed interesting differences.

Avinanda Banerjee; Vikram Rathee†; Rema Krishnaswamy†; Pritha Bhattacharjee; Pulak Ray...Kaushik Sengupta

1.2.1.7 Differential Thermal Stability and Oxidative Vulnerability of the Hemoglobin Variants, HbA₂ and HbE

Apart from few early biophysical studies, the relative thermal instability of HbE has been only shown by clinical investigations. We have compared *in vitro* thermal stability of HbE with HbA₂ and HbA using optical spectroscopy. From absorption measurements in the Soret region, synchronous fluorescence spectroscopy and dynamic light scattering experiments, we have found thermal stability of the three hemoglobin variants following the order HbE < HbA < HbA₂ in terms of structural unfolding and aggregation pattern. We have found formation of intermolecular dityrosine fluorophores with characteristic fluorescence signature, at pH > 11.0 in all the three variants. Under oxidative stress conditions in presence of hydrogen peroxide, HbE has been found to be more vulnerable to aggregation compared to HbA and HbA₂. Taken together, these studies have shown thermal and oxidative instability of HbE and points towards the role of HbE in the upregulation of redox regulators and chaperone proteins in erythrocyte proteome of patients suffering from HbE-beta thalassemia.

Abhijit Chakrabarti; Dipankar Bhattacharya; Sanghamitra Deb; Madhumita Chakraborty

1.2.1.8 2D DIGE based proteomics study of erythrocyte cytosol in sickle cell disease: Altered proteostasis and oxidative stress

Sickle cell disease (SCD) is a hemolytic disorder caused by a mutation in beta-globin gene and affects millions of people worldwide. Though clinical manifestations of the disease are quite heterogeneous, many of them occur due to erythrocyte sickling at reduced oxygen concentration and vascular occlusion mediated via blood cell adhesion to the vessel wall. We have followed proteomic approach to resolve the differentially regulated proteins of erythrocyte cytosol. The deregulated proteins mainly fall in the group of chaperone proteins such as heat shock protein 70, alpha hemoglobin stabilizing protein, and redox regulators such as aldehyde dehydrogenase and peroxiredoxin-2 proteoforms. Proteasomal subunits are found to be upregulated and phospho-catalase level also got altered. Severe oxidative stress inside erythrocyte is evident from the ROS analysis and Oxyblot

(TM) experiments. Peroxiredoxin-2 shows significant dimerization in the SCD patients, a hallmark of oxidative stress inside erythrocytes. One interesting fact is that most of the differentially regulated proteins are also common for hemoglobinopathies such as E β thalassemia. These could provide important clues in understanding the pathophysiology of SCD and lead us to better patient management in the future.

Avik Basu; Sutapa Saha; Shilpita Karmakar; Sudipa Chakravarty; Debasis Banerjee; Bisnu Prasad Dash; Abhijit Chakrabarti

1.2.1.9 Grb2 Is Regulated by Foxd3 and Has Roles in Preventing Accumulation and Aggregation of Mutant Huntingtin

Growth factor receptor protein binding protein 2 (Grb2) is known to be associated with intracellular growth and proliferation related signaling cascades. Huntingtin (Htt), a ubiquitously expressed protein, when mutated, forms toxic intracellular aggregates - the hallmark of Huntington's disease (HD). We observed an elevated expression of Grb2 in neuronal cells in animal and cell models of HD. Grb2 overexpression was predominantly regulated by the transcription factor Forkhead Box D3 (Foxd3). Exogenous expression of Grb2 also reduced aggregation of mutant Htt in Neuro2A cells. Grb2 is also known to interact with Htt, depending on epidermal growth factor receptor (EGFR) activation. Grb2- mutant Htt interaction in the contrary, took place in vesicular structures, independent of EGFR activation that eventually merged with autophagosomes and activated the autophagy machinery helping in autophagosome and lysosome fusion. Grb2, with its emerging dual role, holds promise for a survival mechanism for HD.

Shounak Baksi; Nihar R Jana†; Nitai Pada Bhattacharyya; Debashis Mukhopadhyay

1.2.1.10 Increased Cytoplasmic Localization of p27(kip1) and Its Modulation of RhoA Activity during Progression of Chronic Myeloid Leukemia

The role of p27(kip1) in Chronic Myeloid Leukemia (CML) has been well studied in relation to its function as a cell cycle inhibitor. However, its cytoplasmic function especially in CML remains to be seen. We studied the localization of p27(kip1) and its function during the progression of CML from chronic to blast phase. Our investigations revealed an increased localization of p27(kip1) in the cytoplasm of CD34(+) cells in the blast phase compared to chronic phase. Cytoplasmic p27(kip1) was found to modulate RhoA activity in CD34(+) stem and progenitor cells. Further, RhoA activity was shown to be dependent on cytoplasmic p27(kip1) which in turn was dependent on p210(Bcr-Abl) kinase activity. Interestingly, RhoA activity was observed to affect cell survival in the presence of imatinib through the SAPK/JNK pathway. Accordingly, inhibition of SAPK/JNK pathway using SP600125 increased apoptosis of K562 cells in presence of imatinib. Our results, for the first time, thus reveal a crucial link between cytoplasmic p27(kip1), RhoA activity and SAPK/JNK signalling. To this effect we observed a correlation between increased cytoplasmic p27(kip1), increased RhoA protein levels, decreased RhoA-GTP levels and increased SAPK/JNK phosphorylation in blast phase CD34(+) cells compared to chronic phase CD34(+) cells.

Anita Roy; Lakshmeshri Lahiry; Debasis Banerjee†; Malay Ghosh†; Subrata Banerjee

1.2.1.11 Epstein Barr virus-encoded small non-coding RNAs induce cancer cell chemoresistance and migration

Epstein-Barr virus (EBV) encoded small, non-coding, non-polyadenylated RNAs, known as EBERs are the most abundantly expressed viral transcripts in latently EBV infected cells. We found the specific role of EBERs in cell cycle progression, resistance against chemotherapeutic drug and cellular invasion in gastric cancer cells in vitro. Ectopic expression of EBERs upregulates the expression of IL-6 and activate its downstream STAT3, which is significantly involved in downregulating the expression of cell cycle inhibitor genes p21 and p27. Stable expression of EBERs regulates the activation of pFAK and pPAK1 and the expression of anti-metastatic genes RhoGDI and KAI-1 in gastric cancer cells. In addition, administration of neu-IL-6 antibody and dominant negative STAT3 beta reduces chemoresistance and inhibits invasion of EBERs-expressing gastric cancer cells. Our results thus revealed a novel role of EBERs in the coordination of IL-6-STAT3 signaling pathway to chemoresistance and cellular migration.

Aditi Sengupta Banerjee; Anindita Deb Pal; Subrata Banerjee

1.2.1.12 Molecular basis of recognition of quadruplexes human telomere and c-myc promoter by the putative anticancer agent sanguinarine

Background: Interaction of putative anticancer agent sanguinarine with two quadruplex forming sequences, humantelomeric DNA (H24) and NHE III1 upstream of the P1 promoter of c-myc (Pu27), has been studied to understand the structural basis of the recognition.

Methods: Absorption, fluorescence and circular dichroism spectroscopy have been employed to characterize the association. Energetics of the interaction was studied by isothermal titration and differential scanning calorimetry. TRAP assay was done to assess the inhibitory potential of sanguinarine.

Results: Absorption and fluorescence studies show that sanguinarine has high binding affinity of similar to 10⁵ M⁻¹ for both sequences. Binding stoichiometry is 2:1 for H24 and 3:1 for Pu27. Results suggest stacking interaction between planar sanguinarine moiety and G-quartets. Circular dichroism spectra show that sanguinarine

Conclusion: These results suggest that there is a difference in the structural modes of association of sanguinarine to the quadruplexes. General significance: It helps to understand the role of quadruplex structures as a target of small molecule inhibitors of telomerase.

Saptarni Ghosh; Suman Kalyan Pradhan; Anirban Kar†; S Chowdhury; D Dasgupta

1.2.1.13 Fluorescence Spectroscopic and Calorimetry Based Approaches to Characterize the Mode of Interaction of Small Molecules with DNA

Ethidium bromide displacement assay by fluorescence is frequently used as a diagnostic tool to identify the intercalation ability of DNA binding small molecules. Here we have demonstrated that the method has pitfalls. We have employed fluorescence, absorbance and label free technique such as isothermal titration calorimetry to probe the limitations. Ethidium bromide, a non-specific intercalator, netropsin, a (A-T) specific minor groove binder, and sanguinarine, a (G-C) specific intercalator, have been used in our experiments to study the association of a ligand with DNA in presence of a competing ligand. Here we have shown that netropsin quenches the fluorescence

intensity of an equilibrium mixture of ethidium bromide - calf thymus DNA via displacement of ethidium bromide. Isothermal titration calorimetry results question the accepted interpretation of the observed decrease in fluorescence of bound ethidium bromide in terms of competitive binding of two ligands to DNA. Furthermore, isothermal titration calorimetry experiments and absorbance measurements indicate that the fluorescence change might be due to formation of ternary complex and not displacement of one ligand by another.

Amrita Banerjee; Jasdeep Singh; Dipak Dasgupta

1.2.1.14 Ellipticine Binds to a Human Telomere Sequence: An Additional Mode of Action as a Putative Anticancer Agent?

Polyguanine sequences fold into G-quadruplex structures in the presence of monovalent cations. It is accepted that the telomeric DNA region consists of G-quadruplex structure. There are reports that potential G-quadruplex forming motifs are also present in the promoter region of some proto-oncogenes such as *c-myc*, *c-kit*, *KRAS*, etc. Small molecules with the potential to stabilize the telomeric DNA quadruplex have emerged as potential anticancer agents. We have studied the interaction of ellipticine, a putative anticancer agent from a plant source, with a human telomeric DNA sequence (H24). Spectroscopic and calorimetric studies indicate that the association of ellipticine with H24 is an entropically driven phenomenon with a 2:3 (H24:ellipticine) stoichiometry. Though ellipticine binding does not induce any major structural perturbation in H24, the association leads to formation of a complex with enhanced thermal stability. An assay with the telomerase repeat amplification protocol shows that ellipticine inhibits telomerase activity in MDAMB-231 breast cancer cell line extracts. This is the first report of the quadruplex binding ability of ellipticine. Using the results, we propose that along with DNA intercalation and/or topoisomerase II inhibition, interaction with the telomeric DNA region and the resultant inhibition of telomerase activity might be an additional mode of action for its anticancer property.

Saptaparni Ghosh; Anirban Kar†; Shantanu Chowdhury†; Dipak Dasgupta

1.2.1.15 Structural Alterations of Lamin A Protein in Dilated Cardiomyopathy

Lamin A protein, encoded by the LMNA gene, belongs to the type V intermediate filament protein family and is a major nuclear protein component of higher metazoan organisms, including humans. Lamin A along with B-type lamins impart structural rigidity to the nucleus by forming a lamina that is closely apposed to the inner nuclear membrane and is also present as a filamentous network in the interior of the nucleus. A vast number of mutations that lead to a diverse array of at least 11 diseases in humans, collectively termed laminopathies, are being gradually uncovered in the LMNA gene. Dilated cardiomyopathy (DCM) is one such laminopathy in which ventricular dilation leads to an increase in systolic and diastolic volumes, resulting in cardiac arrhythmia and ultimately myocardial infarction. The point mutations in lamin A protein span the entire length of the protein, with a slight preponderance in the central α -helical coiled-coil forming domain. In this work, we have focused on three such important mutations that had been previously observed in DCM-afflicted patients producing severe symptoms. This is the first report to show that these mutations entail significant alterations in the secondary and tertiary structure of the protein, hence perturbing the intrinsic self-association behavior of lamin A protein. Comparison of the enthalpy changes accompanying the deoligomerization process for the wild type and the mutants suggests a

difference in the energetics of their self-association. This is further corroborated by the formation of the aggregates of different size and distribution formed inside the nuclei of transfected cells.

Pritha Bhattacharjee; Avinanda Banerjee; Amrita Banerjee; Dipak Dasgupta; Kaushik Sengupta

1.2.1.16 Prospect of Bioflavonoid Fisetin as a Quadruplex DNA Ligand: A Biophysical Approach

Quadruplex (G_4) forming sequences in telomeric DNA and c-myc promoter regions of human DNA are associated with tumorigenesis. Ligands that can facilitate or stabilize the formation and increase the stabilization of G_4 can prevent tumor cell proliferation and have been regarded as potential anti-cancer drugs. In the present study, steady state and time-resolved fluorescence measurements provide important structural and dynamical insights into the free and bound states of the therapeutically potent plant flavonoid fisetin (3,3',4',7-tetrahydroxyflavone) in a G_4 DNA matrix. The excited state intramolecular proton transfer (ESPT) of fisetin plays an important role in observing and understanding the binding of fisetin with the G_4 DNA. Differential absorption spectra, thermal melting, and circular dichroism spectroscopic studies provide evidences for the formation of G_4 DNA and size exclusion chromatography (SEC) proves the binding and 1:1 stoichiometry of fisetin in the DNA matrix. Comparative analysis of binding in the presence of EtBr proves that fisetin favors binding at the face of the G-quartet, mostly along the diagonal loop. Time resolved fluorescence anisotropy decay analysis indicates the increase in the restrictions in motion from the free to bound fisetin. We have also investigated the fingerprints of the binding of fisetin in the antiparallel quadruplex using Raman spectroscopy. Preliminary results indicate fisetin to be a prospective candidate as a G_4 ligand.

Bidisha Sengupta; Biswa Pathik Pahari; Laura Blackmon; Pradeep K Sengupta

1.2.1.17 Interactions of Dietary Flavonoids with Proteins: Insights from Fluorescence Spectroscopy and Other Related Biophysical Studies

In 1936, Rusznyak and Szent-Gyorgyi first drew attention to the therapeutically beneficial role of dietary flavonoids, which are the most common group of polyphenols ubiquitously present in plant based food and beverages. Recent years have witnessed a renaissance of interest on these nutraceuticals, which, because of their high potency and low systemic toxicity, are gradually emerging as promising alternatives to conventional therapeutic drugs. There is a mounting evidence that various proteins frequently serve as targets for therapeutically important flavonoids. In this article we present perspectives exemplifying the growing potential of fluorescence spectroscopy as an exquisitely sensitive tool for noninvasive sensing of protein-flavonoid interactions at physiologically relevant concentrations, via measurements of steady state emission parameters as well as decay kinetics studies of the intrinsic fluorescence of the target (protein) and/or ligand (flavonoid). Especially, we highlight novel applications of the remarkably environment sensitive 'two color' fluorescence exhibited by many important flavonoids, which permits multiparametric and ratiometric measurements. To consolidate findings obtained via fluorescence spectroscopy, use of other relevant experimental biophysical techniques and molecular modeling have proved to be valuable and are also discussed here. Such complementary studies provide additional insights regarding the thermodynamics and conformational aspects of the protein-flavonoid interactions, together with details, at atomistic level, of the dominant noncovalent interactions involved in the docking of different

flavonoids to their target proteins.

Sudip Chaudhuri; Bidisha Sengupta; Jasmine Taylor; Biswa Pathik Pahari; Pradeep K Sengupta

1.2.1.18 Alteration of Mitochondrial Proteome Due to Activation of Notch1 Signaling Pathway

The Notch signaling pathway, a known regulator of cell fate decisions, proliferation, and apoptosis, has recently been implicated in the regulation of glycolysis, which affects tumor progression. However, the impact of Notch on other metabolic pathways remains to be elucidated. To gain more insights into the Notch signaling and its role in regulation of metabolism, we studied the mitochondrial proteome in Notch1-activated K562 cells using a comparative proteomics approach. The proteomic study led to the identification of 10 unique proteins that were altered due to Notch1 activation. Eight of these proteins belonged to mitochondria-localized metabolic pathways like oxidative phosphorylation, glutamine metabolism, Krebs cycle, and fatty acid oxidation. Validation of some of these findings showed that constitutive activation of Notch1 deregulated glutamine metabolism and Complex 1 of the respiratory chain. Furthermore, the deregulation of glutamine metabolism involved the canonical Notch signaling and its downstream effectors. The study also reports the effect of Notch signaling on mitochondrial function and status of high energy intermediates ATP, NADH, and NADPH. Thus our study shows the effect of Notch signaling on mitochondrial proteome, which in turn affects the functioning of key metabolic pathways, thereby connecting an important signaling pathway to the regulation of cellular metabolism.

Nandini Pal Basak; Anita Roy; Subrata Banerjee

1.2.2 C&MB

1.2.2.1 Potential of known and short prokaryotic protein motifs as a basis for novel peptide-based antibacterial therapeutics: a computational survey

Short linear motifs (SLiMs) are functional stretches of protein sequence that are of crucial importance for numerous biological processes by mediating protein-protein interactions. These motifs often comprise peptides of less than 10 amino acids that modulate protein-protein interactions. While well-characterized in eukaryotic intracellular signaling, their role in prokaryotic signaling is less well-understood. We surveyed the distribution of known motifs in prokaryotic extracellular and virulence proteins across a range of bacterial species and conducted searches for novel motifs in virulence proteins. Many known motifs in virulence effector proteins mimic eukaryotic motifs and enable the pathogen to control the intracellular processes of their hosts. Novel motifs were detected by finding those that had evolved independently in three or more unrelated virulence proteins. The search returned several significantly over-represented linear motifs of which some were known motifs and others are novel candidates with potential roles in bacterial pathogenesis. A putative C-terminal G[AG]_n motif found in type IV secretion system proteins was among the most significant detected. A KK motif that has been previously identified in a plasminogen-binding protein, was demonstrated to be enriched across a number of adhesion and lipoproteins. While there is some potential to develop peptide drugs against bacterial infection based on bacterial peptides that mimic host components, this could have unwanted effects on host signaling. Thus, novel SLiMs in virulence factors that do not mimic host components but are crucial for bacterial pathogenesis,

such as the type IV secretion system, may be more useful to develop as leads for anti-microbial peptides or drugs.

Heini Ruhanen†; Daniel Hurley†; Ambarnil Ghosh; et al

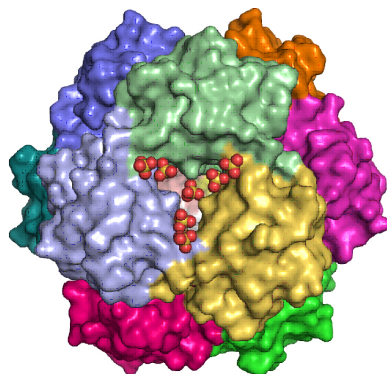
1.2.2.2 Transcription Regulation of HYPK by Heat Shock Factor 1

HYPK (Huntingtin Yeast Partner K) was originally identified by yeast two-hybrid assay as an interactor of Huntingtin, the protein mutated in Huntington's disease. HYPK was characterized earlier as an intrinsically unstructured protein having chaperone-like activity in vitro and in vivo. HYPK has the ability of reducing rate of aggregate formation and subsequent toxicity caused by mutant Huntingtin. Further investigation revealed that HYPK is involved in diverse cellular processes and required for normal functioning of cells. In this study we observed that hyperthermia increases HYPK expression in human and mouse cells in culture. Expression of exogenous Heat Shock Factor 1 (HSF1), upon heat treatment could induce HYPK expression, whereas HSF1 knockdown reduced endogenous as well as heat-induced HYPK expression. Putative HSF1-binding site present in the promoter of human HYPK gene was identified and validated by reporter assay. Chromatin immunoprecipitation revealed in vivo interaction of HSF1 and RNA polymerase II with HYPK promoter sequence. Additionally, acetylation of histone H4, a known epigenetic marker of inducible HSF1 binding, was observed in response to heat shock in HYPK gene promoter. Overexpression of HYPK inhibited cells from lethal heat-induced death whereas knockdown of HYPK made the cells susceptible to lethal heat shock-induced death. Apart from elevated temperature, HYPK was also upregulated by hypoxia and proteasome inhibition, two other forms of cellular stress. We concluded that chaperone-like protein HYPK is induced by cellular stress and under transcriptional regulation of HSF1.

Srijit Das; Nitai Pada Bhattacharyya

1.2.2.3 A Novel 8-nm Protein Cage Formed by *Vibrio cholerae* Acylphosphatase

Here we show the formation of an similar to 8-nm cage formed by the self-assembly of acylphosphatase from *Vibrio cholerae* O395 (Vc-AcP). The 12-subunit cage structure forms spontaneously and is stabilized through binding of sulfate ions at its exterior face and interfacial regions. Crystal



structure and studies in solutions illuminate the basis for the formation of the cage, while a single (Cys20 → Arg) mutation (Vc-AcP-C20R) transforms Vc-AcP to a potent enzyme but disrupts the

assembly into a trimer.

Seema Nath; Ramanuj Banerjee; Udayaditya Sen

1.2.2.4 A turn on ESIPT probe for rapid and ratiometric fluorogenic detection of homocysteine and cysteine in water with live cell-imaging

5(Benzothiazol-2-yl)-4-hydroxyisophthalaldehyde (BHI), an intense ESIPT containing molecule in mixed media loses its properties due to resonance-assisted H-bond (RAHB) in absolute water. Due to resonance-assisted H-bond the o-aldehyde is more reactive than the other one. With addition of cysteine/homocysteine into this solution the o-aldehyde group gets transformed into thiazolidine/thiazine ring, respectively, and the phenolic proton becomes free enough for transfer to nitrogen of the benzothiazole ring in excited state, that is, the ESIPT of BHI is turned on. Thus we can detect cysteine/homocysteine in water as well as in live cells.

Shyamaprosad Goswami†; Abhishek Manna†; Sima Paul†...Anup Kumar Maity; Partha Saha

1.2.2.5 A FRET-based rhodamine-benzimidazole conjugate as a Cu²⁺-selective colorimetric and ratiometric fluorescence probe that functions as a cytoplasm marker

On the basis of fluorescence resonance energy transfer (FRET) from benzimidazole to a rhodamine moiety, a rhodamine-benzimidazole conjugate (RBC) ratiometric fluorescent probe has been designed and synthesized. The RBC selectively binds to Cu²⁺, showing visually observable changes in absorption and emission behavior, and demonstrates an effective intracellular Cu²⁺ imaging ability, allowing it to function as a cytoplasm marker.

Shyamaprosad Goswami†; Sibaprasad Maity†; Annada C Maity†; Anup Kumar Maity...Partha Saha

1.2.2.6 Visual and near IR (NIR) fluorescence detection of Cr³⁺ in aqueous media via spirobenzopyran ring opening with application in logic gate and bio-imaging

A new spirobenzopyran derivative (SPNH) was designed and synthesized which was applied in simultaneous colorimetric and NIR fluorescence detections for Cr³⁺. This spirobenzopyran receptor is normally colorless in aqueous organic media but the formation of merocyanine occurs by Cr³⁺ showing a yellow color. Here the formation of yellow color in UV-vis spectra and strong NIR fluorescence emission at 675 nm makes SPNH a good sensor for Cr³⁺ ion. It is also found to be useful in cell imaging and in construction of logic gate. It shows INHIBIT gate in fluorescence and OR gate in absorption. To the best of our knowledge, this is the first report of NIR fluorescence emission of a spirobenzopyran derivative by Cr³⁺ and its application to cell-biology and also in the logic gate.

Shyamaprosad Goswami†; Avijit Kumar Das†; Anup Kumar Maity...Partha Saha; et al

1.2.2.7 Drought resistance in rice seedlings conferred by seed priming

Seed priming is a method by which seeds are subjected to different stress conditions to impart stress adaptation in seedlings germinating and growing under stressful situations. Drought stress is a major reason behind failure of crops. We studied the effects of hydropriming, dehydration priming (induced by PEG), and osmopriming (induced by NaCl and KH₂PO₄) on subsequent germination, growth and anti-oxidant defense mechanisms of 2-week-old rice seedlings under continuing dehydration stress. Unprimed seeds grown in PEG showed significantly lower germination and growth along with significantly higher reactive oxygen species (ROS) and lipid peroxidation levels. Among the priming methods, 5 % PEG priming was found to be the best in terms of germination and growth rate along with the lowest amount of ROS and lipid peroxidation (malondialdehyde [MDA]) values. MDA levels were reduced significantly by all of the priming methods. Hence, reduction of lipid peroxidation may be a key factor underlying the drought tolerance produced by the priming treatments. Glutathione peroxidase (GPX) activity seemed to bear an excellent correlation with oxidative stress resistance through seed priming. The PEG priming produced minimum peroxidative damage and superior germination and growth rate along with efficient GPX activity, overexpressed MnSOD and maintenance of HSP70 expression in normal as well as in drought condition. Therefore, in PEG-primed seeds the existence of robust protective mechanisms is definitely indicated.

Alakananda Goswami; Rahul Banerjee; Sanghamitra Raha

1.2.2.8 Conformational Barrier of CheY3 and Inability of CheY4 to Bind FliM Control the Flagellar Motor Action in *Vibrio cholerae*

Vibrio cholerae contains multiple copies of chemotaxis response regulator (VcCheY1-VcCheY4) whose functions are elusive yet. Although previous studies suggested that only VcCheY3 directly switches the flagellar rotation, the involvement of VcCheY4 in chemotaxis could not be ruled out. None of these studies, however, focused on the structure, mechanism of activation or molecular basis of FliM binding of the VcCheYs. From the crystal structures of Ca²⁺ and Mg²⁺ bound VcCheY3 we proposed the presence of a conformational barrier composed of the hydrophobic packing of W61, M88 and V106 and a unique hydrogen bond between T90 and Q97 in VcCheY3. Lesser fluorescence quenching and higher K_m value of VcCheY3, compared to its mutants VcCheY3-Q97A and VcCheY3-Q97A/E100A supported our proposition. Furthermore, aforesaid biochemical data, in conjunction with the structure of VcCheY3-Q97A, indicated that the coupling of T90 and Q97 restricts the movement of T90 toward the active site reducing the stabilization of the bound phosphate and effectively promoting autodephosphorylation of VcCheY3. The structure of BeF₃-activated VcCheY3 insisted us to argue that elevated temperature and/or adequacy of phosphate pool might break the barrier of the free-state VcCheY3 and the conformational changes, required for FliM binding, occur upon phosphorylation. Structure of VcCheY4 has been solved in the free and sulfated states. VcCheY4(sulf), containing a bound sulfate at the active site, appears to be more compact and stable with a longer alpha 4 helix, shorter beta 4 alpha 4 loop and hydrogen bond between T82 and the sulfate compared to VcCheY4 free. While pull down assay of VcCheYs with VcFliM(NM) showed that only activated VcCheY3 can interact with VcFliMNM and VcCheY4 cannot, a knowledge based docking explained the molecular mechanism of the interactions between VcCheY3 and VcFliM and identified the limitations of VcCheY4 to interact with VcFliM even in

its phosphorylated state.

Maitree Biswas†; Sanjay Dey†; Susmita Khamrui; Udayaditya Sen; et al

1.2.2.9 Structural and mechanistic basis of anti-termination of Rho-dependent transcription termination by bacteriophage P4 capsid protein Psu

The conserved bacterial transcription terminator, Rho, is a potent target for bactericidal agents. Psu, a bacteriophage P4 capsid protein, is capable of inducing anti-termination to the Rho-dependent transcription termination. Knowledge of structural and mechanistic basis of this anti-termination is required to design peptide-inhibitor(s) of Rho from Psu. Using suppressor genetics, cross-linking, protein foot-printing and FRET analyses, we describe a conserved disordered structure, encompassing 139-153 amino acids of Rho, as the primary docking site for Psu. Also a neighbouring helical structure, comprising 347-354 amino acids, lining its central channel, plays a supportive role in the Rho-Psu complex formation. Based on the crystal structure of Psu, its conformation in the capsid of the P4 phage, and its interacting regions on Rho, we build an energy-minimized structural model of the Rho:Psu complex. In this model, a V-shaped dimer of Psu interacts with the two diagonally opposite subunits of a hexameric Rho, enabling Psu to form a 'lid' on the central channel of the latter. We show that this configuration of Psu makes the central channel of Rho inaccessible, and it causes a mechanical impediment to its translocase activity.

Amitabh Ranjan†; Savita Sharma†; Ramanuj Banerjee; Udayaditya Sen; et al

1.2.2.10 Enhancement of Proteolytic Activity of a Thermostable Papain-Like Protease by Structure-Based Rational Design

Ervatamins (A, B and C) are papain-like cysteine proteases from the plant *Ervatamia coronaria*. Among Ervatamins, Ervatamin-C is a thermostable protease, but it shows lower catalytic efficiency. In contrast, Ervatamin-A which has a high amino acid sequence identity ($\sim 90\%$) and structural homology (C α rmsd 0.4 Å) with Ervatamin-C, has much higher catalytic efficiency (~ 57 times). From the structural comparison of Ervatamin-A and -C, two residues Thr32 and Tyr67 in the catalytic cleft of Ervatamin-A have been identified whose contributions for higher activity of Ervatamin-A are established in our earlier studies. In this study, these two residues have been introduced in Ervatamin-C by site directed mutagenesis to enhance the catalytic efficiency of the thermostable protease. Two single mutants (S32T and A67Y) and one double mutant (S32T/A67Y) of Ervatamin-C have been generated and characterized. All the three mutants show ~ 8 times higher catalytic efficiency (k_{cat}/K_m) than the wild-type. The thermostability of all the three mutant enzymes remained unchanged. The double mutant does not achieve the catalytic efficiency of the template enzyme Ervatamin-A. By modeling the structure of the double mutant and probing the role of active site residues by docking a substrate, the mechanistic insights of higher activity of the mutant protease have been addressed. The *in-silico* study demonstrates that the residues beyond the catalytic cleft also influence the substrate binding and positioning of the substrate at the catalytic centre, thus controlling the catalytic efficiency of an enzyme.

Sruti Dutta; Jiban Kanti Dattagupta; Sampa Biswas

1.2.3 Chemical Sciences

1.2.3.1 Spectroscopic studies of the binding of Cu(II) complexes of oxicam NSAIDs to alternating G-C and homopolymeric G-C sequences

Drugs belonging to the Non-steroidal anti-inflammatory (NSAID) group are not only used as anti-inflammatory, analgesic and anti-pyretic agents, but also show anti-cancer effects. Complexing them with a bioactive metal like copper, show an enhancement in their anti-cancer effects compared to the bare drugs, whose exact mechanism of action is not yet fully understood. For the first time, it was shown by our group that Cu(II)-NSAIDs can directly bind to the DNA backbone. The ability of the copper complexes of NSAIDs namely meloxicam and piroxicam to bind to the DNA backbone could be a possible molecular mechanism behind their enhanced anticancer effects. Elucidating base sequence specific interaction of Cu(II)-NSAIDs to the DNA will provide information on their possible binding sites in the genome sequence. In this work, we present how these complexes respond to differences in structure and hydration pattern of GC rich sequences. For this, binding studies of Cu(II) complexes of piroxicam [Cu(II)-(Px)₂ (L)₂] and meloxicam [Cu(II)-(Mx)₂ (L)] with alternating GC (polydG-dC) and homopolymeric GC (polydG-polydC) sequences were carried out using a combination of spectroscopic techniques that include UV-Vis absorption, fluorescence and circular dichroism (CD) spectroscopy. The Cu(II)-NSAID5 show strong binding affinity to both polydG-dC and polydG-polydC. The role reversal of Cu(II)-meloxicam from a strong binder of polydG-dC ($K_b = 11.5 \times 10^3 \text{ M}^{-1}$) to a weak binder of polydG-polydC ($K_b = 5.02 \times 10^3 \text{ M}^{-1}$), while Cu(II)-piroxicam changes from a strong binder of polydG-polydC ($K_b = 8.18 \times 10^3 \text{ M}^{-1}$) to a weak one of polydG-dC ($K_b = 2.18 \times 10^3 \text{ M}^{-1}$), point to the sensitivity of these complexes to changes in the backbone structures/hydration. Changes in the profiles of UV absorption band and CD difference spectra, upon complex binding to polynucleotides and the results of competitive binding assay using ethidium bromide (EtBr) fluorescence indicate different binding modes in each case.

Sreeja Chakraborty; Madhuparna Bose†; Munna Sarkar

1.2.3.2 Development of a Rhodamine-Rhodanine-Based Fluorescent Mercury Sensor and Its Use to Monitor Real-Time Uptake and Distribution of Inorganic Mercury in Live Zebrafish Larvae

We introduce a new rhodamine-rhodanine-based "turn-on" fluorescent sensor (RR1) and describe its application for detection of mercury, including in solution, in live cells, and in a living vertebrate organism. The sensor RR1, which is a one-pot synthesis from rhodamine B, undergoes a rapid and irreversible 1:1 stoichiometric reaction with Hg^{2+} in aqueous medium. Using fluorescence correlation spectroscopy (FCS), RR1 was shown to detect the presence of as low as a 0.5 pM concentration of Hg^{2+} . It may also lend itself to tagging with biomolecules and nanoparticles, leading to the possibility of organelle-specific Hg detection. Results of experiments with mammalian cells and zebrafish show that RR1 is cell and organism permeable and that it responds selectively to mercury ions over other metal ions. In addition, real-time monitoring of inorganic mercury ion uptake by cells and live zebrafish using this chemosensor shows that saturation of mercury ion uptake occurs within 20-30 min in cells and organisms. We also demonstrate the acquisition of high-resolution real-time distribution maps of inorganic mercury (Hg^{2+}) in the zebrafish brain by

using a simple fluorescence confocal imaging technique.

Kallol Bera; Anand Kant Das†; Moupanya Nag; Soumen Basak

1.2.3.3 Synthesis of radioactive gold nanoparticle in surfactant medium

The present study describes the synthesis of radioactive gold nanoparticle in surfactant medium. Proton irradiated stable ^{197}Au and radioactive ^{198}Au were simultaneously used for production of radioactive gold nanoparticle. Face centered cubic gold nanoparticles with size of 4-50 nm were found in proton irradiated gold foil. However, the size of nanoparticle varies with pH using both stable and radioactive gold.

Swadesh Mandal

1.2.3.4 Separation of no-carrier-added $^{99m}\text{TcO}_4^-$ Tc from ^{99}Mo - ^{99m}Tc equilibrium mixture by PEG based aqueous biphasic separation technique using sodium/potassium salts of citric and tartaric acid

Extraction and separation of no-carrier-added (nca) $^{99m}\text{TcO}_4^-$ Tc from ^{99}Mo - ^{99m}Tc equilibrium mixture was carried out by environmentally benign polyethylene glycol based liquid-liquid aqueous biphasic systems (ABS) consisting various inorganic salts. Among the various inorganic salt trisodium citrate and potassium sodium tartrate showed the suitable salt rich phase for the best separation in this report. The concentration variation of salt rich phase, temperature and PEG phase also exhaustively studied in paper for the achievement of high separation factor. At 40°C temperature in 50 % (w/v) PEG-4000-2M Na_3 citrate showed the highest separation factor ($S\text{-Tc/Mo}$) 1.2×10^7 .

Swadesh Mandal; Ajoy Mandal

1.2.3.5 Effect of phosphate group in switching off electron transfer in different media

We have studied the interactions of individual nucleoside 5'-monophosphates of all the five nucleic acid bases, adenosine 5'-monophosphate (AMP), guanosine 5'-monophosphate (GMP), thymidine 5'-monophosphate (TMP), cytidine 5'-monophosphate (CMP) and uridine 5'-monophosphate (UMP) with two quinones, 9,10-anthraquinone (AQ) and 2-methyl 1,4-naphthoquinone (MQ) commonly known as menadione using laser flash photolysis in two different types of media. Although electron transfer (ET) in excited state is a well-known phenomenon in DNA with quinones, this work reveals a total failure of ET with these isolated 5'-monophosphate molecules in a homogeneous medium (acetonitrile/water), except GMP. Similar experiments in SDS micelles have been repeated but here even GMP failed to transfer electrons. We have attributed the failure of ET in homogeneous medium to a semi-circular conformation adopted by the 5'-monophosphates, which is assumed to pull back the electrons from the electron donor center, the nitrogenous base. In SDS micelles a rapid spin exchange within an abnormally short inter-radical distance has been considered to prevent ET.

Adity Bose†; Samita Basu

1.2.3.6 Polypyrrole decorated graphene nanostructure: Fabrication, depiction and anomalous dimensional crossover in electronic conduction

We had fabricated polypyrrole based graphene nanostructure by using CTAB (cetyl trimethylammonium bromide) surfactant with variation of graphene loading and characterized them by XRD, FT-IR, SEM, TEM, AFM, Raman etc. Variable range hopping (VRH) model had been applied for explication of temperature dependent D.C. conductivity scrutinized from 20 to 300 K. A synergetic effect of pi-electron flow in conducting polymer polypyrrole and 2D graphene layer was appeared to demonstrate the plausible charge-transport mechanism. Dramatically, two peculiar crossovers had been observed simultaneously in the composite samples with variation of temperature. A 3D-2D effective dimensional crossover had been observed at approximate to 100 K with variation of hopping length which can be controlled by temperatures. Below 50K another cross-over between Mott and ES (Efros & Shklovskii) type VRH mechanism had also been explored as resistivity increases with lowering of temperature. Here, charge transport occurred via VRH between intact graphene island and polypyrrole chain.

Debabrata Nandi; Susmita Nandi; Prasun K Pal...Amitabha De; et al

1.2.3.7

Conducting CoMn₂O₄-PEDOT nanocomposites as catalyst in oxygen reduction reaction The present study is on development of easy, facile and rapid synthetic methodologies for producing highly active low-cost bifunctional electrocatalysts for oxygen reduction/evolution reactions (ORR/OER) which are the key barriers in various electrochemical devices such as metal-air batteries, fuel cells and water splitting reaction. The synthesized PEDOT-CoMn₂O₄ nanocomposites from alpha-MnO₂ nanorod favour 4e oxygen reduction process of oxygen to water and exhibit high ORR activities in the stable conducting platform of the polymer. The catalytic effect is studied by Linear Sweep Voltammetry using Rotating Disk Electrode at varying rotation speed (0 to 3000 rpm). Although the α -MnO₂ nanorod does not show any OER/ORR activity, the spinel makes the difference and the nanocomposites of PEDOT - CoMn₂O₄ exhibit unexpected, surprisingly high ORR activities in their conducting and stable form. The enhanced catalytic activity arises from synergetic chemical coupling effects between PEDOT and CoMn₂O₄.

Ankan Dutta Chowdhury; Nidhi Agnihotri; Pintu Sen†; Amitabha De

1.2.3.8 Separation of no-carrier-added rhenium from bulk tantalum by the sodium malonate-PEG aqueous biphasic system

The aqueous biphasic system (ABS) involving sodium malonate-polyethylene glycol (PEG) phases has been applied for the first time for separation of no-carrier-added Re-183 (T-1/2=70 d) from α -particle irradiated bulk tant alum target. The various ABS conditions were applied for investigating the separation by varying pH, temperature, PEG-molecular weight, concentration of salt. The extraction pattern was hardly affected by change in pH and the molecular weight of PEG. One step separation of nca Re-183 from Ta was achieved at the optimal conditions of (i) 50% (w/w) PEG-4000-2 M sodium malonate, 40° C and (ii) 50% (w/w) PEG-4000-3 M sodium malonate, room temperature (27° C).

Binita Dutta; Susanta Lahiri; BS Tomar†

1.2.3.9 Effect of β -cyclodextrin on the molecular properties of myricetin upon nano-encapsulation: Insight from optical spectroscopy and quantum chemical studies

Myricetin, a bioactive plant flavonol, readily forms inclusion complex with the drug delivery vehicle beta-cyclodextrin (β -CD). Appearance of typical "dual emission", consisting of normal (470 nm) and ESIPT tautomer (530 nm) bands, with concomitant rise in fluorescence intensity and dramatically blue shifted normal fluorescence of myricetin with increasing β -CD concentration, indicates facile entry of myricetin into the cavity of β -CD. The stoichiometry of the inclusion complex has been established to be equimolar (1:1), with an equilibrium constant of $439 \pm 18 \text{ M}^{-1}$ at 25°C . The driving force of inclusion is attributed to strong van der Waals interaction and formation of hydrogen bond between host (β -CD) and guest (myricetin). Both experimental and theoretical studies indicate that myricetin possibly incorporates within β -CD through its benzoyl moiety. Inclusion in β -CD increases the antioxidant potency of myricetin which has been attributed to the less delocalised HOMO and reduced HOMO-LUMO energy gap in the confined state.

Sandipan Chakraborty†; Soumalee Basu; Soumen Basak

1.2.3.10 Photophysical properties of 1,8-naphthalic anhydride in aprotic solvents: An electron acceptor in excited state

1,8-Naphthalic anhydride (NAN) has long been known as an intermediate for the synthesis of 1,8-naphthalimide derivatives with diverse applications. Uses of NAN for other purposes are restricted because it hydrolyzes in water and other protic solvents. In the current work we have investigated the absorption, steady-state and time-resolved fluorescence spectroscopy of NAN in eight different aprotic solvents of varying polarity. The compound is found to have different quantum yields in all the solvents. Astoundingly, NAN shows minimal fluorescence yield in dimethyl sulphoxide and N,N-dimethylformamide which is found to originate from pure collisional quenching owing to proton affinity of the solvent. In aprotic solvents acetonitrile and ethyl acetate, fluorescence emission and lifetime of NAN are quenched on addition of aliphatic amines namely triethylamine (TEA), tri-N-butylamine (TBA) and diisopropylethylamine (DIEA). Laser flash photolysis experiments in acetonitrile solvent have been used to find out the transient intermediates, which depict the involvement of photo-induced electron transfer from the amines to NAN. Hence, NAN has the potential to act as an efficient photo-induced electron acceptor in aprotic medium.

Sujay Ghosh; Subhanip Biswas; Mousumi Mondal; Samita Basu

1.2.3.11 Fabrication, nanostructure evaluation, 3D electrical transport and electrochemical capacitance of PEDOT-Ti(IV)-doped iron(III) oxide nanocomposite

Poly[3,4-(ethylenedioxy) thiophene] (PEDOT) nanocomposites (NCs) reinforced by varying titanium(IV)-doped iron(III) nano oxide (NITO) particles have been fabricated in dodecylbenzene sulphonic acid by in situ polymerization process using ammonium perdisulfate as initiator. The samples were characterized by X-ray diffraction, Fourier transform infrared spectroscopy, electron microscopy, BET surface analysis etc. followed by subsequent evaluation of thermal properties, temperature-dependent 3D electrical transport. Thermal stability of the NCs increased with increasing NITO amount in PEDOT matrix. Electrical conductivity of the NCs increased significantly

with increasing NITO content ($0.45\text{--}67.73\text{ S cm}^{-1}$) and also with the temperature ($50\text{--}300\text{ K}$). 3D variable range hopping conduction mechanism explained the conduction pathways. Specific capacitance of NCs are enhanced with higher NITO content in polymer from 107 F g^{-1} (pristine PEDOT) to 158 F g^{-1} (NC) owing to the development of mesoporous (pore size: 4.1 nm and cylindrical pore volume: $0.103\text{ cm}^3\text{ g}^{-1}$) structure and high specific surface area ($\sim 104\text{ m}^2\text{ g}^{-1}$).

Debabrata Nandi†; Arup K Ghosh†; Amitabha De; et al

1.2.3.12 Highly sensitive electrochemical biosensor for glucose, DNA and protein using gold-polyaniline nanocomposites as a common matrix

In this paper, fabrication of a biosensing platform by covalent attachment of biomolecules on PANi nanowire (NW) decorated with gold nanoparticles (AuNP) has been reported. Efficiency of the platform has been evaluated after attachment of three different biomolecules viz. glucose oxidase (GOx), a single stranded DNA (ssDNA) and Lamin A antibody (LAA) for sensing of glucose, complementary DNA strand and Lamin A protein, respectively. Method of immobilization as well as method of detection was somewhat different for different systems. GOx and LAA were attached via NH₂ functionalizations on AuNP while thiol-ended ssDNA was directly attached to AuNP surface. Sensing of glucose was monitored via chronoamperometry and the flow cell techniques while DNA detection was carried out via Differential Pulse Voltametry (DPV) and protein detection employing Electrochemical Impedance Spectroscopic (EIS) technique. Fabrication of the electrode was easy, enzymatic activity was well and reproducibility of the sensing process was good enough for sensing of glucose. The lower detection limit ($1\text{ }\mu\text{ M}$), higher sensitivity ($14.63\text{ }\mu\text{ A mM}^{-1}\text{ cm}^{-2}$), greater stability and the excellent specificity indicated excellence of glucose sensor. For DNA sensor, detection of non complementary and complementary strands, even single base mismatch could be well discriminated up to the analyte concentration as low as $1\text{ }\mu\text{ M}$. The similar detection limit was also obtained for detection of protein all which proves the suitability of the Au-PANI nanocomposites as a general sensor platform.

Ankan Dutta Chowdhury; Rupali Gangopadhyay; Amitabha De

1.2.3.13 Gas Phase Hydrolysis of Formaldehyde To Form Methanediol: Impact of Formic Acid Catalysis

We find that formic acid (FA) is very effective at facilitating diol formation through its ability to reduce the barrier for the formaldehyde (HCHO) hydrolysis reaction. The rate limiting step in the mechanism involves the isomerization of a prereactive collision complex formed through either the HCHO center dot center dot center dot H₂O + FA and/or HCHO + FA center dot center dot center dot H₂O pathways. The present study finds that the effective barrier height, defined as the difference between the zero-point vibrational energy (ZPE) corrected energy of the transition state (TS) and the HCHO center dot center dot center dot H₂O + FA and HCHO + FA center dot center dot center dot H₂O starting reagents, are respectively only similar to 1 and similar to 4 kcal/mol. These barriers are substantially lower than the similar to 17 kcal/mol barrier associated with the corresponding step in the hydrolysis of HCHO catalyzed by a single water molecule (HCHO + H₂O + H₂O). The significantly lower barrier heights for the formic acid catalyzed pathway reveal a new important role that organic acids play in the gas phase hydrolysis of atmospheric carbonyl

compounds.

Montu K Hazra; Joseph S Francisco†; Amitabha Sinha†

1.2.3.14 Combinatorial Recruitment of CREB, C/EBP β and c-Jun Determines Activation of Promoters upon Keratinocyte Differentiation

Background: Transcription factors CREB, C/EBP β and Jun regulate genes involved in keratinocyte proliferation and differentiation. We questioned if specific combinations of CREB, C/EBP β and c-Jun bound to promoters correlate with RNA polymerase II binding, mRNA transcript levels and methylation of promoters in proliferating and differentiating keratinocytes.

Results: Induction of mRNA and RNA polymerase II by differentiation is highest when promoters are bound by C/EBP β alone, C/EBP β together with c-Jun, or by CREB, C/EBP β and c-Jun, although in this case CREB binds with low affinity. In contrast, RNA polymerase II binding and mRNA levels change the least upon differentiation when promoters are bound by CREB either alone or in combination with C/EBP β or c-Jun. Notably, promoters bound by CREB have relatively high levels of RNA polymerase II binding irrespective of differentiation. Inhibition of C/EBP β or c-Jun preferentially represses mRNA when gene promoters are bound by corresponding transcription factors and not CREB. Methylated promoters have relatively low CREB binding and, accordingly, those which are bound by C/EBP β are induced by differentiation irrespective of CREB. Composite "Half and Half" consensus motifs and co localizing consensus DNA binding motifs are overrepresented in promoters bound by the combination of corresponding transcription factors.

Conclusion: Correlational and functional data describes combinatorial mechanisms regulating the activation of promoters. Colocalization of C/EBP β and c-Jun on promoters without strong CREB binding determines high probability of activation upon keratinocyte differentiation.

Julian M Rozenberg†; Paramita Bhattacharya; Raghunath Chatterjee†; et al

1.2.3.15 Separation of No-Carrier-Added Rhenium from Bulk Tantalum By Precipitation Technique

No-carrier-added (NCA) rhenium isotopes have received ample attention for diverse practical applications. In the present study we have produced NCA ^{183}Re isotope via particle bombardment on a tantalum target. The classical precipitation method has been revisited for precipitating out the bulk tantalum matrix as hydrated tantalum hydroxide from solution using sodium carbonate and ammonia solution. In this simple single-step procedure of separation, NCA ^{183}Re activity quantitatively retains in the supernatant phase along with negligible ($\sim 1.2\text{-}1.3\text{ppm}$) chemical contamination of the bulk tantalum. This fast, cost effective separation methodology is an example of the green chemistry approach where minimum chemical consumption (no organic reagents was used) was reported including the target material which can be recovered in different chemical form for further use depending on the specific application of NCA rhenium.

Binita Dutta; Susanta Lahiri; BS Tomar†

1.2.3.16 A mathematical approach to beam matching

Objective: This report provides the mathematical commissioning instructions for the evaluation of beam matching between two different linear accelerators.

Methods: Test packages were first obtained including an open beam profile, a wedge beam profile and a depth-dose curve, each from a 10x10 cm² beam. From these plots, a spatial error (SE) and a percentage dose error were introduced to form new plots. These three test package curves and the associated error curves were then differentiated in space with respect to dose for a first and second derivative to determine the slope and curvature of each data set. The derivatives, also known as bandwidths, were analysed to determine the level of acceptability for the beam matching test described in this study.

Results: The open and wedged beam profiles and depth-dose curve in the build-up region were determined to match within 1% dose error and 1-mm SE at 71.4% and 70.8% for of all points, respectively. For the depth-dose analysis specifically, beam matching was achieved for 96.8% of all points at 1%/1mm beyond the depth of maximum dose.

Conclusion: To quantify the beam matching procedure in any clinic, the user needs to merely generate test packages from their reference linear accelerator. It then follows that if the bandwidths are smooth and continuous across the profile and depth, there is greater likelihood of beam matching. Differentiated spatial and percentage variation analysis is appropriate, ideal and accurate for this commissioning process.

Advances in knowledge: We report a mathematically rigorous formulation for the qualitative evaluation of beam matching between linear accelerators.

B Sarkar†; A Manikandan†; M Nandy; et al

1.2.3.17 Tuning the Solution Phase Photophysics of Two De Novo Designed Hydrogen Bond Sensitive 9-methyl-2,3,4,9-tetrahydro-1H-carbazol-1-one Derivatives

Two new fluorophores, 6,7-dimethoxy-9-methyl-2,3,4,9-tetrahydro-1H-carbazol-1-one (DMTCO) and 5-methyl-8,9-dihydro-5H-[1,3]dioxolo[4,5-b]carbazol-6(7H)-one (MDDCO), first of their kind, have been synthesized from the corresponding methoxy and methylenedioxy derivatives of 2,3,4,9-tetrahydro-1H-carbazol-1-one respectively. Comprehensive photophysical characterization of these compounds has been carried out in sixteen different homogeneous solvents and binary solvent mixtures. Both of these compounds are sensitive to solvent polarity, but the sensitivity is much higher in electronic excited state observed by steady-state and time-resolved fluorescence experiments than in ground state studied by UV-vis absorption spectroscopy. The fluorescence spectral shifts are linearly correlated with the empirical parameters of the protic solvents and also the quantitative influence of the empirical solvent parameters on the emission maxima of the compounds has been calculated. The change in dipole moment of the compounds in their excited state has been calculated from the shifts in corresponding emission maxima in pure solvents. A higher dipole moment change of both DMTCO and MDDCO in protic solvents is due to intermolecular hydrogen bonding which is further confirmed by the comparison of their behaviour in toluene-acetonitrile and toluene-methanol solvent mixtures. From structural features, MDDCO is more planar compared to DMTCO, which is reflected better in fluorescence quenching of the former with organic bases, N,N-dimethylaniline and N,N-diethylaniline. Laser flash photolysis experiments prove that the quenching interaction originates from photoinduced electron transfer from the bases to the

compounds.

Sujay Ghosh; Amrit Krishna Mitra†; Chandan Saha†; Samita Basu

1.2.3.18 Separation of no-carrier-added ^{109}Cd from natural silver target using RTIL 1-butyl-3-methylimidazolium hexafluorophosphate

The room temperature ionic liquid (RTIL), 1-butyl-3-methylimidazolium hexafluorophosphate [C(4)mim][PF₆] has various applications in the separation of a range of metal ions replacing volatile and toxic traditional organic solvents in liquid-liquid extraction systems. In this study, the RTIL [C₄mim][PF₆] was used to separate no-carrier-added (NCA) ^{109}Cd from α -particle irradiated Ag target. A natural Ag foil was bombarded by 30 MeV alpha-particles to produce ^{109}Cd . After the decay of all co-produced short-lived products, NCA ^{109}Cd was separated from the bulk Ag using [C₄mim][PF₆] as extractant from HNO₃ medium. Ammoniumpyrrolidine dithiocarbamate (APDC) was used as a complexing agent. At the optimum condition, 3 M HNO₃, 0.01 M APDC in presence of [C(4)mim][PF₆], ~ 99 % bulk Ag was extracted to the IL phase, leaving NCA ^{109}Cd in the aqueous phase. The amount of Ag became negligibly small after re-extraction in the same condition. The ionic liquid was recovered by washing it with 1 M HCl.

Kaustab Ghosh; Moumita Maiti; Susanta Lahiri

1.2.3.19 Synthesis and spectroscopic exploration of carboxylic acid derivatives of 6-hydroxy-1-keto-1,2,3,4-tetrahydrocarbazole: Hydrogen bond sensitive fluorescent probes

Two new fluorescent carboxylic acid derivatives having 6-hydroxy-1-keto-1,2,3,4-tetrahydrocarbazole moiety, 2-(1-oxo-2,3,4,9-tetrahydro-1H-carbazol-6-yloxy)acetic acid [OTHCA] and 2-(7-methoxy-1-oxo-2,3,4,9-tetrahydro-1H-carbazol-6-yloxy)acetic acid [MOTHCA] were synthesized by Japp-Klingemann reaction followed by Fischer indole cyclization. Extensive spectroscopic investigation has been carried out on the compounds in sixteen different aprotic and protic solvents as well as in binary solvent mixtures using absorption, steady-state and time-resolved fluorescence techniques. Fluorescence maxima of the compounds have shifted consistently to longer wavelength in mediums of higher polarity and hydrogen bonding ability. Dipole moment change of the molecules upon photoexcitation has been calculated using Lippert Mataga theory of solvatochromic shifts. Kamlet-Taft solvatochromic comparison method has been used to determine the dependence of spectral shifts upon empirical solvent parameters. Formation of intermolecular hydrogen bonding of both OTHCA and MOTHCA with protic solvents has been proved by comparing their spectral responses in toluene acetonitrile and toluene methanol solvent mixtures.

Amrit Krishna Mitra†; Sujay Ghosh†; Suchandra Chakraborty†; Samita Basu; Chandan Saha; et al

1.2.3.20 Sensing of hydrophobic cavity of serum albumin by an adenosine analogue: Fluorescence correlation and ensemble spectroscopic studies

Adenosine is a naturally occurring purine nucleoside that plays important role in various biochemical processes. We have studied the binding of TNP-Ado (trinitrophenylated-adenosine), a fluorescent analogue of adenosine (which itself is a weak fluorophore), with a model transport protein,

bovine serum albumin (BSA). The binding affinity was determined using Fluorescence correlation spectroscopy (FCS) and compared with its value obtained from macroscopic fluorescence spectroscopic studies. Fluorescence and circular dichroism (CD) spectroscopies were employed together with molecular docking study to locate the probable binding site of TNP-Ado on BSA and its effect on the conformation and stability of BSA. Fluorescence studies showed that TNP-Ado binds to BSA in 1:1 stoichiometry via an entropically favoured process. Induced CD spectra revealed that a chiro-optical switching of TNP-Ado occurs upon binding to BSA. Results on urea-induced denaturation of BSA and docking study suggested that the binding site for the ligand is in the hydrophobic subdomain IIA of BSA, consistent with the results of other measurements. This study establishes TNP-Ado as a sensor of hydrophobic regions in proteins like serum albumin, having the capability of detecting a minimum concentration of 140 ng/ml protein. FCS measurement of binding interaction of rhodamine-labeled TNP-Ado (RTNP-Ado) with BSA yielded an association constant of $K\text{-FCS} = (1.03 \pm 0.06) \times 10^4 \text{ M}^{-1}$. The association constants ($K\text{-a}$) obtained for binding of BSA with rhodamine-free (i.e. TNP-Ado) and rhodamine-labeled (RTNP-Ado) ligands, obtained using the ensemble spectroscopic technique, were $(2.3 \pm 0.06) \times 10^5 \text{ M}^{-1}$ and $(3.4 \pm 0.03) \times 10^4 \text{ M}^{-1}$, respectively. The difference between the values of $K\text{-a}$ for the free and labeled ligands suggests that fluorescent labeling of small molecules perceptibly interferes with the binding process. On the other hand, the difference in $K\text{-a}$ obtained by FCS and ensemble techniques is due to the fact that while the former measures the change in the diffusion constant (i.e. size) of RTNP-Ado upon binding to BSA, the latter focuses on the change of tryptophan emission properties of BSA due to the presence of bound RTNP-Ado.

Moupriya Nag; Kallol Bera; Sandipan Chakraborty†; Soumen Basak

1.2.3.21 Conducting polymer based manganese dioxide nanocomposite as supercapacitor

Poly 3,4-ethylenedioxythiophene (PEDOT)- and polyaniline (PANI) nanocomposites were synthesized based on manganese dioxide in the form of Nanorod: Suitability of these composites was studied extensively as an electrode material for symmetric supercapacitor in a widened operating voltage window of 1.2 V. Role of manganese dioxide during reverse microemulsion polymerization in n-hexane medium for PEDOT and aqueous dispersion polymerization for PANI, have been accounted through X-ray photoelectron spectroscopy (XPS). Structural morphology as well as thermal characterization was carried out using XRD, SEM, TEM, IR and TGA. Charge storage mechanism in these nanocomposites have been investigated through cyclic voltammetry (CV) at different scan rates (2-20 mV/s), where intercalation of metal ion during reduction and de-intercalation upon oxidation predominate over surface adsorption and desorption of metal ions into electrode material. Higher specific capacitance for PEDOT-MnO₂ (315 F/g) and PANI-MnO₂ (221 F/g) are observed in comparison with its constituent MnO₂ (158 F/g) where the internal pore volume plays a significant role over the total surface area. AC impedance measurement in the frequency range 10 kHz to 10 mHz with potential amplitude of 5 mV were carried out to ascertain the pseudocapacitance (C-Fs) arising from the redox reactions over the electrical double layer capacitance (C-DL) in the composite materials.

Pintu Sen†; Amitabha De; Ankan Dutta Chowdhury...Nidhi Agnihotri; M Mukherjee

1.2.3.22 Production and separation of ^{111}In : an important radionuclide in life sciences: a mini review

^{111}In is amongst the frequently used radionuclides in diagnostic nuclear medicine. Therefore its production and subsequent separation chemistry have been widely investigated since late 40s. ^{111}In is commonly produced in proton or α -particle induced reactions on cadmium or silver targets. However, in recent past, various heavy ion (^7Li , ^{11}B , ^{12}C etc.) activation routes have been proposed for its production. In this mini review, we have tried to portray the production routes of ^{111}In and chemical separation methodologies reported so far in the literature in a concise form. A critical analysis presented in this review will be helpful to select suitable nuclear reaction and radiochemical method to produce high purity ^{111}In for applications.

Susanta Lahiri; Moumita Maiti; Kaustab Ghosh

1.2.3.23 Thick target neutron yield from 145 MeV $^{19}\text{F}+^{27}\text{Al}$ system

The double differential neutron energy distribution has been measured for the $^{19}\text{F}+^{27}\text{Al}$ system at 145 MeV projectile energy. The time of flight technique was used to measure the energy while pulse shape discrimination has been used to separate the neutrons from photons. The results are compared with the statistical nuclear reaction model codes PACE and EMPIRE. The PACE code appears to predict the slope and the end point energy of the experimental spectra fairly well but over predicts the values. The slope obtained from the EMPIRE calculations appears to be harder while the values being closer to the experimental results. The yield from the Hauser-Feshbach based compound nucleus model calculations agree reasonably well with the experimental results at the backward angles but not in the forward directions. The energy integrated angular distribution from 145 MeV projectiles show an enhanced emission in the forward angles compared to the similar results from 110 MeV projectiles. This analysis suggests some contribution from the pre-equilibrium emissions from the system at the higher projectile energy.

C Sunil†; T Bandyopadhyay†; M Nandy; et al

1.2.3.24 Interaction between hemoglobin A and merocyanine 540: A spectroscopic investigation supported by docking

Merocyanine 540 (MC 540) is a clinically important dye and a potent sensitizer of lipid peroxidation in natural cell membrane like erythrocyte ghost. We have studied the binding interaction between this antileukemic drug and Hemoglobin A (HbA) using UV-visible absorption, steady-state, time-resolved fluorescence and circular dichroism spectroscopy. The changes in absorption spectra of HbA in presence of MC 540 suggest a ground state complex formation between them. Thermodynamic analyses of quenching of HbA with MC 540 at different temperatures imply that the interaction is spontaneous and H-bonding as well as van der Waals interactions play the key role in this particular interaction. The binding constant and stoichiometry of the complex are $2.89 \times 10^4 \text{ M}^{-1}$ and 1.0 respectively at 298 K. Circular dichroism and synchronous fluorescence spectra suggest a structural change in HbA in presence of MC 540. Theoretical docking study helps to find out the plausible binding site of MC 540 inside HbA.

Mousumi Banerjee; Abhijit Chakrabarti; Samita Basu

1.2.3.25 Protein interactions of Merocyanine 540: Spectroscopic and crystallographic studies with lysozyme as a model protein

Spectroscopic and crystallographic studies reveal that Merocyanine 540 (MC 540), a well-known therapeutically important anionic cyanine dye, interacts with hen egg white lysozyme in ground state. The formation of the complex is validated by two isosbestic points in absorption spectra of lysozyme with varied concentration of MC 540 and appearance of an isodichroic point in induced CD spectra of MC 540 with lysozyme. The blue shift of fluorescence maximum of lysozyme in presence of MC 540 shows hydrophobic effect on Trp due to complex formation probably through cooperative binding. Above 1:3 M stoichiometric ratio (lysozyme:MC 540) an additional fluorescence hump arises because of structural changes in protein, where MC 540 acts as self-denaturant, inducing non-linearity in Stern-Volmer plot. The van't Hoff isotherms with negative changes in enthalpy at lower concentration and positive changes in entropy for entire concentration range of MC 540 depict the binding forces as hydrogen bonding/van der Waal's and ionic/hydrophobic respectively. Finally X-ray crystallographic structure of the complex shows that MC 540 adopts two conformations, cis and trans, while it binds to lysozyme. Benzoxole moiety of MC 540 interacts with Trp123 through pi-stacking and SO₃²⁻ group is stabilized by ionic interaction/H-bonding with Arg125 of lysozyme.

Piyali Mitra; Mousumi Banerjee; Sampa Biswas; Samita Basu

1.2.4 Computational Science

1.2.4.1 Energy Hyperspace for Stacking Interaction in AU/AU Dinucleotide Step: Dispersion-Corrected Density Functional Theory Study

Double helical structures of DNA and RNA are mostly determined by base pair stacking interactions, which give them the base sequence-directed features, such as small roll values for the purine-pyrimidine steps. Earlier attempts to characterize stacking interactions were mostly restricted to calculations on fiber diffraction geometries or optimized structure using ab initio calculations lacking variation in geometry to comment on rather unusual large roll values observed in AU/AU base pair step in crystal structures of RNA double helices. We have generated stacking energy hyperspace by modeling geometries with variations along the important degrees of freedom, roll, and slide, which were chosen via statistical analysis as maximally sequence dependent. Corresponding energy contours were constructed by several quantum chemical methods including dispersion corrections. This analysis established the most suitable methods for stacked base pair systems despite the limitation imparted by number of atoms in a base pair step to employ very high level of theory. All the methods predict negative roll value and near-zero slide to be most favorable for the purine-pyrimidine steps, in agreement with Calladine's steric clash based rule. Successive base pairs in RNA are always linked by sugar-phosphate backbone with C3'-endo sugars and this demands C1-C1 distance of about 5.4 angstrom along the chains. Consideration of an energy penalty term for deviation of C1-C1 distance from the mean value, to the recent DFT-D functionals, specifically B97X-D appears to predict reliable energy contour for AU/AU step. Such distance-based penalty improves energy contours for the other purine-pyrimidine sequences also.

Sanchita Mukherjee; Senthilkumar Kailasam†; Manju Bansal†; Dhananjay Bhattacharyya

1.2.4.2 RNA structure and dynamics: A base pairing perspective

RNA is now known to possess various structural, regulatory and enzymatic functions for survival of cellular organisms. Functional RNA structures are generally created by three-dimensional organization of small structural motifs, formed by base pairing between self-complementary sequences from different parts of the RNA chain. In addition to the canonical Watson Crick or wobble base pairs, several non-canonical base pairs are found to be crucial to the structural organization of RNA molecules. They appear within different structural motifs and are found to stabilize the molecule through long-range intra-molecular interactions between basic structural motifs like double helices and loops. These base pairs also impart functional variation to the minor groove of A-form RNA helices, thus forming anchoring site for metabolites and ligands. Non-canonical base pairs are formed by edge-to-edge hydrogen bonding interactions between the bases. A large number of theoretical studies have been done to detect and analyze these non-canonical base pairs within crystal or NMR derived structures of different functional RNA. Theoretical studies of these isolated base pairs using ab initio quantum chemical methods as well as molecular dynamics simulations of larger fragments have also established that many of these non-canonical base pairs are as stable as the canonical Watson Crick base pairs. This review focuses on the various structural aspects of non-canonical base pairs in the organization of RNA molecules and the possible applications of these base pairs in predicting RNA structures with more accuracy.

Sukanya Halder; Dhananjay Bhattacharyya

1.2.4.3 Influence of divalent magnesium ion on DNA: molecular dynamics simulation studies

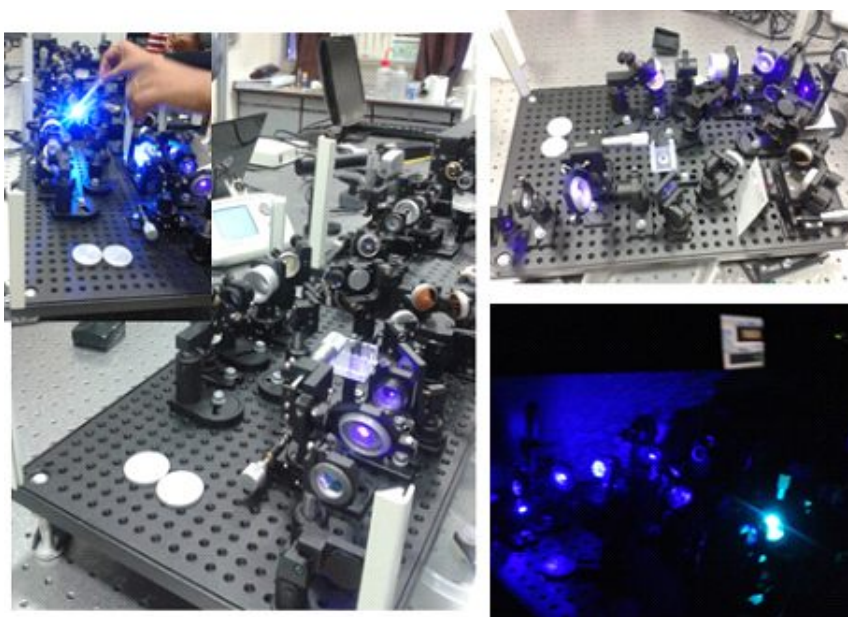
A large amount of experimental evidence is available on the effect of magnesium ions on the structure and stability of DNA double helix. Less is known, however, on how these ions affect the stability and dynamics of the molecule. The static time average pictures from X-ray structures or the quantum chemical energy minimized structures lack understanding of the dynamic DNA-ion interaction. The present work addresses these questions by molecular dynamics simulation studies on two DNA duplexes and their interaction with magnesium ions. Results show typical B-DNA character with occasional excursions to deviated states. We detected expected stability of the duplexes in terms of backbone conformations and base pair parameter by the CHARMM-27 force field. Ion environment analysis shows that Mg^{2+} retains the coordination sphere throughout the simulation with a preference for major groove over minor. An extensive analysis of the influence of the Mg^{2+} ion shows no evidence of the popular predictions of groove width narrowing by dipositive metal ion. The major groove atoms show higher occupancy and residence time compared to minor groove for magnesium, where no such distinction is found for the charge neutralizing Na^+ ions. The determining factor of Mg^{2+} ion's choice in DNA binding site evolves as the steric hindrance faced by the bulky hexahydrated cation where wider major groove gets the preference. We have shown that in case of binding of Mg^{2+} to DNA non electrostatic contributions play a major role. An animated Interactive 3D Complement (I3DC) is available in Proteopedia at <http://proteopedia.org/w/Journal:JBSD:5>.

Sanchita Mukherjee; Dhananjay Bhattacharyya

1.3 Developmental Work

1.3.0.4 Femtosecond Fluorescence Up-conversion Spectrometer

The MAI TAI HP Laser and Femtosecond optically gated fluorescence kinetic measurement system FOG 100-DX were installed at Chemical Sciences Division to measure the lifetime of uorescent transients in February 2014. The sample can be excited from 360-420 nm by second harmonic of



mode-locked Ti-sapphire laser pumped by a 10 W CW Nd:YVO₄ Laser using nonlinear BBO crystal. The uorescence is up-converted in another nonlinear BBO crystal using the fundamental beam as a gate pulse. Maximum delay between excitation and gate pulses is 2.0 ns. The up-converted light is dispersed in a double monochromator and detected by photon counting (maximum 10⁷ counts/sec) electronics.

Samita Basu

1.4 Publications

1.4.1 Publications in Books/Monographs & Edited Volumes

MK Sarangi and S Basu, Distance Dependence of Magnetic Field Effect Inside the Confined Heterogeneous Environment: A Case Study with Acridine and N, N-Dimethyl Aniline Inside AOT Reverse Micelles, in Computational and Experimental Chemistry: Developments and applications; Eds: Tanmoy Chakraborty, Michael J Bucknum, Eduardo A Castro (Apple Academic Press and CRC Press Taylor & Francis Group, Toronto & New Jersey 2014, p127)

Sneh Lata Goyal; PK Saran; PK Sarkar; Maitreyee Nandy, Activation cross sections of ⁷⁴Ga and ⁷¹Zn formed in neutron induced reactions on ⁷⁴Ge, (AIP CONF PROC **1524** 2013, p120)

1.4.2 Publications in Journal

Biophysics and Structural Genomics

D Srivastava; O Chakrabarti, Mahogunin-mediated α -tubulin ubiquitination via noncanonical K6 linkage regulates microtubule stability and mitotic spindle orientation, *Cell Death & Disease* **5** (2014)Art No: e1064

Sutapa Ray; Mickael Blaise; Bappaditya Roy; Saptaparni Ghosh; et al, Fusion with Anticodon Binding Domain of GluRS is Not Sufficient to Alter the Substrate Specificity of a Chimeric Glu-Q-RS, *Protein Journal* **33** (2014)48

Arunabha Chakrabarti; Kasturi Roy; Debashis Mukhopadhyay, Differential Expression of Neuroblastoma Cellular Proteome due to AICD Overexpression, *Journal of Alzheimers Disease* **38** (2014) 845

Kasturi Roy; Mithu Raychaudhuri; Oishee Chakrabarti; Debashis Mukhopadhyay, Growth Factor Receptor-Bound Protein 2 Promotes Autophagic Removal of Amyloid- β Protein Precursor Intracellular Domain Overload in Neuronal Cells, *Journal of Alzheimers Disease* **38** (2014)881

Anita Roy; Srijan Haldar; Nandini Pal Basak; Subrata Banerjee, Molecular cross talk between Notch1, Shh and Akt pathways during erythroid differentiation of K 562 and HEL cell lines, *Experimental Cell Research* **320** (2014) 69

Avinanda Banerjee; Vikram Rathee†; Rema Krishnaswamy†; Pritha Bhattacharjee; Pulak Ray; Ajay K Sood†; Kaushik Sengupta, Viscoelastic Behavior of Human Lamin A Proteins in the Context of Dilate Cardiomyopathy, *PLOS One* **8** (2014)Art No: e83410

Abhijit Chakrabarti; Dipankar Bhattacharya; Sanghamitra Deb; Madhumita Chakraborty, Differential Thermal Stability and Oxidative Vulnerability of the Hemoglobin Variants, HbA₂ and HbE, *PLOS One* **8** (2013)Art No: UNSP e81820

Avik Basu; Sutapa Saha; Shilpita Karmakar; Sudipa Chakravarty; Debasis Banerjee; Bisnu Prasad Dash; Abhijit Chakrabarti, 2D DIGE based proteomics study of erythrocyte cytosol in sickle cell disease: Altered proteostasis and oxidative stress, *Proteomics* **13** (2013) 3233

Shounak Baksi; Nihar R Jana†; Nitai Pada Bhattacharyya; Debashis Mukhopadhyay, Grb2 Is Regulated by Foxd3 and Has Roles in Preventing Accumulation and Aggregation of Mutant Huntingtin, *PLOS One* **8** (2013)Art No: e76792

Anita Roy; Lakshmishri Lahiry; Debasis Banerjee†; Malay Ghosh†, Subrata Banerjee, Increased Cytoplasmic Localization of p27(kip1) and Its Modulation of RhoA Activity during Progression of Chronic Myeloid Leukemia, *PLOS One* **8** (2013)Art No: e76527

Puspendu K Das; Anindita Das; Abhijit Chakrabarti, Metal nanoparticles as better protein-aggregation prevention agents than chaperones, *Abstracts of Papers of the American Chemical Society* **246** (2013) Meeting Abstract: 144-COLL

Aditi Sengupta Banerjee; Anindita Deb Pal; Subrata Banerjee, Epstein Barr virus-encoded small non-coding RNAs induce cancer cell chemoresistance and migration, *Virology* **443** (2013) 294

Saptaparni Ghosh; Suman Kalyan Pradhan; Anirban Kar†; S Chowdhury, D Dasgupta, Molecular basis of recognition of quadruplexes human telomere and c-myc promoter by the putative anticancer agent sanguinarine, *Biochimica et Biophysica Acta-General Subjects* **1830** (2013)4189

Amrita Banerjee; Jasdeep Singh; Dipak Dasgupta, Fluorescence Spectroscopic and Calorimetry Based Approaches to Characterize the Mode of Interaction of Small Molecules with DNA, *Journal of Fluorescence* **23** (2013) 745

Saptaparni Ghosh; Anirban Kar†; Shantanu Chowdhury†; Dipak Dasgupta, Ellipticine Binds to a Human Telomere Sequence: An Additional Mode of Action as a Putative Anticancer Agent?, *Biochemistry* **52** (2013)4127

Pritha Bhattacharjee; Avinanda Banerjee; Amrita Banerjee; Dipak Dasgupta; Kaushik Sengupta, Structural Alterations of Lamin A Protein in Dilated Cardiomyopathy, *Biochemistry* **52** (2013)4229

Bidisha Sengupta; Biswa Pathik Pahari; Laura Blackmon; Pradeep K Sengupta, Prospect of Bioflavonoid Fisetin as a Quadruplex DNA Ligand: A Biophysical Approach, *PLOS One* **8** (2013)Art No: e65383

Sudip Chaudhuri; Bidisha Sengupta; Jasmine Taylor; Biswa Pathik Pahari; Pradeep K Sengupta, Interactions of Dietary Flavonoids with Proteins: Insights from Fluorescence Spectroscopy and Other Related Biophysical Studies, *Current Drug Metabolism* **14** (2013) 491

Malay Patra; Madhurima Mitra, Abhijit Chakrabarti; Chaitali Mukhopadhyay, Binding of polarity sensitive, hydrophobic ligands to erythroid and non-erythroid spectrin: Fluorescence and molecular modeling studies, *J Biomol Struc Dyn* **32** (2014)

Abhijit Chakrabarti; Sumanta Basu; Bisnu Prasad Dash; Sudipa Chakravarty; Debashis Banerjee, Erythrocyte membrane asymmetry in Thalassemia and Sickle Cell Disease, *Proc Ind Ac Sci* **79** (2013) 127

Runu Chakravarty; Dipanwita Das; Neelakshi Sarkar...Isha Sengupta; Chandrima Das; et al, Role of TLR7 Agonist in Hepatitis B Infection: An In Vitro Study, *Journal of Clinical & Experimental Hepatology* **4** (2014) S20

A Chakrabarti; D Mukhopadhyay, Brain Senescence-Omics, *Journal of Proteins & Proteomics* **3** (2013) 15

A Chakrabarti; A Chatterjee; MB Sengupta; P Chattopadhyay; D Mukhopadhyay, Altered Levels of Amyloid Precursor Protein Intracellular Domain-interacting Proteins in Alzheimer Disease, *Alzheimer Disease and Associated Disorders* 2013

Nandini Pal Basak; Anita Roy; Subrata Banerjee, Alteration of mitochondrial proteome due to activation of Notch1 signaling pathway, *Journal of Biological Chemistry* **289** (2014) 7320

C & MB

Heini Ruhanen†; Daniel Hurley†; Ambarnil Ghosh; et al, Potential of known and short prokaryotic protein motifs as a basis for novel peptide-based antibacterial therapeutics: a computational survey, *Frontiers in Microbiology* **5** (2014)

Srijit Das; Nitai Pada Bhattacharyya, Transcription Regulation of HYPK by Heat Shock Factor 1, *PLOS One* **9** (2014) Art No: e85552

Seema Nath; Ramanuj Banerjee; Udayaditya Sen, A Novel 8-nm Protein Cage Formed by *Vibrio cholerae* Acylphosphatase, *Journal of Molecular Biology* **426** (2014)36

Shyamaprosad Goswami†; Abhishek Manna†, Sima Paul†...Anup Kumar Maity; Partha Saha, A turn on ES IPT probe for rapid and ratiometric fluorogenic detection of homocysteine and cysteine in water with live cell-imaging, *Tetrahedron Letters* **55** (2014) 490

Shyamaprosad Goswami†; Sibaprasad Maity†; Annada C Maity†; Anup Kumar Maity...Partha Saha, A FRET-based rhodamine-benzimidazole conjugate as a Cu^{2+} -selective colorimetric and ratiometric fluorescence probe that functions as a cytoplasm marker, *RSC Advances* **4** (2014)6300

Shyamaprosad Goswami†; Avijit Kumar Das†; Anup Kumar Maity...Partha Saha; et al, Visual and near IR (NIR) fluorescence detection of Cr^{3+} in aqueous media via spirobenzopyran ring opening with application in logic gate and bio-imaging, *DALTON Transactions* **43** (2014)231

Alakananda Goswami; Rahul Banerjee; Sanghamitra Raha, Drought resistance in rice seedlings conferred by seed priming, *Protoplasma* **250** (2013) 1115

Maitree Biswas†; Sanjay Dey†; Susmita Khamrui; Udayaditya Sen; et al, Conformational Barrier of CheY3 and Inability of CheY4 to Bind FliM Control the Flagellar Motor Action in *Vibrio cholerae*, *PLOS One* **8** (2013) Art No: e73923

Amitabh Ranjan†; Savita Sharma†; Ramanuj Banerjee; Udayaditya Sen; et al, Structural and mechanistic basis of anti-termination of Rho-dependent transcription termination by bacteriophage P4 capsid protein Psi, *Nucleic Acids Research* **41** (2013) 6839

Sruti Dutta; Jiban Kanti Dattagupta; Sampa Biswas, Enhancement of Proteolytic Activity of a Thermostable Papain-Like Protease by Structure-Based Rational Design, *PLOS One* **8** (2013) Art No: e62619

A Ranjan; R Banerjee; B Pani; U Sen; R Sen, The moonlighting function of bacteriophage P4 capsid protein, Psi, as a transcription antiterminator, *Bacteriophage* **3** (2013) e25657

Chemical Sciences

Sreeja Chakraborty; Madhuparna Bose†; Munna Sarkar, Spectroscopic studies of the binding of Cu(II) complexes of oxicam NSAIDs to alternating G-C and homopolymeric G-C sequences, *Spectrochimica Acta* **A122** (2014)690

Kallol Bera; Anand Kant Das†; Moupriya Nag; et al, Development of a Rhodamine-Rhodanine-Based Fluorescent Mercury Sensor and Its Use to Monitor Real-Time Uptake and Distribution of Inorganic Mercury in Live Zebrafish Larvae, *Analytical Chemistry* **86** (2014)2740

Swadesh Mandal, Synthesis of radioactive gold nanoparticle in surfactant medium, *Journal of Radioanalytical and Nuclear Chemistry* **299** (2014)1209

Swadesh Mandal; Ajoy Mandal, Separation of no-carrier-added $^{99m}\text{TcO}_4^-$ Tc from ^{99}Mo - ^{99m}Tc equilibrium mixture by PEG based aqueous biphasic separation technique using sodium/potassium salts of citric and tartaric acid, *Journal of Radioanalytical and Nuclear Chemistry* **299** (2014)1225

Adity Bose†; Samita Basu, Effect of phosphate group in switching off electron transfer in different media, *Journal of Molecular Liquids* **191** (2014) 92

Debabrata Nandi; Susmita Nandi; Prasun K Pal...Amitabha De; et al, Polypyrrole decorated graphene nanostructure: Fabrication, depiction and anomalous dimensional crossover in electronic conduction, *Applied Surface Science* **293** (2014)90

Ankan Dutta Chowdhury; Nidhi Agnihotri; Pintu Sen†; et al, Conducting CoMn_2O_4 -PEDOT nanocomposites as catalyst in oxygen reduction reaction, *Electrochimica Acta* **118** (2014)81

Binita Dutta; Susanta Lahiri; BS Tomar†, Separation of no-carrier-added rhenium from bulk tantalum by the sodium malonate-PEG aqueous biphasic system, *Applied Radiation and Isotopes* **84** (2014) 8

Sandipan Chakraborty†; Soumalee Basu; Soumen Basak, Effect of β -cyclodextrin on the molecular properties of myricetin upon nano-encapsulation: Insight from optical spectroscopy and quantum chemical studies, *Carbohydrate Polymers* **99** (2014)116

Tanmay Ghosh; Biswarup Satpati; Dulal Senapati, Characterization of bimetallic core-shell nanorings synthesized via ascorbic acid-controlled galvanic displacement followed by epitaxial growth, *Journal of Materials Chemistry* **C2** (2014)2439

Sujay Ghosh; Subhanip Biswas; Mousumi Mondal; Samita Basu, Photophysical properties of 1,8-naphthalic anhydride in aprotic solvents: An electron acceptor in excited state, *Journal of Luminescence* **145** (2014) 410

Kallol Bera; Barun Kumar Maity; Moupriya Nag; et al, Photophysical effects of nitric oxide and S-nitrosocysteine on acridine orange: use as sequential sensing platform for NO, cysteine, cysteine-NO and Hg^{2+} under physiological conditions, *Analytical Methods* **6** (2014) 347

Debabrata Nandi†; Arup K Ghosh†; Amitabha De; et al, Fabrication, nanostructure evaluation, 3D electrical transport and electrochemical capacitance of PEDOT-Ti(IV)-doped iron(III) oxide nanocomposite, *Journal of Materials Science* **49** (2014)776

Ankan Dutta Chowdhury; Rupali Gangopadhyay; Amitabha De, Highly sensitive electrochemical biosensor for glucose, DNA and protein using gold-polyaniline nanocomposites as a common matrix, *Sensors and Actuators* **B190** (2014)348

Montu K Hazra; Joseph S Francisco†; Amitabha Sinha†, Gas Phase Hydrolysis of Formaldehyde To Form Methanediol: Impact of Formic Acid Catalysis, *Journal of Physical Chemistry* **A117** (2013)11704

Julian M Rozenberg†; Paramita Bhattacharya; Raghunath Chatterjee†; et al, Combinatorial Recruitment of CREB, C/EBP β and c-Jun Determines Activation of Promoters upon Keratinocyte Differentiation, *PLOS One* **8** (2013)Art No: e78179

Binita Dutta; Susanta Lahiri; BS Tomar†, Separation of No-Carrier-Added Rhenium from Bulk Tantalum By Precipitation Technique, *Separation Science and Technology* **48** (2013) 2468

B Sarkar†; A Manikandan†; M Nandy; et al, A mathematical approach to beam matching, *British Journal of Radiology* **86** (2013)Art No: 20130238

Sujay Ghosh; Amrit Krishna Mitra†; Chandan Saha†; Samit Basu, Tuning the Solution Phase Photophysics of Two De Novo Designed Hydrogen Bond Sensitive 9-methyl-2,3,4,9-tetrahydro-1H-carbazol-1-one Derivatives, *Journal of Fluorescence* **23** (2013) 1179

Kaustab Ghosh; Moumita Maiti; Susanta Lahiri, Separation of no-carrier-added ^{109}Cd from natural silver target using RTIL 1-butyl-3-methylimidazolium hexafluorophosphate, *Journal of Radioanalytical and Nuclear Chemistry* **298** (2013)1049

Moupriya Nag; Kallol Bera; Sandipan Chakraborty†; Soumen Basak, Sensing of hydrophobic cavity of serum albumin by an adenosine analogue: Fluorescence correlation and ensemble spectroscopic studies, *Journal of Photochemistry and Photobiology* **B127** (2013)202

Pintu Sen†; Amitabha De; Ankan Dutta Chowdhury...Nidhi Agnihotri; M Mukherjee, Conducting polymer based manganese dioxide nanocomposite as supercapacitor, *Electrochimica Acta***108** (2013) 265

Susanta Lahiri; Moumita Maiti; Kaustab Ghosh, Production and separation of ^{111}In : an important radionuclide in life sciences: a mini review, *Journal of Radioanalytical and Nuclear Chemistry* **297** (2013)309

C Sunil†; T Bandyopadhyay†; M Nandy; et al, Thick target neutron yield from 145 MeV $^{19}\text{F}+^{27}\text{Al}$ system, *Nuclear Instruments & Methods in Physics Research* **A721** (2013)21

Mousumi Banerjee; Abhijit Chakrabarti; Samita Basu, Interaction between hemoglobin A and merocyanine 540: A spectroscopic investigation supported by docking, *Dyes and Pigments* **97** (2013) 446

Banabithi Koley Seth; Aurkie Ray; Arpita Saha; Partha Saha; Samita Basu, Potency of photoinduced electron transfer and antioxidant efficacy of pyrrole and pyridine based Cu(II)-Schiff complexes while binding with CT-DNA, *J Photochem Photobiol* **B132** (2014) 72

Piyali Mitra; Mousumi Banerjee; Sampa Biswas; Samita Basu, Protein Interaction of Merocyanine 540: Spectroscopic and Crystallographic Studies with Lysozyme as a Model Protein, *J Photochem*

Photobiol **B121** (2013) 46

Sujay Ghosh; Amrit Krishna Mitra†; Chandan Saha†; Samita Basu, Tuning the solution phase photophysics of two de novo designed hydrogen bond sensitive 9-methyl-2,3,4,9-tetrahydro-1H-carbazol-1-one derivatives, *Journal of Fluorescence* **23** (2013) 1179

Amrit Krishna Mitra†; Sujay Ghosh; Suchandra Chakraborty†; Samita Basu; Chandan Saha†; et al, Synthesis and spectroscopic exploration of carboxylic acid derivatives of 6-hydroxy-1-keto-1,2,3,4-tetrahydrocarbazole: Hydrogen bond sensitive fluorescent probes, *Journal of Luminescence* **143** (2013) 693

Munmun Bardhan; Biswarup Satpati; Tanmay Ghosh; Dulal Senapati, Synergistically controlled nano-templated growth of tunable gold bud-to-blossom nanostructures: a pragmatic growth mechanism, *Journal of Materials Chemistry* **C2** (2014) 3795

Computational Science

Sanchita Mukherjee; Senthilkumar Kailasam†; Manju Bansal†; Dhananjay Bhattacharyya, Energy Hyperspace for Stacking Interaction in AU/AU Dinucleotide Step: Dispersion-Corrected Density Functional Theory Study, *Biopolymers* **101** (2014) 107

Sukanya Halder; Dhananjay Bhattacharyya, RNA structure and dynamics: A base pairing perspective, *Progress in Biophysics & Molecular Biology* **113** (2013) 264

Sanchita Mukherjee; Dhananjay Bhattacharyya, Influence of divalent magnesium ion on DNA: molecular dynamics simulation studies, *Journal of Biomolecular Structure & Dynamics* **31** (2013) 896

1.5 Ph D Awarded

Mousumi Banerjee [Samita Basu and Abhijit Chakrabarti], Spectroscopic studies of interaction of some biologically important small molecules with proteins, Jadavpur University, Mar 7, 2014

Arunabha Chakrabarti [Debashis Mukhopadhyay], Proteomic Characterization of the AICD Interactome, University of Calcutta, Feb 2014

Sudip Majumdar [Udayaditya Sen], Deciphering the Role of the Protein Scaffold of Winged Bean Chymotrypsin Inhibitor (WCI) in the Light of its Inhibitory Power and Stability: Structural and Mutational Studies, University of Calcutta, May 2013

Samir Das [Udayaditya Sen and Debasish Mukhopadhyay], Atomic Resolution Studies on Interaction of Grb2 domains with protein motifs implicated in Alzheimers Disease, University of Calcutta, Sept 2013

Sukanya Halder [Dhananjay Bhattacharyya], Structural Study of Ribonucleic Acids Using The-

oretical Approaches, University of Calcutta, Feb 2014

Swati Panigrahi [Dhananjay Bhattacharyya], Role of Hydrogen Bonding Interactions in Biologically Important Macromolecules, Homi Bhabha National Institute, Dec 2013

Anup Kumar Maity [Partha Saha], Characterization of substrates of an S-phase cell cycle kinase of *Leishmania donovani* with emphasis on a Histone Acetyl Transferase, HBNI, Aug 2013

1.6 Seminars/Lectures given in Conference/Symposium/Schools

Samita Basu

- i. Magnetic Field Effect to identify distance-dependent phenomenon: photoinduced electron transfer between DNA and metal complexes, The Spin Chemistry Meeting 2013 (SCM 2013), Bad Hofgastein, Austria, Apr 22-16, 2013
- ii. Light Amplification by Stimulated Emission of Radiation (LASER) & Its Application in Chemistry, DST-JBNSTS INSPIRE Science Camp, JBNSTS, Kolkata, May 17, 2013
- iii. Some Fundamentals of Photophysics and Photochemistry, Academic Staff College Refresher Course in Chemistry: Education and Research, University of Calcutta, Aug 19, 2013
- iv. BASIC Principle of LASER, Light Amplification by Stimulated Emission of Radiation, DST-JBNSTS INSPIRE SCIENCE CAMP, JBNSTS, Kolkata, Sep 5, 2013
- v. Differentiation of simultaneous photoinduced interactions by steady-state and time-resolved absorption and fluorescence supported by magnetic field effect, National Level Seminar on Recent Developments in Research in Chemistry, Department of Chemistry, West Bengal State University, Barasat, Kolkata 700 126, Nov 23, 2013
- vi. Magnetic Field Effect on Photoinduced Interactions, National Conference on Recent Trends in Chemical Sciences (RTRCS -2014), Manipal University, Jaipur, Feb 21-22, 2014
- vii. How an application of low magnetic field helps to identify photoinduced electron transfer?, International Conference on Light in Chemistry, Materials and Biology (LCMB-2014), IIT, Kharagpur Feb 24-25, 2014
- viii. Magnetic field effect: an assessor of intermolecular separation distance in photoinduced interactions, National Symposium on Recent Trends in Sustainable Chemistry: Frontiers and Challenges (SCFC-2014), North-Eastern Hill University, Shillong, Feb 27-Mar 01, 2014

Udayaditya Sen

- i. 'Knot' and 'Cage': Two New Dimensions in Protein Structures, 42nd National Seminar On Crystallography (NSC42), Delhi, Dec 2013
- ii. Knot and Cage in proteins: As seen in Bacteriophage P4 Psu and *Vibrio cholerae* Acp, 82nd annual meeting of Society of Biological Chemists (India) SBC(I)-82, Hyderabad, Dec 2-5, 2013
- iii. Fructokinase and Ribokinase: Role of Conserved Patches, Structural Flexibility and Divalent Cation During phosphorylation, IUBMB 10th International Symposium, Kolkata, Jan 20-24, 2014
- iv. Protein Knot and Cage: As revealed in the crystal structures of Rho-dependent transcription terminator inhibitor Psu and *Vibrio cholerae* Acylphosphatase ACP, Indian biophysical Society (IBS), Kolkata, Feb 7-11, 2014

Debashis Mukhopadhyay

- i. Proteomics, UGC sponsored workshop organized by the Dept of Biophysics and Molecular Biology, University of Calcutta, Aug 12, 2013
- ii. Talk in "SBC seminar series" organized by the Society of Biological Chemists (I), Kolkata chapter in Bose Institute, Kolkata, Jul 4, 2013
- iii. Talk in IUBMB 10th International Symposium on Biochemical Role of Cell Surface Macromolecules would be organized by Saha Institute of Nuclear Physics, Jan 20-24, 2014
- iv. Talk and acted as a resource person in the workshop on Learning by Doing : Science Mysteries Demystified, Jan 8-9, 2014, in Ramananda College, Bishnupur
- v. Talk in the National Conference on Recent Trends in Protein Structure Biology-2013 (NCRTPSB-2013), Dec 16-18, 2013, Jamia Millia Islamia (Central University), New Delhi, India
- vi. Molecular aspects of Alzheimers disease, NeuroUpdate-2013 meeting, IICB, Kolkata, Nov 29-30, 2013
- vii. Talk in the workshop on Computational Proteomics, Organized by Bioinformatics Centre, Bose Institute, Kolkata, Mar 3-4, 2014
- viii. Talk in the Dept of Microbiology, Moulana Azad College, Kolkata, Aug 17, 2013

Chandrima Das

Bromodomain: An epigenomic reader with versatile function, 17th Transcription Assembly Meeting, JNCASR, Bangalore, Mar 17-18, 2014

Abhijit Chakrabarti

- i. CD19+ cell proteome and interactome in B-ALL, in Indo-French Seminar/Workshop - Recent trends in Proteomics, Angsana Oasis Spa & Resort, Northwest Country, Bangalore, Indo-French Centre for the Promotion of Advanced Research/Centre, Apr 8, 2013
- ii. Proteins, in DST Sponsored INSPIRE camp on Basic Science for high school students organized by Raj Kumar Goel Engineering College, Gaziabad, May 15, 2013
- iii. Lipid-protein cross-talk in red blood cells, in the International Conference on Electron Microscopy and XXXIV Annual Meeting of the Electron Microscopy Society of India (EMSI), Jul 5, 2013, Hyatt Regency, Kolkata
- iv. Protein, Proteins, Proteomics in DST Sponsored INSPIRE camp on Basic Science for high school students organized by JBNSTS, Kolkata, Jul 18, 2013
- v. Erythrocytes, Hematological Disease, Proteomics & Chemical Biology in 20th meeting of TReNDYS in Biochemistry, University of Hyderabad, Nov 22, 2013
- vi. Proteins, in DST Sponsored INSPIRE camp on Basic Science for high school students organized by National Institute of Technology Karnataka (NITK), Surathkal, Dec 16, 2013
- vii. Proteomics study of hemoglobinopathy, in 28th ISMAS (Indian Society for Mass Spectrometry) Symposium cum Workshop on Mass Spectrometry (28th ISMAS-WS-2014) at Timber Trail Heights, Parwanoo, Himachal Pradesh, Mar 10, 2014

Maitreyee Nandy

Quality Assurance of Concrete for Radiological Safety, Manipal Institute of Technology, Mani-

pal, Karnataka, Mar 7, 2014

Dipak Dasgupta

- i. DNA intercalators as dual binders in the context of transcription apparatus chromatin, Dipak Dasgupta & Chandrima Das, Seventeenth Transcription Assembly Meeting 2014, Jawaharlal Nehru Centre for Advanced Scientific Research, Bangalore, INDIA, Mar 17-18, 2014
- ii. Application of Fluorescence Spectroscopy by a Chemical Biologist, National Conference Photo-science: Contemporary Challenges and Future Perspectives, Jadavpur University, Kolkata, INDIA, Dec 12-14, 2013
- iii. Small molecule-chromatin Interaction, Biochemistry Department of Indian Institute of Science, Bangalore

IUBMB 10th International Symposium on Biochemical Role of Eukaryotic Cell Surface Macromolecules

A series of International Symposia on the Biochemical Role of Eukaryotic Cell Surface Macromolecules (ISCSM) are being organized since past 30 years in India, initiated by the pioneer Biochemist of India, Late Prof. Bimal K Bachhawat. We've organized the 10th ISCSM in Kolkata



during January 20-24, 2014. The symposium was attended by eminent glycobiologists and membrane biologists providing golden opportunities to young graduate students and faculty members to get exposure and interact with a galaxy of internationally reputed scientists in the area of cell

surface macromolecules and membrane biology. The meeting accommodated about 100 participants with about 40 of them coming from different parts of Europe, Japan & the United States of America. There were about 13 scientific sessions during four and half day long symposia including an ISN Symposium on Neurochemistry & Biology of Cell Surface Glycoconjugates and excluding two poster sessions and one session dedicated to short presentations by young Indian investigators. The proceeding of the symposium would be published in a peer reviewed journal of Springer named *Advanced Experimental Medicine & Biology* by the end of 2014.

1.7 Teaching elsewhere

Debashis Mukhopadhyay

- i. Proteomics; M Sc, Department of Biophysics, Molecular Biology and Genetics, University of Calcutta Proteomics/ Crystallography;
- ii. Proteomics; M Sc 3rd Semester of Biotechnology (GCGEB), CU
- iii. Proteomics; M Sc 3rd Semester of the Department of Genetics, CU
- iv. Proteomics; M Sc 3rd Semester of the Department of Microbiology, CU
- v. Proteomics; M Sc 3rd Semester of Neurosciences (SNPCN), CU
- vi. Proteomics; M Sc 3rd Semester of the Department of Biochemistry, CU
- vii. Molecular Phylogenetics; Integrated M Sc, Departments of Biotechnology, St Xaviers College, Kolkata
- viii. Molecular Modeling; M.Sc (Pharma), NIPER, Kolkata

Chandrima Das

Histone chaperones, M Sc, Biochemistry Department, Calcutta University of Calcutta

Samita Basu

- i. M Sc (Inorganic Chemistry special), Calcutta University on Spectroscopy, Jan-Mar, 2014
- ii. M Sc (Physical Chemistry special), Midnapore College, Vidyasagar University, West Bengal, on Photochemistry, Mar 2014

Munna Sarkar

- i. New functions for painkillers: membrane fusion, UGC Academic Staff College Jadavpur University, Refresher Course on Contemporary Teaching and Research in Chemistry Jan 02-22, 2014

Maitreyee Nandy

- i. Radioactivity, M Sc, Biophysics & Molecular Biology, University of Calcutta, III semester, 2013-2014
- ii. Radioactivity, M Sc, Bioinformatics, University of Calcutta, III semester, 2013-2014
- iii. Nuclear Medicine, M Sc, Physics, Semester III, Lady Brabourne College, University of Calcutta, 2013-2014

1.8 Miscellany

Debashis Mukhopadhyay

Associate Editor, Journal of Alzheimers Disease

Chapter 2

Condensed Matter Physics including Surface Physics and NanoScience

2.1 Summary of Research Activities of Divisions

2.1.1 Condensed Matter Physics

Colossal piezoresistance effect in $\text{Sm}_{0.55}(\text{Sr}_{0.5}\text{Ca}_{0.5})_{0.45}\text{MnO}_3$ single crystal has been observed. A huge piezoresistance ($\sim 10^7\%$) at a small pressure (0.09 GPa) and a remarkable increase (at the rate of ~ 80 K/GPa) of metal-insulator transition temperature have been observed for uniaxial pressure applied along the *c*-axis. [APL 102, 092406 (2013)].

They have presented a new mechanism whereby doping a correlated band insulator leads to a half-metallic ferrimagnet. This mechanism is quite distinct from the mechanisms in well-known materials that exhibit this phenomenon like the manganites, double perovskites, or Heusler alloys. Their study can motivate a search for materials having the predicted properties and open up new opportunities in the area of spintronics [PRL 112, 106406].

They show that a charge qubit, comprising of an electron tunneling between two dots in an oxide-based double quantum dot (DQD), has very DQD. They show that the stronger the electron couples to the environment the lesser is the qubit decoherence. [PRB 89, 064311 (2014)].

Enhanced dielectric response has been observed for the $\text{Gd}_2\text{Ti}_2\text{O}_7$ - SiO_2 nano-composite with smaller $\text{Gd}_2\text{Ti}_2\text{O}_7$ particles. There is a peak broadening of ϵ' (real part of dielectric constant) versus temperature curves on increasing frequency which suggests die phase transition. This work is expected to raise interest in similar materials as potential candidates for device application such as in gate dielectrics. [Mat. Res. Bull., 50 26 (2014)].

They address why gamma-like distributions arise in different contexts irrespective of different dynamical rules. Study a broad class of mass transport models and show that the variance of the subsystem mass in these models is proportional to the square of its mean. This form of the variance constrains the subsystem mass distribution to be a gamma distribution. [PRL 112, 030601 (2014)].

A bundle of fibers has been considered as a model for composite materials, where breaking of the fibers occur due to a combined influence of applied load and external noise [see RMP for

ber bundle review]. They show that there exists a robust phase boundary between continuous (no waiting time) and intermittent fracturing regimes. They propose a prediction scheme that can tell when the system is expected to reach the continuous fracturing point from the intermittent phase. [PRE 88, 012123 (2013)].

They consider a hydrodynamic description of the spherically symmetric outward flow of nuclear matter, using a nuclear model that introduces a weakly dispersive effect in the flow. They show that even arbitrarily small values of dispersion make the horizon fully opaque to any acoustic disturbance propagating against the bulk flow. [PRC 88, 055205 (2013)].

They have achieved giant enhancement of magnetoresistance (MR) by the formation of $\text{La}_{0.67}\text{Sr}_{0.33}\text{MnO}_3$ (LSMO)/ $\text{Pr}_{0.67}\text{Ca}_{0.33}\text{MnO}_3$ (PCMO) core-shell nanostructure. The observed giant enhancement is the result of significantly weakened charge ordered state in the created ferromagnetic-charge ordered core-shell nanostructure. Their study could be important for magnetic field sensor technology. [APL 103, 202406 (2013)].

2.1.2 Surface Physics and Material Science

Research activities of the Surface Physics Division mainly encompass the physical and chemical methods of growing low-dimensional structures with tunable morphology and mechanical/ electrical/magnetic/optical properties, epitaxial growth of semiconductor quantum structures and their applications in micro-nano technology. Modifications of materials using medium and low-energy ion beams, such as fabrication of decorated and modified surfaces as growth templates, synthesis of quantum dot-composites for photonic/plasmonic applications, etc. are also active areas of our ongoing research. The division has also been involved in the growth of magnetic and photonic structures through nano-manipulation and self-assembly, development of polymer-based photovoltaics and other molecular electronic systems and study of their morphology-transport correlations. Glimpses of some important activities are given in the following. Morphological and structural characterizations of Molecular Beam epitaxy (MBE) - grown Si/Ge superlattice structures have been extensively done using simultaneous analysis of x-ray reflectivity and x-ray diffraction data. Consistent analysis of the data collected in the Indian Beamline at Photon Factory Synchrotron (KEK, Japan) has allowed for the determination of electron density and strain profiles as a function of depth in the multilayer stacks. A procedure for accurate compositional analysis of such Si/Ge superlattice structures and MBE-grown $\text{Si}_{1-x}\text{Ge}_x$ ($0 < x < 0.72$) alloys has been proposed based on MCsN+-SIMS approach. The new methodology has proved to be an efficient approach for Matrix effect minimization in SIMS quantification. Formation mechanisms of multiply-charged secondary ions in sputtering process have been explained in the framework of symmetric and asymmetric collisions. Appreciable nonlinear optical responses in ion-beam induced silver nanoclusters in sapphire with temporal responses in picosecond to femtosecond time domain have shown great relevance to futuristic switching materials in nanophotonics. Cathodoluminescence (CL) in high-resolution scanning electron microscopy (HRSEM) has demonstrated to be an important study on ion-induced ripple patterns on Si. A blue shift of the red peak to a yellow peak (at 575 nm) in CL has been observed for recrystallized patterned sample under high temperature annealing. Localized surface plasmon resonances associated with photon emission in a truncated tetrahedral gold nanoparticle on a silicon substrate are specially mapped showing stronger photon emission in the visible range near the tips of the particle in contact with the substrate compared to the edges of the particle. FDTD simulations of the spectra and cathodoluminescence images are reported to be for the first time. Variable polarization synchrotron radiation has been utilized to map the valence band electronic structure

of graphite by angle-resolved photoemission spectroscopy (ARPES). The measured ARPES has shown asymmetry in intensity around M point of the Brillouin zone mimicking different partial wave character of s1 and s3 bands. Study on micron-sized pit formation on Ge surfaces due to 26 keV Si- ion bombardment is another area of research on materials modifications using medium and low-energy ion beams. A two-field continuum model developed for small slope approximations has described the pit formation and growth at the very beginning stage of ion bombardment. The growth of the pits at later times (high fluence) has been explained by the gradient-dependent erosion mechanisms due to primary ion beam as well by secondary flux of particles originating from steep slopes. Periodic ripple formation on GaAs under 60 keV Ar ion bombardment has been observed. Parameters like rms roughness, ripple wavelength, amplitude, etc. have been measured through AFM image analysis. Study on magnetism in ZnO nanoparticle samples with intrinsic Fe impurities (50 ppm) has shown super-paramagnetic behavior. Under annealing a magnetic hysteresis along with coercive field below the blocking temperature has been found to be almost independent of the cooling field. A simple model has been proposed to explain the reduction of magnetization as being due to a vortex-statelike flux closure formation. Study on structural and magnetic properties of NiO particles through x-ray diffraction, extended x-ray absorption fine structure (EXAFS) and magnetization measurements has demonstrated an unusual finite magnetic moment in antiferromagnetic materials. Incorporation of gold in polypyrrole nanotubes using a cost-effective template based single-step chemical synthesis technique have exhibited switching transition that reduces the resistance of the wires by several orders of magnitude under certain bias around and below 30 K. A deviation from a perfect 2D-hexagonal ($p6m$) structure for CTAB-silica mesostructured films has been observed through X-ray reflectivity and grazing incidence small angle X-ray scattering. The deviation has been understood in terms of the shape and ordering of the micelles inside the film with or without the silica coating-layers contribution. Swelling dynamics of spin-coated ultrathin polyacrylamide films, annealed at the onset of thermal degradation temperature (220 C) of polyacrylamide, have been studied using in-situ X-ray reflectivity to understand the effects of thermal modification of the polymer to their swelling dynamics.

The X-ray reflectivity studies reveal pristine film consists of three layers i.e. lateral stacks of three layers of DNA molecules whereas the salted film has lesser thickness 1.5 times of DNA chain width, indicating enhanced lateral entanglement. Pressure area isotherm of a stearic acid monolayer is recorded and the corresponding image viewed using a Brewster Angle Microscope. Au nanoparticles have been introduced into the monolayer at two different concentrations. The changes in the pressure area isotherm of the system as it progressively changes from a complex to a simpler two dimensional liquid have been studied. The relationship between the change in viscosity of a solution of 50 g asphaltene in 100 ml toluene and the methyl to methylene (CH_3/CH_2) ratio of the asphaltene, when exposed to ultrasonic irradiation, has been studied. The asphaltene used was extracted from refinery sedimentation. Adopting Fourier transform infrared spectroscopy (FTIR) and viscosity measurement as the probing tools, it is found that the viscosity initially decreases but eventually it starts to increase with prolonged duration of ultrasound irradiation. Viscosity decrease is accompanied by an increase in CH_3/CH_2 ratio, which, however, is reversed as the viscosity starts rising in the latter period of irradiation. Thus a clear correspondence exists between the two, viz. when asphaltene is exposed to ultrasonic irradiation its viscosity is inversely proportional to its CH_3/CH_2 ratio. The accuracy of the photo-acoustic (PA) technique to assess blood oxygen saturation (SO_2) using two laser beams was examined theoretically. A Monte Carlo technique was used to simulate 2D tissue configurations, and the PA signals from many red blood cells (RBCs) were constructed by summing the signals emitted by the individual cells. The level of oxygenation of each cell was assumed to be identical in a configuration. The cellular oxygenation state defined the blood oxygen saturation (SO_2) and also controlled the PA signal amplitude. The PA amplitude

was observed to vary linearly with blood SO₂. It was nearly 4.6 times less and 8.2 times greater at SO₂=100% than that of 0% for the 600 and 1064 nm incident optical radiations, respectively. The blood SO₂ was estimated using the PA amplitudes generated at these wavelengths. The estimated values matched perfectly with that of the actual SO₂ confirming the suitability of the PA technique to determine blood SO₂ noninvasively.

2.2 Research Activities

2.2.1 Condensed Matter Physics

2.2.1.1 Doping a Correlated Band Insulator: A New Route to Half-Metallic Behavior

We demonstrate in a simple model the surprising result that turning on an on-site Coulomb interaction U in a doped band insulator leads to the formation of a half-metallic state. In the undoped system, we show that increasing U leads to a first order transition at a finite value U -AF between a paramagnetic band insulator and an antiferromagnetic Mott insulator. Upon doping, the system exhibits half-metallic ferrimagnetism over a wide range of doping and interaction strengths on either side of U -AF. Our results, based on dynamical mean field theory, suggest a new route to half metallicity, and will hopefully motivate searches for new materials for spintronics.

Arti Garg; HR Krishnamurthy†; Mohit Randeria†

2.2.1.2 Polaron dynamics and decoherence in an interacting two-spin system coupled to an optical-phonon environment

We study two anisotropically interacting spins coupled to optical phonons; we restrict our analysis to the regime of strong coupling to the environment, to the antiadiabatic region, and to the subspace with zero value for S_T^z (the z component of the total spin). In the case where each spin is coupled to a different phonon bath, we assume that the system and the environment are initially uncorrelated (and form a simply separable state) in the polaronic frame of reference. By analyzing the polaron dynamics through a non-Markovian quantum master equation, we find that the system manifests a small amount of decoherence that decreases both with increasing nonadiabaticity and with enhancing strength of coupling; whereas, under the Markovian approximation, the polaronic system exhibits a decoherence-free behavior. For the situation where both spins are coupled to the same phonon bath, we also show that the system is decoherence-free in the subspace where S_T^z is fixed. To suppress decoherence through quantum control, we employ a train of π pulses and demonstrate that unitary evolution of the system can be retained. We propose realization of a weakly decohering charge qubit from an electron in an oxide-based (tunnel-coupled) double-quantum-dot system.

Amit Dey; Sudhakar Yarlagadda

2.2.1.3 Interacting particles in a periodically moving potential: Traveling wave and transport

We study a system of interacting particles in a periodically moving external potential, within the simplest possible description of paradigmatic symmetric exclusion process on a ring. The model describes diffusion of hardcore particles where the diffusion dynamics is locally modified at a uniformly moving defect site, mimicking the effect of the periodically moving external potential. The

model, though simple, exhibits remarkably rich features in particle transport, such as polarity reversal and double peaks in particle current upon variation of defect velocity and particle density. By tuning these variables, the most efficient transport can be achieved in either direction along the ring. These features can be understood in terms of a traveling density wave propagating in the system. Our results could be experimentally tested, e.g., in a system of colloidal particles driven by a moving optical tweezer.

Rakesh Chatterjee; Sakuntala Chatterjee†; Punyabrata Pradhan†; et al

2.2.1.4 Enhanced dielectric response of Gd₂Ti₂O₇ nanoparticles in SiO₂ matrix

Dielectric properties of Gd₂Ti₂O₇ nanoparticles in SiO₂ matrix are remarkably different in comparison with the Gd₂Ti₂O₇ single crystal. Gd₂Ti₂O₇-SiO₂ nanocomposite exhibits significant increase in the dielectric constant (epsilon') for smaller Gd₂Ti₂O₇ nanoparticles (GdT900). epsilon'(T) behavior suggests diffuse phase transition (DPT) near room temperature (RT). The estimated value of the diffuseness exponent (gamma) related to DPI is 1.35 for GdT900, indicating an incomplete DPT. The dielectric relaxation near DPT has been associated with the thermally activated oxygen vacancies. The P(E) loops for GdT900 near RT are slim with low values of remnant polarization (P-r similar to 0.15 mu C/cm(2)) and coercive field (E-c similar to 0.85 kV/cm). Nyquist plot for GdT900 indicates that Gd₂Ti₂O₇ nanoparticles play dominant role in electrical conduction. The frequency activated behavior of ac conductivity in the DPT regime suggests that the conduction is due to hopping of bound charge carriers like small polarons.

Papri Dasgupta; S Mukherjee†; RN Bhowmik†; Asok Poddar; Chandan Mazumdar; R Ranganathan

2.2.1.5 Gammalike Mass Distributions and Mass Fluctuations in Conserved-Mass Transport Processes

We show that, in conserved-mass transport processes, the steady-state distribution of mass in a subsystem is uniquely determined from the functional dependence of variance of the subsystem mass on its mean, provided that the joint mass distribution of subsystems is factorized in the thermodynamic limit. The factorization condition is not too restrictive as it would hold in systems with short-ranged spatial correlations. To demonstrate the result, we revisit a broad class of mass transport models and its generic variants, and show that the variance of the subsystem mass in these models is proportional to the square of its mean. This particular functional form of the variance constrains the subsystem mass distribution to be a gamma distribution irrespective of the dynamical rules.

Sayani Chatterjee; Punyabrata Pradhan†; PK Mohanty

2.2.1.6 Field-Induced Spin-Structural Transition and Giant Magnetostriction in Ising Chain α -CoV₂O₆

We have investigated the temperature and magnetic field dependence of magnetization, specific heat (C_p), and relative sample length change ($\Delta L/L_0$) for understanding the field-induced spin-structural change in quasi-one-dimensional spin chain α -CoV₂O₆ which undergoes antiferromagnetic (AFM) transition below $T_N = 15$ K. Analysis of $C_p(T)$ shows that an effective $S = 1/2$

Ising state is realized below 20 K, though the magnetic fluctuations persist well above T_N . C_p and the coefficient of linear thermal expansion (α) exhibit strong H dependence in the AFM state. We also observe a huge positive magnetostriction [$\Delta L(H)/L_0$] below 20 K which does not show any tendency of saturation up to 9 T. With increasing field, a sharp and symmetric peak emerges below T_N in both $C_p(T)$ and $\alpha(T)$ due to field-induced first-order ferrimagnetic/ferromagnetic-paramagnetic transitions. The large value of magnetostriction below T_N suggests strong spin lattice, coupling in α - CoV_2O_6 .

Moumita Nandi; Nazir Khan; Dilip Bhoi; Arindam Midya; Prabhat Mandal

2.2.1.7 Structure-function hierarchies and von Karman-Howarth relations for turbulence in magnetohydrodynamical equations

We generalize the method of A. M. Polyakov, [Phys. Rev. E 52, 6183 (1995)] for obtaining structure-function relations in turbulence in the stochastically forced Burgers equation, to develop structure-function hierarchies for turbulence in three models for magnetohydrodynamics (MHD). These are the Burgers analogs of MHD in one dimension [Eur. Phys. J.B 9, 725 (1999)], and in three dimensions (3DMHD and 3D Hall MHD). Our study provides a convenient and unified scheme for the development of structure-function hierarchies for turbulence in a variety of coupled hydrodynamical equations. For turbulence in the three sets of MHD equations mentioned above, we obtain exact relations for third-order structure functions and their derivatives; these expressions are the analogs of the von Karman-Howarth relations for fluid turbulence. We compare our work with earlier studies of such relations in 3DMHD and 3D Hall MHD.

Abhik Basu; Ali Najit†; Rahul Pandit†

2.2.1.8 Field induced ferromagnetic phase transition and large magnetocaloric effect in $\text{Sm}_{0.55}\text{Sr}_{0.45}\text{MnO}_3$ phase separated manganites

This paper reports about the magnetocaloric effect and relative cooling power based on the first order magnetic phase transition in $\text{Sm}_{0.55}\text{Sr}_{0.45}\text{MnO}_3$ polycrystalline phase separated manganites. Upon 60 kOe applied magnetic field, the magnetic entropy change (—DSM—) of bulk sample reaches a maximum value of 8.48 J/kg-K with a large relative cooling power (RCP) value of 574 J/kg around its Curie temperature (TC)-172 K after the correction for hysteretic losses caused by the first order magnetic phase transition. The corresponding adiabatic temperature change is 2.38 K for magnetic field of 10 kOe. The magnetic field induced change of entropy and specific heat vary with temperature and have their maximum around the first order magnetic phase transition. We also report the magnetic field dependence of the order of the ferromagnetic (FM) to paramagnetic (PM) phase transition in bulk and nanometric manganites. It has been shown that bulk to nanometric samples exhibit first order FM \rightarrow PM phase transition under low magnetic field accompanied by magnetization with thermal hysteresis in the field cooled cooling and warming cycle. However, the samples exhibit a second order magnetic phase transition above a critical field H_{CR} . All the signatures of the first-order magnetic phase transition in bulk and nanometric sample disappear above the critical field H_{CR} . The magnetocaloric effect is thus modified by the field induced order of magnetic phase transition. The field induced paramagnetic to ferromagnetic transition is confirmed to be first order in nature from dc magnetization measurements and Arrott plots using a criteria given by Banerjee. The magnetic phase transition is also accompanied by a large change in

resistivity with thermal hysteresis. The observed value of magnetic entropy change in bulk sample is much higher than the value generally observed in other perovskite manganites of comparable T-C. This large change mainly originates from a sharp magnetization jump, associated with a first-order metamagnetic transition and coalescence of ferromagnetic clusters in the paramagnetic state. Such noticeable magnetic entropy change at low magnetic field makes this material useful for the application of active magnetic refrigerant (AMR) materials.

SK Giri†; Papri Dasgupta; A Poddar; et al

2.2.1.9 Distribution of microRNA co-targets exhibit universality across a wide class of species

MicroRNAs (miRNAs) are small non-coding RNAs which regulate gene expression by binding to the 3' UTR of the corresponding messenger RNAs. We construct miRNA co-target networks for a wide class of species (22 in total) using a target prediction database, MicroCosm Targets. For each species, miRNA pairs having one or more common target genes are connected and the number of co-targets are assigned as the weight of these links. We show that the link weight distributions of all the species collapse remarkably onto each other when scaled suitably-the scale-factor turns out to be a measure of complexity of the species. A simple model, where targets are chosen randomly by miRNAs, could provide the correct scaling function and suggest that the increase of species complexity is related to the increase of the fraction of genes typically targeted by their miRNAs.

Mahashweta Basu; Nitai P Bhattacharyya; PK Mohanty

2.2.1.10 Quantum dynamics of a dissipative and confined cyclotron motion

We study the dissipative dynamics of a charged oscillator in a magnetic field by coupling (a la Caldeira and Leggett) it to a heat bath consisting of non-interacting harmonic oscillators. We derive here the autocorrelation functions of the position and momentum and study its behavior at various limiting situations. The equilibrium (steady state) dispersions of position and momentum are obtained from their respective autocorrelation functions. We analyze the equilibrium position and momentum dispersions at low and high temperatures for both low and high magnetic field strengths. We obtain the classical diffusive behavior (at long times) as well as the equilibrium momentum dispersion of the free quantum charged particle in a magnetic field, in the limit of vanishing oscillator potential coo. We establish the relations between the reduced partition function and the equilibrium dispersions of the dissipative and confined cyclotron problem.

Jishad Kumar

2.2.1.11 Quasi-2D J(1)-J(2) antiferromagnet Zn₂VO(PO₄)(2) and its Ti-substituted derivative: A spin-wave analysis

In this study, we present non-linear spin wave analysis of a quasi 2D spin-1/2 J(1)-J(2) antiferromagnet at the parameter regime relevant for the recently studied compound Zn₂VO(PO₄)(2). We obtain the temperature dependence of the spin wave energy, susceptibility and magnetization using Green's function technique and Tyablikov's decoupling or Hartree-Fock factorization. The comparison of our numerical results with the experimental findings is discussed. Magnetic structure factor

is calculated and compared with powder neutron diffraction data. We also study the spin wave behavior of the compound $\text{Zn}_2\text{Ti}_{0.25}\text{V}_{0.75}\text{O}(\text{PO}_4)_2$ obtained by partial chemical substitution of Ti at V sites of the compound $\text{Zn}_2\text{VO}(\text{PO}_4)_2$ [Kanungo, et al., Phys. Rev. B 87 (2013) 054431]. Due to the superlattice structure of the spin lattice, the substituted compound possesses multiple spin wave modes. The spin wave analysis confirms the quasi-1D nature of the substituted system.

Satyaki Kar; Tanusri Saha-Dasgupta†

2.2.1.12 Low energy spin dynamics in trimer spin chain compound $\text{Ca}_3\text{Cu}_2\text{Ni}(\text{PO}_4)_4$: P-31 NMR study

P-31 nuclear-magnetic-resonance (NMR) study in the trimer spin chain compound $\text{Ca}_3\text{Cu}_2\text{Ni}(\text{PO}_4)_4$ is performed in the presence of different external magnetic fields in the temperature range 4-300 K. The results suggest that the three magnon mediated scattering process which was the dominant contribution to $1/T_1$ in the pure compound $\text{Ca}_3\text{Cu}_3(\text{PO}_4)_4$, has negligible contribution in $\text{Ca}_3\text{Cu}_2\text{Ni}(\text{PO}_4)_4$, with the two magnon mediated Raman process being dominant. The linear variation of nuclear spin lattice relaxation rate $1/T_1T$ with the magnetic susceptibility χ indicates that the Q component of magnetic susceptibility $\chi(Q)$ is nearly proportional to χ , where Q is the antiferromagnetic wave vector. A change in the slope of $1/T_1T$ with respect to χ near 15 K suggests a change in the antiferromagnetic spin fluctuation spectrum. Below 15 K, the spin diffusion mechanism governs the $1/T_1$ process. This could be a signature of the development of short range magnetic correlation or due to the contribution arising from the paramagnetic impurity spins.

M Ghosh; K Ghoshray; M Majumder; Amitabha Ghoshray

2.2.1.13 Dependence of asymptotic decay exponents on initial condition and the resulting scaling violation

There are several examples which show that the critical exponents can be dependent on the initial condition of the system. In such situations, there are many systems where various issues related to the universal behavior, e. g., the existence of universality, the splitting of the universality class, scaling violations, whether the initial dependence should persist even after a sufficiently long time or is a transient effect, the reasons for such features, etc. are not yet quite clear. In this article, with the simple example of the conserved lattice gas model (CLG), we investigate such issues and clearly show that under certain situations the asymptotic decay exponents are, in fact, dependent on the initial condition of the system. We show that such an effect arises because of the existence of two competing time scales and identify the initial conditions which capture the universal features of the system.

Sourish Bondyopadhyay

2.2.1.14 Thermal rectification and negative differential thermal resistance in a driven two segment classical Heisenberg chain

Using computer simulation we investigate thermal transport in a two segment classical Heisenberg spin chain with nearest neighbor interaction and in the presence of an external magnetic field. The system is thermally driven by heat baths attached at the two ends and transport properties are studied using energy conserving dynamics. We demonstrate that by properly tuning the parameters thermal rectification can be achieved-the system behaves as a good conductor of heat along one direction but becomes a bad conductor when the thermal gradient is reversed, and crucially depends on nonlinearity and spatial asymmetry. Moreover, suitable tuning of the system parameters gives rise to the counterintuitive and technologically important feature known as negative differential thermal resistance (NDTR). We find that the crucial factor responsible for the emergence of NDTR is a suitable mechanism for impeding the current in the bulk of the system.

Debarshee Bagchi

2.2.1.15 Temperature-dependent structural property and power factor of n type thermoelectric Bi_{0.90}Sb_{0.10} and Bi_{0.86}Sb_{0.14} alloys

Thermal variation of structural property, linear thermal expansion coefficient (α), resistivity (ρ), thermopower (S), and power factor (PF) of polycrystalline Bi_{1-x}Sb_x ($x=0.10$ and 0.14) samples are reported. Temperature-dependent powder diffraction experiments indicate that samples do not undergo any structural phase transition. Rietveld refinement technique has been used to perform detailed structural analysis. Temperature dependence of α is found to be stronger for Bi_{0.90}Sb_{0.10}. Also, PF for direct band gap Bi_{0.90}Sb_{0.10} is higher as compared to that for indirect band gap Bi_{0.86}Sb_{0.14}. Role of electron-electron and electron-phonon scattering on ρ , S , and PF has been discussed.

K Malik†; Diptasikha Das†; S Bandyopadhyay†; P Mandal...Velaga Srihari, et al

2.2.1.16 Thermally driven classical Heisenberg model in 1D with a local time varying field

We study thermal transport in the one-dimensional classical Heisenberg model driven by boundary heat baths and in the presence of a local time varying magnetic field. We find that, in the steady state, the energy current shows thermal resonance as the frequency of the time-periodic forcing is varied. Even in the absence of a thermal bias a steady nonzero energy current can be induced in the system, whereas for the thermally driven system a current reversal can be achieved in the bulk by suitably tuning the system parameters. When the amplitude of the forcing field is increased the system exhibits multiple resonance peaks. Thermal resonance survives in the thermodynamic limit and their magnitude increases as the temperature of the system is decreased. We find that the resonance frequency is an intrinsic frequency of the model and is related to its spin wave dispersion spectrum. Finally we show that, similar to other generic force-driven systems, there is no thermal pumping despite the current reversal in the bulk of the system.

Debarshee Bagchi

2.2.1.17 Alloying of Fe₃O₄ and Co₃O₄ to develop Co_{3x}Fe_{3(1-x)}O₄ ferrite with high magnetic squareness, tunable ferromagnetic parameters, and exchange bias

Ferromagnetic (FM) Fe₃O₄ and antiferromagnetic (AFM) Co₃O₄ has been alloyed to form the ferrite composition Co_{3x}Fe_{3(1-x)}O₄ ($x = 0.1, 0.3, 0.5$). Three different routes, viz., mechanical alloying at room temperature, annealing of the mechanically alloyed sample and solid state sintering, have been followed to develop the ferrite. X-ray diffraction pattern showed incomplete alloying in as milled samples. Single phased cubic spinel structure has formed after annealing of the mechanical alloyed samples at 950 degrees C, and also in solid state routed samples. The single phase has not formed for the samples at low Co content ($x = 0.1$), but the single phased cubic spinel structure is stabilized for the higher value of Co content ($x = 0.3, 0.5$). All samples showed FM loop at room temperature. The FM parameters (magnetization, squareness, coercivity) of the mechanically alloyed samples after annealing at 950 degrees C showed higher values in comparison with as milled and solid state routed samples with similar composition. Amongst the studied samples, the composition Co_{0.9}Fe_{2.1}O₄ (for $x = 0.3$) exhibited better FM properties in comparison with samples for the compositions $x = 0.1$ and 0.5 . The present work highlighted few more unusual ferromagnetic features, e.g., different types of exchange bias effect, applied field controlled freezing of the ferromagnetic domains, tailoring of the Verwey transition of Fe₃O₄ in the presence of AFM Co₃O₄, and field driven de-pinning of the domain wall motion at lower temperature that can be manipulated for developing next generation advanced magnetic ferrites.

RN Bhowmik†; V Vasanthi†; Asok Poddar

2.2.1.18 Large magnetocapacitance in electronic ferroelectric manganite systems

We have observed a sizable positive magnetocapacitance (similar to 5%-90%) in perovskite Pr_{0.55}Ca_{0.45}MnO₃ and bilayer Pr(Sr_{0.1}Ca_{0.9})₂Mn₂O₇ system under 5 T magnetic field across 20-100 K below the magnetic transition point T-N. The magnetodielectric effect, on the other hand, exhibits a crossover: (a) from positive to negative for the perovskite system and (b) from negative to positive for the bilayer system over the same temperature range. The bilayer Pr(Sr_{0.1}Ca_{0.9})₂Mn₂O₇ system exhibits a sizable anisotropy as well. We have also noticed the influence of magnetic field on the dielectric relaxation characteristics of these systems. These systems belong to a class of improper ferroelectrics and are expected to exhibit charge/orbital order driven ferroelectric polarization below the transition point T-CO. Large magnetocapacitance in these systems shows a typical multiferroic behavior even though the ferroelectric polarization is small in comparison to that of other ferroelectrics.

Ujjal Chowdhury†; Sudipta Goswami†; Dipten Bhattacharya†; Arindam Midya; P Mandal; et al

2.2.1.19 Acoustic horizons in steady spherically symmetric nuclear fluid flows

We consider a hydrodynamic description of the spherically symmetric outward flow of nuclear matter, using a nuclear model that introduces a weakly dispersive effect in the flow. On the resulting stationary conditions of the flow, we apply an Eulerian scheme to derive a fully nonlinear equation of a time-dependent radial perturbation. In its linearized limit, with no dispersion, this equation implies the static acoustic horizon of an analog gravity model. This horizon also defines the minimum radius of the steady flow. We model the perturbation as a high-frequency traveling wave,

in which the weak dispersion is taken iteratively. A WKB analysis shows that even arbitrarily small values of dispersion make the horizon fully opaque to any acoustic disturbance propagating against the bulk flow, with the amplitude and the energy flux of the radial perturbation decaying exponentially just outside the horizon. Nonlinear effects shift the horizon from its steady position.

Niladri Sarkar; Abhik Basu; Jayanta K Bhattacharjee†; et al

2.2.1.20 Response of the two-dimensional kinetic Ising model under a stochastic field

We study, using Monte Carlo dynamics, the time (t) dependent average magnetization per spin $m(t)$ behavior of the 2D kinetic Ising model under a binary ($\pm h_0$) stochastic field $h(t)$. The time dependence of the stochastic field is such that its average over each successive time interval τ is assured to be zero (without any fluctuation). The average magnetization $Q = (1/\tau) \int_0^\tau m(t) dt$ is considered as an order parameter of the system. The phase diagram in (h_0, τ) plane is obtained. Fluctuations in the order parameter and their scaling properties are studied across the phase boundary. These studies indicate that the nature of the transition is Ising like (static Ising universality class) for field amplitudes h_0 below some threshold value $h_0^c(\tau)$ (dependent on tau values; $h_0^c \rightarrow 0$ as $\tau \rightarrow$ infinity across the phase boundary). Beyond these $h_0^c(\tau)$, the transition is no longer continuous.

Asim Ghosh; Bikas K Chakrabarti

2.2.1.21 Spin-orbit interaction induced spin selective transmission through a multi-terminal mesoscopic ring

Spin dependent transport in a multi-terminal mesoscopic ring is investigated in presence of Rashba and Dresselhaus spin-orbit interactions. Within a tight-binding framework, we use a general spin density matrix formalism to evaluate all three components (P_x , P_y , and P_z) of the polarization vector associated with the charge current through the outgoing leads. It explores the dynamics of the spin polarization vector of current propagating through the system subjected to the Rashba and/or the Dresselhaus spin-orbit couplings. The sensitivity of the polarization components on the electrode-ring interface geometry is discussed in detail. Our present analysis provides an understanding of the coupled spin and electron transport in mesoscopic bridge systems.

Moumita Dey; Santanu K Maiti†; Sreekantha Sil†; et al

2.2.1.22 Self-organized dynamics in local load-sharing fiber bundle models

We study the dynamics of a local load-sharing fiber bundle model in two dimensions under an external load (which increases with time at a fixed slow rate) applied at a single point. Due to the local load-sharing nature, the redistributed load remains localized along the boundary of the broken patch. The system then goes to a self-organized state with a stationary average value of load per fiber along the (increasing) boundary of the broken patch (damaged region) and a scale-free distribution of avalanche sizes and other related quantities are observed. In particular, when the load redistribution is only among nearest surviving fiber(s), the numerical estimates of the exponent values are comparable with those of the Manna model. When the load redistribution is

uniform along the patch boundary, the model shows a simple mean-field limit of this self-organizing critical behavior, for which we give analytical estimates of the saturation load per fiber values and avalanche size distribution exponent. These are in good agreement with numerical simulation results.

Soumyajyoti Biswas; Bikas K Chakrabarti

2.2.1.23 Phases and fluctuations in a model for asymmetric inhomogeneous fluid membranes

We propose and analyze a model for phase transitions in an inhomogeneous fluid membrane, that couples local composition with curvature nonlinearly. For asymmetric membranes, our model shows generic non-Ising behavior and the ensuing phase diagram displays either a first- or a second-order phase transition through a critical point (CP) or a tricritical point (TP), depending upon the bending modulus. It predicts generic nontrivial enhancement in fluctuations of asymmetric membranes that scales with system size in a power-law fashion at the CP and TP in two dimensions, not observed in symmetric membranes. It also yields two-dimensional Ising universality class for symmetric membranes, in agreement with experimental results.

Niladri Sarkar; Abhik Basu

2.2.1.24 Lattice bosons in a quasi-disordered environment

In this paper, we study non-interacting bosons in a quasi-disordered one-dimensional optical lattice in a harmonic potential. We consider the case of deterministic quasi-disorder produced by an Aubry-Andre potential. Using exact diagonalization, we investigate both the zero temperature and the finite temperature properties. We investigate the localization properties by using an entanglement measure. We find that the extreme sensitivity of the localization properties to the number of lattice sites in finite size closed chains disappear in open chains. This feature continues to be present in the presence of a harmonic confining potential. The quasi-disorder is found to strongly reduce the Bose-Einstein condensation temperature and the condensate fraction in open chains. The low temperature thermal depletion rate of the condensate fraction increases considerably with increasing quasi-disorder strength. We also find that the critical quasi-disorder strength required for localization increases with increasing strength of the harmonic potential. Further, we find that the low temperature condensate fraction undergoes a sharp drop to 0.5 in the localization transition region. The temperature dependence of the specific heat is, found to be only marginally affected by the quasi-disorder.

R Ramakumar†; AN Das

2.2.1.25 Equivalence of the train model of earthquake and boundary driven Edwards-Wilkinson interface

A discretized version of the Burridge-Knopoff train model with (non-linear friction force replaced by) random pinning is studied in one and two dimensions. A scale free distribution of avalanches and the Omori law type behaviour for after-shocks are obtained. The avalanche dynamics of this

model becomes precisely similar (identical exponent values) to the Edwards-Wilkinson (EW) model of interface propagation. It also allows the complimentary observation of depinning velocity growth (with exponent value identical with that for EW model) in this train model and Omori law behaviour of after-shock (depinning) avalanches in the EW model.

Soumyajyoti Biswas; Purusattam Ray†; Bikas K Chakrabarti

2.2.1.26 Role of inhomogeneous cation distribution in magnetic enhancement of nano-sized $\text{Ni}_{0.35}\text{Zn}_{0.65}\text{Fe}_2\text{O}_4$: A structural, magnetic, and hyperfine study

In this paper, we report the structural, microstructural, and magnetic properties of nanosized (particle size ranging from 20 to 30 nm) $\text{Ni}_{0.35}\text{Zn}_{0.65}\text{Fe}_2\text{O}_4$ (MA4) system synthesized via mechanochemical route followed by annealing. The Rietveld refinement is used for the first time to precisely resolve the crystal structure of a ferrite system at nanoscale. MA4 is a cubic spinel of $\text{Fd}\bar{3}\text{m}$ symmetry. According to XRD and HRTEM studies, it is a well crystalline sample which possesses large microstrain. In spite of its nanometric size, MA4 has displayed some notably distinct magnetic properties like, enhancement of magnetization (64 emu g^{-1} at 15 K), magnetic order, magnetic ordering temperature, coercivity (1000 Oe at 15 K), magnetic anisotropy energy, and reduction of superparamagnetic relaxation compared with its counterparts synthesized by chemical route. It exhibits clear hysteresis loop ($H_C = 50 \text{ Oe}$) at 300 K and ferrimagnetic ordering below the blocking temperature ($\sim 250 \text{ K}$). These improvements in magnetic properties of the system are likely to be very helpful for its technological applications. Again, particles in the sample possess a ferrimagnetically aligned core (with small canting) surrounded by a magnetically disordered shell with canted spin structure. The magnetically disordered surface region of MA4 has an equilibrium cation distribution, whereas the ferrimagnetic core region possesses a nonequilibrium cation distribution. Moreover, the infield Mossbauer spectroscopic study reveals that the nearest neighbor ion configuration about [B] site Fe^{3+} ions is not identical. Thus, there is local chemical inhomogeneity in the sample. The cation redistribution, chemical inhomogeneity, lattice strain are identified as the causes for magnetic enhancement in MA4.

S Dey; SK Dey; B Ghosh; P Dasgupta; A Poddar; et al

2.2.1.27 3d-4f spin interaction induced giant magnetocaloric effect in zircon-type DyCrO_4 and HoCrO_4 compounds

We have investigated the influence of 3d-4f spin interaction on magnetic and magnetocaloric properties of DyCrO_4 and HoCrO_4 compounds by magnetization and heat capacity measurements. Both the compounds exhibit complicated magnetic properties and huge magnetic entropy change around the ferromagnetic transition due to the strong competition between ferromagnetic and antiferromagnetic superexchange interactions. For a field change of 8 T, the maximum values of magnetic entropy change (ΔS_M^{max}), adiabatic temperature change (ΔT_{ad}), and refrigerant capacity (RC) reach $29 \text{ J kg}^{-1} \text{ K}^{-1}$, 8 K, and 583 J kg^{-1} , respectively, for DyCrO_4 whereas the corresponding values for HoCrO_4 are $31 \text{ J kg}^{-1} \text{ K}^{-1}$, 12 K, and 622 J kg^{-1} . ΔS_M^{max} , ΔT_{ad} , and RC are also quite large for a moderate field change. The large values of magnetocaloric parameters suggest that the zircon-type DyCrO_4 and HoCrO_4 could be the potential magnetic refrigerant materials for lique-

faction of hydrogen.

A Midya; N Khan; D Bhoi; P Mandal

2.2.1.28 Formation of Nanosize Griffiths-like Clusters in Solid Solution of Ferromagnetic Manganite and Cobaltite

We report the existence of a Griffiths-like phase over a wide range of x due to the formation of nanosize ferromagnetic clusters in $\text{La}_{0.6}\text{Sr}_{0.4}\text{Mn}_{1-x}\text{Co}_x\text{O}_3$, the solid solution of ferromagnetic $\text{La}_{0.6}\text{Sr}_{0.4}\text{MnO}_3$ and $\text{La}_{0.6}\text{Sr}_{0.4}\text{CoO}_3$, from the magnetization measurements. In the studied compound, this phase arises due to the quenching of randomly distributed Co-O-Mn antiferromagnetic bonds in the ferromagnetic background. In contrary to the divalent alkaline-earth-doped manganites, the Griffiths-like phase in $\text{La}_{0.6}\text{Sr}_{0.4}\text{Mn}_{1-x}\text{Co}_x\text{O}_3$ can exist entirely in the metallic state above T_c (for $x < 0.10$). Based on the present study, a magnetoelectronic phase diagram is drawn.

D Bhoi; N Khan; A Midya...P Mandal

2.2.1.29 Generic instabilities in a fluid membrane coupled to a thin layer of ordered active polar fluid

We develop an effective two-dimensional coarse-grained description for the coupled system of a planar fluid membrane anchored to a thin layer of polar ordered active fluid below. The macroscopic orientation of the active fluid layer is assumed to be perpendicular to the attached membrane. We demonstrate that activity or nonequilibrium drive of the active fluid makes such a system generically linearly unstable for either signature of a model parameter $\Delta\mu$ that characterises the strength of activity. Depending upon boundary conditions and within a range of the model parameters, underdamped propagating waves may be present in our model. We discuss the phenomenological significance of our results.

Niladri Sarkar; Abhik Basu

2.2.1.30 Positional dependence of energy gap on line defect in armchair graphene nanoribbons: Two-terminal transport and related issues

The characteristics of energy band spectrum of armchair graphene nanoribbons in the presence of line defect are analyzed within a simple non-interacting tight-binding framework. In metallic nanoribbons, an energy gap may or may not appear in the band spectrum depending on the location of the defect line, while in semiconducting ribbons, the gaps are customized, yielding the potential applicabilities of graphene nanoribbons in nanoscale electronic devices. With a more general model, we also investigate two-terminal electron transport using Green's function formalism.

Paramita Dutta; Santanu K Maiti†; SN Karmakar

2.2.1.31 Noise-induced rupture process: Phase boundary and scaling of waiting time distribution

A bundle of fibers has been considered here as a model for composite materials, where breaking of the fibers occur due to a combined influence of applied load (stress) and external noise. Through numerical simulation and a mean-field calculation we show that there exists a robust phase boundary between continuous (no waiting time) and intermittent fracturing regimes. In the intermittent regime, throughout the entire rupture process avalanches of different sizes are produced and there is a waiting time between two consecutive avalanches. The statistics of waiting times follows a Γ distribution and the avalanche distribution shows power-law scaling, similar to what has been observed in the case of earthquake events and bursts in fracture experiments. We propose a prediction scheme that can tell when the system is expected to reach the continuous fracturing point from the intermittent phase.

Srutarshi Pradhan; Anjan Kumar Chandra; Bikas K Chakrabarti

2.2.1.32 Nonequilibrium dynamics of ultracold Fermi superfluids

The aim of this mini review is to survey the literature on the study of nonequilibrium dynamics of Fermi super fluids in the BCS and BEC limits, both in the single channel and dual channel cases. The focus is on mean field approaches to the dynamics, with specific attention drawn to the dynamics of the Ginzburg-Landau order parameters of the Fermi and composite Bose fields, as well as on the microscopic dynamics of the quantum degrees of freedom. The two approaches are valid approximations in two different time scales of the ensuing dynamics. The system is presumed to evolve during and/or after a quantum quench in the parameter space. The quench can either be an impulse quench with virtually instantaneous variation, or a periodic variation between two values. The literature for the order parameter dynamics, described by the time-dependent Ginzburg-Landau equations, is reviewed, and the works of the author in this area highlighted. The mixed phase regime in the dual channel case is also considered, and the dual order parameter dynamics of Fermi-Bose mixtures reviewed. Finally, the nonequilibrium dynamics of the microscopic degrees of freedom for the superfluid is reviewed for the self-consistent and non self-consistent cases. The dynamics of the former can be described by the Bogoliubov de-Gennes equations with the equilibrium BCS gap equation continued in time and self-consistently coupled to the BdG dynamics. The latter is a reduced BCS problem and can be mapped onto the dynamics of Ising and Kitaev models. This article reviews the dynamics of both impulse quenches in the Feshbach detuning, as well as periodic quenches in the chemical potential, and highlights the author's contributions in this area of research.

Analabha Roy

2.2.1.33 Study of gamma ray response of R404A superheated droplet detector using a two-state model

The superheated droplet detector (SOD) is known to be gamma ray insensitive below a threshold temperature which made them excellent candidates for neutron detection in the presence of gamma rays. Above the threshold temperature, the gamma ray detection efficiency increases with increase in temperature. In this work the gamma ray threshold temperature has been studied for SDD

using R404A as the active liquid and is compared to the theoretical prediction. The temperature variation of gamma ray detection efficiency and interstate transition kinetics has also been studied using a two-state model. The experiments are performed at the ambient pressure of 1 atm and in the temperature range of 17-32 degrees C using a 662 keV Cs-137 gamma ray source.

PK Mondal; BK Chatterjee†

2.2.1.34 Magnetic structures in RNi₄B (R=Nd, Tb, Ho, Er)

Neutron diffraction has been performed on RNi₄B (R=Nd, Tb, Ho, Er) polycrystals. The orthorhombic structure for NdNi₄B and the CeCO₄B structure type (hexagonal) for TbNi₄B and HoNi₄B are confirmed. Our data also show that this last structure is currently the best approximant for ErNi₄B. The RNi₄B (R=Nd, Tb, Ho, Er) order ferromagnetically at respectively 11.0, 18.1, 6.2 and 10.0 K. The crystal electric field (CEF) interaction controls the magnetic anisotropy in this series leading to an easy axis similar to 30 deg above the basal plane in RNi₄B (R=Nd, Tb, Ho) and parallel to the c-axis in ErNi₄B at 1.6 K. The RNi₄B (R=Nd, Tb, Ho) display a spin re-orientation below T_c which arises from a competition between the second order term and the higher order terms of the CEF hamiltonian.

E Alleno; C Mazumdar

2.2.1.35 Comparison of Modules of Wild Type and Mutant Huntingtin and TP53 Protein Interaction Networks: Implications in Biological Processes and Functions

Disease-causing mutations usually change the interacting partners of mutant proteins. In this article, we propose that the biological consequences of mutation are directly related to the alteration of corresponding protein protein interaction networks (PPIN). Mutation of Huntingtin (HTT) which causes Huntington's disease (HD) and mutations to TP53 which is associated with different cancers are studied as two example cases. We construct the PPIN of wild type and mutant proteins separately and identify the structural modules of each of the networks. The functional role of these modules are then assessed by Gene Ontology (GO) enrichment analysis for biological processes (BPs). We find that a large number of significantly enriched ($p < 0.0001$) GO terms in mutant PPIN were absent in the wild type PPIN indicating the gain of BPs due to mutation. Similarly some of the GO terms enriched in wild type PPIN cease to exist in the modules of mutant PPIN, representing the loss. GO terms common in modules of mutant and wild type networks indicate both loss and gain of BPs. We further assign relevant biological function(s) to each module by classifying the enriched GO terms associated with it. It turns out that most of these biological functions in HTT networks are already known to be altered in HD and those of TP53 networks are altered in cancers. We argue that gain of BPs, and the corresponding biological functions, are due to new interacting partners acquired by mutant proteins. The methodology we adopt here could be applied to genetic diseases where mutations alter the ability of the protein to interact with other proteins.

Mahashweta Basu; Nitai P Bhattacharyya; Pradeep K Mohanty

2.2.1.36 Microwave spectral studies of 2, 4-difluorobenzaldehyde: O-trans conformer

The ground state microwave rotational spectra of 2,4-difluorobenzaldehyde (2,4-DFBD) vapor have been investigated in the frequency range 18.037.0GHz using conventional microwave as well as Radiofrequency-Microwave Double Resonance (RFMWDR) spectroscopic techniques. A least-squares analysis of 50 a-type R-branch lines provides a set of rotational and centrifugal distortion constants which corresponds to the O-trans conformer of the molecule. The rotational constants are: $A = 2498.977$ (39)MHz, $B = 958.043$ MHz and $C = 692.394$ MHz. Detailed DFT calculations were carried out with various functional and basis sets to evaluate the spectroscopic constants, dipole moment and various structural parameters of the O-trans conformer of 2,4-DFBD for the ground state. It was found that the optimized geometry with B3LYP/6-311++g(2d,2p) basis set shows good agreement with the experimental values of the rotational constants. The ground state microwave rotational spectrum of 2,4-difluorobenzaldehyde was measured and analyzed. O-trans conformer was found to be predominant in the gas phase. Detailed DFT calculations were performed to evaluate spectroscopic constants and structural parameters.

Rangana Bhattacharya; AI Jaman

2.2.1.37 Periodic dynamics of fermionic superfluids in the BCS regime

We study the zero temperature non-equilibrium dynamics of a fermionic superfluid in the BCS limit and in the presence of a drive leading to a time-dependent chemical potential $\mu(t)$. We choose a periodic driving protocol characterized by a frequency ω and compute the fermion density, the wavefunction overlap, and the residual energy of the system at the end of N periods of the drive. We demonstrate that the BCS self-consistency condition is crucial in shaping the long time behaviour of the fermions subjected to the drive and provide an analytical understanding of the behaviour of the fermion density n_{k_F} (where $k(F)$ is the Fermi momentum vector) after a drive period and for large ω . We also show that the momentum distribution of the excitations generated due to such a drive bears the signature of the pairing symmetry and can be used, for example, to distinguish between s- and d-wave superfluids. We propose experiments to test our theory.

Analabha Roy; Raka Dasgupta†; Sanhita Modak†; et al

2.2.1.38 Local electromagnetic properties of magnetic pnictides: a comparative study probed by NMR measurements

^{75}As and ^{31}P NMR studies are performed in PrCoAsO and NdCoPO respectively. The Knight shift data in PrCoAsO indicate the presence of an antiferromagnetic interaction between the 4f moments along the c axis in the ferromagnetic state of Co 3d moments. We propose a possible spin structure in this system. The ^{75}As quadrupolar coupling constant, ν_Q , increases continuously with decrease of temperature and is found to vary linearly with the intrinsic spin susceptibility, K_{iso} . This indicates the possibility of the presence of a coupling between charge density and spin density fluctuations. Further, the ^{31}P NMR Knight shift and spin-lattice relaxation rate ($1/T_1$) in the paramagnetic state of NdCoPO indicate that the differences of LaCoPO and NdCoPO from SmCoPO are due to the decrement of the interlayer separation and not due to the moments of the 4f electrons. The nuclear spin-lattice relaxation time (T_1) in NdCoPO shows weak anisotropy at 300 K. Using the self-consistent renormalization (SCR) theory of itinerant ferromagnets, it is shown

that in the *ab* plane, the spin fluctuations are three-dimensional ferromagnetic in nature. From SCR theory the important spin-fluctuation parameters (T_0, T_A, \overline{F}_1) are evaluated. The similarities and dissimilarities of the NMR results in As and P based systems with different rare earths are also discussed.

M Majumder; K Ghoshray; A Ghoshray; et al

2.2.1.39 Vortex dynamics and second magnetization peak in $\text{PrFeAsO}_{0.60}\text{F}_{0.12}$ superconductor

We have studied the vortex dynamics in the $\text{PrFeAsO}_{0.60}\text{F}_{0.12}$ superconducting sample by dc magnetization and dynamic magnetization-relaxation rate (Q) measurements. The field dependence of the superconducting irreversible magnetization M_s reveals a second magnetization peak or fishtail effect. The large value of Q is an indication of moderate vortex motion and relatively weak pinning energy. Data analysis based on the generalized inversion scheme suggests that the vortex dynamics can be described by the collective pinning model. The temperature dependence of the critical current is consistent with the pinning due to the spatial variation in the mean free path near a lattice defect (δl -pinning). The temperature and field dependence of Q indicate a crossover from elastic to plastic vortex creep with increasing temperature and magnetic field. Finally, we have constructed the vortex phase diagram based on the present data.

D Bhoi; P Mandal; P Choudhury†

2.2.1.40 Critical exponents and irreversibility lines of $\text{La}_{0.9}\text{Sr}_{0.1}\text{CoO}_3$ single crystal

We have studied the dynamic and static critical behavior of spin glass transition in insulating $\text{La}_{0.9}\text{Sr}_{0.1}\text{CoO}_3$ single crystal by ac susceptibility and dc magnetization measurements in the vicinity of its freezing temperature (T_f). The dynamic scaling analysis of the frequency dependence of ac susceptibility data yields the characteristic time constant $\tau_0 = 1.6(9) \times 10^{-12}$ s, the dynamic critical exponent $z\nu = 9.5(2)$, and a frequency dependence factor $K = \Delta T_f / T_f (\Delta \log f) = 0.017$, indicating that the sample enters into a canonical spin-glass phase below $T_f = 34.8(2)$ K. The scaling analysis of non-linear magnetization in the vicinity of T_f through the static scaling hypothesis yields critical exponents $\beta = 0.89(1)$ and $\gamma = 2.9(1)$, which match well with that observed for well known three-dimensional (3D) Heisenberg spin glasses. From the longitudinal component of zero-field-cooled and field-cooled magnetization measurement, we have constructed the $H - T$ phase diagram which represents the field evolution of two characteristic temperatures: the upper one, $T_w(H)$, indicates the onset of spin freezing in a uniform external field H , while the lower one, $T_s(H)$, marks the onset of strong irreversibility of the frozen state. The low field $T_s(H)$ follows the critical line suggested by d'Almeida-Thouless model for canonical spin glass, whereas the $T_w(H)$ exhibits a re-entrant behavior with a maximum in the $T_w(H)$ at a nonzero field above which it follows the Gabay-Toulouse (GT) critical line which is a characteristic of Heisenberg spin glass. The reentrant behavior of the GT line resembles that predicted theoretically for n -component vector spin glasses in the presence of a uniaxial anisotropy field.

N Khan; A Midya; P Mandal; et al

2.2.1.41 The universal behavior of inverse magnetocaloric effect in antiferromagnetic materials

We report the universal behavior of inverse magnetocaloric effect (IMCE) in antiferromagnetic materials. In contrast to the universal behavior of conventional magnetocaloric effect often observed in ferromagnetic systems, a phenomenological universal master curve can be constructed to describe the temperature dependence of magnetic entropy change for IMCE without rescaling the temperature axis. The proposed universal curve method allows extrapolating the magnetic entropy change of an IMCE material, which would be imperative to judge its suitability in actual magnetic refrigeration devices. (C) 2013 American Institute of Physics.

Anis Biswas†; Sayan Chandra†; Tapas Samanta...I Das; et al

2.2.1.42 Absorbing phase transition in energy exchange models

We study energy exchange models with dissipation (λ) and noise (of amplitude σ) and show that in presence of a threshold these models undergo an absorbing phase transition when either dissipation or noise strength or both are varied. Using Monte Carlo simulations we find that the behaviour along the critical line, which separates the active phase from the absorbing one, belongs to directed percolation (DP) universality class. We claim that the conserved version with $\lambda = 1$ and $\sigma = 0$ also shows a DP transition; the apparent non-DP behaviour observed earlier is an artifact of undershooting in the decay of activity density starting from a random initial condition.

U Basu; M Basu; PK Mohanty

2.2.1.43 Universality in the entropy change for the inverse magnetocaloric effect

A comprehensive study of the temperature (T) and magnetic field (H) dependence of magnetic entropy change ($\Delta S-M$) for different materials exhibiting inverse magnetocaloric effect (IMCE) is reported. We show that $\Delta S-M$ follows a power-law dependence of H ($\Delta S-M \sim H^{-n}$; n is an exponent) for these compounds. In contrast to conventional magnetocaloric effect (CMCE), n is independent of H and T in the case of IMCE. As a result, a universal master curve can be constructed to describe $\Delta S-M$ (T) of the IMCE systems for different H without rescaling the temperature axis. This is completely different from that reported for CMCE, where the rescaling of the temperature axis with the introduction of at least one reference temperature is needed for constructing a universal curve. The different universal behavior of IMCE is attributed to the constant value of n in any field and temperature, which is a generic feature of IMCE systems irrespective of their magnetic state and nature of phase transition. From the proposed phenomenological universal curve, one can extrapolate the magnetocaloric properties of IMCE systems in any temperature and magnetic field range, which would be helpful in designing controlled active magnetic refrigeration devices.

Anis Biswas†; Sayan Chandra†; Tapas Samanta...; I Das; et al

2.2.1.44 Electric field driven destabilization of the insulating state in nominally pure LaMnO_3

We report an electric field driven destabilization of the insulating state in nominally pure LaMnO_3 single crystal with a moderate field which leads to a resistive state transition below 300 K. The

transition is between the insulating state in LaMnO_3 and a high resistance bad metallic state that has a temperature independent resistivity. The transition occurs at a threshold field (E_{th}) that shows a steep enhancement on cooling. While at lower temperatures the transition is sharp and involves a large change in resistance, it softens on heating and is eventually absent above 280 K. When the Mn^{4+} content is increased by Sr substitution up to $x = 0.1$, the observed transition, although observable in a certain temperature range, softens considerably. This observation has been explained as a bias driven percolation type transition between two co-existing phases, where the majority phase is a charge and orbitally ordered polaronic insulating phase and the minority phase is a bad metallic phase. The mobile fraction f of the bad metallic phase deduced from the experimental data follows an activated kinetics as $f = f_o(E)\exp(-\Delta/k_B T)$ with the activation energy $\Delta \approx 200$ meV, and the pre-factor $f_o(E)$ is a strong function of the field that leads to a rapid enhancement of f on application of field, leading to the resistive state transition. We suggest likely scenarios for such co-existing phases in nominally pure LaMnO_3 that can lead to the bias driven percolation type transition.

Rajib Nath†; AK Raychaudhuri†; Ya M Mukovskii†...P Mandal

2.2.1.45 Dynamical percolation transition in the two-dimensional ANNNI model

The dynamical percolation transition of the two-dimensional axial next nearest-neighbor Ising model due to a pulsed magnetic field has been studied by finite size scaling analysis (by Monte Carlo simulation) for various values of frustration parameters, pulse width and temperature (below the corresponding static transition temperature). It has been found that the size of the largest geometrical cluster shows a transition for a critical field amplitude. Although the transition points shift, the critical exponents remain invariant for a wide range of frustration parameters. They are also the same as those obtained for the 2d Ising model. This suggests that although the static phase diagrams of these two models differ significantly in various aspects, the dynamical percolation transitions of these models belong to the same universality class.

Anjan Kumar Chandra

2.2.1.46 Crossover behaviors in one and two dimensional heterogeneous load sharing fiber bundle models

We study the effect of heterogeneous load sharing in the fiber bundle models of fracture. The system is divided into two groups of fibers (fraction ρ and $1-\rho$) in which one group follows the completely local load sharing mechanism and the other group follows global load sharing mechanism. Patches of local disorders (weakness) in the loading plate can cause such a situation in the system. We find that in 2d a finite crossover (between global and local load sharing behaviours) point comes up at a finite value of the disorder concentration (near $\rho_c \sim 0.53$), which is slightly below the site percolation threshold. We numerically determine the phase diagrams (in 1d and 2d) and identify the critical behavior below ρ_c with the mean field behavior (completely global load sharing) for both dimensions. This crossover can occur due to geometrical percolation of disorders in the loading plate. We also show how the critical point depends on the loading history, which is identified as a special property of local load sharing.

Soumyajyoti Biswas; Bikas K Chakrabarti

2.2.1.47 Electronic transport minimum in SmCuAs_2 at low temperatures and structural anomalies

Temperature dependent x-ray diffraction and electrical transport under pressure have been reported on SmCuAs_2 , which has been known to exhibit an unusual transport behaviour (a pronounced minimum much before long range magnetic order (Sampathkumaran et al., 2003 [6])) at low temperatures. The Neel temperature as well as the pronounced resistivity upturn observed before the onset of magnetic ordering is found to decrease sluggishly with pressure up to 15 kbar. External magnetic field has insignificant effect both at ambient and under pressure. Thus the anomalies are quite robust to applied pressure and magnetic field. Low temperature x-ray diffraction reveals no symmetry change, but the system exhibits lattice distortions along both a- and c-axes in the temperature region of interest, thereby suggesting that the resistivity anomalies could be associated with structural anomalies in this system.

K Sengupta; KK Iyer†; R Ranganathan; et al

2.2.2 Surface Physics and Material Science

2.2.2.1 Synthesis of SiGe layered structure in single crystalline Ge substrate by low energy Si ion implantation

Nanometer-thickness SiGe alloy layers were synthesized by direct Si ion implantation in Ge (100) wafers at different fluences followed by high temperature annealing. The cross-sectional transmission electron microscopy and secondary ion mass spectrometry reveal the formation of a thin Si-rich crystalline layer in the near-surface region. The micro-Raman spectroscopy and X-ray reflectivity techniques were used to determine the composition and strain in SiGe alloy layers. The photoluminescence measurements of the annealed samples showed a broad emission, peaking around 500 nm. The peak intensity is, however, dependent on the bombarding fluence.

SA Mollick; D Ghose; SR Bhattacharyya; S Bhunia; NR Ray, et al

2.2.2.2 Development of hydrophobicity of mica surfaces by ion beam sputtering

The hydrophilic mica surface can be made hydrophobic by low energy Ar^+ ion sputtering. The ion sputtering leads to both topographical and physicochemical changes of the surface which are thought to be responsible for the water repelling behavior. The sessile drop method is used to evaluate the wetting properties of the sputtered mica surfaces. It has been shown that the sputter-pattern at the nano-length scale has little influence on the development of hydrophobicity. On the other hand, the wettability appears to be strongly connected with the chemistry of the bombarded surface. We have also studied the temporal evolution of contact angle as the water evaporates due to difference in vapor pressures between the droplet surface and the surroundings. The analysis offers a simple method to estimate the diffusion coefficient of water vapor.

Amaresh Metya; Debabrata Ghose; Nihar Ranjan Ray

2.2.2.3 Enhancement of supercapacitance property of electrochemically deposited MnO₂ thin films grown in acidic medium

In this communication we present supercapacitance property of MnO₂ thin-films which are fabricated on stainless steel (SS) substrate by electro-deposition method carried out in different pH of the electrolyte. A significant improvement of the device performance of acid mediated grown (AMG) MnO₂ over normal MnO₂ (grown in neutral medium) has been achieved. We have also investigated role of interfacial structure on the internal resistance of the device material. AMG MnO₂ film exhibits superior device performance with specific capacitance of 652 F/g which is 2 times better than that obtained in normal MnO₂ and also energy density of 90.69 Wh/kg.

SK Jana; VP Rao; S Banerjee

2.2.2.4 Inverse magnetocaloric effect in Mn₂NiGa and Mn_{1.75}Ni_{1.25}Ga magnetic shape memory alloys

Inverse magnetocaloric effect is demonstrated in Mn₂NiGa and Mn_{1.75}Ni_{1.25}Ga magnetic shape memory alloys. The entropy change at the martensite transition is larger in Mn_{1.75}Ni_{1.25}Ga, and it increases linearly with magnetic field in both the specimens. Existence of inverse magnetocaloric effect is consistent with the observation that magnetization in the martensite phase is smaller than the austenite phase. Although the Mn content is smaller in Mn_{1.75}Ni_{1.25}Ga, from neutron diffraction, we show that the origin of inverse magnetocaloric effect is the antiferromagnetic interaction between the Mn atoms occupying inequivalent sites.

Sanjay Singh; S Esakki Muthu†; A Senyshyn†...SR Barman

2.2.2.5 An unusual μ -(1,2,3)-squarato-bridged two dimensional coordination polymer: Crystal structure, thermal, photoluminescence and magnetic studies

A new 2D coordination polymer, [Ni-II(squarate)(2,2'-bipy)(H₂O)]center dot H₂O(n), [squarate = 3,4-dihydroxycyclo-but-3-ene-1,2-dionate, 2,2'-bipy = 2,26'-bipyridine], has been synthesized by using multi-oxygen donor squaric acid ligand and characterized by single crystal X-ray crystallographic and various spectroscopic studies. The structural analysis has revealed that the complex crystallizes in orthorhombic P-bca space group and it has 3D supramolecular structure. Within the complex, the squarato-dianion exhibits unusual μ -(1,2,3) bridging mode with Ni(II) ions and 2D coordination sheets are formed through bridging the metal ions by squarato-anions. The 2D coordination sheets are packed along crystallographic b-axis and the 2,2'-bipyridyl (blocking ligand) moieties are hanging in the interlamellar spaces between the 2D coordination sheets. These 2D coordination sheets are further bridged by supramolecular π ... π interactions using 2,2'-bipyridyl ligands leading to the formation of 3D supramolecular framework which acts as a metal-organic supramolecular host (MOSH). During formation of 3D supramolecular structure, 1D supramolecular channels are formed along the crystallographic c-axis. The guest water molecules get stability within such supramolecular channels through hydrogen bonding interactions with free oxygen atoms of bridging squarate ions. The thermal study indicates that the complex decomposes in three steps. The variable temperature magnetic measurements suggest that the complex is antiferromagnetic in nature. The complex exhibits solid-state photoluminescence spectra at room temperature due to $\pi - \pi^* / n - \pi^*$ transition of the squarate and 2,2'-bipyridine ligands. The present study points to

the squarato-bridged metal complexes as unique model system to carry out the study on different bridging modes exhibited by the ligand.

Somen Goswami; Rajat Saha; Ian M Steele...Papri Dasgupta; Asok Poddar; et al

2.2.2.6 Anomalous patterns and nearly defect-free ripples produced by bombarding silicon and germanium with a beam of gold ions

We demonstrate that surface ripples with an exceptionally high degree of order can develop when germanium is bombarded with a broad beam of gold ions. In contrast, if silicon is sputtered with an Au- beam, patches of ripples with two distinct wave vectors can emerge. These types of order can be understood if the coupling between the surface morphology and composition is taken into account.

Mollick, Safiul Alam; Debabrata Ghose; Patrick D Shipman†; et al

2.2.2.7 Hydrostatic pressure effects on martensitic transition, magnetic and magnetocaloric effect in Si doped Ni-Mn-Sn Heusler alloys

We report the hydrostatic pressure dependence of martensitic, magnetic and magnetocaloric effect in the $\text{Ni}_{48}\text{Mn}_{39}\text{Sn}_{13-x}\text{Si}_x$ ($x = 1$ and 4) Heusler alloys. The martensitic transition temperature increased with respect to pressure at the rate of 2.37 K/kbar and 0.7 K/kbar for $x = 1$ and 4 alloys respectively and decreases with the application of magnetic field at the rate of 1.2 K/T and 0.8 K/T for $x = 1$ and 4 alloys respectively. The Curie temperature of austenite phase changes marginally under pressure. The maximum magnetic entropy change (ΔS_M) of 5.13 J kg⁻¹ K⁻¹ at 0 kbar and 24.5 J kg⁽⁻¹⁾ K⁻¹ at 9.7 kbar were observed for $x = 1$ alloy. However the magnetic entropy change for $x = 4$ alloy seems to decrease as a function of pressure.

S Esakki Muthu†; M Kanagaraj†; Sanjay Singh; et al

2.2.2.8 Anomalous behaviour of magnetic coercivity in graphene oxide and reduced graphene oxide

In this report, we present the temperature dependence of the magnetic coercivity of graphene oxide (GO) and reduced graphene oxide (RGO). We observe an anomalous decrease in coercivity of GO and RGO with decreasing temperature. The observation could be understood by invoking the inherent presence of wrinkles on graphene oxide due to presence of oxygen containing groups. Scanning electron microscopic image reveals high wrinkles in GO than RGO. We observe higher coercivity in RGO than in GO. At room temperature, we observe antiferromagnetic and ferromagnetic behaviours in GO and RGO, respectively. Whereas, at low temperatures (below $T = 60-70$ K), both materials show paramagnetic behaviour.

K Bagani; A Bhattacharya; J Kaur; A Rai Chowdhury; B Ghosh...S Banerjee

2.2.2.9 Study of density-dependent swelling of ultrathin water soluble polymer films

The effects of density on the swelling dynamics of ultrathin polymer films have been demonstrated. In order to examine the effect of density on the swelling dynamics, films of nearly identical thicknesses with different densities were fabricated by a spin coating method. Swelling dynamics of these films have been studied by monitoring their thicknesses with time in a saturated water vapor environment using an in situ X-ray reflectivity technique. We observed that the electron density of the films increases with the concentration of the solutions used for the preparation of the films. Interestingly, our results reveal a systematic decrease in free diffusion coefficients and an increase of the free chain fraction with an increase in film density.

Mojammel H Mondal; M Mukherjee

2.2.2.10 Characterization of bimetallic core-shell nanorings synthesized via ascorbic acid-controlled galvanic displacement followed by epitaxial growth

This paper describes the role of ascorbic acid in synthesizing bimetallic core-shell nanorings at room temperature. Using two-dimensional (2D) triangular silver nanoparticles as templates, we first synthesized 2D triangular gold (Au) nanorings via the galvanic replacement reaction and then overgrown Ag on Au nanorings via an epitaxial growth process. Transmission Electron Microscopy (TEM) and associated techniques were used for in-depth characterization. The TEM study revealed that single crystalline Ag nanoparticles led to the formation of continuous Au nanorings with single crystalline walls, and the void spaces which corroborate with the template shapes only when ascorbic acid was added to the growth solution. Both the silver nanoplates and gold nanorings have (111) planes as the basal planes. Subsequently we synthesized Au-core-Ag-shell nanorings using the previously synthesized Au nanorings as templates. Energy dispersive X-ray (EDX) line profile spectra and imaging, along with high-angle annular dark field scanning/transmission electron microscopy (STEM-HAADF), were used extensively for compositional studies in addition to energy filtered TEM (EFTEM) imaging.

Tanmay Ghosh; Biswarup Satpati; Dulal Senapati

2.2.2.11 Facile synthesis and the photo-catalytic behavior of core-shell nanorods

Sodium niobate nanorods (SNRs) have been synthesized by a facile surfactant free hydrothermal method. To explore their potential for photoelectrochemical water splitting under visible light, core-shell nanorods were fabricated by grafting CdS on sodium niobate nanorods. The TEM analysis shows the formation of sodium niobate nanorods which are in the order of 40 +/- 5 nm in width and 1300 +/- 100 nm in length. The presence of a thin layer on nanorods, as observed in a TEM image, and XRD and SAD analysis, reveals the grafting of hexagonal CdS on orthorhombic sodium niobate nanorods. This was further confirmed by dual band gap values (E-g: 3.6 for sodium niobate and 2.59 eV for CdS) determined from diffuse reflectance data of the CdS-sodium niobate nanorod sample. The CdS-sodium niobate nanorods show drastic enhancement in the current density ($J(\text{an})$: 7.6 mA cm⁻²) at 0.2 V vs. SHE) when irradiated with monochromatic UV light (300 nm), many folds higher than that observed for bare sodium niobate nanorods ($J(\text{an})$: 2.5 mA cm⁻²) at 0.2 V vs. SHE), bulk sodium niobate ($J(\text{an})$: 0.6 mA cm⁻²) at 0.2 V vs. SHE) and CdS. The conduction band (CB) minima calculations show a downhill offset of the CB edges of

CdS-sodium niobate. Such a downhill staggered band gap and smooth lattice matched interface, as shown by HRTEM, seem to facilitate an efficient charge separation followed by a photo-generated $e(-)$ transfer from the CdS CB to the sodium niobate CB and, therefore, appear responsible for the enhancement of the photocurrent density of CdS-sodium niobate nanorods. This is further corroborated by the time resolved photoluminescence decay measurements which show a longer average decay time ($\langle \tau \rangle$) for CdS-sodium niobate nanorods in the order of 8.06 ns than that for sodium niobate nanorods (6.45 ns). Furthermore, better light harvesting efficiency and incident to photon conversion efficiency (23.91% at 300 nm) observed for CdS-sodium niobate nanorods imply a better photo-generated charge carrier separation than those observed for bare sodium niobate nanorods and bulk sodium niobate. The synthesis of CdS modified sodium niobate nanorods, detailed results on the photoelectrochemical behaviour of CdS modified sodium niobate nanorods and underlying mechanism are presented.

Kamala Kanta Nanda†; Smrutirekha Swain†; Biswarup Satpati; et al

2.2.2.12 Production of ordered and pure Si nanodots at grazing ion beam sputtering under concurrent substrate rotation

Hexagonal array of Si-nanodots is spontaneously generated by low energy Ar⁺ sputtering of a Si (100) surface at grazing incidence angle (75 degrees) under continuous rotation of the substrate holder. The effects of rotation speed, beam current density and beam energy on the dot morphology are investigated by atomic force microscopy. The transmission electron microscopy of the dot microstructure shows that the dots are crystalline and are not induced by metal contaminants. Moreover, the dots are found to be capped by negligibly thin amorphous layer.

Debasree Chowdhury; Debabrata Ghose; Biswarup Satpati

2.2.2.13 Formation of Au-Ge nanodots by Au- ion sputtering of Ge

Energetic Au ion sputtering of crystalline Ge surface at normal incidence and room temperature can produce nanodot morphology, which has been studied by atomic force microscopy. The cross-sectional transmission electron microscopy of the dot structure reveals that the implanted Au does not form solid solution with Ge, but preferentially segregates at the top edges of the dots as well as near the amorphous/crystalline interface. The mechanism of dot formation is discussed in the light of local transient melting of the surface due to a high rate of energy deposition by the Au ions and the subsequent cooling.

Safiqul Alam Mollick; Debabrata Ghose; Biswarup Satpati

2.2.2.14 Simultaneous detection of guanine, adenine, thymine, and cytosine at polyaniline/MnO₂ modified electrode

In this study, PANI/MnO₂ nanocomposite was synthesized by the reaction of polyaniline (PANI) and KMnO₄ in the aqueous medium. Material was characterized by X-ray diffraction, nitrogen sorption, scanning electron microscopy, transmission electron microscopy, thermogravimetric analysis, and FTIR. PANI/MnO₂ modified electrode was investigated in the simultaneous detection of

all four DNA bases (guanine, adenine, thymine, and cytosine) using cyclic and differential pulse voltammetries. pH was optimized to obtain the best peak potential separation and response current. This enabled us for the simultaneous voltammetric determination of all four DNA bases at physiological condition (pH 7). PANI/MnO₂ nanocomposite exhibited high-current sensitivity for these analytes compared to MnO₂ and PANI modified electrodes. Under the optimum conditions, PANI/MnO₂ exhibited low detection limit, good sensitivity, and wide linear range for the simultaneous detection of G, A, T, and C. Moreover, the proposed method was successfully applied in the determination of G, A, T, and C contents in a calf thymus DNA sample with satisfactory results. The reliability and stability of the modified electrode provide a good possibility for applying the technique in the routine analysis for a selected class of electroactive organic/bio-molecules.

MU Anu Prathap†; Rajendra Srivastava†; Biswarup Satpati

2.2.2.15 Variations in Magnetic Properties of Nanostructured Nickel

The magnetic properties of carbon nanotube encapsulated nickel nanowires (C. E. nanowires of diameter similar to 10 nm), and its comparison to other forms of Ni are carried out in this work. The saturation magnetization (M_s) and coercivity (H_c) for C. E. nanowires are 1.0 emu/g and 230 Oe. The temperature dependence of coercivity follows T^{-0.77} dependence indicating a superparamagnetic behavior. The field-cooled and zero-field-cooled plots indicate that the blocking temperature (T_B) similar to 300 K. These altered magnetic properties of C. E. nanowires are mainly due to the nanoscale confinement effect from carbon nanotube encapsulation. The shape and magnetic environment enhance the total magnetic anisotropy of C. E. nanowires by a factor of four.

Paramita Kar Choudhury†; S Banerjee; S Ramaprabhu†; et al

2.2.2.16 Highly Efficient Nanocrystalline Zirconosilicate Catalysts for the Aminolysis, Alcoholysis, and Hydroamination Reactions

Nanocrystalline zirconosilicates and titanosilicates with MFI framework structure were hydrothermally synthesized by the addition of organosilanes in the synthesis composition of conventional zirconosilicate and titanosilicate materials. Materials were characterized by a complementary combination of X-ray diffraction, nitrogen sorption, scanning/transmission electron microscopy (S/TEM), ammonia temperature-programmed desorption (TPD), Fourier transform infrared (FT-IR) spectroscopy, and ultraviolet visible (UV-vis) spectroscopic investigations. Nanocrystalline zeolite catalysts of the present study are reusable. They exhibit significantly higher catalytic activities in aminolysis and alcoholysis compared with the hitherto known catalysts. A range of beta-amino alcohols/beta-alkoxy alcohols with high regioselectivity were synthesized using zirconosilicates. Application of these materials was also extended in the synthesis of aminoesters by the hydroamination reaction of methyl acrylates and amines. Structure activity relationship was explained based on acidity measurements, reactivity of amines/alcohols, and adsorption of reactants on catalysts.

Rajkumar Kore†; Rajendra Srivastava†; Biswarup Satpati

2.2.2.17 Structural, optical and photocatalytic properties of flower-like ZnO nanostructures prepared by a facile wet chemical method

Flower-like ZnO nanostructures were synthesized by a facile wet chemical method. Structural, optical and photocatalytic properties of these nanostructures have been studied by X-ray diffraction (XRD), scanning electron microscopy (SEM), transmission electron microscopy (TEM), photoluminescence (PL) and UV-vis absorption spectroscopy. SEM and TEM studies revealed flower-like structures consisting of nanosheets, formed due to oriented attachment of ZnO nanoparticles. Flower-like ZnO structures showed enhanced photocatalytic activity towards sun-light driven photodegradation of methylene blue dye (MB) as compared to ZnO nanoparticles. XRD, UV-vis absorption, PL, FTIR and TEM studies revealed the formation of Zn(OH)(2) surface layer on ZnO nanostructures upon ageing. We demonstrate that the formation of a passivating Zn(OH)(2) surface layer on the ZnO nanostructures upon ageing deteriorates their efficiency to photocatalytically degrade of MB.

Kuriakose Sini†; Neha Bhardwaj†; Jaspal Singh†; Biswarup Satpati; et al

2.2.2.18 Facile preparation of Ni(OH)(2)-MnO2 hybrid material and its application in the electrocatalytic oxidation of hydrazine

A surfactant-free synthetic methodology is reported for the preparation of Ni(OH)(2)-MnO2 hybrid nanostructures. For comparative study, MnO2 and Ni(OH)(2) were also synthesized. Materials were characterized by X-ray diffraction, nitrogen sorption, scanning electron microscopy, and transmission electron microscopy. Ni(OH)(2)-MnO2 modified electrode is fabricated for the determination of hydrazine. The electrochemical oxidation of hydrazine was investigated using cyclic, linear sweep voltammetries, and chronoamperometry methods. The Ni(OH)(2)-MnO2 modified electrode showed hydrazine oxidation with decrease in the over voltage and increase in the oxidation peak current, when compared to MnO2, Ni(OH)(2), and bare GCE. pH was optimized to obtain the best peak potential and current sensitivity. Chronoamperometry was used to estimate the diffusion coefficient of hydrazine. The kinetic parameters such as overall number of electrons involved in the catalytic oxidation of hydrazine and the rate constant (k) for the oxidation of hydrazine at Ni(OH)(2)-MnO2 modified electrode were determined. The Ni(OH)(2)-MnO2 modified electrode exhibited good sensitivity, stability, and reproducibility in hydrazine sensing.

MU Anu Prathap†; V Anuraj†; Biswarup Satpati; et al

2.2.2.19 SEM analysis of ion implanted SiC

SiC is a material used in two future energy production technologies, firstly as a photovoltaic layer to harness the UV spectrum in high efficient power solar cells, and secondly as a diffusion barrier material for radioactive fission products in the fuel elements of the next generation of nuclear power plants. For both applications, there is an interest in the implantation of reactive and non-reactive ions into SiC and their effects on the properties of the SiC. In this study 360 key Ag+, I+ and Xe+ ions were separately implanted into 6H-SiC and in polycrystalline SiC at various substrate temperatures. The implanted samples were also annealed in vacuum at temperatures ranging from 900 degrees C to 1600 degrees C for various times. In recent years, there had been significant advances in scanning electron microscopy (SEM) with the introduction of an in-lens detector combined with

field emission electron guns. This allows defects in solids, such as radiation damage created by the implanted ions, to be detected with SEM. Cross-sectional SEM images of 6H-SiC wafers implanted with 360 keV Ag⁺ ions at room temperature and at 600 degrees C and then vacuum annealed at different temperatures revealed the implanted layers and their thicknesses. A similar result is shown of 360 keV I⁺ ions implanted at 600 degrees C into 6H-SiC and annealed at 1600 degrees C. The 6H-SiC is not amorphized but remained crystalline when implanted at 600 degrees C. There are differences in the microstructure of 6H-SiC implanted with silver at the two temperatures as well as with reactive iodine ions. Voids (bubbles) are created in the implanted layers into which the precipitation of silver and iodine can occur after annealing of the samples. The crystallinity of the substrate via implantation temperature caused differences in the distribution and size of the voids. Implantation of xenon ions in polycrystalline SiC at 350 degrees C does not amorphize the substrate as is the case with room temperature heavy ion bombardment. Subsequent annealing of the implanted polycrystalline samples leads to increased thermal etching effects such as grain boundary grooving. Damage due to channelling (or non-channelling) in the different crystallites resulted also in differences in thermal etching in the crystallites.

Johan B Malherbe†; NG van der Berg†; AJ Botha...P Chakraborty; et al

2.2.2.20 Effect of antbsite formation on magnetic properties of nickel zinc ferrite particles

In this report, we have investigated the effect of antbsite ordering on the magnetic behavior of Ni_xZn_{1-x}Fe₂O₄ nanoparticles for $x = 0, 0.25, 0.5, 0.75,$ and 1. Observed magnetization versus temperature data show systematic gradual changes from antiferromagnetic to ferrimagnetic phase with increasing amount of Ni concentration. Saturation magnetization of the parent Zn ferrite increases when substituted by Ni and then decreases for concentration greater than $x = 0.5$. Coercivity also shows a concentration dependence. Saturation magnetization has no dependence on cooling field at all concentrations. For $x = 0.5$ the system act as an extremely soft magnetic material with highest saturation magnetization and lowest coercivity. Site occupancy by cations plays an important role for local moment imbalance between different antiferromagnetic sublattices giving rise to ferrimagnetic interaction upon Ni substituted in Zn ferrite.

B Ghosh; M Sardar†; S Banerjee

2.2.2.21 Designing Novel pH-Induced Chitosan-Gum Odina Complex Coacervates for Colon Targeting

This paper investigates the design of novel polyelectrolyte complex (PEC) coacervates of chitosan (Ch) with gum Odina (GO) as potential candidates for colon targeting. Potentiometric titration experiments established that 1:1 charge stoichiometry occurred at a Ch/GO weight ratio of 1:5. The coacervate formed at pH 4.5 displayed the highest storage modulus (G') values. FTIR, XPS, WAXS, TGA, and DSC results suggested the strong ionic (NH₃⁺-center dot center dot center dot COO⁻) bond formation between these two biopolymers. Through in vitro viability tests, the pH-induced PECs were shown to be nontoxic. In vitro biodegradation rates of their microspheres revealed insolubility in simulated gastric fluid and simulated intestinal fluid and degradation by cell-associated portions of rat cecal and colonic enzymes rather than the extracellular portions. The microsphere of pH 3.0 showed the highest degradation, and LVSEM micrographs revealed notably

high amount of macropores in cell-associated enzymes, in contrast to extracellular enzymes.

Partha Sarathi Roy†; Amalesh Samanta†; Manabendra Mukherjee; et al

2.2.2.22 Giant enhancement of magnetoresistance in core-shell ferromagnetic-charge ordered nanostructures

We have achieved giant enhancement of magnetoresistance (MR) by the formation of $\text{La}_{0.67}\text{Sr}_{0.33}\text{MnO}_3$ (LSMO)- $\text{Pr}_{0.67}\text{Ca}_{0.33}\text{MnO}_3$ (PCMO) core-shell nanostructure. Astonishingly, 1143% enhancement of MR in the core-shell nanostructure has been observed with respect to the parent PCMO nanoparticles at 100 K and 2 T magnetic field. The observed giant enhancement is the result of significantly weakened charge ordered state in the created ferromagnetic-charge ordered core-shell nanostructure. Our study clearly indicates a method to achieve huge enhancement of magnetoresistance that can eventually give rise to artificially created superior materials important for magnetic field sensor technology.

Kalipada Das; R Rawat†; B Satpati; I Das

2.2.2.23 Comparison of Three Scattering Models for Ultrasound Blood Characterization

Ultrasonic backscattered signals from blood contain frequency-dependent information that can be used to obtain quantitative parameters reflecting the aggregation level of red blood cells (RBCs). The approach is based on estimating structural aggregate parameters by fitting the spectrum of the backscattered radio-frequency echoes from blood to an estimated spectrum considering a theoretical scattering model. In this study, three scattering models were examined: a new implementation of the Gaussian model (GM), the structure factor size estimator (SFSE), and the new effective medium theory combined with the structure factor model (EMTSFM). The accuracy of the three scattering models in determining mean aggregate size and compactness was compared by 2-D and 3-D computer simulations in which RBC structural parameters were controlled. Two clustering conditions were studied: 1) the aggregate size varied and the aggregate compactness was fixed in both 2-D and 3-D cases, and 2) the aggregate size was fixed and the aggregate compactness varied in the 2-D case. For both clustering conditions, the EMTSFM was found to be more suitable than GM and SFSE for characterizing RBC aggregation.

Emilie Franceschini†; Ratan K Saha; Guy Cloutier†

2.2.2.24 Simultaneous and sensitive determination of ascorbic acid, dopamine, uric acid, and tryptophan with silver nanoparticles-decorated reduced graphene oxide modified electrode

In this paper, we report the synthesis of silver nanoparticle-decorated reduced graphene oxide composite (AgNPs/rGO) by heating the mixture of graphene oxide and silver nitrate aqueous solution in the presence of sodium hydroxide. This material was characterized by means of X-ray diffraction, UV-vis spectroscopy, and transmission electron microscopy. AgNPs/rGO based electrochemical sensor was fabricated for the simultaneous determination of ascorbic acid, dopamine, uric

acid, and tryptophan. Electrochemical studies were carried out by using cyclic voltammetry, linear sweep voltammetry, and chronoamperometry. AgNPs/rGO modified electrode exhibited excellent electrocatalytic activity, stability, sensitivity, and selectivity with well-separated oxidation peaks toward ascorbic acid, dopamine, uric acid, and tryptophan in the simultaneous determination of their quaternary mixture. The analytical performance of this material as a chemical sensor was demonstrated for the determination of ascorbic acid and dopamine in commercial pharmaceutical samples such as vitamin C tablets and dopamine injections, respectively. The applicability of this sensor was also extended in the determination of uric acid in human urine samples.

Balwinder Kaur†; Thangarasu Pandiyan†; Biswarup Satpati; et al

2.2.2.25 Studies on resistive switching characteristics of aluminum/graphene oxide/semiconductor nonvolatile memory cells

We report semiconductor-based resistive switching nonvolatile memory devices with graphene oxide (GO) as an active layer which is sandwiched between aluminum (Al) metal and semiconductors such as Si and Ge. Semiconductors (p-Si or p-Ge) are used as bottom electrodes on which a layer of GO is deposited and Al electrodes are then formed on the top of it by thermal evaporation. From current-voltage characteristics, it is found that the devices show diode like rectifying switching behavior, which can suppress the cross talk between adjacent cells. In these structures, during initial voltage biasing, the current conduction is found to be due to thermionic emission and in later stages, it is driven by space charge. The maximum on/off ratio in Al/GO/p-Si and Al/GO/p-Ge structures is 110 (at -1.2 V) and 76 (at -1.7 V), respectively. However, breakdown occurs in the memory cells fabricated on p-Ge after switching to low resistance state due to lack of stable oxide at the interface between Ge and GO unlike in the cells on Si where stable native SiO₂ prevents such breakdown. The mechanism of resistive switching in semiconductor based memory cells has been explained using X-ray photoelectron spectroscopy and capacitance-voltage characteristics.

S Mahaboob Jilani†; Tanesh D Gamot†; P Banerji†; S Chakraborty

2.2.2.26 Core level photoemission studies on conducting polypyrrole polymer nanotubes showing switching transitions

Conducting polypyrrole (PPY) nanotubes is a classical model system for strongly correlated disordered materials showing intriguing switching transitions from low to high conductivity states at low temperature. This switching behaviour can be tuned by incorporating gold nanoclusters to form composite nanotubes (AuPPY). Here, we present core level electronic structure studies on PPY and AuPPY nanotubes with different diameters using hard X-ray photoemission spectroscopy at room temperature. The spectroscopic data provide information on the role of diameter as well as metal cluster incorporation for a modification of the electronic structure of this important class of nanotubes. Furthermore, electrical transport measurements were performed at low temperature to extract the change in localization length and doping level in these nanotubes. Based on these results, we explain the observed electrical transport behavior of these nanotubes as the interplay of disorder and carrier concentration.

I Sarkar†; A Sarma; MK Sanyal; et al

2.2.2.27 Investigation of ion beam induced nanopattern formation near the threshold energy

The nanoscale ripple formation on mica surface is studied at off-normal ion incidence angles θ under Ar^+ bombardment at energies E close to or below the threshold energy for physical sputtering. A phase diagram for domains of pattern formation is presented as a function of θ and E , which shows the stability/instability bifurcation angle close to 40° . The instability grows as ripple-like structures at lower angles, while at grazing angles the pattern emerges as dense array of needles. The results support the pure mass redistribution based paradigm for surface patterning as the erosion due to sputtering essentially tends to zero.

Amaresh Metya; Debabrata Ghose

2.2.2.28 Local electron beam excitation and substrate effect on the plasmonic response of single gold nanostars

We performed cathodoluminescence (CL) spectroscopy and imaging in a high-resolution scanning electron microscope to locally and selectively excite and investigate the plasmonic properties of a multi-branched gold nanostar on a silicon substrate. This method allows us to map the local density of optical states from the nanostar with a spatial resolution down to a few nanometers. We resolve, both in the spatial and spectral domain, different plasmon modes associated with the nanostar. Finite-difference time-domain (FDTD) numerical simulations are performed to support the experimental observations. We investigate the effect of the substrate on the plasmonic properties of these complex-shaped nanostars. The powerful CL-FDTD combination helps us to understand the effect of the substrate on the plasmonic response of branched nanoparticles.

Pabitra Das; Abhitosh Kedia†; Pandian Senthil Kumar†...Tapas Kumar Chini

2.2.2.29 Microstructure, magnetic and electrical transport properties of melt-spun Ni-Mn-Sb ribbons

The $\text{Ni}_{50}\text{Mn}_{37}\text{Sb}_{13}$ ribbons were prepared by melt-spinning technique to overcome the brittleness of bulk. A single phase austenite with $L2_1$ structure was confirmed in the as-spun and annealed ribbons at room temperature similar to bulk. We observe increments in the martensite transformation temperature (T_M) from 238 K to 252 K and in Curie temperature of austenite phase (T_C^A) from 336 K to 342 K after annealing the as-spun ribbon. The exchange bias, magnetic entropy change (ΔS_M), and magnetoresistance are found to increase from 380 Oe to 415 Oe, 1 J/kg-K to 3 J/kg-K ($\Delta H = 50$ kOe), and -4% to -13% ($\Delta H = 50$ kOe), respectively, after annealing the as-spun ribbon. The possible reasons for observed behaviour are discussed.

Mayukh K Ray; K Bagani; RK Singh†...S Banerjee

2.2.2.30 Crossover of spin glass characteristics as a function of field in an NiMnSnAl alloy

The magnetic state in martensitic phase of $\text{Ni}_{50}\text{Mn}_{34}\text{Sn}_6\text{Al}_{10}$ shows interesting glassy behaviour. The irreversibility was observed in d.c. magnetization measurement below martensitic transformation temperature. Further measurements at lower temperature showed the presence of exchange

bias field in sample. H-T phase diagram of the irreversibility showed that the system was in Heisenberg like spin glass state at low field, which changed its type when the external field was above the exchange bias field. In order to determine the cause of cross over, a. c. susceptibility measurements were performed in zero and d.c. biasing fields. This switching of glassy nature of the system is a novel phenomenon.

Sandeep Agarwal†; S Banerjee; PK Mukhopadhyay†

2.2.2.31 Formation of single-crystalline CuS at the organic-aqueous interface

We report here the results of a study to understand the formation mechanism of single crystals of the transition metal chalcogenide, CuS, at the water-toluene interface through an interfacial reaction. Systematic measurements carried out using synchrotron x-ray scattering, electron microscopy, atomic force microscopy and calorimetric techniques clearly show that nano-crystallites of CuS form within a few minutes at the interface as the reagents are brought from the organic (upper) and aqueous (lower) layers to the interface, then crystallization of CuS proceeds over a few hours only by reorganization, despite the large excess available in both upper and lower liquid phases. The interface confinement and passivation by organics is critical here in the formation of single crystals having sizes of 6 and 200 nm along the normal and in-plane directions of the liquid-liquid interface.

Santanu Maiti; Milan K Sanyal; Neenu Varghese†; B Satpati; D Dasgupta; et al

2.2.2.32 Comparative study of the microstructural and magnetic properties of fly ashes obtained from different thermal power plants in West Bengal, India

This paper deals with the physical nature of the fly ashes obtained from two thermal power plants, situated in West Bengal, India. The fly ash samples are characterized by using comprehensive techniques with an emphasis on their ultrafine nature. The particle sizes of the samples are estimated using scanning electron microscopy (SEM) and found to lie within 0.18-5.90 μ m. For morphology and compositional analysis, we also use SEM coupled with energy dispersive X-ray spectrometry. From X-ray study of the fly ashes the nature of conglomeration is seen to be crystalline, and the major components are mullite ($\text{Al}_6\text{Si}_2\text{O}_{13}$) and quartz (SiO_2). The magnetic measurement of the fly ash samples was carried out by SQUID magnetometer. Fe-57 Mossbauer spectra are obtained using a conventional constant-acceleration spectrometer with a Co-57/Rh Mossbauer source. The hyperfine parameters obtained, in general, support the findings as made from XRD analysis and provide a quantitative measure of different iron ions present in the samples. The paper presents experimental data on the physical aspects of the fly ash samples of the thermal power plants which comprise coarse, fine, and ultrafine magnetic particulate materials and attempts to provide an exhaustive analysis.

Ashis Bhattacharjee†; Haradhan Mandal†; Madhusudan Roy; et al

2.2.2.33 Linear current fluctuations in the power-law region of metallic carbon nanotubes

We study low-frequency noise in a non-Ohmic region of metallic single walled and multiwalled carbon nanotubes. The generalized relative noise appears to be independent of applied bias in the power-law regime of the tubes and in agreement with theoretical predictions. Beyond the power-law regime the suppression of conductance due to scattering with optical phonons is accompanied by a reduction of relative noise by an order of magnitude. Mobility fluctuations in the tubes due to optical phonon scattering cause the unexpected reduction in the relative noise magnitude which is modeled using a modified mobility fluctuation picture. The findings have important implications for metallic nanotubes being used as interconnects in nanoelectronic devices.

D Talukdar; P Yotprayoonsak; O Herranen; M Ahlskog

2.2.2.34 Correlated Charge Carrier-like Photoresponse of Polymer Nanowires

Size confinement at nanometer length scales gives rise to many new and tunable properties of organic materials that are absent in their bulk state. Here we report, the appearance of large photoconduction property of a conducting polymer when it forms nanowires. The photoresponse and the external photoconductive gain were found to be $> 10(5) \%$ and $> 200\%$, respectively, even at low bias (< 1 V) voltage. These nanowires show a resistance switching transition at low temperature above a threshold bias, and below this transition, the resistance changes by more than 3 orders of magnitude under illumination of light. The photoresponse increases superlinearly and the resistance switching threshold voltage decreases with increasing illumination intensity. These properties are absent in the bulk polymer, and the observed photoresponse is not bolometric or excitonic in nature, nor it can be explained by free carrier generation or Schottky barrier modulation, rather it is consistent with the photoexcitation of correlated charge carriers.

Atikur Rahman; Milan K Sanyal

2.2.2.35 Facile preparation of polyaniline/MnO₂ nanofibers and its electrochemical application in the simultaneous determination of catechol, hydroquinone, and resorcinol

In this study, polyaniline/MnO₂ nanofibers were synthesized by the simple mixing of aqueous dispersed solution of polyaniline (PANI) nanofibers and KMnO₄ aqueous solution. Materials were characterized by X-ray diffraction, nitrogen sorption, scanning electron microscopy, transmission electron microscopy, thermogravimetric analysis, and FT-IR. The electrochemical oxidation of hydroquinone, catechol, and resorcinol was investigated using cyclic and differential pulse voltammeteries at PANI/MnO₂ modified electrode. PANI/MnO₂ exhibited high current sensitivity for these analytes compared to MnO₂ and PANI modified electrodes, which is due to the presence of highly dispersed MnO₂ in PANI matrix. The performance of this material was demonstrated in the detection of hydroquinone, catechol, and resorcinol in water samples. The reliability and stability of the modified electrode provides a good possibility for applying the technique in routine analysis for a selected class of electroactive organic/bio-molecules.

MU Anu Prathap†; Biswarup Satpati; Rajendra Srivastava†

2.2.2.36 Diameter-dependent coercivity of cobalt nanowires

We show that the coercivity of electrochemically grown cobalt nanowires (NWs) within the pores of a polycarbonate membrane can be changed to a large extent by tuning their diameters. The face centered cubic crystalline structure of the NWs having diameter in the range of 10 to 200 nm could be retained. Smaller diameter wires (below 30 nm) are found to be single crystalline and oriented in the [110] growth direction, but for higher diameter wires the crystallite size became very small. Magnetization measurements with an applied field parallel to the axis of the NWs show that the nature of the M-H loop changes from square to linear as the diameter of the NWs increases. The coercivity was found to be 1700 Oe and 480 Oe at 5 K (1000 Oe and 250 Oe at 300 K) for 10 nm and 100 nm wires, respectively. The observed changes in the nature of the M-H loop and in coercivity could be explained following the Stoner-Wohlfarth model and using the fact that the domain size reduces as the diameter of the wires increases.

Sirshendu Gayen; Milan K Sanyal; Biswarup Satpati; Atikur Rahman

2.2.2.37 DNA-Mediated Wirelike Clusters of Silver Nanoparticles: An Ultrasensitive SERS Substrate

Stable metal nanoclusters (NCs) with uniform interior nanogaps reproducibly offer a highly robust substrate for surface-enhanced Raman scattering (SERS) because of the presence of abundant hot spots on their surface. The synthesis of such an SERS substrate by a simple route is a challenging task. Here, we have synthesized a highly stable wirelike cluster of silver nanoparticles (Ag-NPs) with an interparticle gap of similar to 1.7 ± 0.2 nm using deoxyribonucleic acid (DNA) as the template by exploiting an easy and inexpensive chemical route. The red shift in the surface plasmon resonance (SPR) band of Ag-NCs compared to SPR of a single Ag-NP confirms the strong interplasmonic interaction. Methylene Blue (MB) is used as a representative Raman probe to study the SERS effect of the NCs. The SERS measurements reveal that uniform, reproducible, and strong Raman signals were observed up to the single-molecule level. The intensity of the Raman signal is not highly dependent on the polarization of the excitation laser. The DNA-based Ag-NCs as a substrate show better isotropic behavior for their SERS intensity compared to the dimer, as confirmed from both the experimental and theoretical simulation results. We believe that in the future the DNA-based Ag-NCs might be useful as a potential SERS substrate for ultrasensitive trace detection, biomolecular assays, NP-based photothermal therapeutics, and a few other technologically important fields.

Dipanwita Majumdar†; Achintya Singha†; Prasanna Kumar Mondal; et al

2.2.2.38 Thickness dependent electronic structure and morphology of rubrene thin films on metal, semiconductor, and dielectric substrates

The evolution of the electronic structure and morphology of rubrene thin films on noble-metal, semiconductor and dielectric substrates have been investigated as a function of thickness of deposited films by using photoelectron spectroscopy and atomic force microscopy. The clean polycrystalline Au and Ag were used as noble-metals, whereas, H passivated and SiO₂ coated Si (100) were used as semiconductors and dielectric substrates. Discussion and comparison on interface dipole, energy level alignment, and surface morphology for the four cases are presented. The formation of

dipole at metallic interfaces is found to occur due to push back effect. S parameter obtained from the variation of barrier height with the change of work function of the contacting metal indicates moderately weak interaction between rubrene and the metal substrates. The thickness dependent energy level alignment of the physisorbed rubrene films on different substrates is explained by a dielectric model in terms of electrostatic screening of photo-holes or photoemission final state relaxation energy. Films on all the substrates are found to grow following Stranski-Krastnov type growth mode and are more ordered at higher coverage.

Sumona Sinha; M Mukherjee

2.2.2.39 Investigation of the influence of hydrostatic pressure on the magnetic and magnetocaloric properties of $\text{Ni}_{2-X}\text{Mn}_{1+X}\text{Ga}$ ($X=0, 0.15$) Heusler alloys

The effect of hydrostatic pressure on the magnetic and magnetocaloric properties of $\text{Ni}_{2-X}\text{Mn}_{1+X}\text{Ga}$ ($X = 0, 0.15$) Heusler alloys around the martensitic transformation temperature (T_M) has been investigated. We find that magnetic field increases and decreases the characteristic transitions temperature for $X = 0$ and 0.15 , respectively, and increases the saturation magnetization of martensite phase for both the alloys. However, the hysteresis width decreases for both the alloys as we increase the magnetic field to 5 T. Application of hydrostatic pressure increases (decreases) the T_M for $X = 0$ and 0.15 . Pressure stabilizes the martensite phase with the increase of T_M for Ni_2MnGa , whereas the austenite phase gets stabilized with the decrease of T_M in $\text{Ni}_{1.85}\text{Mn}_{1.15}\text{Ga}$ ($x = 0.15$). Metamagnetic-like transition is suppressed for both the specimens with increasing pressure. The maximum magnetic entropy change (ΔS_{Mmax}) is found to reduce from $19.2 \text{ J kg}^{-1} \text{ K}^{-1}$ ($P = 0$) to $6.04 \text{ J kg}^{-1} \text{ K}^{-1}$ ($P = 9.69$ kilobars) around T_M for Ni_2MnGa and it decreases from $8.9 \text{ J kg}^{-1} \text{ K}^{-1}$ ($P = 0$) to $1.27 \text{ J kg}^{-1} \text{ K}^{-1}$ ($P = 7.4$ kilobars) around T_M for $\text{Ni}_{1.85}\text{Mn}_{1.15}\text{Ga}$.

U Devarajan†; S Esakki Muthu†; S Arumugam†; Sanjay Singh; SR Barman

2.2.2.40 Power law in swelling of ultra-thin polymer films

Steady state and dynamic behaviour of swelling of spin coated polyacrylamide films have been studied at room temperature in a precisely controlled environment of 12-99% relative humidity (RH). Swelling of the films was monitored by measuring the thickness of the films using X-ray reflectivity and Atomic Force Microscopy. Swellibility of the films was observed to be independent of thickness of the films indicating no significant influence of substrate polymer interaction or confinement effect in swelling. The water content of the films swelled at different humidity conditions was calculated comparing the electron density of the dry and the swelled films. The volume fraction of water in the swelled films and their swellibility were found to follow double power law behaviour as a function of relative humidity and the transition from one regime to the other was observed around 75% RH value. The behaviour was explained in terms of transition from short to long diffusing channels in the films. Comparison of time evolution of relative humidity of the experimental chamber with that of the dynamics of swellings of the films shows that diffusion of water into the environment was several orders of magnitude faster than the swelling dynamics. The observed values of the diffusion coefficients for the films at different humidity were same whereas the excluded volume parameter, that determine the saturated thickness of the films, was found to have dependence on

relative humidity and film thickness.

M Mukherjee; M Souheib Chebil†; Nicolas Delorme†; et al

2.2.2.41 Photoacoustic response of suspended and hemolyzed red blood cells

The effect of confinement of hemoglobin molecules on photoacoustic (PA) signal is studied experimentally. The PA amplitudes for samples with suspended red blood cells (SRBCs) and hemolyzed red blood cells (HRBCs) were found to be comparable at each hematocrit for 532 nm illumination. The difference between the corresponding amplitudes increased with increasing hematocrit for 1064 nm irradiation. For example, the PA amplitude for the SRBCs was about 260% higher than that of the HRBCs at 40% hematocrit. This observation may help to develop a PA method detecting hemolysis noninvasively.

Ratan K Saha; Subhajit Karmakar; Madhusudan Roy

2.2.2.42 Nanoparticle-induced morphological transition of *Bombyx mori* nucleopolyhedrovirus: a novel method to treat silkworm grasserie disease

Grasserie, a polyorganotrophic disease caused by *Bombyx mori* nucleopolyhedrovirus (BmNPV), accounts for lethal infection to fifth instar silkworm larvae. It was found that nanoparticle (NP)-induced morphological transformation of BmNPV polyhedra could reduce the infectivity of BmNPV both in cell line and in silkworm larvae. Initially, 11 NPs were screened for evaluation of their nature of interaction with polyhedra surface through scanning electron microscopy. Amongst these NPs, lipophilically coated silica nanoparticle (SNPL), alumina nanoparticles in the hexagonal close-packed a structure and aspartate capped gold nanoparticle transformed polyhedra were tested for their infectivity in *B. mori* cell line using cytopathic effect and plaque reduction assay. SNPL was evaluated for its bio-efficacy in fifth instar silkworm larvae. The study of polyhedra morphology as a function of NP concentration showed severe 'roughening' of the polyhedra with replacement of the regular facets by a large number of irregular ones by SNPL, and this caused transition of highly infectious polyhedra into a nearly spherical, non-infectious structure. A moderate polyhedra roughening was observed for alumina NPs, and no roughening was noticed for gold NPs. The morphological changes could be correlated with reduction of virus-induced cytopathic effect and plaque formation, and increased survival rate of SNPL transformed polyhedra infected silkworm larvae to 70.09 +/- 6.61 % after 96 h. In this group, 61.04 +/- 8.03 % larvae formed normal cocoons from which moths eclosed, laid eggs and larvae emerged. This study could lead to open up newer pathways for designing nano pharmaceuticals to combat other viral diseases.

Sumistha Das†; Ankita Bhattacharya†; Nitai Debnath†; Alokmay Datta; et al

2.2.2.43 Structural and microstructural characterizations of nanocrystalline hydroxyapatite synthesized by mechanical alloying

Single phase nanocrystalline hydroxyapatite (HAp) powder has been synthesized by mechanical alloying the stoichiometric mixture of CaCO₃ and CaHPO₄ powders in open air at room temperature, for the first time, within 2 h of milling. Nanocrystalline hexagonal single crystals are obtained

by sintering of 2 h milled sample at 500 degrees C. Structural and microstructural properties of as-milled and sintered powders are revealed from both the X-ray line profile analysis and transmission electron microscopy. Shape and lattice strain of nanocrystalline HAp particles are found to be anisotropic in nature. Particle size of HAp powder remains almost invariant up to 10 h of milling and there is no significant growth of nanocrystalline HAp particles after sintering at 500 degrees C for 3 h. Changes in lattice volume and some primary bond lengths of as-milled and sintered are critically measured, which indicate that lattice imperfections introduced into the HAp lattice during ball milling have been reduced partially after sintering the powder at elevated temperatures. We could achieve similar to 96.7% of theoretical density of HAp within 3 h by sintering the pellet of nanocrystalline powder at a lower temperature of 1000 degrees C. Vickers microhardness (VHN) of the uni-axially pressed (6.86 MPa) pellet of nanocrystalline HAp is 4.5 GPa at 100 gm load which is close to the VHN of bulk HAp sintered at higher temperature. The strain-hardening index (n) of the sintered pellet is found to be >2 , indicating a further increase in microhardness value at higher load.

S Lala†; B Satpati; T Kar†; et al

2.2.2.44 Morphology and chemical properties of silver-triblock copolymer nanocomposite thin films

The triblock copolymer PEO-PPO-PEO is thermoresponsive and have demonstrated excellent properties to act as a reducing as well as capping agent for synthesis of metal nanoparticles. Effect of reaction temperature in growth, morphology and chemical properties of self-assembled structures of silver PEO -PPO-PEO nanocomposites on silicon substrates is described here. The polymer-metal composites are deposited on hydrophilic and hydrophobic silicon substrates through adsorption from solution at different temperatures. Morphologies of the nanocomposite films observed by SEM are strongly dependent on reaction temperature as well as on philicity/phobicity of silicon substrates. Detailed investigations of the chemical properties of nanocomposite materials are performed using XPS and NEXAFS. At lower reaction temperatures, mainly thermoresponsive behavior of the copolymer controls nanocomposite formation and their organization on the substrates. Whereas at higher reaction temperatures, chemical nature of the copolymer that directly take part in the reaction is changed drastically and alters the nanocomposite formation process as well as the nature of self-assembly. The resemblance in spectroscopic data of this modified/degraded copolymer with that of fatty acid molecules indicate formation of fatty acid-like molecules at higher temperature.

AKM Maidul Islam; S Mukherjee†; S Nannarone†; M Mukherjee

2.2.2.45 Wetting and Surface Energy of Vertically Aligned Silicon Nanowires

The vertically aligned silicon nanowires (SiNWs) have been synthesized by metal assisted chemical etching process on commercially available p type silicon wafer. The aspect ratios of the SiNWs have been modified by simply varying the etching time. The microstructures of the as prepared samples have been investigated with the field emission scanning electron microscope as well as with a high resolution transmission electron microscope. The bonding information has been obtained by Fourier transformed infrared spectroscopy and X-ray photoelectron spectroscopy. The contact angles for water with the as-prepared SiNWs films were measured and found to be highly dependent upon the aspect ratio of the as synthesized wires. For obtaining a deep insight regarding

the reasons behind this dependence the surface energies of the as prepared SiNWs films have been calculated by Owens method using two liquids, water and glycerol. The porosity of the films has been calculated indirectly from the equilibrium equations. It has been found that the etching time has a profound effect on the aspect ratio and thus on the surface energy of SiNWs that governs the wetting behaviour of the as prepared samples.

S Jana; S Mondal; SR Bhattacharyya

2.2.2.46 Microstructure and optical characterizations of mechanosynthesized nanocrystalline (Ti_{0.9}Si_{0.1})N

The nanostructured (Ti_{0.9}Si_{0.1})N powder has been mechanosynthesized by ball-milling the elemental stoichiometric mixture of alpha-Ti (0.9 mol fraction) and Si (0.1 mol fraction) powders at room temperature under nitrogen atmosphere. After 1 h of milling, the alpha-Ti (hcp) phase partially transformed to metastable beta-Ti (cubic) phase and the initiation of (Ti_{0.9}Si_{0.1})N (fcc) phase is noticed. Completely stoichiometric nanocrystalline (Ti_{0.9}Si_{0.1})N phase is obtained after 7 h of milling. Microstructure of unmilled and ball-milled powders is characterized by analyzing their XRD patterns employing the Rietveld structure refinement method and by HRTEM images. The analysis reveals the inclusion of Si and nitrogen atoms into the Ti lattice on the way to formation of (Ti_{0.9}Si_{0.1})N phase. Presence of Si and nitrogen in the ball milled powders is also confirmed from EDX spectra. The average size of almost monodispersed spherical particles of (Ti_{0.9}Si_{0.1})N is similar to 4 nm. Optical band gaps of TiN and TiSiN powders are measured from UV-vis absorption spectra and it has been found that the optical band gap of highly insulating TiN nanoparticles (band gap similar to 5.56 eV) can be substantially reduced towards semiconductors (band gap similar to 3.96 eV) by incorporating a small amount of Si into TiN matrix.

UK Bhaskar†; B Satpati; SK Pradhan†

2.2.2.47 Direct Experimental Evidence of Nucleation and Kinetics Driven Two-Dimensional Growth of Core-Shell Structures

We report the appearance of different anisotropic one-dimensional (1D) and two-dimensional (2D) gold (Au) core-silver (Ag) shell nanostructures in a single reaction environment. High-resolution transmission electron microscopy (HRTEM) images taken from the core region of a core shell nanostructure revealed the prominent presence of the hexagonal-shaped gold seed leading to formation of a triangular final particle. The HRTEM studies provide the direct experimental evidence of the "silver halide" model proposed by Sigmund et al. (Lofton, C.; Sigmund, W. *Adv. Funct Mater.* 2005, 15, 1197-1208) to explain the kinetic growth mechanism behind their formation. It is important that this information cannot be identified from a single composite nanoparticle due to the lack of atomic number (Z) contrast difference. We have studied energy-dispersive X-ray line profile spectra and elemental mapping using the high-angle annular dark-field scanning/transmission electron microscopy (STEM-HAADF) technique corresponding to the Au-M and Ag-K energies from the similar core shell structures. This confirms the composition of the core to be made of gold and that of the shell of silver. The line profile along the relative thickness map of a hexagonal and triangular nanoplate obtained using energy-filtered TEM indicates the formation of nearly uniform 2D structures. The nearly equal thicknesses of the core and outside shell of a core shell nanoplate measured using electron energy loss spectroscopy in STEM mode also confirm the 2D growth of a

gold seed forming a triangular core shell nanoplate.

Tanmay Ghosh; Biswarup Satpati

2.2.2.48 Influence of Si substitution on the structure, magnetism, exchange bias and negative magnetoresistance in $\text{Ni}_{48}\text{Mn}_{39}\text{Sn}_{13}\text{Si}_x$ Heusler alloys

The effect of partial Si substitution for Sn on the structure, magnetism, magnetic entropy change, exchange bias and negative magnetoresistance in $\text{Ni}_{48}\text{Mn}_{39}\text{Sn}_{13-x}\text{Si}_x$ ($1 \leq x \leq 4$) Heusler alloy systems is investigated. A small amount of Si in the Sn position influences the characteristic transition temperatures and the magnetocaloric effect. A maximum positive entropy change of $5.13 \text{ J kg}^{-1} \text{ K}^{-1}$ is observed for a field change of 9 T in the $\chi=1$ alloy. An increase in Si content increases the exchange bias field. The exchange bias field and the coercive field strongly depend on the Si content. For the $\chi=4$ alloy, an exchange bias field of 354 Oe is observed. In addition, a negative magnetoresistance is observed in this alloy system, which decreases with Si content. The increase in resistivity at the martensitic transition could be attributed to the formation of superzone boundary gaps that changes the density of states near the Fermi surface.

S Esakki Muthu†; Sanjay Singh; R Thiyagarajan†; et al

2.2.2.49 Destruction of ferromagnetism in Cu-doped ZnO upon thermal annealing: role of oxygen vacancy

We report on the role that oxygen vacancies have in determining the magnetic properties of Cu-doped ZnO. The observed magnetic hysteresis and the temperature dependence (irreversibility) of magnetization behave like supermoments blocked along random directions for a low-temperature annealed sample. The magnetic hysteresis (finite coercivity and low field saturation) and the irreversibility of temperature-dependent magnetization are destroyed upon thermal annealing. We propose that oxygen vacancies play an important role in inducing supermoments to explain the observations.

B Ghosh; M Sardar†; S Banerjee

2.2.2.50 Preparation of manganese-doped ZnO thin films and their characterization

In this study, pure and manganese-doped zinc oxide (Mn:ZnO) thin films were deposited on quartz substrate following successive ion layer adsorption and reaction (SILAR) technique. The film growth rate was found to increase linearly with number of dipping cycle. Characterization techniques of XRD, SEM with EDX and UV-visible spectra measurement were done to investigate the effect of Mn doping on the structural and optical properties of Mn:ZnO thin films. Structural characterization by X-ray diffraction reveals that polycrystalline nature of the films increases with increasing manganese incorporation. Particle size evaluated using X-ray line broadening analysis shows decreasing trend with increasing manganese impurification. The average particle size for pure ZnO is 29 center dot 71 nm and it reduces to 23 center dot 76 nm for 5% Mn-doped ZnO. The strong preferred c-axis orientation is lost due to manganese (Mn) doping. The degree of polycrystallinity increases and the average microstrain in the films decreases with increasing Mn incorporation. Incorporation of

Mn was confirmed from elemental analysis using EDX. As the Mn doping concentration increases the optical bandgap of the films decreases for the range of Mn doping reported here. The value of fundamental absorption edge is 3 center dot 22 eV for pure ZnO and it decreases to 3 center dot 06 eV for 5% Mn:ZnO.

S Mondal†; SR Bhattacharyya; P Mitra†

2.2.2.51 Reinforcing effect of reclaim rubber on natural rubber/polybutadiene rubber blends

Mechanochemically devulcanized ground rubber tire (GRT) was revulcanized in a composition with natural rubber (NR) and polybutadiene rubber (PBR). Reclaiming of GRT was carried out by tetra methyl thiuram disulfide (TMTD) in the presence of spindle oil, a paraffin base rubber process oil. The cure characteristics and tensile properties of NR/PBR compounds were investigated. Results indicate that the minimum torque and Mooney viscosity of the NR/PBR compounds increase with increasing reclaim rubber (RR) loading whereas the scorch time remains unaltered but optimum cure time exhibits a decreasing trend due to the presence of active crosslinking sites in the reclaim rubber. The (re) vulcanization of different NR-PBR/RR blends was found to give a new low cost product with adequate properties. The mechanical properties before and after aging of NR-PBR/RR blend system and different proportions of carbon black loaded NR-PBR/RR blend system were studied. Tensile strength increases with increasing the proportion of reclaim rubber, but for all the vulcanizates the values are less than those of the control formulation. Thermogravimetric analysis of RR, NR-PBR and different NR-PBR/RR vulcanizates was carried out in order to get thermal stability of the vulcanizates. The effects of variations of RR loading on dynamic mechanical properties like loss tangent, storage and loss modulus were studied.

Debapriya De†; Prabir Kr Panda†; Madhusudan Roy; Satyaban Bhunia

2.2.2.52 Solventless synthesis of hematite nanoparticles using ferrocene

Ferrite nanoparticles of 40 nm size have been obtained under the thermal decomposition of bis-(cyclopentadienyl)iron-ferrocene in the presence of oxalic acid at 453 K. The solventless solid state thermal reaction has been monitored by thermogravimetry. Morphology and structure of the ferrites obtained are investigated by scanning electron microscopy and X-ray powder diffraction technique, respectively, while the magnetic property of these materials are studied by dc magnetization study as well as Fe-57 Mossbauer spectroscopy. The results, observed from X-ray powder diffraction, magnetization measurement and Mossbauer spectroscopy, establish unequivocally that the ferrite materials obtained are hematite. The solid state reaction process has been discussed too. To the best of our knowledge, the presently observed solid state reaction leading to the formation of hematite nanoparticles using ferrocene takes place at the lowest temperature reported so far.

A Bhattacharjee; A Roop; M Roy; et al

2.2.2.53 The hydrophilic/hydrophobic nature of a Cl-terminated Si surface

The hydrophilic/hydrophobic nature of a Cl-terminated Si surface, which is slightly controversial, was investigated on the molecular level by depositing CTAB-silica 2D-hexagonal mesostructured

films on it as well as on OH- and H-terminated Si surfaces and determining their structures by combining X-ray reflectivity and grazing incidence small angle X-ray scattering measurements. The contact angle measurements, which provide macroscopic level information, confirm that the Cl-Si surface is hydrophilic in nature but less hydrophilic than the OH-Si surface. The initial attachment of a film (through a silica layer) and the (near circular) shape of the micelles, which provide microscopic level information, clearly indicate that the Cl-Si surface is hydrophilic in nature and its hydrophilicity is comparable to that of the OH-Si surface. The relatively strong electronegativity of Cl is probably the reason for the hydrophilic nature of the Cl-Si surface, while the lack of hydrogen bonding and/or the lack of complete chlorination are a hindrance.

Paramita Chatterjee; Satyajit Hazra

2.2.2.54 Enhanced vacuum-photoconductivity of chemically synthesized ZnO nanostructures

We report on the enhanced ultraviolet (UV) photoconductivity of zinc oxide (ZnO) nanostructures in vacuum. Nanoparticles and nanorods of ZnO were fabricated using a simple cost-effective solid state grinding method. Morphology of the nanostructures was studied using transmission electron microscopy, while the optical properties were investigated using UV-visible absorption and photoluminescence spectroscopy. The emission spectra of the nanostructures revealed the existence of various native defect states of ZnO and also indicated the presence of surface adsorbed water molecules. In the photoconductivity measurements, although the ZnO nanoparticles exhibited lower photoconductivity in comparison to the nanorods, a similar trend of photoresponse was observed for both the cases. An initial decrease in the photoconductivity followed by a large enhancement was observed in vacuum compared to that in ambient condition. Such unusually increased photoconductivity has been correlated to the desorption of physisorbed water molecules from nanostructure surfaces under vacuum. This desorption is responsible for the rise in dark current and an initial decrease in photoconductivity. Continual UV irradiation in vacuum leads to the desorption of chemisorbed water molecules from the defect sites of the nanostructures, resulting in the occurrence of high photoconductivity.

Sayan Bayana; Sheo K Mishra; Purushottam Chakraborty; et al

2.2.2.55 A facile approach for in situ synthesis of graphene-branched-Pt hybrid nanostructures with excellent electrochemical performance

A facile and green approach for the synthesis of highly electroactive branched Pt nanostructures well dispersed on graphene has been developed by in situ reduction of graphene oxides and Pt(IV) ions in an aqueous medium. The as-synthesized branched Pt and graphene hybrid nanomaterials (GR-BPtNs) were thoroughly characterized using Transmission Electron Microscope (TEM), UV-Visible spectroscopy, Fourier transform infrared spectroscopy (FT-IR), thermogravimetric analysis (TGA) and Raman spectroscopy. This report clearly exploits the decisive role of the graphene support, the pH of the solution and the stabiliser on shaping the branched morphology of the Pt nanostructures well dispersed on graphene. Cyclic voltammetry, chronoamperometry and electrochemical impedance spectroscopy (EIS) measurements were employed to investigate the electrocatalytic performance and durability of GR-BPtNs towards methanol oxidation and oxygen reduction. The

results reveal that the synergetic effect of the graphene support and the branched morphology triggers electrocatalytic performance and robust tolerance to surface poisoning of GR-BPtNs.

Subash Chandra Sahu†; Aneeya K Samantara†, Biswarup Satpati

2.2.2.56 Synergistically controlled nano-templated growth of tunable gold bud-to-blossom nanostructures: a pragmatic growth mechanism

A novel nano-templating method with a unique nanocrystal growth mechanism has been introduced for the single-pot production of variable-size (110-360 nm), intrinsically monodispersed, single-shaped, tunable plasmonic (580-1300 nm) gold nanomaterials showing a man-made replica of nature's bud-to-blossom steps associated with the gigantic SERS activity. In the first growth step, we synthesized 45 +/- 3 nm gold nano-popcorns (GNPops) from 4.3 +/- 1.4 nm spherical gold nano-seeds, and in the second growth step, we used GNPops as templates for controlled overgrowth and to produce bigger gold nano-flowers (GNFs) simply by controlling the viscosity of the surfactant. TEM-based electron tomography (ET) of highly structured GNFs provides their actual morphology with no Bragg diffraction artefacts. Due to their broad plasmon tunability throughout the Vis-NIR region and extraordinarily high Raman activity, these materials are suitable for applications in tunable Plasmon spectroscopy, high-throughput Raman sensing and efficient photothermal therapy in the biological window.

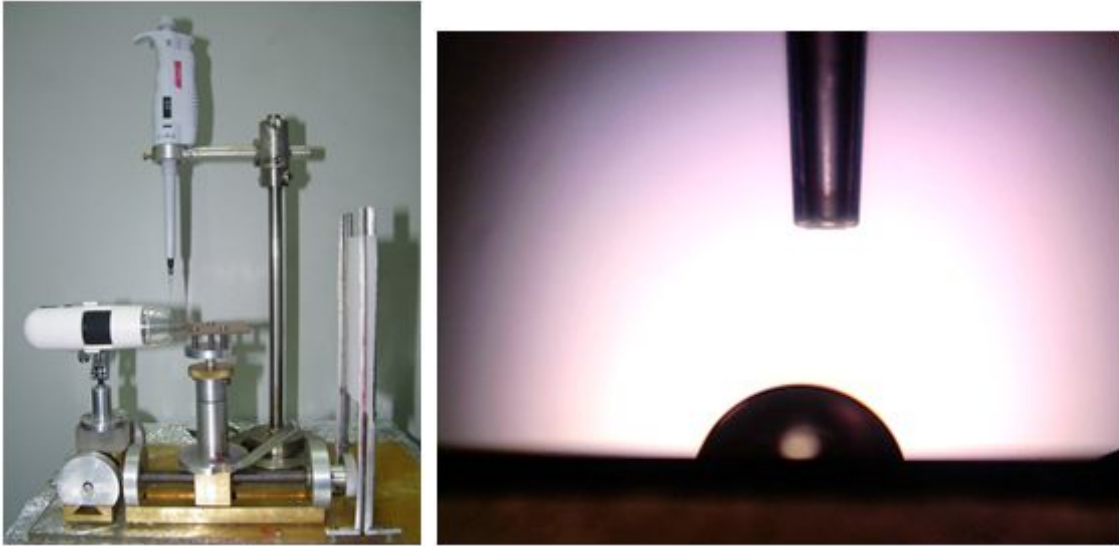
Munmun Bardhan; Biswarup Satpati; Tanmay Ghosh; Dulal Senapati

2.3 Developmental Work

2.3.1 Contact Angle Measurement System

One of the methods for surface energy estimation depends on correct measurement of contact angles. During contact angle measurement drop size, mechanical shock and evaporation of liquid are very important. Keeping all these in mind a setup for measuring static and dynamic contact angles of suitable liquid on various surfaces has been developed and is ready to work with. The whole instrument is designed and fabricated in this institute with the help of institute workshop very cost effectively.

This instrument is integrated by a digital microscope, sample stage, micropipette (21-201) and a light diffuser. The light diffuser is made by using flash light at the backside of stage. Magnification of the digital microscope is about 10X-300X, connected with computer for getting the video of liquid drop and contact angle is measured by using ImageJ software from the snap shot of the video in offline mode so that we can get the time evolution of contact angle.



This instrument is integrated by a digital microscope, sample stage, micropipette (2l-20l) and a light diffuser. The light diffuser is made by using flash light at the backside of stage. Magnification of the digital microscope is about 10X-300X, connected with computer for getting the video of liquid drop and contact angle is measured by using ImageJ software from the snap shot of the video in offline mode so that we can get the time evolution of contact angle.

Shyamal Mondal; Debraj Dey; Satyaranjan Bhattacharyya

2.4 Publications

2.4.1 Publications in Books/Monographs & Edited Volumes

i. Sputter-ripple formation on flat and rough surfaces a case study with Si - Safiul Alam Mollick and Debabrata Ghose in: Nanofabrication by Ion-Beam Sputtering: Fundamentals and Applications (Eds.: T Som and D Kanjilal), (Pan Stanford Publishing Pte Ltd, Singapore, 2013, p41)

2.4.2 Publications in Journal

2.4.2.1 Condensed Matter Physics

Arti Garg, HR Krishnamurthy†, Mohit Randeria†, Doping a Correlated Band Insulator: A New Route to Half-Metallic Behavior, *Physical Review Letters* **112** (2014) Art No: 106406

Amit Dey; Sudhakar Yarlagadda, Polaron dynamics and decoherence in an interacting two-spin system coupled to an optical-phonon environment, *Physical Review* **B89** (2014) Art No: 064311

Rakesh Chatterjee; Sakuntala Chatterjee†; Punyabrata Pradhan†; et al, Interacting particles in a periodically moving potential: Traveling wave and transport, *Physical Review* **E89** (2014) Art No: 022138

Papri Dasgupta; S Mukherjee†; RN Bhowmik†; Asok Poddar, Chandan Mazumdar, R Ranganathan, Enhanced dielectric response of Gd₂Ti₂O₇ nanoparticles in SiO₂ matrix, *Materials Research Bulletin* **50** (2014) 26

Sayani Chatterjee; Punyabrata Pradhan; PK Mohanty, Gammalike Mass Distributions and Mass Fluctuations in Conserved-Mass Transport Processes, *Physical Review Letters* **112** (2014) Art No: 030601

Moumita Nandi; Nazir Khan; Dilip Bhoi; et al, Field-Induced Spin-Structural Transition and Giant Magnetostriction in Ising Chain α -CoV₂O₆, *Journal of Physical Chemistry* **C118** (2014)1668

Abhik Basu; Ali Naji†; Rahul Pandit†, Structure-function hierarchies and von Karman-Howarth relations for turbulence in magnetohydrodynamical equations, *Physical Review* **E89** (2014) Art No: 012117

SK Giri†; Papri Dasgupta; A Poddar; et al, Field induced ferromagnetic phase transition and large magnetocaloric effect in Sm_{0.55}Sr_{0.45}MnO₃ phase separated manganites, *Journal of Alloys and Compounds* **582** (2014)609

Mahashweta Basu; Nitai P Bhattacharyya; PK Mohanty, Distribution of microRNA co-targets exhibit universality across a wide class of species, *EPL* **105** (2014)Art No: 28007

Jishad Kumar, Quantum dynamics of a dissipative and confined cyclotron motion, *Physica* **A393** (2014) 182

Satyaki Kar; Tanusri Saha-Dasgupta†, Quasi-2D J(1)-J(2) antiferromagnet Zn₂VO(PO₄)(₂) and its Ti-substituted derivative: A spin-wave analysis, *Physica* **B432** (2014)71

M Ghosh; K Ghoshray; M Majumder; Amitabha Ghoshray, Low energy spin dynamics in trimer spin chain compound Ca₃Cu₂Ni(PO₄)(₄): P-31 NMR study, *Physica* **B431** (2013) 19

Sourish Bondyopadhyay, Dependence of asymptotic decay exponents on initial condition and the resulting scaling violation, *Physical Review* **E88** (2013)Art No: 062125

Debarshee Bagchi, Thermal rectification and negative differential thermal resistance in a driven two segment classical Heisenberg chain, *Journal of Physics-Condensed Matter* **25** (2013)Art No: 496006

Malik†; Diptasikha Das†; S Bandyopadhyay†; P Mandal...Velaga Srihari, et al, Temperature-dependent structural property and power factor of n type thermoelectric Bi_{0.90}Sb_{0.10} and Bi_{0.86}Sb_{0.14} alloys, *Applied Physics Letters* **103** (2013)Art No: 242108

Debarshee Bagchi, Thermally driven classical Heisenberg model in 1D with a local time varying field, *Journal of Statistical Mechanics-Theory and Experiment,* Art No: P12005 (2013)

RN Bhowmik†; V Vasanthi†; Asok Poddar, Alloying of Fe₃O₄ and Co₃O₄ to develop Co_{3x}Fe_{3(1-x)}O₄ ferrite with high magnetic squareness, tunable ferromagnetic parameters, and exchange bias, *Journal of Alloys and Compounds* **578** (2013)585

Ujjal Chowdhury†; Sudipta Goswami†; Dipten Bhattacharya†; Arindam Midya; P Mandal; et al, Large magnetocapacitance in electronic ferroelectric manganite systems, *Journal of Applied Physics* **114** (2013)Art No: 194104

Niladri Sarkar; Abhik Basu; Jayanta K Bhattacharjee†; et al, Acoustic horizons in steady spherically symmetric nuclear fluid flows, *Physical Review* **C88** (2013)Art No: 055205

Asim Ghosh; Bikas K Chakrabarti, Response of the two-dimensional kinetic Ising model under a stochastic field, *Journal of Statistical Mechanics-Theory and Experiment* (2013) Art No: P11015

Moumita Dey; Santanu K Maiti†; Sreekantha Sil†; et al, Spin-orbit interaction induced spin selective transmission through a multi-terminal mesoscopic ring, *Journal of Applied Physics* **114** (2013)Art No: 164318

Soumyajyoti Biswas; Bikas K Chakrabarti, Self-organized dynamics in local load-sharing fiber bundle models, *Physical Review* **E88** (2013)Art No: 042112

Niladri Sarkar; Abhik Basu, Phases and fluctuations in a model for asymmetric inhomogeneous fluid membranes, *Physical Review* **E88** (2013)Art No: 042106

R Ramakumar†; AN Das, Lattice bosons in a quasi-disordered environment, *Physica* **A392** (2013)4271

Mayukh K Ray; K Bagani; RK Singh†...S Banerjee, Microstructure, magnetic and electrical transport properties of melt-spun Ni-Mn-Sb ribbons, *Journal of Applied Physics* **114** (2013)Art No: 123904

Soumyajyoti Biswas; Purusattam Ray†; Bikas K Chakrabarti, Equivalence of the train model of earthquake and boundary driven Edwards-Wilkinson interface, *European Physical Journal* **B86** (2013)Art No: 388

S Dey; SK Dey; B Ghosh; P Dasgupta; A Poddar; et al, Role of inhomogeneous cation distribution in magnetic enhancement of nanosized $\text{Ni}_{0.35}\text{Zn}_{0.65}\text{Fe}_2\text{O}_4$: A structural, magnetic, and hyperfine study, *Journal of Applied Physics* **114** (2013)Art No: 093901

A Midya; N Khan; D Bhoi; P Mandal, 3d-4f spin interaction induced giant magnetocaloric effect in zircon-type DyCrO_4 and HoCrO_4 compounds, *Applied Physics Letters* **103** (2013) Art No: 092402

D Bhoi; N Khan; A Midya...P Mandal, Formation of Nanosize Griffiths-like Clusters in Solid Solution of Ferromagnetic Manganite and Cobaltite, *Journal of Physical Chemistry* **C117** (2013) 16658

Niladri Sarkar; Abhik Basu, Generic instabilities in a fluid membrane coupled to a thin layer of ordered active polar fluid, *European Physical Journal* **E36** (2013)Art No: 86

Paramita Dutta; Santanu K Maiti†; SN Karmakar, Positional dependence of energy gap on line

defect in armchair graphene nanoribbons: Two-terminal transport and related issues, *Journal of Applied Physics* **114** (2013) Art No: 034306

Srutarshi Pradhan; Anjan Kumar Chandra; Bikas K Chakrabarti, Noise-induced rupture process: Phase boundary and scaling of waiting time distribution, *Physical Review* **E88** (2013) Art No: 012123

Analabha Roy, Nonequilibrium dynamics of ultracold Fermi superfluids, *European Physical Journal-Special Topics* **222** (2013) 975

PK Mondal; BK Chatterjee†, Study of gamma ray response of R404A superheated droplet detector using a two-state model, *Applied Radiation and Isotopes* **77**(2013) 61

E Alleno; C Mazumdar, Magnetic structures in RNi₄B (R=Nd, Tb, Ho, Er), *Journal of Solid State Chemistry* **202** (2013) 15

Mahashweta Basu; Nitai P Bhattacharyya; Pradeep K Mohanty, Comparison of Modules of Wild Type and Mutant Huntingtin and TP53 Protein Interaction Networks: Implications in Biological Processes and Functions, *PLOS One* **8** (2013) Art No: UNSP e64838

S Esakki Muthu†; Sanjay Singh; R Thiyagarajan†; et al, Influence of Si substitution on the structure, magnetism, exchange bias and negative magnetoresistance in Ni₄₈Mn₃₉Sn₁₃ Heusler alloys, *Journal of Physics* **D46** (2013) Art No: 205001

Rangana Bhattacharya; AI Jaman, Microwave spectral studies of 2, 4-difluorobenzaldehyde: O-trans conformer (vol 1039C, pg 174, 2013), *Journal of Molecular Structure* **1040** (2013) 254

Analabha Roy; Raka Dasgupta†; Sanhita Modak†; et al, Periodic dynamics of fermionic superfluids in the BCS regime, *Journal of Physics-Condensed Matter* **25** (2013) Art No: 205703

M Majumder; K Ghoshray; A Ghoshray; et al, Local electromagnetic properties of magnetic pnictides: a comparative study probed by NMR measurements, *Journal of Physics-Condensed Matter* **25** (2013) Art No: 196002

D Bhoi; P Mandal; P Choudhury†, Vortex dynamics and second magnetization peak in PrFeAsO_{0.60}F_{0.12} superconductor, *Journal of Applied Physics* **113** (2013) Art No: 183902

N Khan; A Midya; P Mandal; et al, Critical exponents and irreversibility lines of La_{0.9}Sr_{0.1}CoO₃ single crystal, *Journal of Applied Physics* **113** (2013) Art No: 183909

Anis Biswas†; Sayan Chandra†; Tapas Samanta...I Das; et al, The universal behavior of inverse magnetocaloric effect in antiferromagnetic materials, *Journal of Applied Physics* **113** (2013) Art No: 17A902

U Basu; M Basu; PK Mohanty, Absorbing phase transition in energy exchange models, *European Physical Journal* **B86** (2013) Art No: 236

Anis Biswas†; Sayan Chandra†; Tapas Samanta...I Das; et al, Universality in the entropy change

for the inverse magnetocaloric effect, *Physical Review* **B87** (2013) Art No: 134420

Rajib Nath†; AK Raychaudhuri†; Ya M Mukovskii†...P Mandal, Electric field driven destabilization of the insulating state in nominally pure LaMnO_3 , *Journal of Physics-Condensed Matter* **25** (2013) Art No: 155605

Anjan Kumar Chandra, Dynamical percolation transition in the two-dimensional ANNNI model, *Journal of Physics-Condensed Matter* **25** (2013) Art No: 136002

Soumyajyoti Biswas; Bikas K Chakrabarti, Crossover behaviors in one and two dimensional heterogeneous load sharing fiber bundle models, *European Physical Journal* **B86** (2013) Art No: 160

K Sengupta; KK Iyer†; R Ranganathan; et al, Electronic transport minimum in SmCuAs_2 at low temperatures and structural anomalies, *Solid State Communications* **159** (2013) 29

Barnana Pal; S Kundu, Anomalous Ultrasonic Attenuation in Aqueous NaCl Solutions, *Universal Journal of Chemistry* **1** (2013) 96

2.4.2.2 Surface Physics and Material Science

SA Mollick; D Ghose; SR Bhattacharyya; S Bhunia; NR Ray, et al, Synthesis of SiGe layered structure in single crystalline Ge substrate by low energy Si ion implantation, *Vacuum* **101** (2014)387

Amaresh Metya; Debabrata Ghose; Nihar Ranjan Ray, Development of hydrophobicity of mica surfaces by ion beam sputtering, *Applied Surface Science* **293** (2014)18

SK Jana; VP Rao; S Banerjee, Enhancement of supercapacitance property of electrochemically deposited MnO_2 thin films grown in acidic medium, *Chemical Physics Letters* **593** (2014) 160

Sanjay Singh; S Esakki Muthu†; A Senyshyn†...SR Barman, Inverse magnetocaloric effect in Mn_2NiGa and $\text{Mn}_{1.75}\text{Ni}_{1.25}\text{Ga}$ magnetic shape memory alloys, *Applied Physics Letters* **104** (2014)Art No: 051905

Somen Goswami; Rajat Saha; Ian M Steele...Papri Dasgupta; Asok Poddar; et al, An unusual μ -(1,2,3)-squarato-bridged two dimensional coordination polymer: Crystal structure, thermal, photoluminescence and magnetic studies, *Inorganica Chimica Acta* **410** (2014)111

Safiul Alam Mollick; Debabrata Ghose; Patrick D Shipman†; et al, Anomalous patterns and nearly defect-free ripples produced by bombarding silicon and germanium with a beam of gold ions, *Applied Physics Letters* **104** (2014)Art No: 043103

S Esakki Muthu†; M Kanagaraj†; Sanjay Singh; et al, Hydrostatic pressure effects on martensitic transition, magnetic and magnetocaloric effect in Si doped Ni-Mn-Sn Heusler alloys, *Journal of Alloys and Compounds* **584** (2014) 175

K Bagani; A Bhattacharya; J Kaur; A Rai Chowdhury; B Ghosh...S Banerjee, Anomalous be-

haviour of magnetic coercivity in graphene oxide and reduced graphene oxide, *Journal of Applied Physics* **115** (2014) Art No: 023902

Mojammel H Mondal; M Mukherjee, Study of density-dependent swelling of ultrathin water soluble polymer films, *Journal of Polymer Research* **21** (2004) Art No: 343

Tanmay Ghosh; Biswarup Satpati; Dulal Senapati, Characterization of bimetallic core-shell nanorings synthesized via ascorbic acid-controlled galvanic displacement followed by epitaxial growth, *Journal of Materials Chemistry* **C2** (2014) 2439

Kamala Kanta Nanda†; Smrutirekha Swain†; Biswarup Satpati; et al, Facile synthesis and the photo-catalytic behavior of core-shell nanorods, *RSC Advances* **4** (2014) 10928

Debasree Chowdhury; Debabrata Ghose; Biswarup Satpati, Production of ordered and pure Si nanodots at grazing ion beam sputtering under concurrent substrate rotation, *Materials Science and Engineering* **B179** (2014) 1

Safiqul Alam Mollick; Debabrata Ghose; Biswarup Satpati, Formation of Au-Ge nanodots by Au-ion sputtering of Ge, *Vacuum* **99** (2014) 289

MU Anu Prathap†; Rajendra Srivastava†; Biswarup Satpati, Simultaneous detection of guanine, adenine, thymine, and cytosine at polyaniline/MnO₂ modified electrode, *Electrochimica Acta* **114** (2014) 285

Paramita Kar Choudhury†; S Banerjee; S Ramaprabhu†; et al, Variations in Magnetic Properties of Nanostructured Nickel, *Journal of Nanoscience and Nanotechnology* **13** (2013) 8162

Rajkumar Kore†; Rajendra Srivastava†; Biswarup Satpati, Highly Efficient Nanocrystalline Zirconosilicate Catalysts for the Aminolysis, Alcoholysis, and Hydroamination Reactions, *ACS Catalysis* **3** (2013) 2891

Kuriakose Sini†; Neha Bhardwaj†; Jaspal Singh†; Biswarup Satpati; et al, Structural, optical and photocatalytic properties of flower-like ZnO nanostructures prepared by a facile wet chemical method, *Beilstein Journal of Nanotechnology* **4** (2013) 763

MU Anu Prathap†; V Anuraj†; Biswarup Satpati; et al, Facile preparation of Ni(OH)₂-MnO₂ hybrid material and its application in the electrocatalytic oxidation of hydrazine, *Journal of Hazardous Materials* **262** (2013) 766

Johan B Malherbe†; NG van der Berg†; AJ Botha...P Chakraborty; et al, SEM analysis of ion implanted SiC, *Nuclear Instruments & Methods in Physics Research* **B315** (2013) 136

B Ghosh; M Sardar†; S Banerjee, Effect of antisite formation on magnetic properties of nickel zinc ferrite particles, *Journal of Applied Physics* **114** (2013) Art No: 183903

Partha Sarathi Roy†; Amallesh Samanta†; Manabendra Mukherjee; et al, Designing Novel pH-Induced Chitosan-Gum Odina Complex Coacervates for Colon Targeting, *Industrial & Engineering Chemistry Research* **52** (2013) 15728

Kalipada Das; R Rawat†; B Satpati et al, Giant enhancement of magnetoresistance in core-shell ferromagnetic-charge ordered nanostructures, *Applied Physics Letters* **103** (2013)Art No: 202406

Emilie Franceschini†; Ratan K Saha; Guy Cloutier†, Comparison of Three Scattering Models for Ultrasound Blood Characterization, *IEEE Transactions on Ultrasonics Ferroelectrics and Frequency Control* **60** (2013)2321

Balwinder Kaur†; Thangarasu Pandiyan†; Biswarup Satpati; et al, Simultaneous and sensitive determination of ascorbic acid, dopamine, uric acid, and tryptophan with silver nanoparticles-decorated reduced graphene oxide modified electrode, *Colloids and Surfaces* **B111** (2013)97

S Mahaboob Jilani†; Tanesh D Gamot†; P Banerji†; S Chakraborty, Studies on resistive switching characteristics of aluminum/graphene oxide/semiconductor nonvolatile memory cells, *Carbon* **64** (2013) 187

I Sarkar†; A Sarma; MK Sanyal; et al, Core level photoemission studies on conducting polypyrrole polymer nanotubes showing switching transitions, *Journal of Applied Physics* **114** (2013)Art No: 163707

Amaresh Metya; Debabrata Ghose, Investigation of ion beam induced nanopattern formation near the threshold energy, *Applied Physics Letters* **103** (2013) Art No: 161602

Pabitra Das; Abhitosh Kedia†; Pandian Senthil Kumar†...Tapas Kumar Chini, Local electron beam excitation and substrate effect on the plasmonic response of single gold nanostars, *Nanotechnology* **24** (2013)Art No: 405704

Sandeep Agarwal†; S Banerjee; PK Mukhopadhyay, Crossover of spin glass characteristics as a function of field in an NiMnSnAl alloy, *Journal of Applied Physics* **114** (2013)Art No: 133904

Santanu Maiti; Milan K Sanyal; Neenu Varghese†; et al, Formation of single-crystalline CuS at the organic-aqueous interface, *Journal of Physics-Condensed Matter* **25** (2013)Art No: 395401

Ashis Bhattacharjee; Haradhan Mandal†; Madhusudan Roy; et al, Comparative study of the microstructural and magnetic properties of fly ashes obtained from different thermal power plants in West Bengal, India, *Environmental Monitoring and Assessment* **185** (2013)8673

D Talukdar; P Yotprayoosak; O Herranen; et al, Linear current fluctuations in the power-law region of metallic carbon nanotubes, *Physical Review* **B88** (2013)Art No: 125407

Atikur Rahman; Milan K Sanyal, Correlated Charge Carrier-like Photoresponse of Polymer Nanowires, *ACS Nano* **7** (2013) 7894

MU Anu Prathap†; Biswarup Satpati; Rajendra Srivastava†, Facile preparation of polyaniline/MnO₂ nanofibers and its electrochemical application in the simultaneous determination of catechol, hydroquinone, and resorcinol, *Sensors and Actuators* **B186** (2013)67

Sirshendu Gayen; Milan K Sanyal; Biswarup Satpati; et al, Diameter-dependent coercivity of cobalt

nanowires, Applied Physics **A112** (2013)775

Dipanwita Majumdar; Achintya Singha†; Prasanna Kumar Mondal; et al, DNA-Mediated Wirelike Clusters of Silver Nanoparticles: An Ultrasensitive SERS Substrate, ACS Applied Materials & Interfaces **5** (2013) 7798

Sumona Sinha; M Mukherjee, Thickness dependent electronic structure and morphology of rubrene thin films on metal, semiconductor, and dielectric substrates, Journal of Applied Physics **114** (2013) Art No: 083709

U Devarajan†; S Esakki Muthu†; S Arumugam†; Sanjay Singh; SR Barman, Investigation of the influence of hydrostatic pressure on the magnetic and magnetocaloric properties of Ni_{2-X}Mn_{1+X}Ga (X=0, 0.15) Heusler alloys, Journal of Applied Physics **114** (2013) Art No: 053906

M Mukherjee; M Souheib Chebil†; Nicolas Delorme†; et al, Power law in swelling of ultra-thin polymer films, Polymer **54** (2013)4669

Ratan K Saha; Subhajit Karmakar; Madhusudan Roy, Photoacoustic response of suspended and hemolyzed red blood cells, Applied Physics Letters **103** (2013) Art No: 044101

Sumistha Das; Ankita Bhattacharya; Nitai Debnath†; et al, Nanoparticle-induced morphological transition of Bombyx mori nucleopolyhedrovirus: a novel method to treat silkworm grasserie disease, Applied Microbiology and Biotechnology **97** (2013)6019

S Lala†; B Satpati; T Kar†; et al, Structural and microstructural characterizations of nanocrystalline hydroxyapatite synthesized by mechanical alloying, Materials Science & Engineering C-Materials for Biological Applications **33** (2013) 2891

AKM Maidul Islam; S Mukherjee; S Nannarone†; et al, Morphology and chemical properties of silver-triblock copolymer nanocomposite thin films, Materials Chemistry and Physics **140** (2013)284

S Jana; S Mondal; SR Bhattacharyya, Wetting and Surface Energy of Vertically Aligned Silicon Nanowires, Journal of Nanoscience and Nanotechnology **13** (2013)3983

UK Bhaskar†; B Satpati; SK Pradhan, Microstructure and optical characterizations of mechanosynthesized nanocrystalline (Ti_{0.9}Si_{0.1})N, Powder Technology **241** (2013)28

Tanmay Ghosh; Biswarup Satpati, Direct Experimental Evidence of Nucleation and Kinetics Driven Two-Dimensional Growth of Core-Shell Structures, Journal of Physical Chemistry **C117** (2013) 10825

B Ghosh; M Sardar†; S Banerjee, Destruction of ferromagnetism in Cu-doped ZnO upon thermal annealing: role of oxygen vacancy, Journal of Physics **D46** (2013) Art No: 135001

S Mondal; SR Bhattacharyya; P Mitra†, Preparation of manganese-doped ZnO thin films and their characterization, Bulletin of Materials Science **36** (2013) 223

Debapriya De; Prabir Kr Panda†; Madhusudan Roy; et al, Reinforcing effect of reclaim rubber

on natural rubber/polybutadiene rubber blends, *Materials & Design* **46** (2013)142

A Bhattacharjee; A Roj; M Roy; et al, Solventless synthesis of hematite nanoparticles using ferrocene, *Journal of Materials Science* **48** (2013) 2961

Subash Chandra Sahu†; Aneeya K Samantara†, Biswarup Satpati, A facile approach for in situ synthesis of graphene-branched-Pt hybrid nanostructures with excellent electrochemical performance, *Nanoscale* **5**(2013) 11265

Debasree Chowdhury; Debabrata Ghose; Safiul Alam Mollick, Homoepitaxy of germanium by hyperthermal ion irradiation, *Vacuum* **107** (2014) 23

Paramita Chatterjee; Satyajit Hazra, The hydrophilic/hydrophobic nature of a Cl-terminated Si surface, *Soft Matter* **9** (2013) 9799

Sayan Bayana; Sheo K Mishra; Purushottam Chakraborty; et al, Enhanced vacuum photoconductivity of chemically synthesized ZnO Nanostructures, *Philosophical Magazine* **94** (2014) 914

Biswajit Saha; Purushottam Chakraborty, M_{Csn}⁺- SIMS: an innovative approach for direct compositional analysis of materials without standards, *Energy Propedia* **41** (2013) 80

2.5 Ph D Awarded

Sanjoy Kr Mahatha [Krishnakumar SR Menon], Electronic Structure of Two-Dimensional Materials and Ultra-Thin Overlayers using Angle-Resolved Photoemission Spectroscopy, University of Calcutta, Dec 2013

Sahinur Reja [Sudhakar Yarlagadda], Strong electron-phonon interactions in some strongly correlated systems, Cambridge University, Nov 2013

2.6 Seminars/Lectures given in Conference/Symposium/Schools

Biswarup Satpati

- i. TEM Sample Preparation for Materials Science, Workshop on Spectroscopy in SEM and TEM: Material Science Applications in International Conference on Electron Nanoscopy and XXXIV Annual Meeting of EMSI, Saha Institute of Nuclear Physics (SINP), Kolkata, Jul 1-2, 2013
- ii. Transmission Electron Microscopy (TEM) and associated techniques for the investigation of bimetallic nanoparticles, International Conference on Electron Nanoscopy and XXXIV Annual Meeting of EMSI, Saha Institute of Nuclear Physics, Kolkata, Jul 3-5, 2013
- iii. Understanding the Appearance of Different Anisotropic Nanostructures in Chemical Synthesis using Transmission Electron Microscopy and Associated Techniques, International Conference on Structural and Physical Properties of Solids (SPPS 2013) having Focal Theme, Smart Materials at

- Nano and Micro Scale, Indian School of Mines, Dhanbad 826004, India, Nov 18-20, 2013
- iv. Transmission Electron Microscopy and Associated Techniques for Characterization of Nanomaterials” in the short term course on Advanced Functional Materials (SAFM-2013), Department of physics, National Institute of Technology (NIT), Durgapur, Nov 18-22, 2013
 - v. Formation of Triangular Bimetallic Core-Shell Nanorings from Hexagonal Monometallic Nanoparticles, Workshop on Imaging and Spectroscopy in Advanced TEM (WISAT-2014), Nasik, Maharashtra, Jan 28-31, 2014
 - vi. Two Lectures and a practical demonstration in a three-day workshop on ”Electron Microscopy in Physical Sciences”, Sophisticated Analytical Instrument Facility, North Eastern Hill University, Shillong, Mar 4-6, 2014

Purushottam Chakraborty

- i. National Seminar on Thin Film and MEMs Science & Technology, Institute of Chemical Engineers, Jadavpur University, India, Mar 21-22, 2014
- ii. 3rd International Conference on Physics at Surfaces and Interfaces (PSI2014), Puri, India, Feb 24-28, 2014
- iii. 5th National Conference on Nanotechnology and Materials Science 2013, Department of Physics, University of Lucknow, India, Dec 21-23, 2013
- iv. International Conference on Electron Microscopy and XXXIV Annual Meeting of the Electron Microscope Society of India (EMSI), Hyatt Regency Kolkata, India, Jul 30, 2013

Barnana Pal

- i. Ultrasound: A Nondestructive Probe in Material Science, One Day Seminar under DBT-STAR College Program, Lady Brabourne College, Kolkata, Dec 7, 2013

Prabhat Mandal

- i. 3d-4f spin interaction and field-induced metamagnetism in RXO_4 ($R=Ho, Gd, Lu; X=Cr, V$) compounds, 58th Annual Conference on Magnetism and Magnetic Materials, Denver, Colorado, Nov 4-8, 2013

Sudhakar Yarlagadda

- i. Oxide devices – the next revolution, National Seminar (2014) on Recent Advances in Physics, Berhampur Univ, organized by Berhampur Univ and IOP, Bhubaneswar
- ii. Polaron dynamics and decoherence in an interacting two-spin system coupled to optical phonon environment, International meeting on quantum information processing and applications, Harish-Chandra Research Institute, Allahabad, Dec 2-8, 2013

2.7 Teaching elsewhere

Purushottam Chakraborty

- i. Physics Department, Pontifical Catholic University of Rio de Janeiro, Brazil, Atomic Colli-

sions in Solids, Secondary Ion Mass Spectrometry, Oct 13-Nov 7, 2013

ii. Department of Physics, University of Pretoria, South Africa, Ion-Surface Interactions, May-Jun, 2013

2.8 Miscellany

Purushottam Chakraborty

i. Visiting Professor, University of Pretoria, South Africa, May-Jun, 2013

ii. Visiting Professor, Pontifical Catholic University of Rio de Janeiro, Brazil, Oct 13-Nov 7, 2013

Barnana Pal

Recipient of Bharat Jyoti Award presented by India International Friendship Society at a function held at India International Centre, New Delhi on 26th March 2014

Chapter 3
Experimental Nuclear and Particle Physics

Chapter 3

Experimental Nuclear and Particle Physics

3.1 Summary of Research Activities of Divisions

3.1.1 Applied Nuclear Physics

Applied Nuclear Physics Division is carrying out research work in the interdisciplinary areas mostly involving techniques and methods developed for Nuclear Physics research. Research conducted during 2013-2014 are in the subject areas of exploration of atomic structure and molecular dynamics using x-rays of various types and origin; investigation on the structure, evolution and phase transition of nanomaterials, crystalline materials, soft matter and bio-materials; development, characterization and optimization of radiation detectors; and model based simulation. Fragmentation and ionization of complex molecules by femtosecond lasers and ion beams are explored using pump-probe method and multi-event time of flight (TOF) imaging techniques. Attempts are made at explaining the findings in the light of Coulomb explosion model. Inner shell ionization in heavy elements, such as Lead and Bismuth, by electron impact at energies 15 to 40 keV was investigated. These studies have their importance in the quantitative trace element analysis. Attempts are made at explaining the energy dependence on the basis distorted wave Born approximation (DWBA) and modified relativistic binary encounter Bethe (MRBEB) model. Positron annihilation studies of different class of materials, such as nanosemiconductors, nanospinels, graphene, etc. were done and the new results were communicated. Systematic investigation of the Positronium life time of soft materials, nanocomposites synthesized by chemical route, has revealed structural modification due to subtle changes in the chemical composition. In the PAC spectroscopy laboratory, identification of phase transition in crystalline metal and metal oxides were done over a wide range of temperatures using ^{181}Hf as the probe nucleus. These studies manifest many interesting results including the coexistence of defects and their reversible / irreversible transformation through annealing of the materials. Our divisional scientists are also continuing with their involvement in the research planning, simulation and development of radiation detectors for the RD-51 collaboration in CERN, and also in the proposed India-based Neutrino Observatory (INO) as part of the national multi-institutional collaboration. Simulation of detector performance and design optimization of various grid based

gaseous detectors, micropattern gaseous detectors (MPGD), resistive plate chambers (RPC) and time projection chamber (TPC) detectors are successfully done by the scientists involved. A systematic study of the temperature and humidity dependence on the performance of bakelite based RPC detectors, operated in both avalanche and streamer modes are completed. A completely indigenous set up involving sensor based real time monitoring was developed and utilized for the above purpose. Interpretation of results on the basis of underlying physics and through simulation techniques is undertaken. Members of our division are concentrating on various phenomena associated with visual perception, where the models are inspired mainly by vision. These studies are supplemented by suitable cognitive science experiments. An equipped laboratory with vision based measurements and interpretation of the results are routinely carried out.

3.1.2 High Energy Nuclear and Particle Physics

The High Energy Nuclear and Particle Physics division is involved in two major experiments at the Large Hadron Collider at CERN. SINP has been involved in the ALICE experiment since 1997. The experiment, focused for studies of minimum bias events in proton-proton and lead-lead collisions has started taking data since late 2009. The Large Hadron Collider has provided large amount of data during the period between 2010 and 2012. The beam energy has gone up during 2012 to reveal new features in the data. The ALICE group in the institute constructed a part of the forward muon spectrometer which has been working satisfactorily during the entire period. Some collision data are collected with no magnetic field and these data are used to align different components of the spectrometer to the desired accuracy. The high level trigger for muons, also designed by the SINP group, has been performing with very high efficiency. The data show evidence of suppression of charged particle production, jet quenching and other features which are some of the signatures of formation of very dense medium in Pb-Pb collisions. The group is actively pursuing analysis of heavy quark and quarkonia production and also phenomenological studies of photon production in quark gluon plasma and heavy fermion in dense and warm plasma. A group is formed within the institute which applied for participation in the Compact Muon Solenoid (CMS) experiment and has been welcome within the CMS collaboration. The group has major responsibilities in two activities: detector performance studies of the hadron calorimeter and data quality monitoring. In addition, the group has the highest level expertise in detector simulation and some of the simulation coordination effort is coming to the group. The group has undertaken responsibilities in the upgrade program of the hadron calorimeter and there the main emphasis is on the back end electronics of the forward hadron calorimeter which needs to be replaced during the long shut down period between 2013-14. During this year members of the Division published several important papers validating various aspects of the Standard Model and from studies of heavy ion collision where suppression of heavy quark final states including quarkonia and jet quenching are reported. The two experiments, ALICE and CMS collected data with a very high efficiency and members of the HENPP Division of SINP took active parts in the data collection, data analysis and extracting important physics results from these experiments. Members of ALICE collaboration are responsible for the Muon Spectrometer which is used to study heavy quark formation at the extreme forward angles in proton-proton as well as heavy ion collisions.

We have set up a local Tier-3 scale computing cluster for CMS with about 300 computing cores and roughly 60 Tera Bytes(TB) of raw storage. Each computing server is a part of a GPFS cluster for

transparent and efficient data access from anywhere on the cluster. We run Condor as the batch scheduler. The computing center, which is become an essential part of CMS activities, is being used regularly for Monte Carlo event generation, simulation and reconstruction as well as for data processing and analysis.

3.1.3 Nuclear Physics

Research activities in Nuclear Physics Division revolves around the experimental study of low & intermediate energy nuclear physics using different accelerator centres in India and a few abroad. In addition, members of the division are also actively involved in the setting up of the FRENA facility for nuclear astrophysics research. The other major activities are: theoretical research, developmental activities and EDXRF spectrometry. Several faculty members of the division actively participated in the summer students programme of the Institute and also undertook teaching courses both in SINP and other neighbouring universities.

Nuclear Structure: The level schemes of the nuclei ^{34}Cl & ^{33}S have been extended and modified utilizing data from gamma-gamma coincidence, directional correlation and linear polarization measurements. Evolution of collectivity has been studied experimentally as well as theoretically in these nuclei. Large basis shell model calculations have been performed to understand the microscopic origin of these levels. In odd-odd ^{154}Ho , the total Routhian Surface calculations indicate a deformed character for this nucleus along with a secondary minimum for an oblate structure. There seems to be an indication of stable octupole deformation. Detailed analysis is in progress.

Nuclear Reactions: A measurement of the quasi-elastic scattering excitation function for $^7\text{Li}+^{159}\text{Tb}$, starting from near-barrier to deep-subbarrier energies, has been carried out at the BARC-TIFR Pelletron accelerator. The deep-subbarrier cross sections will be used to determine the surface diffuseness parameters. The experimental measurements of fusion excitation function and quasi-elastic barrier distribution function of $^7\text{Li}+^{64}\text{Ni}$ have been completed at the BARC-TIFR Pelletron Facility. Analysis of the data has already been completed. The investigation of the fusion excitation function close to the barrier for the $^6\text{Li}+^{64}\text{Ni}$ system has also been completed. The work on the systematic R-matrix analysis of $^{13}\text{C}(p,\gamma)^{14}\text{N}^*$ capture reaction along with the low energy $^{13}\text{C}(p,p)$ elastic scattering data using the code **AZURE II** is complete. Study of the $^{12}\text{C}(\alpha,\gamma)$ reaction at 300 keV has been carried out using the indirect method. The analysis of the $^{12}\text{C}(^6\text{Li},d)$ reaction was completed during this period. The spectroscopic amplitudes of seven states of ^{16}O were extracted by a comparison of the CDCC-CRC formalism in the R-matrix framework. The major finding is that for the population of the bound states of ^{16}O , the transfer process is influenced by projectile breakup. This affects evaluation of the E2 S-factor to the ground state.

Developmental activities: A ^{22}Ne implanted target has been prepared by using 75 keV ions from an ECR ion source at TIFR, Mumbai. The bulk characterization of this target have been completed by the $^{22}\text{Ne}(p,?)^{23}\text{Na}$ resonance reaction at 851 keV. The proton beam was delivered from a 5MV accelerator at University of Notre Dame, USA. Besides, a ^{14}N implanted target with Ta backing has also been prepared at TIFR, Mumbai. The thickness of this target, measured by nuclear resonance reaction $^{14}\text{N}(p,)^{15}\text{O}$, was found to be $(23 \pm 4 \text{ keV})$.

Theoretical Work: The experimental data on ^{153}Ho have been extensively analysed through Particle Rotor Model calculations. The lifetimes of the three isomers in the positive parity states have been specially analysed to verify the claim of prolate deformation for these states. The calculated results clearly show that especially at higher spins, the prolate shape of the nucleus is favoured compared to oblate.

3.2 Research Activities

3.2.1 Applied Nuclear Physics

3.2.1.1 Positron annihilation studies of vacancy-type defects and room temperature ferromagnetism in chemically synthesized Li-doped ZnO nanocrystals

In this article, we have investigated the effects of Li incorporation on the lattice defects and room-temperature $d(0)$ ferromagnetic behaviour in ZnO nanocrystals by correlating X-ray photoelectron, photoluminescence and positron annihilation spectroscopic study in details. It is found that at low doping level (< 7 at.%), Li¹⁺ is an effective substituent of Zn site, but it prefers to occupy the interstitial positions when Li-doping exceeds 7 at.% resulting in lattice expansion and increase of particle sizes. The pristine ZnO nanocrystals exhibit ferromagnetic behaviour which is further enhanced significantly after few percentage of Li-doping in ZnO. The magnitude of both saturation magnetizations (M-S) as well as the Curie temperature (T-C) are found to increase considerably up to Li concentration of 10 at.% and then started to decrease on further Li-doping. The gradual enhancement of Zn vacancy (V-Zn) defects in ZnO nanocrystals due to Li substitution as confirmed from photoluminescence and positron annihilation spectroscopy measurements might be responsible to induce paramagnetic moments within ZnO host. The ferromagnetic exchange interaction between the localised moments of V-Zn defects can be mediated through the holes arising due to Li-substitutional (Li-Zn) acceptor defects within ZnO. Hence, Li doping in ZnO favours in stabilizing considerable V-Zn defects and thus helps to sustain long-range high-TC ferromagnetism in ZnO which can be a promising material in future spintronics.

S Ghosh†; Gobinda Gopal Khan†; K Mandal†; PMG Nambissan

3.2.1.2 Transition between Mechanisms of Laser-Induced Field-Free Molecular Orientation

The transition between two distinct mechanisms for the laser-induced field-free orientation of CO molecules is observed via measurements of orientation revival times and subsequent comparison to theoretical calculations. In the first mechanism, which we find responsible for the orientation of CO up to peak intensities of 8×10^{13} W/cm², the molecules are impulsively oriented through the hyperpolarizability interaction. At higher intensities, asymmetric depletion through orientation-selective ionization is the dominant orienting mechanism. In addition to the clear identification of the two regimes of orientation, we propose that careful measurements of the onset of the orientation depletion mechanism as a function of the laser intensity will provide a relatively simple route to calibrating absolute rates of nonperturbative strongfield molecular ionization.

I Znakovskaya†; M Spanner†; S De, et al

3.2.1.3 Probe-impurity interaction in dilute alloy $Zr(x)Hf(1-xx) \sim 0.98$: Results from perturbed angular correlation measurements

Time-differential perturbed angular correlation measurements have been performed in Zr metal with ~ 2 at% Hf to understand the results of previous measurements. From present measurements at different temperatures two interaction frequencies have been found. One of these produces an asymmetry parameter $\eta=0$ as expected for a hcp crystal while the other one gives a non-zero

value of η . The component with $\eta=0$ gives a value of quadrupole frequency $\omega_Q=47.4(3)$ Mrad/s at 298 K while the second component produces values of $\omega_Q=49.5(2)$ Mrad/s, $\eta=0.22(1)$ at room temperature. The component with $\eta=0$ has been attributed to a configuration where all the 12 nearest neighbor (NN) to the probe has Zr atoms while the non-zero eta component arises due to the presence of 1 NN HE. The site fractions for these two components depend on temperature and it is found that with increase in temperature, the ratio $f/(1 - f)$ decreases following the Arrhenius behavior, f is the component fraction for the probe-impurity interaction. The entropy of formation and binding energy for the probe-impurity pair have been determined in the present report.

CC Dey

3.2.1.4 High energy (MeV) ion fluence dependent nano scale free volume defects studies of PMMA films

A systematic study on the dependence of the free volume at nanoscale in carbon ions irradiated polymethylmethacrylate polymer samples was carried out by means of positron annihilation lifetime spectroscopy and Doppler broadening spectroscopy (DBS). An investigation about the evolution of cross-linking in the polymeric chains after ion irradiation was carried out from the calculated values of hole radius, free volume and fractional free volume using Tao-Eldrup Model. The role of rise in temperature on the growth of free volume was observed at higher fluences. The results were supported by variations in the S parameter of DBS study. The structural analyses were carried out using XRD to investigate for the modification in the structural nature, degree of crystallinity and average crystallite size of the polymer after ion irradiation. Additional information on the modifications of optical and chemical properties was extracted by means of UV-visible and FTIR spectroscopy respectively.

Paramjit Singh†; Rajesh Kumar†; Jincemon Cyriac†...PMG Nambissan; et al

3.2.1.5 Effects of process parameters on the defects in graphene oxide-polyaniline composites investigated by positron annihilation spectroscopy

Graphene oxide (GO)-polyaniline (PANI) composites were prepared with different relative abundance of PANI and GO by in situ polymerization of aniline in the presence of GO and ammonium persulphate at different temperatures. In the process, GO also got reduced to graphene. Positron lifetimes and coincidence Doppler broadening of the electron-positron annihilation gamma ray spectra originating from the composite samples were measured and the results are reported. The positron lifetimes indicated the presence of very large size defects in the form of vacancy clusters within the samples. Another interesting observation was the increase of relative intensity of the defect specific positron lifetime component when an increase in relative abundance of PANI led to increased reduction of GO to graphene. The reduction also shrank the volume occupied by GO and the free volume thereby released added to the overall defect concentration, resulting in a simultaneous increase of the intensity of the positron lifetime component. The variation of the positron lifetime and its intensity with the synthesis temperature suggested an optimum temperature suitable for the process. The above observations are corroborated by other experimental investigations like electron microscopy, X-ray diffraction and electrical conductivity.

Utpal Rana†; PMG Nambissan; Sudip Malik†; Kuntal Chakrabarti

3.2.1.6 A positron annihilation spectroscopic investigation of europium-doped cerium oxide nanoparticles

Doping in ceria (CeO_2) nanoparticles with europium (Eu) of varying concentrations (0, 0.1, 0.5, ..., 50 atom%) is studied using complementary experimental techniques and novel observations were made during the investigation. The immediate observable effect was a distinct reduction in particle sizes with increasing Eu concentration attributed to the relaxation of strain introduced due to the replacement of Ce^{4+} ions by Eu^{3+} ions of larger radius. However, this general trend was reversed in the doping concentration range of 0.1–1 atom% due to the reduction of Ce^{4+} to Ce^{3+} and the formation of anion vacancies. Quantum confinement effects became evident with the increase of band gap energy when the particle sizes reduced below 7–8 nm. Positron annihilation studies indicated the presence of vacancy type defects in the form of vacancy clusters within the nanoparticles. Some positron annihilation was also seen on the surface of crystallites as a result of diffusion of thermalized positrons before annihilation. Coincidence Doppler broadening measurements indicated the annihilation of positrons with electrons of different species of atoms and the characteristic S-W plot showed a kink-like feature at the particle sizes where quantum confinement effects began.

Atul V Thorat†; Tandra Ghoshal†; Justin D Holmes†; PMG Nambissan; et al

3.2.1.7 Comparison of bulk Micromegas with different amplification gaps

The bulk Micromegas detector is considered to be a promising candidate for building TPCs for several future experiments including the projected linear collider. The standard bulk with a spacing of 128 μm has already established itself as a good choice for its performances in terms of gas gain uniformity, energy and space point resolution, and its capability to efficiently pave large readout surfaces with minimum dead zone. The present work involves the comparison of this standard bulk with a relatively less used bulk Micromegas detector having a larger amplification gap of 192 μm . Detector gain, energy resolution and electron transparency of these Micromegas have been measured under different conditions in various Argon based gas mixtures to evaluate their performance. These measured characteristics have also been compared in detail to numerical simulations using the Garfield framework that combines packages such as neBEM, Magboltz and Heed. Further, we have carried our another numerical study to determine the effect of dielectric spacers on different detector features. A comprehensive comparison of the two detectors has been presented and analyzed in this work.

Purba Bhattacharya; Sudeb Bhattacharya; Nayana Majumdar; Supratik Mukhopadhyay; Sandip Sarkar; et al

3.2.1.8 Gadolinium substitution induced defect restructuring in multiferroic BiFeO_3 : case study by positron annihilation spectroscopy

Positron annihilation spectroscopy (PAS) comprising of the measurements of positron lifetime and coincidence Doppler broadening spectra has been carried out to understand and monitor the evolution of the vacancy-type defects arising from the ionic deficiencies at lattice points of the multiferroic perovskite bismuth ferrite (BiFeO_3) doped with 1, 5 and 10 at% gadolinium Gd^{3+} ions. Negatively charged defects in the form of Bi^{3+} monovacancies (V_{Bi}^{3-}) were present in the undoped nanocrystallites, which strongly trapped positrons. During the successive doping by Gd^{3+} ions, the positron trapping efficiency decreased while the doped ions combined with the vacancies to form complexes,

which became neutral. A fraction of the positrons got annihilated at the crystallite surfaces too, being evident from the very large positron lifetimes obtained and confirming the nano-size-specific characteristics of the samples. Further, the intercrystallite regions provided favourable sites for orthopositronium formation, although in minute concentrations. The dopant ion-complex formation was also depicted clearly by the defect characteristic S-W plot. Also, the large change of electrical resistivity with Gd concentration has been explained nicely by invoking the defect information from the PAS study. The study has demonstrated the usefulness of an excellent method of defect identification in such a novel material system, which is vital information for exploiting them for further technological applications.

A Mukherjee†; M Banerjee†; S Basu†; PMG Nambissan; et al

3.2.1.9 Femtosecond photoelectron diffraction on laser-aligned molecules: Towards time-resolved imaging of molecular structure

We demonstrate an experimental method to record snapshot diffraction images of polyatomic gas-phase molecules, which can, in a next step, be used to probe time-dependent changes in the molecular geometry during photochemical reactions with femtosecond temporal and angstrom spatial resolution. Adiabatically laser-aligned 1-ethynyl-4-fluorobenzene (C_8H_5F) molecules were imaged by diffraction of photoelectrons with kinetic energies between 31 and 62 eV, created from core ionization of the fluorine (1s) level by ≈ 80 fs x-ray free-electron-laser pulses. Comparison of the experimental photoelectron angular distributions with density functional theory calculations allows relating the diffraction images to the molecular structure.

R Boll†; D Anielski†; C Bostedt†...S De; et al

3.2.1.10 Electric quadrupole and magnetic dipole interactions at ^{181}Ta impurity in Zr_2Ni_7 intermetallic compound: Experiment and first-principles calculations

Electric quadrupole interactions at ^{181}Ta impurity in the intermetallic compound Zr_2Ni_7 have been studied by perturbed angular correlation technique. It has been found that there are two electric field gradients (EFG) at the ^{181}Ta site due to two different crystalline configurations in Zr_2Ni_7 , while contradictory results were reported from previous investigations. The values of EFG at room temperature have been found to be $V_{zz}=7.9 \times 10^{17}$ V/cm² and 7.1×10^{17} V/cm² corresponding to present experimental values of quadrupole frequencies and asymmetry parameters for the two sites: $\omega_Q^1=70.7(1)$ Mrad/s, $\eta=0.28(1)$, $\delta=0.8(2)\%$ (site fraction 84%) and $\omega(2)(Q)=63(1)$ Mrad/s, $\eta=0.35(5)$, $\delta \sim 0$ (site fraction 9%). Electric field gradients and asymmetry parameters have been computed from the complementary first-principles density functional theory (DFT) to compare with present experimental results. Our calculated values of EFG are found to be in close agreement with the experimental results. No magnetic interactions in Zr_2Ni_7 have been observed at 298 and 77 K which implies that there is no ferromagnetic ordering in this material down to 77 K. This observation is corroborated by theoretical calculations, wherein no magnetic moment or hyperfine field is found at any atomic site.

CC Dey; SK Srivastava†

3.2.1.11 Recoil Induced Room Temperature Stable Frenkel Pairs in alpha-Hafnium Upon Thermal Neutron Capture

Ultrapure hafnium metal (110 ppm zirconium) was neutron activated with a thermal neutron flux of $6.6 \cdot 10^{12} \text{ cm}^{-2}\text{s}^{-1}$ in order to obtain ^{181}Hf for subsequent time differential perturbed angular correlation (TDPAC) experiments using the nuclear probe $^{181}\text{Hf}(\beta^-)^{181}\text{Ta}$. Apart from the expected nuclear quadrupole interaction (NQI) signal for a hexagonal close-packed (hcp) metal, three further discrete NQIs were observed with a few percent fraction each. The TDPAC spectra were recorded for up to 11 half lives with extreme statistical accuracy. The fitted parameters vary slightly within the temperature range between 248 K and 373 K. The signals corresponding to the three additional sites completely disappear after 'annealing' at 453 K for one minute. Based on the symmetry of the additional NQIs and their temperature dependencies, they are tentatively attributed to Frenkel pairs produced by recoil due to the emission of a prompt 5.694 MeV gamma-ray following thermal neutron capture and reported by the nuclear probe in three different positions. These Frenkel pairs are stable up to at least 373 K.

Tilman Butz†; Satyendra K Das†; Chandu C Dey; et al

3.2.1.12 Investigations of Zr-Ni intermetallic compounds by perturbed angular correlations

The hyperfine interactions experienced by ^{181}Ta in ZrNi_5 and Zr_2Ni_7 intermetallic compounds have been investigated by the perturbed angular correlation (PAC) technique. In ZrNi_5 , a strong electric quadrupole interaction ($\sim 40\%$) with $\omega(Q)=72.0(1) \text{ Mrad/s}$, $\eta=0.25(1)$, $\delta=0$ at room temperature has been found due to the presence of Zr_2Ni_7 contaminating phase produced during sample preparation in the arc furnace. A weak quadrupole interaction of Zr_2Ni_7 ($\sim 5\%$) with $\omega(Q)=65(1) \text{ Mrad/s}$, $\eta=0.24(6)$, $\delta=0$ has also been observed. The cubic component of ZrNi_5 also has been observed ($\sim 40\%$ at room temperature) in this sample along with associated defect ($\sim 5\%$). It is found that at 873 K, the cubic fraction increases to $\sim 54\%$ at the cost of its defect fraction. No magnetic interaction in ZrNi_5 has been observed which supports the earlier PAC results but rules out the result of strong magnetic ordering found from magnetization measurement. In Zr_2Ni_7 , two regular fractions corresponding to two different crystallographic sites of Zr have been clearly identified with the parameters $\omega(Q)(1)=70.9(1) \text{ Mrad/s}$, $\eta(1)=0.28(1)$, $\delta=1.3(3)\%$ and $\omega(Q)(2)=64(1) \text{ Mrad/s}$, $\eta(2)=0.34(8)$, $\delta=0$ while contradictory results were reported from previous measurements.

CC Dey

3.2.1.13 Inner-shell multiple ionization of polyatomic molecules with an intense x-ray free-electron laser studied by coincident ion momentum imaging

The ionization and fragmentation of two selenium containing hydrocarbon molecules, methylselenol (CH_3SeH) and ethylselenol ($\text{C}_2\text{H}_5\text{SeH}$), by intense ($>10^{17} \text{ W cm}^{-2}$) 5 fs x-ray pulses with photon energies of 1.7 and 2 keV has been studied by means of coincident ion momentum spectroscopy. Measuring charge states and ion kinetic energies, we find signatures of charge redistribution within the molecular environment. Furthermore, by analyzing fragment ion angular correlations, we can determine the laboratory-frame orientation of individual molecules and thus investigate the fragmentation dynamics in the molecular frame. This allows distinguishing protons originating from

different molecular sites along with identifying the reaction channels that lead to their emission.

B Erk†; D Rolles†; L Foucar†...Sankar De; et al

3.2.1.14 Orientation enhancement in early visual processing can explain time course of brightness contrast and White's illusion

Dynamics of orientation tuning in V1 indicates that computational model of V1 should not only comprise of bank of static spatially oriented filters but also include the contribution for dynamical response facilitation or suppression along orientation. Time evolution of orientation response in V1 can emerge due to time- dependent excitation and lateral inhibition in the orientation domain. Lateral inhibition in the orientation domain suggests that Ernst Mach's proposition can be applied for the enhancement of initial orientation distribution that is generated due to interaction of visual stimulus with spatially oriented filters and subcortical temporal filter. Oriented spatial filtering that appears much early (70 ms) in the sequence of visual information processing can account for many of the brightness illusions observed at steady state. It is therefore expected that time evolution of orientation response might be reflecting in the brightness percept over time. Our numerical study suggests that only spatio-temporal filtering at early phase can explain experimentally observed temporal dynamics of brightness contrast illusion. But, enhancement of orientation response at early phase of visual processing is the key mechanism that can guide visual system to predict the brightness by "Max-rule" or "Winner Takes All" (WTA) estimation and thus producing White's illusions at any exposure.

Subhajit Karmakar; Sandip Sarkar

3.2.1.15 Evolution of Vacancy-Type Defects, Phase Transition, and Intrinsic Ferromagnetism during Annealing of Nanocrystalline TiO₂ Studied by Positron Annihilation Spectroscopy

The evolution of vacancy-type crystalline defects across the transition from anatase to rutile structure of titanium dioxide (TiO₂) nanoparticles during high-temperature annealing in oxygen and argon is studied by using positron lifetime and coincidence Doppler broadening spectroscopic measurements. The TiO₂ nanoparticles were synthesized through a simple sol-gel chemical route. The changes in the crystalline phase and lattice parameters of the nanoparticles upon thermal treatment were investigated by X-ray diffraction and high-resolution transmission electron microscopy, and the results were correlated with those of photoluminescence spectroscopy and positron annihilation measurements. The structural defects, mostly 3D vacancy clusters, in the nanoparticles were found to decrease in concentration during the annealing in O₂ rather than in Ar at elevated temperatures. In the case of annealing in Ar, the vacancy-type defects persisted even at the highest annealing temperature of 900° C used in the experiment and the transition was, as a result, found to be delayed and partial. The annihilation of positrons at the nanocrystalline grain interfaces also contributed to the long positron lifetime component, but variations due to annealing were clearly visible as it also contained the contributions from annihilation within the vacancy clusters. The role of the vacancy type defects on the magnetic property of the TiO₂ nanoparticles is also investigated.

S Ghosh†; Gobinda Gopal Khan†; K Mandal†; Anirban Samanta; PMG Nambissan; et al

3.2.2 High Energy Nuclear and Particle Physics

3.2.2.1 Modifications to the pulsar kick velocity due to magnetic interactions in dense plasma

In this work we calculate the pulsar kick velocity of a magnetized neutron star (NS) composed of a degenerate quark matter core with non-Fermi liquid (NFL) correction. Both the leading order (LO) and next to LO (NLO) corrections to the kick velocity have been incorporated. In addition, the NFL corrections to the specific heat of magnetized quark matter have been presented. This has been taken into account to calculate the kick velocity of the NS. The results show a significant departure from the normal Fermi liquid estimates. The relation between radius and temperature has been shown with a kick velocity of 100 km s⁻¹ with and without NFL corrections.

SP Adhya; PK Roy; AK Dutt-Mazumder

3.2.2.2 Wake potential in collisional anisotropic quark-gluon plasma

Within the framework of the Boltzmann transport equation with a Bhatnagar-Gross-Krook collisional kernel, we study the wake potential induced by fast partons traveling through the high-temperature QCD plasma which is anisotropic in momentum space. We calculate the dielectric response function of a collisional anisotropic quark-gluon plasma for small ξ (anisotropic parameter) limit. Using this, the wake potential for various combinations of the anisotropy parameter (ξ) and the collision rate (ν) is evaluated both for parallel and perpendicular directions of motion of the fast parton. It is seen that the inclusion of the collision modifies the wake potential, and the amount, as well as the nature, of the potential depends on the combinations of ξ and ν .

Mahatsab Mandal; Pradip Roy

3.2.2.3 Ψ AND Υ PRODUCTION IN pp COLLISIONS AT 7.0 TeV

This is an extension of recent studies for $\Upsilon(nS)$ and $\Psi(1S, 2S)$ production at the LHC in pp collisions, $\sqrt{s} = 7.0$ TeV, with the ALICE detector.

Leonard S Kisslinger†; Debasish Das

3.2.2.4 Multiplicity dependence of two-particle azimuthal correlations in pp collisions at the LHC

We present the measurements of particle pair yields per trigger particle obtained from di-hadron azimuthal correlations in pp collisions at $\sqrt{s} = 0.9, 2.76,$ and 7TeV recorded with the ALICE detector. The yields are studied as a function of the charged particle multiplicity. Taken together with the single particle yields the pair yields provide information about parton fragmentation at low transverse momenta, as well as on the contribution of multiple parton interactions to particle production. Data are compared to calculations using the PYTHIA6, PYTHIA8, and PHOJET event generators.

B Abelev†; J Adam†; D Adamova†; S Chattopadhyay; D Das; K Das; AK Dutta Majumdar; P Khan; B Paul; P Roy; T Sinha; et al

3.2.2.5 Heavy quark damping rate in hot viscous QCD plasma

We derive an expression for the heavy quark damping rate in hot quark gluon plasma in the presence of flow. Here all the bath particles are out of equilibrium due to the existence of nonzero velocity gradient. The magnetic sector shows similar infrared divergences even after hard thermal loop corrections as one encounters in the case of nonviscous plasma. We estimate the first order correction in (η/s) for heavy quark damping rate due to the nonzero viscosity of the QCD plasma.

Sreemoyee Sarkar; Abhee K Dutt-Mazumder

3.2.2.6 Structure of nearly degenerate dipole bands in ^{108}Ag

The high spin negative parity states of Ag-108 have been investigated with the $^{11}\text{B} + ^{100}\text{Mo}$ reaction at 39 MeV beam energy using the INCA facility at TIFR, Mumbai. From the gamma-gamma coincidence analysis, an excited negative parity band has been established and found to be nearly degenerate with the ground state band. The spin and parity of the levels are assigned using angular correlation and polarization measurements. This pair of degenerate bands in ^{108}Ag is studied using the recently developed microscopic triaxial projected shell model approach. The observed energy levels and the ratio of the electromagnetic transition probabilities of these bands in this isotope are well reproduced by the present model. Further, it is shown that the partner band has a different quasiparticle structure as compared to the yrast band.

J Sethi†; R Palit†; S Saha†; S Chattopadhyay; et al

3.2.2.7 UPSILON PRODUCTION IN pp COLLISIONS FOR FORWARD RAPIDITIES AT LHC

This is a continuation of recent studies of $\Upsilon(nS)$ production at the LHC in pp collisions. Our previous studies were for rapidity $y = -1$ to 1 for the CMS detector, while the present study is for $y = 2.5$ to 4.0 at the LHC.

Leonard S Kisslinger†; Debasish Das

3.2.2.8 Non-Fermi liquid behavior of thermal relaxation time in degenerate electron plasma

The thermal relaxation time (T-kee) for the degenerate electron plasma has been calculated by incorporating non-Fermi liquid corrections both for the thermal conductivity and specific heat capacity. Perturbative results are presented by making expansion in $T/m(D)$ with next to leading order corrections. We see that the next to leading order non-Fermi liquid corrections further reduce the decrease in relaxation time due to the leading order corrections.

Sreemoyee Sarkar; Abhee K Dutt-Mazumder

3.2.3 Nuclear Physics

3.2.3.1 High spin spectroscopy in ^{34}Cl

High spin states of ^{34}Cl populated through $^{27}\text{Al}(^{12}\text{C}, \alpha n)^{34}\text{Cl}$ reaction at $E(^{12}\text{C}) = 40$ MeV, have been studied using the Indian National Gamma Array facility. The level scheme has been extended up to 10.6 MeV utilizing the results of intensity, directional correlation, and linear polarization measurements. Lifetimes of a few excited states have been estimated for the first time using the Doppler shift attenuation method. Large-basis shell-model calculations within the $sd - pf$ space have been done to understand the microscopic origin of the excited states. Involvement of pf orbitals have been found to be essential to reproduce the negative-parity as well as high spin positive-parity states. Onset of collectivity manifested through short half-lives and large $B(E2)$ values have been reproduced well in the calculations.

Abhijit Bisoi; M Saha Sarkar; S Sarkar†; S Ray...R Kshetri; et al

3.2.3.2 Shape coexistence in the near-spherical ^{142}Sm nucleus

High spin states of ^{142}Sm have been investigated using the fusion-evaporation reaction $^{116}\text{Cd}(^{31}\text{P}, p4n)$ at beam energy 148 MeV using the Indian National Gamma Array (INGA). Approximately sixty new gamma transitions have been placed in the proposed level scheme, which has been extended up to ≈ 12.5 MeV. Several band-like structures including one dipole band and three quadrupole bands have been observed in the proposed level scheme. Lifetimes of several levels in the dipole band and quadrupole bands have been measured using doppler shift attenuation method (DSAM). The deduced $B(M1)$ values for the dipole band have been compared with the semiclassical shears mechanism with the principle axis cranking (SPAC) model, and the dipole band has been interpreted as a magnetic rotational band. Comparisons between the experimental characteristics and cranked Nilsson-Strutinsky (CNS) calculations for the observed quadrupole bands indicate that these bands have been formed on the triaxial deformed shape of ^{142}Sm .

S Rajbanshi; Abhijit Bisoi; Somnath Nag†;...S Chattopadhyay...M Saha Sarkar...A Goswami

3.2.3.3 Measurement of the Dipole Polarizability of the Unstable Neutron-Rich Nucleus ^{68}Ni

The E1 strength distribution in ^{68}Ni has been investigated using Coulomb excitation in inverse kinematics at the (RB)³B-LAND setup and by measuring the invariant mass in the one-and two-neutron decay channels. The giant dipole resonance and a low-lying peak (pygmy dipole resonance) have been observed at 17.1(2) and 9.55(17) MeV, respectively. The measured dipole polarizability is compared to relativistic random phase approximation calculations yielding a neutron-skin thickness of 0.17(2) fm. A method and analysis applicable to neutron-rich nuclei has been developed, allowing for a precise determination of neutron skins in nuclei as a function of neutron excess.

DM Rossi†; P Adrich†; F Aksouh†...U Datta Pramanik; et al

3.2.3.4 Study of the ^{14}Be Continuum: Identification and Structure of its Second 2^+ State

The coupling between bound quantum states and those in the continuum is of high theoretical interest. Experimental studies of bound drip-line nuclei provide ideal testing grounds for such investigations since they, due to the feeble binding energy of their valence particles, are easy to excite into the continuum. In this Letter, continuum states in the heaviest particle-stable Be isotope, ^{14}Be , are studied by employing the method of inelastic proton scattering in inverse kinematics. New continuum states are found at excitation energies $E^* = 3.54(16)$ MeV and $E^* = 5.25(19)$ MeV. The structure of the earlier known 2_1^+ state at 1.54(13) MeV was confirmed with a predominantly $(0d_{5/2})^2$ configuration while there is very clear evidence that the 2_2^+ state has a predominant $(1s_{1/2}, 0d_{5/2})$ structure with a preferential three-body decay mechanism. The region at about 7 MeV excitation shows distinct features of sequential neutron decay via intermediate states in ^{13}Be . This demonstrates that the increasing availability of energetic beams of exotic nuclei opens up new vistas for experiments leading towards a new understanding of the interplay between bound and continuum states.

Yu Aksyutina†; T Aumann†; K Boretzky† ...U Datta Pramanik; et al

3.2.3.5 Importance of the 1n-stripping process in the $^6\text{Li}+^{159}\text{Tb}$ reaction

The inclusive cross sections of the α particles produced in the reaction $^6\text{Li} + ^{159}\text{Tb}$ have been measured at energies around the Coulomb barrier. The measured cross sections are found to be orders of magnitude larger than the calculated cross sections of ^6Li breaking into α and d fragments, thus indicating contributions from other processes. The experimental cross sections of 1n-stripping and 1n-pickup processes have been determined from an entirely different measurement, reported earlier. Apart from incomplete fusion and d-transfer processes, the 1n-stripping process is found to be a significant contributor to the inclusive α -particle cross sections in this reaction.

MK Pradhan; A Mukherjee; Subinit Roy; P Basu; A Goswami; R Kshetri...M Saha Sarkar; et al

3.2.3.6 Band structures and intruder $\pi i_{13/2}$ state in ^{197}Tl

The excited states in the odd-A ^{197}Tl nucleus have been studied by populating them using the $^{197}\text{Au}(\alpha, 4n)^{197}\text{Tl}$ reaction at a beam energy of 48 MeV. The $\gamma - \gamma$ coincidence data were taken using a combination of clover, low-energy photon spectrometer (LEPS), and single-crystal high-purity germanium (HPGe) detectors. Precise spin and parity assignments of the excited states have been done through polarization and directional correlation from oriented states (DCO) measurements. A new band structure has been identified and evidence for a possible intruder $\pi i_{13/2}$ state has been found for the first time. Possible configurations of the observed bands have been discussed. The total Routhian surface calculations have been performed to study the shape of $i^{197}\text{Tl}$ for different configurations.

H Pait†; G Mukherjee†; S Bhattacharya†...S Rajbanshi; A Goswami; et al

3.2.3.7 Superdeformation and α -cluster structure in ^{35}Cl

A superdeformed (SD) band has been identified in a non-alpha-conjugate nucleus ^{35}Cl . It crosses the negative-parity ground band above $11/2^-$ and becomes the yrast at $15/2^-$. Lifetimes of all relevant states have been measured to follow the evolution of collectivity. Enhanced $B(E2)$, $B(E1)$ values as well as energetics provide evidence for superdeformation and existence of parity doublet cluster structure in an odd-A nucleus in the $A \simeq 40$ region. Large-scale shell-model calculations assign $(sd)^{16}(pf)^3$ as the origin of these states. Calculated spectroscopic factors correlate the SD states in ^{35}Cl to those in ^{36}Ar .

Abhijit Bisoi; M Saha Sarkar; S Sarkar†...S Ray; Debasmita Kanjilal...A Goswami; et al

3.2.3.8 Shape evolution in ^{123}Cs and ^{124}Ba nuclei

Lifetime measurements have been carried out for high spin states in ^{123}Cs and ^{124}Ba using the Doppler shift attenuation method. The transition quadrupole moments $Q(t)$ measured in the present work show a loss of collectivity after the alignment of neutron $h_{11/2}$ orbitals. The experimental results are compared with the existing theoretical calculations within the framework of the cranked shell model. The results are consistent with the evolution of triaxial shape due to the alignment of $\nu h_{11/2}$ orbitals. However, larger deformation parameters β_2 have been measured compared with the values predicted by the model calculations in both the nuclei.

K Selvakumar; AK Singh; Subhashri Das...A Goswami; R Raut; A Mukherjee; U Datta Pramanik; et al

3.2.3.9 Chemical composition of soil evolving from municipal solid waste using energy dispersive X-ray fluorescence

Municipal solid waste (MSW) generated in the city of Kolkata, India has been dumped at a site known as Dhapa', situated in the eastern fringes of the city, since the middle of 19th century. The soil in this area is expected to be evolving from several layers of dumped MSW through many decades. Earlier chemical composition study of surface soil of the site revealed the existence of heavy elements at comparatively higher concentrations than non-contaminated soil. It becomes primary environmental prerogative to investigate further the bulk elemental composition of the soil at various depths. Samples from three different layers had been collected from six selected spots spanning a length of around 2km, starting from the present core dumping area to a bypass highway dividing the rest of the city from Dhapa. Samples were studied first using radio-isotope induced energy dispersive X-ray fluorescence (RI-EDXRF) spectrometer and later augmented by using a commercial (Epsilon 5, PANalytical B.V., Netherlands) high-energy polarized-beam variety (HE-P-EDXRF) to cover a wider range of heavy elements. In RI-EDXRF, the backscatter fundamental parameter algorithm had been used with the readily available and/or preparable single elemental foils and/or compound pellets as calibration standards for elemental quantification. Whereas in the more sensitive HE-P-EDXRF, influence coefficient method was employed, which ideally requires several similar matrix geological soil standards. In the absence of optimum number of soil standards for HE-P-EDXRF, the RI-EDXRF with backscatter fundamental parameter proved useful in covering the dynamic concentration range of certain important heavy metals in the MSW contaminated soil such as Cu, Zn, and Pb. NIST SRM 2586 comprising Pb contaminated soil was used for quality control. Potentially toxic heavy metals were observed at all levels (surface, middle, and lower with

geometric mean concentrations in mg/kg) viz.: Cr (320, 250, 100); Ni (70, 70, 55); Cu(315, 320, 360); Zn (940, 810, 625); Cd (2.5, 1.8, 1.1); Sb (5.3, 8.9, 12.4); Ba (1050, 1050, 880); and Pb (530, 520, 724). There is a general trend of higher accumulation of Sb and Pb at lowest level, whereas there is a general trend of decrease with depth for Cr, Zn, and Cd.

Dhrubajyoti Gupta; Subinit Roy; Rita Ghosh; Ajoy Kumar Mitra

3.2.3.10 Structure of the unbound nucleus ^{13}Be : One-neutron knockout reaction data from ^{14}Be analyzed in a holistic approach

At the ALADIN-LAND setup at GSI the unbound nucleus ^{13}Be has been produced in one-neutron knockout reactions from a 304 MeV/nucleon relativistic beam of ^{14}Be ions impinging on a liquid hydrogen target. An analysis of the data including all available information about ^{13}Be , and in particular recent data from a similar experiment performed at RIKEN, has been performed. A consistent description is reached. It is found that the excitation spectrum is dominated by s-waves at low energy, which solves problems from previous seemingly contradictory interpretations. A possible interference between two s-states in ^{13}Be is also discussed. The results indicate that the ground-state wave function of ^{14}Be is dominated by valence neutrons in the s-shell contributing with 60-75% of the total neutron knockout cross section.

Yu Aksyutina†; T Aumann†; K Boretzky†...U Datta Pramanik; et al

3.3 Developmental Work

3.3.1

3.3.1.1 Energy - time measurement and pulse-shape discrimination with a simple spectrometer consisting of scintillators and a digital oscilloscope

The aim of this work is to develop a simple gamma and neutron spectrometer based on digital signal processing of gamma and neutron pulses from detectors by utilizing a dual channel digital oscilloscope. This spectrometer was also used for gamma and neutron spectroscopy for measurement of energy and time differences in a Time of Flight set-up. We have developed algorithm for pulse shape discrimination to distinguish between neutrons and gammas incident on a liquid scintillator detector from a ^{252}Cf fission source. This work has been done with undergraduate associates and summer project students.

Tuhin Malik†; Rutuparna Rath†; Uttiyoarnab Saha†...M Saha Sarkar

3.3.1.2 High Voltage Test of Cathode Pad Chamber (CPC) with gas mixture Ar/CO₂ (85:15) using Mass Flow Controller (MFC)

The High Voltage validation was done for the Cathode Pad Chamber flushing with Ar/CO₂ (85:15) using the facility MFC in the laboratory of HENPP division. The High Voltage (HV) was put to the detector after conditioning with Ni₂ flushing for three hours. The HV went up to 1500 V within 1 hour. The leakage current as a function of high voltage was linear. This existing CPC chamber

in the HENPP laboratory is identical to the quadrant chambers of the Second Tracking Station of MUON spectrometer of ALICE detector at CERN. This HV testing was necessary to obtain the inputs for the service of CPC chambers of CERN.

Tinku Sinha; D Das; L Das; Debasish Das; Sukalyan Chattopadhyay

3.3.1.3 Response of Multi-strip Multi-gap Resistive Plate Chamber using pulsed electron beam

We developed a special laboratory at SINP, Kolkata for developing ultra fast radiation detector [Multi gap multi strip resistive plate chamber (MMRPC)]. In this laboratory, for the first time in India, technologically challenging, low cost, multi purpose detector with timing resolution better than 100 ps with efficiency 99% has been developed.

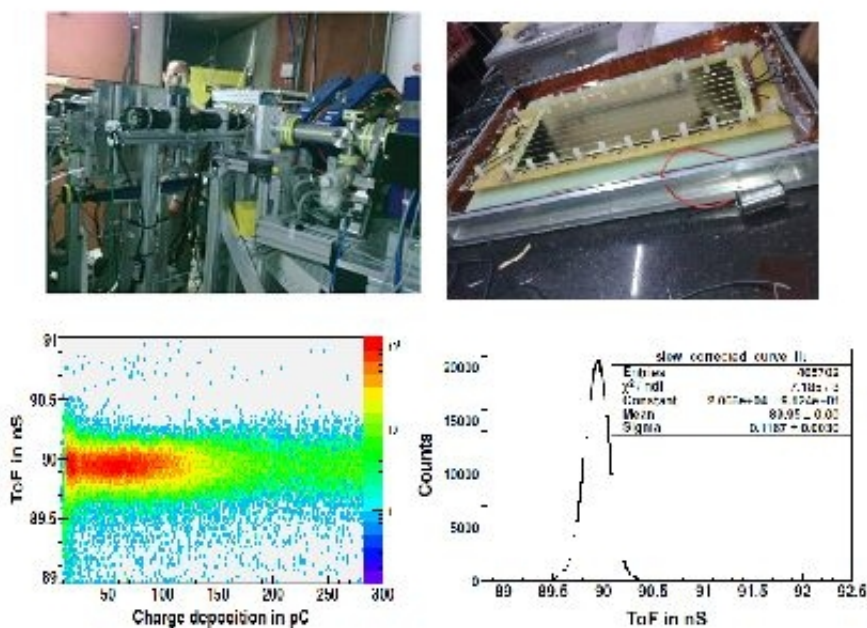


Figure 1. (Top-left) Photograph of experimental setup at ELBE during experiment using the MRPC (Top-right) anode plate developed at SINP laboratory. (Bottom-left) Spectra of deposited charge against time after slew correction using pulsed electron beam (Bottom-right). Projected timing spectra of the MRPC for pulsed electron.

Detailed response of the developed detector (SINP developed MMRPC) with different controlling parameters was studied with the pulsed electron beam from ELBE at Helmholtz-Zentrum Dresden-Rossendorf. The obtained time resolution (dt) of the detector after slew correction was 91.5 (3) ps. Position resolution measured along (s_x) and across (s_y) the strip was 1.9(0.7) cm and 0.58 cm, respectively. The measured absolute efficiency of the detector for minimum ionizing particle like electron was 95.8(1.3) %. Better timing resolution of the detector can be achieved by restricting the events to a single strip and/or using graphical cut at charge distribution plot. The response of the detector was mainly in avalanche mode but a few percentage of streamer mode response was also observed. A comparison of the response of these two modes with trigger rate was studied.

This detector has wide range of utility in both fundamental science such as particle physics, astrophysics, nuclear physics etc and applied physics like medical imaging, security etc. A paper has been submitted for publication.

U Datta Pramanik; S Chakraborty; A Rahaman; P Basu; J Basu...S Chatterjee; PK Das...J Panjaa; et al

CMS

a. A detailed description is reported of the analysis used by the CMS Collaboration in the search for the standard model Higgs boson in pp collisions at the LHC, which led to the observation of a new boson. The data sample corresponds to integrated luminosities up to 5.1 fb⁻¹ at $\sqrt{s} = 7$ TeV, and up to 5.3 fb⁻¹ at $\sqrt{s} = 8$ TeV. The results for five Higgs boson decay modes, $\gamma\gamma$, WW , ZZ , bb , and $\tau\tau$, which show a combined local significance of 5 standard deviations near 125 GeV, are reviewed. A fit to the invariant mass of the two high resolution channels, $\tau\tau$ and ZZ , gives a mass estimate of 125.3 ± 0.4 (stat.) ± 0.5 (syst.) GeV. The measurements are interpreted in the context of the standard model Lagrangian for the scalar Higgs field interacting with fermions and vector bosons. The measured values of the corresponding couplings are compared to the standard model predictions. The hypothesis of custodial symmetry is tested through the measurement of the ratio of the couplings to the W and Z bosons. All the results are consistent, within their uncertainties, with the expectations for a standard model Higgs boson. *J. High Energy Phys.* 06 (2013) 081 b. Results are presented of a search for compositeness in electrons and muons using a data sample of pp collisions at a center-of-mass energy $\sqrt{s} = 7$ TeV collected with the CMS detector at the LHC and corresponding to an integrated luminosity of 5.0 inverse femtobarns. Excited leptons (l^*) are assumed to be produced via contact interactions in conjunction with a standard model lepton and to decay via $l^* \rightarrow l \gamma$, yielding a final state with two energetic leptons and a photon. The number of events observed in data is consistent with that expected from the standard model. The 95% confidence upper limits for the cross section for the production and decay of excited electrons (muons), with masses ranging from 0.6 to 2 TeV, are 1.48 to 1.24 fb (1.31 to 1.11 fb). Excited leptons with masses below 1.9 TeV are excluded for the case where the contact interaction scale equals the excited lepton mass. These are the best limits published to date. *Phys. Lett. B* 720 (2013) 309-329

3.4 Publications

3.4.1 Publications in Journal

3.4.1.1 Applied Nuclear Physics

S Ghosh†; Gobinda Gopal Khan†; K Mandal†; PMG Nambissan, Positron annihilation studies of vacancy-type defects and room temperature ferromagnetism in chemically synthesized Li-doped ZnO nanocrystals, *Journal of Alloys and Compounds* **590** (2014) 396

I Znakovskaya†; M Spanner†, S De et al, Transition between mechanisms of laser-induced field-free molecular orientation, *Physical Review Letters* **112** (2014) 113005

CC Dey, Probe-impurity interaction in dilute alloy $Zr(x)Hf(1-x) \sim 0.98$: Results from perturbed angular correlation measurements, *Solid State Communications* **179** 92014)43

Paramjit Singh†; Rajesh Kumar†; Jincemon Cyriac†...PMG Nambissan; et al, High energy (MeV)

ion fluence dependent nano scale free volume defects studies of PMMA films, Nuclear Instruments & Methods in Physics Research **B320** (2014)64

Utpal Rana†; PMG Nambissan; Sudip Malik†; Kuntal Chakrabarti, Effects of process parameters on the defects in graphene oxide-polyaniline composites investigated by positron annihilation spectroscopy, Physical Chemistry Chemical Physics **16** (2014) 3292

Atul V Thorat†; Tandra Ghoshal†; Justin D Holmes†; PMG Nambisan; et al, A positron annihilation spectroscopic investigation of europium-doped cerium oxide nanoparticles, Nanoscale **6** (2014) 608

Purba Bhattacharya; Sudeb Bhattacharya; Nayana Majumdar; Supratik Mukhopadhyay; Sandip Sarkar; et al, Comparison of bulk Micromegas with different amplification gaps, Nuclear Instruments & Methods in Physics Research **A732** (2013) 208

A Mukherjee†; M Banerjee†; S Basu†; PMG Nambissan; et al, Gadolinium substitution induced defect restructuring in multiferroic BiFeO₃: case study by positron annihilation spectroscopy, Journal of Physics **D46** (2013) Art No: 495309

R Boll†; D Anielski†; C Bostedt†...S De; et al, Femtosecond photoelectron diffraction on laser-aligned molecules: Towards time-resolved imaging of molecular structure, Physical Review **A88** (2013) Art No: 061402

CC Dey; SK Srivastava†, Electric quadrupole and magnetic dipole interactions at ¹⁸¹Ta impurity in Zr₂Ni₇ intermetallic compound: Experiment and first-principles calculations, Physica **B427** (2013) 126

Tilman Butz†; Satyendra K Das†; Chandni C Dey; et al, Recoil Induced Room Temperature Stable Frenkel Pairs in alpha-Hafnium Upon Thermal Neutron Capture, Zeitschrift fur Naturforschung **A68** (2013)610

CC Dey, Investigations of Zr-Ni intermetallic compounds by perturbed angular correlations, Journal of Magnetism and Magnetic Materials **342** (2013) 87

B Erk†; D Rolles†; L Foucar†...Sankar De; et al, Inner-shell multiple ionization of polyatomic molecules with an intense x-ray free-electron laser studied by coincident ion momentum imaging, Journal of Physics **B46** (2013) Art No: 164031

Subhajit Karmakar; Sandip Sarkar, Orientation enhancement in early visual processing can explain time course of brightness contrast and White's illusion, Biological Cybernetics **107** (2013)337

S Ghosh†; Gobinda Gopal Khan†; K Mandal†; Anirban Samanta; PMG Nambissan; et al, Evolution of Vacancy-Type Defects, Phase Transition, and Intrinsic Ferromagnetism during Annealing of Nanocrystalline TiO₂ Studied by Positron Annihilation Spectroscopy, Journal of Physical Chemistry C **117** (2013) 8458

Shaibal Saha, Minimal digital electronic relay-feedback control for sequential movement of observatory shutters, Int Journal Scientific & Engineering Research **4** (2013) 1081

D Abbaneo; M Abbrescia; M Abi Akl...N Majumdar; S Mukhopadhyay; et al, Studies on the upgrade of the muon system in the forward region of the CMS experiment at LHC with GEMs, Journal of Instrumentation **9** (2014) Art No: C01053

N Majumdar; S Mukhopadhyay, Development of the data acquisition system for the Triple-GEM detectors for the upgrade of the CMS forward muon spectrometer, Journal of Instrumentation **9** (2014) C03052

Sreetama Dutta; Bichitra Nandi Ganguly, Characteristics of Dispersed ZnO-Folic acid Conjugate in Aqueous Medium, Advances in Nanoparticles **3** (2014) 23

Sreetama Dutta; Sourav Sarkar; Bichitra Nandi Ganguly, Positron Annihilation Study of ZnO Nanoparticles Grown Under Folic Acid Template, J Material Sci Eng **3** (2014) 1000134

PMG Nambissan; VK Lakhanit; KB Modit, Positron and positronium annihilation as probes to identify cation substitution effects in $\text{CoCr}_x\text{Fe}_{2-x}\text{O}_4$, Materials Science Forum **733** (2013) 215

PMG Nambissan; O Mondalit; S Chakrabarty; et al, Ni-substitution induced inversion in ZnFe_2O_4 seen by positron annihilation, Materials Science Forum **733** (2013) 219

PMG Nambissan, Nano sulfide and oxide semiconductors as promising materials for studies by positron annihilation, Journal of Physics: Conference Series **443** (2013) 012040

AV Thorat, T Ghoshal; MA Morris; PMG Nambissan, Eu-Doped Cerium Oxide Nanoparticles Studied by Positron Annihilation, Acta Physica Polonica **A125** (2014) 756

3.4.1.2 High Energy Nuclear and Particle Physics

SP Adhya; PK Roy; AK Dutt-Mazumder, Modifications to the pulsar kick velocity due to magnetic interactions in dense plasma, Journal of Physics **G41** (2014) Art No: 025201

Mahatsab Mandal; Pradip Roy, Wake potential in collisional anisotropic quark-gluon plasma, Physical Review **D88** (2013) Art No: 074013

Leonard S Kisslinger; Debasish Das, Ψ AND Υ PRODUCTION IN pp COLLISIONS AT 7.0 TeV, Modern Physics Letters **A28** (2013) Art No: 1350120 (205 HEP)

B Abelev; J Adam; D Adamova; S Chattopadhyay; D Das; K Das; AK Dutta Majumdar; P Khan; B Paul; P Roy; T Sinha; et al, Multiplicity dependence of two-particle azimuthal correlations in pp collisions at the LHC, Journal of High Energy Physics, **Issue: 9** (2013) Art No: 049

Sreemoyee Sarkar; Abhee K Dutt-Mazumder, Heavy quark damping rate in hot viscous QCD plasma, Physical Review **D88** (2013) Art No: 054006

J Sethi; R Palit; S Saha; S Chattopadhyay; et al, Structure of nearly degenerate dipole bands

in ^{108}Ag , Physics Letters **B725** (2013) 85

Leonard S Kisslinger†; *Debasish Das*, UPSILON PRODUCTION IN pp COLLISIONS FOR FORWARD RAPIDITIES AT LHC, Modern Physics Letters **A28** (2013) Art No: 1350067

Santosh Roy; S Chattopadhyay, Comment on "Evidence of antimagnetic rotation in odd-A Cd-105", Physical Review **C87** (2013) Art No: 059801

Sreemoyee Sarkar; Abhee K Dutt-Mazumder, Non-Fermi liquid behavior of thermal relaxation time in degenerate electron plasma, Physical Review **D87** (2013) Art No: 076003

D Abbaneo; M Abbrescia; M Abi Akl; et al, Studies on the upgrade of the muon system in the forward region of the CMS experiment at LHC with GEMs, Journal of Instrumentation **9** (2014) Art No: C01053

3.4.1.3 ALICE Collaboration

ALICE Collaboration, Two- and three-pion quantum statistics correlations in Pb-Pb collisions at root S-NN=2.76 TeV at the CERN Large Hadron Collider, Physical Review **C89** (2014) Art No: 024911

ALICE Collaboration, J/psi production and nuclear effects in p-Pb collisions at=5.02 TeV, Journal of High Energy Physics **Issue: 2** (2014) Art No: 073

ALICE Collaboration, Multiplicity dependence of pion, kaon, proton and lambda production in p-Pb collisions at root s(NN)=5.02 TeV, Physics Letters **B728** (2014)25

ALICE Collaboration, Multi-strange baryon production at mid-rapidity in Pb-Pb collisions at root s(NN)=2.76 TeV, Physics Letters **B728** (2014)216

ALICE Collaboration, Multiplicity dependence of the average transverse momentum in pp, p-Pb, and Pb-Pb collisions at the LHC, Physics Letters **B727** (2013) 371

ALICE Collaboration, Directed Flow of Charged Particles at Midrapidity Relative to the Spectator Plane in Pb-Pb Collisions at root s(NN)=2.76TeV, Physical Review Letters **111** (2013) Art No: 232302

ALICE Collaboration, K-S(0) and Lambda Production in Pb-Pb Collisions at root s(NN)=2: 76 TeV, Physical Review Letters **111** (2013) Art No: 222301

ALICE Collaboration, Charmonium and e(+)e(-) pair photoproduction at mid-rapidity in ultra-peripheral Pb-Pb collisions at root s(NN)=2.76 TeV, European Physical Journal **C73** (2013) Art No: 2617

ALICE Collaboration, Centrality dependence of the pseudorapidity density distribution for charged particles in Pb-Pb collisions at root s(NN)=2.76 TeV, Physics Letters **B726** (2013)610

ALICE Collaboration, J/psi Elliptic Flow in Pb-Pb Collisions at $\sqrt{s(NN)}=2.76$ TeV, Physical Review Letters **111** (2013) Art No: 162301

ALICE Collaboration, Centrality dependence of pi, K, and p production in Pb-Pb collisions at $\sqrt{s(NN)}=2.76$ TeV, Physical Review **C88** (2013) Art No: 044910

ALICE Collaboration, Centrality determination of Pb-Pb collisions at $\sqrt{s(NN)}=2.76$ TeV with ALICE, Physical Review **C88** (2013) Art No: 044909

ALICE Collaboration, Long-range angular correlations of pi, K and p in p-Pb collisions at $\sqrt{s(NN)}=5.02$ TeV, Physics Letters **B726** (2013) 164

ALICE Collaboration, Performance of the ALICE VZERO system, Journal of Instrumentation **8** (2013) Art No: P10016

ALICE Collaboration, D Meson Elliptic Flow in Noncentral Pb-Pb Collisions at $\sqrt{s(NN)}=2.76$ TeV, Physical Review Letters **111** (2013) Art No: 102301

ALICE Collaboration, Mid-rapidity anti-baryon to baryon ratios in pp collisions at $\sqrt{s}=0.9, 2.76$ and 7 TeV measured by ALICE, European Physical Journal **C73** (2013) Art No: 2496

ALICE Collaboration, Charge correlations using the balance function in Pb-Pb collisions at $\sqrt{s(NN)}=2.76$ TeV, Physics Letters **B723** (2013) 267

ALICE Collaboration, Measurement of inelastic, single- and double-diffraction cross sections in proton-proton collisions at the LHC with ALICE, European Physical Journal **C73** (2013) Art No: 2456

ALICE Collaboration, Measurement of the inclusive differential jet cross section in pp collisions at $\sqrt{s}=2.76$ TeV, Physics Letters **B722** (2013) 262

ALICE Collaboration, Net-Charge Fluctuations in Pb-Pb Collisions at $\sqrt{s(NN)}=2.76$ TeV, Physical Review Letters **110** (2013) Art No: 152301

ALICE Collaboration, Measurement of electrons from beauty hadron decays in pp collisions at $\sqrt{s}=7$ TeV, Physics Letters **B721** (2013) 13

3.4.1.4 CMS Collaboration

CMS Collaboration, Measurement of the $t\bar{t}$ production cross section in the dilepton channel in pp collisions at $\sqrt{s} = 8$ TeV (vol 2, 024, 2014), Journal of High Energy Physics, **Issue: 2** (2014) Art No: 102

CMS Collaboration, Studies of azimuthal dihadron correlations in ultra-central PbPb collisions at $\sqrt{s_{NN}}=2.76$ TeV, Journal of High Energy Physics, **Issue: 2** (2014) Art No: 088

CMS Collaboration, Measurement of the $t\bar{t}$ production cross section in the dilepton channel in pp collisions at $\sqrt{s}=8$ TeV, Journal of High Energy Physics, **Issue: 2** (2014) Art No: 024

CMS Collaboration, Search for the standard model Higgs boson produced in association with a W or a Z boson and decaying to bottom quarks, Physical Review **D89** (2014) Art No: UNSP 012003

CMS Collaboration, Determination of the top-quark pole mass and strong coupling constant from the $t\bar{t}$ production cross section in pp collisions at $\sqrt{s}=7$ TeV, Physics Letters **B728** (2014) 496

CMS Collaboration, Measurement of Higgs boson production and properties in the WW decay channel with leptonic final states, Journal of High Energy Physics, **Issue: 1** (2014) Art No: 096

CMS Collaboration, Rapidity distributions in exclusive Z plus jet and gamma plus jet events in pp collisions at $\sqrt{s}=7$ TeV, Physical Review **D88** (2013) Art No: 112009

CMS Collaboration, Measurement of the prompt J/ψ and $\psi(2S)$ polarizations in pp collisions at $\sqrt{s}=7$ TeV, Physics Letters **B727** (2013) 381

CMS Collaboration, Jet and underlying event properties as a function of charged-particle multiplicity in proton-proton collisions at $\sqrt{s}=7$ TeV, European Physical Journal **C73** (2013) Art No: 2674

CMS Collaboration, Measurement of the cross section and angular correlations for associated production of a Z boson with b hadrons in pp collisions at $\sqrt{s}=7$ TeV, Journal of High Energy Physics, **Issue: 12** (2013) Art No: 039

CMS Collaboration, Measurement of the differential and double-differential Drell-Yan cross sections in proton-proton collisions at $\sqrt{s}=7$ TeV, Journal of High Energy Physics, **Issue: 12** (2013) Art No: 030

CMS Collaboration, Search for Top Squarks in R-Parity-Violating Supersymmetry Using Three or More Leptons and b-Tagged Jets, Physical Review Letters **111** (2013) Art No: 221801

CMS Collaboration, Searches for new physics using the $t\bar{t}$ over-bar invariant mass distribution in pp collisions at $\sqrt{s}=8$ TeV, Physical Review Letters **111** (2013) Art No: 211804

CMS Collaboration, Search for a non-standard-model Higgs boson decaying to a pair of new light bosons in four-muon final states, Physics Letters **B726** (2013) 564

CMS Collaboration, Search for a Higgs boson decaying into a Z and a photon in pp collisions at $\sqrt{s}=7$ and 8 TeV, Physics Letters **B726** (2013) 587

CMS Collaboration, The performance of the CMS muon detector in proton-proton collisions at $\sqrt{s}=7$ TeV at the LHC, Journal of Instrumentation **8** (2013) Art No: P11002

CMS Collaboration, Search for a new bottomonium state decaying to $Upsilon(1S)\pi^+\pi^-$ in

pp collisions at $\sqrt{s}=8$ TeV, Physics Letters **B727** (2013) 57

CMS Collaboration, Angular analysis and branching fraction measurement of the decay $B^0 \rightarrow K^{*0}\mu^+\mu^-$, Physics Letters **B727** (2013) 77

CMS Collaboration, Measurement of the $\Upsilon(1S)$, $\Upsilon(2S)$, and $\Upsilon(3S)$ cross sections in pp collisions at $\sqrt{s}=7$ TeV, Physics Letters **B727** (2013)101

CMS Collaboration, Measurement of the W^+W^- cross section in pp collisions at and limits on anomalous $WW\gamma$ and WWZ couplings, European Physical Journal **C73** (2013)Art No: 2610

CMS Collaboration, Measurement of the production cross section for $Z \gamma \rightarrow \nu\bar{\nu}\gamma$ in pp collisions at $\sqrt{s}=7$ TeV and limits on $ZZ \gamma$ and $Z \gamma\gamma$ triple gauge boson couplings, Journal of High Energy Physics,**Issue: 10** (2013)Art No: 164

CMS Collaboration, Measurement of the W-boson helicity in top-quark decays from $t\bar{t}$ production in lepton plus jets events in pp collisions at $\sqrt{s}=7$ TeV, Journal of High Energy Physics, **Issue: 10** (2013)Art No: 167

CMS Collaboration, Measurement of the ratio of the inclusive 3-jet cross section to the inclusive 2-jet cross section in pp collisions at $\sqrt{s}=7$ TeV and first determination of the strong coupling constant in the TeV range, European Physical Journal **C73** (2013)Art No: 2604

CMS Collaboration, Search for gluino mediated bottom- and top-squark production in multijet final states in pp collisions at 8 TeV, Physics Letters **B725** (2013) 243

CMS Collaboration, Interpretation of searches for supersymmetry with simplified models, Physical Review **D88** (2013)Art No: 052017

CMS Collaboration, Search for supersymmetry in hadronic final states with missing transverse energy using the variables α_T and b-quark multiplicity in pp collisions at $\sqrt{s}=8$ TeV, European Physical Journal **C73** (2013) Art No: 2568

CMS Collaboration, Measurement of the $B_s^0 \rightarrow \mu^+\mu^-$ Branching Fraction and Search for $B^0 \rightarrow \mu^+\mu^-$ with the CMS Experiment, Physical Review Letters **111** 2013 Art No: 101804

CMS Collaboration, Measurement of neutral strange particle production in the underlying event in proton-proton collisions at $\sqrt{s}=7$ TeV, Physical Review **D88** (2013)Art No: UNSP052001

CMS Collaboration, Inclusive Search for Supersymmetry Using Razor Variables in pp Collisions at $\sqrt{s}=7$ TeV, Physical Review Letters**111** (2013) Art No: 081802

CMS Collaboration, Searches for Higgs bosons in pp collisions at $\sqrt{s}=7$ and 8 TeV in the context of four-generation and fermiophobic models, Physics Letters **B725** (2013) 36

CMS Collaboration, Multiplicity and transverse momentum dependence of two- and four-particle correlations in pPb and PbPb collisions, Physics Letters **B724** (2013)213

CMS Collaboration, search for new physics in events with same-sign dileptons and b jets in pp collisions at $\sqrt{s} = 8$ TeV (vol 3, pg 037, 2013), Journal of High Energy Physics, **Issue: 7** (2013)Art No: 041

CMS Collaboration, Measurement of the Λ_b^0 lifetime in pp collisions at $\sqrt{s}=7$ TeV, Journal of High Energy Physics,**Issue: 7** 2013)Art No: 163

CMS Collaboration, Searches for long-lived charged particles in pp collisions at $\sqrt{s}=7$ and 8 TeV, Journal of High Energy Physics, **Issue: 7** (2013)Art No: 122

CMS Collaboration, Study of exclusive two-photon production of W^+W^- in pp collisions at $\sqrt{s}=7$ TeV and constraints on anomalous quartic gauge couplings, Journal of High Energy Physics, **Issue: 7** (2013)Art No: 116

CMS Collaboration, Search for microscopic black holes in pp collisions at $\sqrt{s}=8$ TeV, Journal of High Energy Physics,**Issue: 7** (2013)Art No: UNSP 178

CMS Collaboration, Measurement of masses in the $t(\tilde{t})$ system by kinematic endpoints in pp collisions at $\sqrt{s}=7$ TeV, European Physical Journal **C73** (2013)Art No: 2494 (266)

CMS Collaboration, Measurement of the $X(3872)$ production cross section via decays to $J/\psi\pi^+\pi^-$ in pp collisions at $\sqrt{s}=7$ TeV, Journal of High Energy Physics,**Issue: 4** (2013)Art No: 154

CMS Collaboration, Search for physics beyond the standard model in events with tau leptons, jets, and large transverse momentum imbalance in pp collisions at $\sqrt{s}=7$ TeV, European Physical Journal **C73** (2013)Art No: UNSP 2493)

CMS Collaboration, Search for heavy resonances in the W/Z-tagged dijet mass spectrum in pp collisions at 7 TeV, Physics Letters **B723** (2013) 280

CMS Collaboration, Search for narrow resonances using the dijet mass spectrum in pp collisions at $\sqrt{s}=8$ TeV, Physical Review **D87** (2013) Art No: 114015

CMS Collaboration, Measurements of differential jet cross sections in proton-proton collisions at $\sqrt{s}=7$ TeV with the CMS detector, Physical Review **D87** (2013)Art No: UNSP 112002

CMS Collaboration, Measurement of inelastic, single- and double-diffraction cross sections in proton-proton collisions at the LHC with ALICE, European Physical Journal **C73** (2013)Art No: 2469

CMS Collaboration, Search for a standard-model-like Higgs boson with a mass in the range 145 to 1000 GeV at the LHC, European Physical Journal **C73** (2013)Art No: 2469

CMS Collaboration, Observation of a new boson with mass near 125 GeV in pp collisions at $\sqrt{s}=7$ and 8 TeV, Journal of High Energy Physics,**Issue: 6** (2013)Art No: 081

CMS Collaboration, Search for a Higgs boson decaying into a b-quark pair and produced in association with b quarks in proton-proton collisions at 7 TeV, Physics Letters **B722** (2013) 207

CMS Collaboration, Event shapes and azimuthal correlations in Z plus jets events in pp collisions at $\sqrt{s}=7$ TeV, Physics Letters **B722** (2013) 238

CMS Collaboration, Search for long-lived particles in events with photons and missing energy in proton-proton collisions at $\sqrt{s}=7$ TeV, Physics Letters **B722** (2013) 273

CMS Collaboration, Search for fractionally charged particles in pp collisions at $\sqrt{s}=7$ TeV, Physical Review **D87** (2013) Art No: 092008

CMS Collaboration, Measurement of the inelastic proton-proton cross section at $\sqrt{s}=7$ TeV, Physics Letters **B722** (2013) 5

CMS Collaboration, Search for anomalous production of highly boosted Z bosons decaying to $\mu^+\mu^-$ in proton-proton collisions at $\sqrt{s}=7$ TeV, Physics Letters **B722** (2013) 28

CMS Collaboration, Measurement of the $t\bar{t}$ production cross section in the all-jet final state in pp collisions at $\sqrt{s}=7$ TeV, Journal of High Energy Physics, **Issue: 5** (2013) Art No: UNSP 065

CMS Collaboration, Search for the standard model Higgs boson produced in association with a top-quark pair in pp collisions at the LHC, Journal of High Energy Physics, **Issue: 5** (2013) Art No: 145

CMS Collaboration, Studies of jet mass in dijet and W/Z plus jet events, Journal of High Energy Physics, **Issue: 5** (2013) Art No: UNSP 090

CMS Collaboration, Search for supersymmetry in pp collisions at $\sqrt{s}=7$ TeV in events with a single lepton, jets, and missing transverse momentum, European Physical Journal **C73** (2013) Art No: UNSP 2404

CMS Collaboration, Measurement of associated production of vector bosons and top quark-antiquark pairs in pp collisions at $\sqrt{s}=7$ TeV, Physical Review Letters **110** (2013) Art No: 172002

CMS Collaboration, Measurement of the W^+W^- and ZZ production cross sections in pp collisions at $\sqrt{s}=8$ TeV, Physics Letters **B721** (2013) 190

CMS Collaboration, Search for new physics in final states with a lepton and missing transverse energy in pp collisions at the LHC, Physical Review **D87** (2013) Art No: 072005

CMS Collaboration, Search for pair-produced dijet resonances in four-jet final states in pp collisions at $\sqrt{s}=7$ TeV, Physical Review Letters **110** (2013) Art No: 141802

CMS Collaboration, Search for Z' resonances decaying to $t\bar{t}$ in dilepton plus jets final states in pp collisions at $\sqrt{s}=7$ TeV, Physical Review **D87** (2013) Art No: 072002

CMS Collaboration, Search for supersymmetry in events with opposite-sign dileptons and missing transverse energy using an artificial neural network, Physical Review **D87** (2013) Art No: 072001 (352 HEP)

CMS Collaboration, Study of the underlying event at forward rapidity in pp collisions at $\sqrt{s}=0.9, 2.76, \text{ and } 7 \text{ TeV}$, *Journal of High Energy Physics*, **Issue: 4** (2013) Art No: 072

CMS Collaboration, Measurement of the $t(\bar{t})$ production cross section in the tau plus jets channel in pp collisions at $\sqrt{s}=7 \text{ TeV}$, *European Physical Journal* **C73** (2013) Art No: 2386

CMS Collaboration, Identification of b-quark jets with the CMS experiment, *Journal of Instrumentation* **8** (2013) Art No: P04013

3.4.1.5 Nuclear Physics

Abhijit Bisoi; M Saha Sarkar; S Sarkar†; S Ray...R Kshetri; et al, High spin spectroscopy in ^{34}Cl , *Physical Review* **C89** (2014) Art No: 024303

S Rajbanshi; Abhijit Bisoi; Somnath Nag†...S Chattopadhyay...M Saha Sarkar...A Goswami, Shape coexistence in the near-spherical ^{142}Sm nucleus, *Physical Review* **C89** (2014) Art No: 014315

DM Rossi†; P Adrich†; F Aksouh†...U Datta Pramanik; et al, Measurement of the Dipole Polarizability of the Unstable Neutron-Rich Nucleus ^{68}Ni , *Physical Review Letters* **111** (2013) Art No: 242503

Yu Aksyutina†; T Aumann†; K Boretzky†...U Datta Pramanik; et al, Study of the ^{14}Be Continuum: Identification and Structure of its Second 2^+ State, *Physical Review Letters* **111** (2013) Art No: 242501

MK Pradhan; A Mukherjee; Subinit Roy; P Basu; A Goswami; R Kshetri...M Saha Sarkar; et al, Importance of the 1n-stripping process in the $^6\text{Li}+^{159}\text{Tb}$ reaction, *Physical Review* **C88** (2013) Art No: 064603

H Pai†; G Mukherjee†; S Bhattacharya†...S Rajbanshi; A Goswami; et al, Band structures and intruder $\pi i_{13/2}$ state in ^{197}Tl , *Physical Review* **C88** (2013) Art No: 064302

Abhijit Bisoi; M Saha Sarkar; S Sarkar†...S Ray; Debasmitta Kanjilal...A Goswami; et al, Superdeformation and α -cluster structure in ^{35}Cl , *Physical Review* **C88** (2013) Art No: 034303

K Selvakumar; AK Singh; Subhashri Das...A Goswami; R Raut; A Mukherjee; U Datta Pramanik; et al, Shape evolution in ^{123}Cs and ^{124}Ba nuclei, *Physical Review* **C88** (2013) Art No: 024313

Dhrubajyoti Gupta; Subinit Roy; Rita Ghosh; Ajoy Kumar Mitra, Chemical composition of soil evolving from municipal solid waste using energy dispersive X-ray fluorescence, *X-Ray Spectrometry* **42** (2013) 268

Yu Aksyutina†; T Aumann†; K Boretzky†...U Datta Pramanik; et al, Structure of the unbound nucleus ^{13}Be : One-neutron knockout reaction data from ^{14}Be analyzed in a holistic approach, *Physical Review* **C87** (2013) Art No: 064316

C Langer; O Lepyoshkina; Yu Aksyutina†... U Datta Pramanik; et al, Thermonuclear reaction $^{30}\text{S}(p, \gamma)^{31}\text{Cl}$ studied via Coulomb breakup of ^{31}Cl , Phys Rev **C89** (2014) 035806

S Chakraborty; U Datta Pramanik; T Aumann†...S Chatterjee... G De...A Rahaman...J Ray... et al, Study of the Ground-state Configuration of Neutron-rich Aluminium Isotopes through Coulomb Break, EPJ **66** (2014) 02019

J Ray; U Datta Pramanik; RK Bhowmik; I Ray; A Rahaman; A Chakraborty; S Chakraborty, Exotic decay of hot rotating nuclei near proton drip line, EPJ **66** (2014) 02089

Yu Aksyutina†; T Aumann†; K Boretzky†...U Datta Pramanik, Momentum profile analysis in one-neutron knockout from Borromean nuclei, Phys Lett **B 718** (2013) 1309 (2013)

A Rahaman; U Datta Pramanik; T Aumann†, Study of ground state configuration of neutron-rich Na isotopes via Coulomb breakup, EPJ **66** (2014) 02087

C Caesar; T Aumann†; K Boretzky†, Beyond the neutron drip line: The unbound oxygen isotopes ^{25}O and ^{26}O Phys Rev C88 (2013) 024313

3.5 Ph D Awarded

Debasmita Kanjilal [Satyajit Saha], Spectroscopy of Trans-Lead Nuclei, Jadavpur University, Oct 2013

3.6 Seminars/Lectures given in Conference/Symposium/Schools

Debasish Das

- i. Bottomonium Physics, National meeting on the physics of Heavy Flavor(HF-2013) meet, IIT Bombay, Apr 29-May 1, 2013
- ii. Quarkonia Overview, Workshop in High Energy Physics and Phenomenology(WHEPP) XIII, Puri, Odhisa, Dec 12-21, 2013

Bichitra Nandi Ganguly

- i. Positron-Positronium Interaction in Herbal NanoMedicine, POSITRON-2013 meeting, BARC, Mumbai, Dec 9, 2013
- ii. Structural Features in Nano-ZnO-Folic acid Conjugate system, ICT, Hyderabad, Dec 11, 2013

Sankar De

- i. Ion-induced dissociation dynamics of polyatomic molecules Seminar in the Quantum Science and Engineering Center, Kyoto University, Japan, 6th December, 2013
- ii. Tracking wave packets dynamics in oxygen molecules with few-cycle infrared laser pulses Seminar in the Dept. of Chemistry, Osaka City University, Japan, 5th December, 2013
- iii. Following wave packet dynamics in diatomic molecules with few-cycle infrared laser pulses

Atomic Physics group seminar, Tokyo Metropolitan University, Japan, 2nd December, 2013

iv. Following dynamic nuclear wave packets in O₂ and CO with few-cycle infrared laser pulses M. Takahashi and K. Ueda groups joint seminar, Institute of Multidisciplinary Research for Advanced Materials, Tohoku University, Sendai, Japan, 26th November, 2013

v. Dynamic field-free orientation of polar molecules by intense two-color femtosecond laser pulses DAE - BRNS Theme Meeting on Ultrafast Science (UFS 2013), IIT Kharagpur, 24th - 26th October, 2013

M Saha Sarkar

i. Superdeformation and alpha-cluster structure in sd-shell nuclei (Plenary talk), Oct 1, 2013, International Conference in Subatomic Physics and Applications (CIPSA 2013), Constantine 1 University, Constantine, Algeria, Sept 30 - Oct 02, 2013

ii. Shell evolution in neutron rich nuclei, Sept 30, 2013, 9th International Conference in Subatomic Physics and Applications (CIPSA 2013), Constantine 1 University, Constantine, Algeria, Sept 30 - Oct 02, 2013

iii. What are the interests and relevance of Nuclear Physics in the present day world?, Physics Department, North Eastern Hill University, Shillong, Meghalaya, Apr 1, 2013

iv. Why and how do we detect gamma rays and x-rays?, Physics Department, North Eastern Hill University, Shillong, Meghalaya, Mar 26, 2014

PMG Nambissan

i. Blending of positron annihilation with nano semiconductors and spinel studies, National Seminar on Positron Annihilation, Department of Nuclear Physics, University of Madras, Chennai, Sept 3, 2013

ii. Eu-doped cerium oxide nanoparticles studied by positronannihilation, 41st Polish Seminar on Positron Annihilation, Lublin, Poland, Sept 9-13, 2013

iii. Nanocrystalline aspects of certain oxide semiconductors explored through recent positron annihilation studies, DAE-BRNS Theme Meeting on Positron Annihilation Spectroscopy (Positron-2013), Bhabha Atomic Research Centre, Mumbai, Dec 9-10, 2013

iv. Growing with a temperament in science, DST-Sponsored INSPIRE Science Internship Camp, Sacred Heart College, Thevara, Kerala, Jan 21-25, 2014

v. National Seminar on Facets of Nuclear and Radiation Physics (FNRP-14), Payyanur College, Payyanur, Kerala, Feb 13-14, 2014

vi. Growing with a temperament in science, National Seminar on Facets of Nuclear and Radiation Physics (FNRP-14), Payyanur College, Payyanur, Kerala, Feb 13-14, 2014

vii. Review of positron annihilation studies in multiferroic nanocrystalline compounds, International Conference on Nanoscience and Nanotechnology (ALIGARH NANO IV), Aligarh Muslim University, Aligarh, Mar 8-10, 2014

viii. Nanocrystallinity of materials as an avenue for positron annihilation studies, Indira Gandhi Centre for Atomic Research, Kalpakkam, October 28, 2013

Chinmoy Basu

i. Experimental results using loosely bound projectiles and Indirect method, Workshop on Secondary RIB using HYRA, IUAC, New Delhi, Nov 14-15, 2013

Ushasi Datta Pramanik

i. Coulomb Breakup as a Novel spectroscopic tool to probe quantum numbers of loosely bound nucleon(s) of exotic nuclei, 10th Latin American Symposium on Nuclear Physics and Applications,

Montevideo, Uruguay, Dec 1-6, 2013

- ii. Measurement of mass of neutrino from unique technique beta-decay measurement at SINP laboratory in the International School of Nuclear Physics, 35th Course, Neutrino Physics: Present and Future, Erice-Sicily, Sep 16-24, 2013
- iii. Direct probe to the ground state configuration of Island of Inversion neutron-rich nuclei through Coulomb Breakup, International Nuclear Physics Conference, Firenze, Jun 3, 2013
- iv. Nuclear Energy and research with Radioactive ion beam facility, International workshop on At the Crossroads Of Africa, Asia and Europe: Challenges and Perspective, Humboldt-Kolleg, Venice International University, Venezia, May 30-Jun 1, 2013

Sunanda Banerjee

- i. Higgs boson - have we seen it?, IOP Colloquium, May 2013
- ii. High Energy Physics and India", "Future of CMS, Workshop for Contemporary Trends in High Energy Physics and Experimentation, Panjab University, Mar 10-11, 2014
- iii. Higgs results from CMS, Triggering Discoveries in HEP, Jammu, Sep 2013
- iv. Performance of Geant4, 18th Geant4 Meeting, Seville, Sep 23-27, 2013
- v. SUSY searches at CMS, SUSY-DM workshop at CHEP, Bangalore, Oct 3-5, 2013
- vi. Lecture series on "Detector Simulation and Event Reconstruction, 2013 IEEE NSS/MIC/RTSD, Seoul, Oct 30-Nov 2, 2013
- vii. Search of Higgs boson at the LHC, Emerging Trends in Applied Mathematics, University of Calcutta, Feb 2014
- viii. New Particle and the Large Hadron Collider, National Test House, Calcutta, Aug 2013
- ix. The Universe and the Higgs boson, Konnagar Municipality, Sept 2013
- x. Exciting Tune in Higgs Huntingi, Bidhannagar Municipality, Sept 2013
- xi. Discovery of Higgs boson, IIT Guwahati, Mar 2014
- xii. Discovery of Higgs boson, Govt Teachers' Training College, Feb 8, 2014

Subir Sarkar

- i. The Computing Challenges at the Large Hadron Collider at CERN, Workshop on Recent Advances in Particle Physics, Astro Physics and Cosmology, University of Calcutta, Aug 7-8, 2013
- ii. Big Science and the Future of Science, Govt Teachers' Training College, Feb 8, 2014

Suchandra Dutta

- i. Electron Triggers (Track Trigger Integration Working Group), CMS Upgrade Week, DESY, Hamburg, Germany, Jun 3-7, 2013
- ii. The CMS Experiment at the Large Hadron Collider at CERN, Workshop on Recent Advances in Particle Physics, Astro Physics and Cosmology, University of Calcutta, Aug 7-8, 2013

Satyaki Bhattacharya

- i. Invited public lecture at Indian Association of Physics Teachers Convention, Oct 27, 2013
- ii. Invited public lecture at Gadbeta college, Feb 2014
- iii. Series of 4 pedagogic lectures on multivariate techniques in HEP, on invitation by RECAPP, HRI, Allahabad Feb 12-18, 2014
- iv. Invited talk in "School Leadership Conference: Encouraging Innovation in Classroom Practice", by the British Council, Chennai

Raman Khurana

- i. Higgs-IV: Search for standrad model Higgs boson in tau final states, Trieste Workshop: Work-

shop on Higgs and BSM physics, Jun 24-28, 2013, ICTP, Trieste, Italy

3.7 Teaching elsewhere

Chinmoy Basu

MSc (Pure Physics) Special paper: Nuclear Reactions and Astrophysics, Rajabazar Science College, University of Calcutta, Jan 2-Mar 31, 2014

3.8 Miscellany

Bichitra Nandi Ganguly

Received Rastriya Gourv award from India International Friendship Society a India Govt registered body at NewDelhi, in a seminar, presided by several dignitaries on Jun 12, 2014, India International Centre, New Delhi

Sankar De

Invitation fellowship (short term) from Japan Society for the Promotion of Science (JSPS) to perform research in collaboration with Prof Haruo Shiromaru of Tokyo Metropolitan University, November–December, 2013

CMS

We organized the 5-day long Asian CMS Data Analysis School(CMSDAS) in November 2013. CMSDAS is a technical, hands-on, computing intensive school where the students learn CMS software and data analysis techniques from the global experts. The local computing cluster was extensively used during the school by more than fifty participants. This is the first time that such a high profile CMS school was held in India.

Chapter 4

Plasma Physics

4.1 Summary of Research Activities of Divisions

4.1.1 Plasma Physics

Research activities in the plasma physics division encompass a variety of theoretical and experimental topics in the field of linear and nonlinear wave propagation. Theoretical studies using nonlinear analysis in Lagrange variables for various types of electrostatic modes in unmagnetized and magnetized plasmas have been carried out to demonstrate wave breaking phenomena due to phase-mixing processes. Such studies have relevance to electron energization and plasma particle heating in astrophysical environments and laboratory experiments. Using Lagrange fluid approach, collapse type processes associated with magnetosonic waves have been identified to be a possible mechanism for generation of strongly localized magnetic fields that are important in the astrophysical context of magnetic star formation. Studies are also being pursued to understand the formation of different types of nonlinear structures in classical as well as quantum plasmas.

In the field of strongly coupled dusty plasmas, effects of velocity shear have been extensively studied to show new types of instabilities in dust acoustic and shear waves. In non-Newtonian plasmas, shear flow-rate dependent viscosity in the shear thickening and thinning regimes is shown to modify the growth rates of Kelvin-Helmholtz instability. The stability of large scale vortex in a strongly coupled dusty plasma is being studied with short scale perturbations. It is shown that the free energy related to the velocity shear of the elliptical vortex flow can drive secondary instabilities of transverse shear wave when the resonance condition between vortex rotation frequency and secondary wave frequency are met. Such process can transfer energy from long scale vortex to the short scale secondary wave ultimately contributing to turbulence.

Experimental activities are being carried out in the MaPLE (Magnetized Plasma Linear Experiment), Double Layer Experiment (DLX), glow discharge plasma and the tokamak devices. In MAPLE nitrogen plasma produced by ECR discharge is used to study the parametric decay of waves in the ion cyclotron frequency range of frequencies into linear modes. Along with a mode whose frequency lies in the range of density gradient driven drift wave, sidebands of incident wave are also observed when the amplitude of the exciter signal goes above a threshold value. Sideband of the second harmonic is also observed. Preliminary analysis shows the possibility of ion Bernstein

waves in the device. Wave dispersion studies to confirm the identity of the excited waves are in progress.

In DLX, 2D measurements in a plasma diffusing in a diverging magnetic field have been carried out showing U-shaped potential contours and hollow conical density structures defined by the maximum diverging magnetic field lines passing through the radial edge of the exit aperture of the source. We observe a slow increase of the peak density along a hollow conical surface under various conditions indicating that the phenomenon is generic in nature.

Nonlinear dynamic experiments are being carried out in the DC glow discharge plasma device to study homoclinic and inverse homoclinic bifurcation and intermittent chaos. Different statistical and spectral methods have been used to explore the complex dynamics of the system. Theoretical and numerical modelling based on plasma fluid models leading to third order autonomous differential equation known as jerk equation explain a number of interesting chaotic phenomena based on bifurcation diagrams.

4.2 Research Activities

4.2.1 Plasma Physics

4.2.1.1 Velocity shear effect on the longitudinal wave in a strongly coupled dusty plasma

The characteristics of longitudinal dust acoustic wave (DAW) in presence of velocity shear have been investigated in a strongly coupled dusty plasma using the generalized hydrodynamic (GH) model. In the hydrodynamic regime ($\omega \tau \ll 1$), i.e. when characteristic time τ is slower than inverse of wave frequency, the viscosity in the GH model plays the usual role of wave damping, whereas in the kinetic regime ($\omega \tau \gg 1$), i.e. when characteristic time τ is larger than inverse of wave frequency, viscosity shows energy storing property in the wave. In the kinetic regime, we have studied the longitudinal mode (where ω is the frequency, k is the wave number, c_d is the dust acoustic velocity and c_s is the longitudinal velocity that arises due to viscosity) in presence of velocity shear. It is shown that velocity shear can destabilize this mode. Both nonmodal and modal techniques are employed to demonstrate the growth rate of the instability.

S Garai; D Banerjee; MS Janaki; N Chakrabarti

4.2.1.2 An exact solution in a gravitating fluid with a density-dependent viscosity

An exact nonlinear solution for a cold fluid in presence of a gravitational field and viscous dissipation is obtained using Lagrange variable. It is shown that with a density-dependent viscosity the nonlinear equation can be exactly solved. The solution indicates that in absence of viscosity and initial fluid velocity shear, density collapse occurs at time of the order of inverse Jeans frequency. The effect of viscosity is to delay the collapse but it can not halt the collapse. The initial fluid velocity shear can act in both directions: a positive one leads to delay, a negative one to a speeding up of the density collapse. This nonlinear solution may have some bearing with the structure

formations in the universe.

Nikhil Chakrabarti; Hans Schamel†

4.2.1.3 Nonlinear electron acoustic waves in presence of shear magnetic field

Nonlinear electron acoustic waves are studied in a quasineutral plasma in the presence of a variable magnetic field. The fluid model is used to describe the dynamics of two temperature electron species in a stationary positively charged ion background. Linear analysis of the governing equations manifests dispersion relation of electron magneto sonic wave. Whereas, nonlinear wave dynamics is being investigated by introducing Lagrangian variable method in long wavelength limit. It is shown from finite amplitude analysis that the nonlinear wave characteristics are well depicted by KdV equation. The wave dispersion arising in quasineutral plasma is induced by transverse magnetic field component. The results are discussed in the context of plasma of Earth's magnetosphere.

Manjitha Dutta†; Samiran Ghosh†; Manoranjan Khan†; Nikhil Chakrabarti

4.2.1.4 Nonlinear electron oscillations in a warm plasma

A class of nonstationary solutions for the nonlinear electron oscillations of a warm plasma are presented using a Lagrangian fluid description. The solution illustrates the nonlinear steepening of an initial Gaussian electron density disturbance and also shows collapse behavior in time. The obtained solution may indicate a class of nonlinear transient structures in an unmagnetized warm plasma.

Anwesa Sarkar; Chandan Maity; Nikhil Chakrabarti

4.2.1.5 Comparative study on nonlinear dynamics of magnetized and un-magnetized dc glow discharge plasma

Various nonlinear dynamical behaviors are experimentally observed to exist in magnetized dc glow discharge plasma. Nonlinear plasma fluctuations are seen evolving when the initial parameters such as discharge voltage, filling pressures, etc are changed in the presence of external magnetic field. A transition pattern of chaotic to quasiperiodicity is experimentally observed when a magnetic field is applied, which is not the case in the un-magnetized one. Hence, a comparative analysis is being conducted for both the cases of magnetized and un-magnetized plasma. The nonlinear behavior of the plasma oscillations are diagnosed by different techniques namely: power spectrum, phase space plotting, correlation dimension, Liapunov exponent, fractal dimension and Hurst exponent. Furthermore, it is noticed that with increasing discharge voltage, the glow emerges from the cathode, slowly moves toward the anode and finally sinks into the anode in a ballooning manner.

Bornali Sarma†; Sourabh S Chauhan†; AM Wharton; AN Sekar Iyengar

4.2.1.6 Continuous wavelet transform analysis for self-similarity properties of turbulence in magnetized DC glow discharge plasma

Characterization of self-similarity properties of turbulence in magnetized plasma is being carried out in DC glow discharge plasma. The time series floating potential fluctuation experimental data are acquired from the plasma by Langmuir probe. Continuous wavelet transform (CWT) analysis considering db4 mother wavelet has been applied to the experimental data and self-similarity properties are detected by evaluating the Hurst exponent from the wavelet variance plotting. From the CWT spectrum, effort is made to extract a highly correlated frequency by locating the brightest spot. Accordingly, those signals are treated for finding out correlation dimension and the Liapunov exponent so that the exact frequency responsible for the chaotic behavior could be found out.

Bornali Sarma†; Sourabh S Chauhan†; AM Wharton; AN Sekar Iyengar

4.2.1.7 Selective Excitation of Low Frequency Drift Waves by Density Modulation and Parametric Excitation of Higher Frequency Mode

Excitation of low frequency drift waves in a radial region of a weak density gradient is demonstrated experimentally by strong temporal modulation of the plasma density. Though a parallel electron current can destabilize drift waves throughout the region, we observe mode selection at the resonant location matching the frequency of modulation. Parametric mode-mode interaction among two excited drift modes to destabilize a higher frequency one is reported under the specific condition of the growth rate. Theoretically estimated growth rates fit well with the experiment.

Subir Biswas; Debjyoti Basu; Rabindranath Pal; Nikhil Chakrabarti

4.2.1.8 Nonstationary magnetosonic wave dynamics in plasmas exhibiting collapse

In a Lagrangian fluid approach, an explicit method has been presented previously to obtain an exact nonstationary magnetosonic-type wave solution in compressible magnetized plasmas of arbitrary resistivity showing competition among hydrodynamic convection, magnetic field diffusion, and dispersion [Chakrabarti et al., Phys. Rev. Lett. 106, 145003 (2011)]. The purpose of the present work is twofold: it serves (i) to describe the physical and mathematical background of the involved magnetosonic wave dynamics in more detail, as proposed by our original Letter, and (ii) to present an alternative approach, which utilizes the Lagrangian mass variable as a new spatial coordinate [Schamel, Phys. Rep. 392, 279 (2004)]. The obtained exact nonlinear wave solutions confirm the correctness of our previous results, indicating a collapse of the magnetic field irrespective of the presence of dispersion and resistivity. The mean plasma density, on the other hand, is less singular, showing collapse only when dispersive effects are negligible. These results may contribute to our understanding of the generation of strongly localized magnetic fields (and currents) in plasmas, and they are expected to be of special importance in the astrophysical context of magnetic star formation.

Nikhil Chakrabarti; Chandan Maity; Hans Schamel†

4.2.1.9 Phase-mixing of electrostatic modes in a cold magnetized electron-positron plasma

In a fluid description, we study space-time evolution of electrostatic oscillations in a cold magnetized electron-positron plasma. Nonlinear results up to third order, obtained by employing a simple perturbation technique, indicate phase-mixing and thus breaking of excited oscillations, and provide an expression for the phase-mixing time. It is shown that an increase in the strength of ambient magnetic field results in an increase in the phase-mixing time. The results of our investigation will be of relevance to astrophysical environments as well as laboratory experiments.

Chandan Maity; Nikhil Chakrabarti; Sudip Sengupta

4.2.1.10 Network of seismo-geochemical monitoring observatories for earthquake prediction research in India

Present paper deals with a brief review of the research carried out to develop multi-parametric gas-geochemical monitoring facilities dedicated to earthquake prediction research in India by installing a network of seismo-geochemical monitoring observatories at different regions of the country. In an attempt to detect earthquake precursors, the concentrations of helium, argon, nitrogen, methane, radon-222 (Rn-222), polonium-218 (Po-218), and polonium-214 (Po-214) emanating from hydrothermal systems are monitored continuously and round the clock at these observatories. In this paper, we make a cross correlation study of a number of geochemical anomalies recorded at these observatories. With the data received from each of the above observatories we attempt to make a time series analysis to relate magnitude and epicentral distance locations through statistical methods, empirical formulations that relate the area of influence to earthquake scale. Application of the linear and nonlinear statistical techniques in the recorded geochemical data sets reveal a clear signature of long-range correlation in the data sets.

Hirok Chaudhuri†; Chiranjib Barman†; AN Sekar Iyengar; et al

4.2.1.11 Kelvin-Helmholtz instability in non-Newtonian complex plasma

The Kelvin-Helmholtz (KH) instability is studied in a non-Newtonian dusty plasma with an experimentally verified model [Phys. Rev. Lett. 98, 145003 (2007)] of shear flow rate dependent viscosity. The shear flow profile used here is a parabolic type bounded flow. Both the shear thinning and shear thickening properties are investigated in compressible as well as incompressible limits using a linear stability analysis. Like the stabilizing effect of compressibility on the KH instability, the non-Newtonian effect in shear thickening regime could also suppress the instability but on the contrary, shear thinning property enhances it. A detailed study is reported on the role of non-Newtonian effect on KH instability with conventional dust fluid equations using standard eigenvalue analysis.

D Banerjee; S Garai; MS Janaki; Nikhil Chakrabarti

4.2.1.12 Nonlinear dynamical modelling of chaotic electrostatic ion cyclotron oscillations by jerk equations

Plasma being a nonlinear and complex system, is capable of sustaining a wide spectrum of waves, oscillations and instabilities. These fluctuations interact nonlinearly amongst themselves and also

with particles: electrons/ions and thus lead to nonlinear wave-wave or wave-particle interaction. In the presence of coherent waves the particles are accelerated whereas irregular oscillations can give rise to particle heating which is also called stochastic heating. Particle orbits are known to be randomized by the wave fields such that their motion can also become stochastic. For fusion to be sustained one needs a very high temperature plasma for an extended duration. It quite common to deploy external waves like electron cyclotron waves or ion cyclotron waves for plasma heating and current drive. These external waves also work only in certain regimes. Conventional plasma techniques have been able to answer several of the observations of the above processes related to heating transport etc, but nonlinear dynamics as a tool has helped in comprehending the plasma oscillations better. We have for the first time obtained a Third Order nonlinear ordinary differential equation (TONLODE) also known as jerk equation to describe the electrostatic ion cyclotron plasma oscillations in a magnetic field. The interesting feature of this equation is that it does not require an external forcing term to obtain chaotic behaviour.

AM Wharton; MS Janaki; ANS Iyengar

4.2.1.13 Long range correlation in earthquake precursory signals

Research on earthquake prediction has drawn serious attention of the geophysicist, geologist and investigators in different fields of science across the globe for many decades. Researchers around the world are actively working on recording pre-earthquake changes in non-seismic parameters through a variety of methods that include anomalous changes in geochemical parameters of the Earth's crust, geophysical properties of the lithosphere as well as ionosphere etc. Several works also have been done in India to detect earthquake precursor signals using geochemical and geophysical methods. However, very few works have been done so far in India in this field through the application of nonlinear techniques to the recorded geophysical and geochemical precursory signals for earthquakes. The present paper deals with a short review of the early works on geochemical precursors that have been carried out in India as yet. With a view to detect earthquake precursory signals by means of gas-geochemical method we developed a network of seismo-geochemical monitoring observatories in India in hot springs and mud volcano crater. In the last few years we detected several geochemical anomalies and those were observed prior to some major earthquakes that occurred within a radius of 1500 km from the test sites. In the present paper we have applied nonlinear techniques to the long term, real-time and natural data sets of radon-222 and associated gamma originated out of the terrestrial degassing process of the earth. The results reveal a clear signature of the long range correlation present in the geochemical time series. This approach appears to be a potential tool to explore intrinsic information hidden within the earthquake precursory signals.

H Chaudhuri; C Barman; ANS Iyengar; et al

4.2.1.14 Wave-Breaking Phenomena in a Relativistic Magnetized Plasma

We study the wave-breaking phenomenon of relativistic upper-hybrid (UH) oscillations in a cold magnetoplasma. For our purposes, we use the electron continuity and relativistic electron momentum equations, together with Maxwell's equations, as well as introduce Lagrangian coordinates to obtain an exact nonstationary solution of the governing nonlinear equations. It is found that bursts in the electron density appear in a finite time as a result of relativistic electron mass variations in the UH electric field, indicating a phase mixing or breaking of relativistic UH oscillations. We

highlight the relevance of our investigation of the UH wave phase-mixing or UH wave-breaking process to electron energization and plasma particle heating.

Chandan Maity; Anwesa Sarkar; Padma Kant Shukla†; Nikhil Chakrabarti

4.2.1.15 Disruption avoidance in the SINP-Tokamak by means of electrode-biasing at the plasma edge

Control of plasma disruption by a biased edge electrode is reported in SINP-Tokamak. The features that characterize a plasma disruption are reduced with increasing bias potential. The disruption can be completely suppressed with the concomitant stabilization of observed MHD modes that are allegedly precursors of the disruption. An $m = 3/n = 1$ tearing mode, which apparently causes disruption can be stabilized when a negative biasing potential is applied near the edge. These changes in the disruptive behavior with edge biasing are hypothesized to be due to changes in the current density profile.

Debjyoti Basu; Rabindranath Pal; Julio J Martinell†; et al

4.2.1.16 Phase mixing of upper hybrid oscillations in a cold inhomogeneous plasma placed in an inhomogeneous magnetic field

We study phase mixing/wave breaking phenomena of upper hybrid modes in a cold inhomogeneous plasma placed in an inhomogeneous magnetic field. Inhomogeneities both in the background ion density and magnetic field profile are treated as periodic in space but independent in time. The Lagrangian fluid description is employed to obtain an exact solution of this fully nonlinear problem. It is demonstrated that the upper hybrid modes, excited by an initial local charge imbalance, break via phase mixing, induced by the inhomogeneities. It is also shown that it is possible to avoid phase mixing in excited upper hybrid oscillations in an inhomogeneous plasma containing a finite amplitude ion density fluctuation. The choice of external magnetic field is shown to have a key role in avoiding phase mixing in such oscillations. The relevance of our investigation regarding the particle acceleration in an inhomogeneous plasma has also been discussed.

Anwesa Sarkar; Chandan Maity; Nikhil Chakrabarti

4.2.1.17 Nonlinear electron acoustic cyclotron waves in presence of uniform magnetic field

Nonlinear electron acoustic cyclotron waves (EACW) are studied in a quasineutral plasma in presence of uniform magnetic field. The fluid model is used to describe the dynamics of two temperature electron species in a stationary charge neutral inhomogeneous background. In long wavelength limit, it is shown that the linear electron acoustic wave is modified by the uniform magnetic field similar to that of electrostatic ion cyclotron wave. Nonlinear equations for these waves are solved by using Lagrangian variables. Results show that the spatial solitary wave-like structures are formed due to nonlinearities and dispersions. These structures transiently grow to larger amplitude unless dispersive effect is actively operative and able to arrest this growth. We have found that the wave dispersion originated from the equilibrium inhomogeneity through collective effect and is responsible for spatiotemporal structures. Weak dispersion is not able to stop the wave collapse and

singular structures of EACW are formed. Relevance of the results in the context of laboratory and space plasmas is discussed.

Manjistha Dutta†; Samiran Ghosh†; Rajkumar Roychoudhury†; Nikhil Chakrabarti

4.2.1.18 New nonlinear structures in a degenerate one-dimensional electron gas

The collective dynamics of nonlinear electron waves in an one-dimensional degenerate electron gas is treated using the Lagrangian fluid approach. A new class of solutions with a nontrivial space and time dependence is derived. Both analytical and numerical results demonstrate the formation of stable, breather-like modes, provided certain conditions are met. For large amplitudes of the initial density perturbation, a catastrophic collapse of the plasma density is predicted, even in the presence of the quantum statistical pressure and quantum diffraction dispersive effects. The results are useful for the understanding of the properties of general nonlinear structures in dense plasmas.

S Ghosh†; N Chakrabarti; F Haas†

4.2.1.19 Wave breaking of nonlinear electron oscillations in a warm magnetized plasma

Wave breaking phenomena of nonlinear electron oscillations around a homogeneous background of massive ions have been studied in a warm magnetized plasma by using Lagrangian variables. An inhomogeneity in the background magnetic field is shown to induce phase mixing and thus breaking of the oscillations. A nonlinear analysis in Lagrangian variables predicts that wave breaking may disappear above a critical value of the electron temperature. An estimate for the critical temperature has been provided.

Sourav Pramanik; Chandan Maity; Nikhil Chakrabarti

4.3 Developmental Work

4.3.1 Plasma Physics

4.3.1.1 The double layer experiment (DLX) and study of plasma diffusing in a diverging magnetic field

An experimental setup has been constructed for the study of plasma propulsion using the concept of electric double layer and study of plasma diffusing in a diverging magnetic field. A compensated Langmuir probe using passive external RF filter for measurements of density, a retarding field analyzer to find the ion energy distribution and an emissive probe to measure plasma potential have been developed. All three diagnostics are mounted on L-shaped configurations with the axial movements done by vacuum bellows and precision guide rail systems, with the carriages driven by stepper motors which can be controlled from a computer for precise movements.

S Chowdhury; MS Janaki; Abhijit Ghosh; et al

4.4 Publications

4.4.1 Publications in Journal

4.4.1.1 Plasma Physics

S Garai; D Banerjee; MS Janaki; N Chakrabarti, Velocity shear effect on the longitudinal wave in a strongly coupled dusty plasma, *Astrophysics and Space Science***349** (2014)789

Nikhil Chakrabarti; Hans Schamel†, An exact solution in a gravitating fluid with a density-dependent viscosity, *Journal of Plasma Physics***79** (2013)1075

Manjistha Dutta†; Samiran Ghosh†; Manoranjan Khan†; Nikhil Chakrabarti, Nonlinear electron acoustic waves in presence of shear magnetic field, *Physics of Plasmas***20** (2013)Art No: 122112

Anwesa Sarkar; Chandan Maity; Nikhil Chakrabarti, Nonlinear electron oscillations in a warm plasma, *Physics of Plasmas***20** (2013)Art No: 122303

Bornali Sarma†; Sourabh S Chauhan†; AM Wharton; AN Sekar Iyengar, Comparative study on nonlinear dynamics of magnetized and un-magnetized dc glow discharge plasma, *Physica Scripta***88** (2013)Art No: 065005

Bornali Sarma†; Sourabh S Chauhan†; AM Wharton; AN Sekar Iyengar, Continuous wavelet transform analysis for self-similarity properties of turbulence in magnetized DC glow discharge plasma, *Journal of Plasma Physics***79** (2013)885

Subir Biswas; Debjyoti Basu; Rabindranath Pal; Nikhil Chakrabarti, Selective Excitation of Low Frequency Drift Waves by Density Modulation and Parametric Excitation of Higher Frequency Mode, *Physical Review Letters***111** (2013)Art No: 115004

Nikhil Chakrabarti; Chandan Maity; Hans Schamel†, Nonstationary magnetosonic wave dynamics in plasmas exhibiting collapse, *Physical Review* **E88** (2013)Art No: 023102

Chandan Maity; Nikhil Chakrabarti; Sudip Sengupta, Phase-mixing of electrostatic modes in a cold magnetized electron-positron plasma, *Physics of Plasmas***20** (2013)Art No: 082302

Hirok Chaudhuri†; Chiranjib Barman†; AN Sekar Iyengar; et al, Network of seismo-geochemical monitoring observatories for earthquake prediction research in India, *Acta Geophysica***61** (2013) 1000

D Banerjee; S Garai; MS Janaki; Nikhil Chakrabarti, Kelvin-Helmholtz instability in non-Newtonian complex plasma, *Physics of Plasmas***20** (2013)Art No: 073702

AM Wharton; MS Janaki; AN Sekar Iyengar, Nonlinear dynamical modelling of chaotic electrostatic ion cyclotron oscillations by jerk equations, *European Physical Journal-Special Topics***222** (2013)751

H Chaudhuri; C Barman; AN Sekar Iyengar; et al, Long range correlation in earthquake precursory signals, *European Physical Journal-Special Topics* **222** (2013) 827

Chandan Maity; Anwesa Sarkar; Padma Kant Shukla†; Nikhil Chakrabarti, Wave-Breaking Phenomena in a Relativistic Magnetized Plasma, *Physical Review Letters* **110** (2013) Art No: 215002

Debjyoti Basu; Rabindranath Pal; Julio J Martinell†; et al, Disruption avoidance in the SINP-Tokamak by means of electrode-biasing at the plasma edge, *Physics of Plasmas* **20** (2013) Art No: 052502

Anwesa Sarkar; Chandan Maity; Nikhil Chakrabarti, Phase mixing of upper hybrid oscillations in a cold inhomogeneous plasma placed in an inhomogeneous magnetic field, *Physics of Plasmas* **20** (2013) Art No: 052301

Manjistha Dutta†; Samiran Ghosh†; Rajkumar Roychoudhury†; Nikhil Chakrabarti, Nonlinear electron acoustic cyclotron waves in presence of uniform magnetic field, *Physics of Plasmas* **20** (2013) Art No: 042301

Sourav Pramanik; Chandan Maity; Nikhil Chakrabarti, Wave breaking of nonlinear electron oscillations in a warm magnetized plasma, *Physics of Plasmas* **21** (2014) 022308

S Ghosh†; N Chakrabarti; F Haas†, New nonlinear structures in a degenerate one-dimensional electron gas, *Euro Phys Letters* **105** (2014) 30006

4.5 Ph D Awarded

Debabrata Banerjee [Nikhil Chakrabarti and MS Janaki], Waves and instabilities in inhomogeneous strongly coupled dusty plasma, HBNI, Jan 2014

4.6 Seminars/Lectures given in Conference/Symposium/Schools

Nikhil Chakrabarti

- i. Nonlinear Waves in a strongly coupled dusty plasma, the 3rd International symposium on Complex dynamical systems and applications, Indian Statistical Institute, Kolkata, Mar 10-12, 2014
- ii. Nonlinear wave propagation in a strongly coupled collisional dusty plasma, 7th International conference on the Physics of Dusty Plasma, University of Delhi, Mar 03-07, 2014
- iii. Lagrangian Fluid description to study nonlinear oscillations and waves in Plasmas, National conference on Union Radio Science, Symbiosis Institute of Technology, Pune, Jan 02-05, 2014
Chaired a session of Commission-H

MS Janaki

1. Waves and Instabilities in Strongly Coupled Dusty Plasma, Regional Conference on Radio Science, Symbiosis Institute of Technology, Pune, Jan 2-4, 2014
- ii. Magnetic structures as kinetic equilibria, Frontiers of Applied Mathematics, organized by Dept of applied mathematics, JU, Mar 27, 2014

4.7 Teaching elsewhere

Nikhil Chakrabarti

- i. Three lectures on basic plasma physics in refresher course organized by Mathematics Department, Jadavpur University on Nov 23 & 26, 2013
- ii. Ten Lectures on basic plasma physics to the M Sc Students of Gourbanga University, Malda, Aug 20-24, 2013

Chapter 5
Theoretical Physics & Astroparticle Physics

Chapter 5

Theoretical Physics & Astroparticle Physics

5.1 Summary of Research Activities of Divisions

5.1.1 Astroparticle Physics and Cosmology

The Astroparticle Physics & Cosmology (APC) Division carries out advanced research in the interface areas spanning High Energy Astrophysics, Cosmology, and Particle & Nuclear physics. During the year under review, members of the Division have carried out research on a variety of topics in AstroParticle Physics observational, experimental and theoretical.

Some highlights are given below:

(i) Experimental research on various aspects of Superheated Droplet Detectors (SDD) in connection with the international PICASSO Collaboration for search for the weakly interacting massive particle (WIMP) candidates of dark matter (DM). The PICASSO experiment is currently underway at the SNOLAB underground facility in Sudbury, Canada. The SINP group has performed research pertaining to (a) study of using low frequency acoustic signals to identify and discriminate between neutron and gamma-ray induced bubble nucleation events in SDDs, (b) study of a possible universal energy calibration curve valid for different liquids used in SDDs, and (c) determination of the nucleation parameter for heavy-ion induced bubble nucleation in SDDs.

(ii) High Energy Gamma Ray Astronomy: Members of APC Division have participated in several studies of multiwavelength observation as well as modeling of Very High Energy (VHE) gamma ray emission from various sources including blazars, TeV gamma ray emitting binary systems, supernova remnants (SNRs), and so forth. These studies have thrown new lights on possible physical mechanisms of emission of very high energy gamma rays from energetic astrophysical objects, as well as on the nature of the extragalactic background light (EBL) and the intergalactic magnetic field (IGMF).

(iii) Physics of Neutron Star interiors : Isospin dependence of entrainment in superfluid neutron stars in a relativistic model has been studied. It has been shown that the inclusion of rho meson exchange in baryon-baryon interaction strongly influences the entrainment parameter in a superfluid neutron star.

(iv) Theoretical research on Dark Matter and Dark Energy: Several theoretical as well as phenomenological issues pertaining to Dark Energy (DE) and direct as well as indirect detection of WIMP Dark Matter (DM) have been investigated.

In the area of DE, a two-parameter generalization for the dark energy equation of state (EOS) for thawing dark energy models, that includes various other thawing models as limiting cases, has been proposed and confronted with the latest observational data, and possible ways to distinguish between various models using observational data have been studied.

In another work the possibility of obtaining the observed late-time acceleration of the Universe within the context of a theory of a slow-moving Galileon field has been studied, and the constraints on the parameters of the theory from various observational data have been studied.

In the area of DM, the velocity distribution function (VDF) of the WIMPs hypothesized to constitute the DM halo of the Galaxy has been determined by inverting, the well-known NFW universal density profile of the DM halo by using Eddington's method, with the parameters of the NFW halo density profile determined from the observed rotation curve (RC) data of Galaxy by the Markov chain Monte Carlo technique. The derived most-likely isotropic VDF has been found to significantly differ from the Maxwellian form assumed in the so-called standard halo model customarily used in the analysis of the results of WIMP direct-detection experiments. The implications of the non-Maxwellian nature of the VDF for the analysis of the results of WIMP direct-detection experiments have also been studied. A two-component dark matter model has been proposed to explain the possible 130 GeV gamma-ray line from the galactic centre claimed to have been detected by some authors from their analysis of the Fermi-LAT satellite data. The model is based on an extension of the Standard Model by adding an inert Higgs doublet and a gauge singlet scalar with a $Z(2) \times Z(2)$ symmetry imposed on the full model. The gamma-ray line arises from self-annihilation of the DM particles and the model is shown to also give rise to the correct relic abundance of DM.

In another work, gamma ray and neutrino flux resulting from the annihilation of neutralinos (which are good candidate for WIMP DM) at the Galactic centre region have been calculated within the minimal anomaly mediated supersymmetry breaking (mAMSB) model, and the detection prospects of such gamma rays and neutrinos have been studied.

(v) Neutrino physics and astrophysics : Work has been continued towards understanding the neutrino masses and mixing angles. It has been shown that invoking type-I seesaw mechanism within the context of a neutrino mass matrix derived from a broken cyclic symmetry, all the neutrino oscillation data can be explained with a small (about 10 percent) breaking of the cyclic symmetry provided the neutrino masses follow a normal mass hierarchy. The Dirac phase and three Majorana phases are also numerically calculated.

In another work, it has been shown that current best-fit ranges of neutrino mass squared differences and mixing angles, including a value of θ_{13} in the observed range, can be accommodated within the context of type-I seesaw mechanism by perturbing (to lowest order) the $\mu - \tau$ symmetric four- and three zero neutrino Yukawa textures by introducing small $\mu - \tau$ symmetry breaking terms, provided all the light neutrinos have an inverted mass ordering.

Work has also been done in the area of neutrino astrophysics. The possibility of observing supernova (SN) neutrinos through the process of coherent elastic neutrino-nucleus scattering (CENNS) in future ton-scale detectors designed primarily for direct detection of dark matter has been investigated. In particular, the possibility of distinguishing the various phases of the SN neutrino emission has been investigated.

(vi) Gravitation: Various aspects of extremal and non-extremal spacetimes have been studied. These include a study of the inner-most stable circular orbits (ISCO) in extremal and non-extremal Kerr-Taub-NUT spacetimes, and the Lense-Thirring precession in Plebanski-Demianski Spacetimes. It has been found that the ISCO coincides with the horizon in the exactly extremal situa-

tion. It is also shown that there is no stable circular orbit in massless NUT spacetimes for timelike geodesics. In the study of Lense-Thirring precession, an exact expression of Lense-Thirring precession rate has been derived for non-extremal and extremal Plebanski-Demianski spacetimes, and the formula is used to find the exact Lense-Thirring precession rate in various axisymmetric spacetimes i.e., Kerr-Newman, Kerr-deSitter etc.

In another work, thermodynamics of quantum isolated horizons (QIH) have been studied with the most general structure possible for the Hamiltonian operator associated with the QIH. It is shown that for a quantum spacetime admitting a thermodynamically stable QIH as its internal boundary, there must exist a specific bound on the Barbero-Immirzi parameter if the entropy of the QIH obeys the Bekenstein-Hawking area law.

5.1.2 Theory

a) Particle Physics Phenomenology

An important ingredient to the full NNLO QCD correction to graviton mediated hadronic scattering processes namely the gluon and quark form factors of energy momentum tensor of the QCD part of the SM upto two-loop level in QCD has been computed.

A technically natural supersymmetric scenario for light uncolored and heavy colored superpartners has been constructed. Minimal supersymmetry has been confronted with latest experimental measurements. Properties of two-Higgs-doublet models have been analysed.

b) Non-perturbative Studies of Quantum Field Theories

Lattice QCD with Standard Wilson gauge and quark action was studied using domain decomposed Hybrid Monte Carlo (DD-HMC) algorithm. Autocorrelations of different observables and the low-lying spectrum were investigated. A first-time result that autocorrelations of topological susceptibility was found to be significantly reduced in presence of lighter quarks is expected to boost research in this area. Low-lying spectrum was found to be consistent with expectations from NLO chiral perturbation theory, another first result with naive Wilson quarks.

Topological susceptibility in lattice Yang-Mills theory with open boundary condition was studied. Open Boundary Condition, Wilson Flow and the Scalar Glueball Mass were explored. With open boundary conditions, trapping in topological sectors was largely avoided and results at smaller lattice spacings were also possible.

Transverse spin sum rules, relevant for polarized deep inelastic scattering were investigated.

c) Gravity and Cosmology

Previous calculations of black hole entropy in loop quantum gravity had led to a dominant term proportional to the area, but there was always a correction involving the logarithm of the area, the Chern-Simons level being assumed to be large. It has now been found that the calculations actually yield an entropy proportional to the area eigenvalue with no such correction if the Chern-Simons level is finite, so that the area eigenvalue can be relatively large.

Aspects of research in cosmology and its connection with particle physics have been explored. In particular, a viable model of dark energy that is stable under quantum corrections has been constructed. Further study is involved in finding theoretical inconsistencies of certain modified theories of gravity. Also work has been done on embedding certain inflationary models in string theory where N fields collectively drive inflation.

d) Strings

A class of 1/4 BPS supersymmetric D_p -brane solutions which interpolate between Lifshitz vacua in the IR and AdS solutions in the UV have been proposed. The properties of these classical solutions near the two fixed points have been studied in detail. These interpolating solutions are used to find

the entanglement entropy of boundary subsystems after compactification of the lightcone coordinate. Observations are made about the electric-magnetic duality and the thermal entropy of the dual Lifshitz Dp-brane systems.

It is observed that the (intersecting) branes of M/string theory, which are known to give AdS geometry (directly or upto a conformal transformation) in the near horizon limit, do also lead to Schrödinger/Lifshitz dual space-times (without or with hyperscaling violation) upon using appropriate solution generating transformation and dimensional reduction.

Several examples were given to illustrate the claim. Hyperscaling violating ‘strange metal’ phase of heavy fermion compounds can be described holographically by probe D-branes in the background of a Lifshitz space-time with hyperscaling violation. A zero sound mode, analogous to Fermi liquid, has been shown to exist in such system in some cases. AC conductivity has also been computed in this system.

Further (Super) Yang-Mills theory at finite heavy-quark density has been studied. This attempt tries to identify the correct ground state for a strongly coupled large N gauge theory at finite density. A family of solutions of 10-dimensional supergravity has been constructed, which are dual to the infra-red limit of strongly coupled large N gauge theories at finite density. The effect of a non-vanishing chemical potential on the thermalization time for a prototypical strongly coupled large N gauge theory are being analysed by studying the gravitational collapse dynamics in an asymptotically anti de-Sitter space-time.

e) QCD at Finite Temperature and Density

The dual heavy-ion colliders at RHIC and LHC have given opportunity to look simultaneously at the signatures of hot and dense QCD matter (QGP). The efforts are made in understanding data emerging from the era of dual Collider to move in new directions. On the other hand recent numerical lattice QCD (LQCD) has provided first principle information on various thermodynamic properties of QGP. A very successful effort is made to understand various static quantities with a state-of-the-art perturbation theory, known as Hard Thermal Loop perturbation theory.

f) Nuclear Theory

Information content of the weak-charge form factor in asymmetric nuclei are studied. Accurate measurements of the weak-charge form factor of ^{48}Ca and ^{208}Pb will have a profound impact on many aspects of nuclear theory and hadronic measurements of neutron skins of exotic nuclei at radioactive-beam facilities. The electric dipole polarizability in ^{208}Pb is studied using a large and representative set of microscopic mean field models. The prediction of droplet model that the product of dipole polarizability and the nuclear symmetry energy at saturation density is better correlated with the neutron skin thickness of ^{208}Pb than the polarizability alone is confirmed for the first time.

g) Mathematical Physics

Novel exactly solvable variants of the BC_N type of spin Calogero model have been constructed by using polarized spin reversal operators (PSRO). The strong coupling limit of such spin Calogero models leads to the BC_N type of Polychronakos spin chains with PSRO. Exact spectra of the BC_N type of spin Calogero models with PSRO have been derived and partition functions of the related spin chains have been computed. An interesting relation between the partition functions of the BC_N type and A_{N-1} type of Polychronakos spin chains has been found.

Unravelling hidden dimensions in integrable systems a novel quasi-higher dimensional nonlinear Schroedinger equation is introduced, lump-soliton solution of which, aided by ocean current, could model oceanic surface rogue waves. Further, bending of an optical solitonic beam along an arbitrary curve is achieved theoretically, controlling the boundary condition of the doped resonant medium, through which the beam propagates.

Noncommutative geometry is a model of Planck scale physics. The noncommutative corrections to black hole entropy have been analytically calculated within the kappa-Minkowski framework and

the renormalization of the Newton's constant has been obtained. In another line of work, effect of topological defects of Friedel sum rule in graphene has been calculated.

5.2 Research Activities

5.2.1 Astroparticle Physics and Cosmology

5.2.1.1 Inner-most stable circular orbits in extremal and non-extremal Kerr-Taub-NUT spacetimes

We study causal geodesics in the equatorial plane of the extremal Kerr-Taub-NUT spacetime, focusing on the inner-most stable circular orbit (ISCO), and we compare its behavior with extant results for the ISCO in the extremal Kerr spacetime. Calculations of the radii of the direct ISCO, its Kepler frequency, and the rotational velocity show that the ISCO coincides with the horizon in the exactly extremal situation. We also study geodesics in the strong non-extremal limit, i.e., in the limit of a vanishing Kerr parameter (i.e., for Taub-NUT and massless Taub-NUT spacetimes as special cases of this spacetime). It is shown that the radius of the direct ISCO increases with NUT charge in Taub-NUT spacetime. As a corollary, it is shown that there is no stable circular orbit in massless NUT spacetimes for timelike geodesics.

Chandrachur Chakraborty

5.2.1.2 A three-year multi-wavelength study of the very-high-energy γ -Ray Blazar 1ES 0229+200

The high-frequency-peaked BL Lacertae object 1ES 0229+200 is a relatively distant ($z = 0.1396$), hard-spectrum ($\Gamma \sim 2.5$), very-high-energy (VHE; $E > 100$ GeV) emitting gamma-ray blazar. VHE measurements of this active galactic nucleus have been used to place constraints on the intensity of the extragalactic background light and the intergalactic magnetic field (IGMF). A multi-wavelength study of this object centered around VHE observations by Very Energetic Radiation Imaging Telescope Array System (VERITAS) is presented. This study obtained, over a period of three years, an 11.7 standard deviation detection and an average integral flux $F(E > 300 \text{ GeV}) = (23.3 \pm 2.8_{stat} \pm 5.8_{sys}) \times 10^{-9} \text{ photons m}^{-2} \text{ s}^{-1}$, or 1.7% of the Crab Nebula's flux (assuming the Crab Nebula spectrum measured by H. E. S. S). Supporting observations from Swift and RXTE are analyzed. The Swift observations are combined with previously published Fermi observations and the VHE measurements to produce an overall spectral energy distribution which is then modeled assuming one-zone synchrotron-self-Compton emission. The χ^2 probability of the TeV flux being constant is 1.6%. This, when considered in combination with measured variability in the X-ray band, and the demonstrated variability of many TeV blazars, suggests that the use of blazars such as 1ES 0229+200 for IGMF studies may not be straightforward and challenges models that attribute hard TeV spectra to secondary γ -ray production along the line of sight.

E Aliu†; S Archambault†; T Arlen†...P Majumdar; et al

5.2.1.3 Observing supernova neutrino light curve in future dark matter detectors

The possibility of observing supernova (SN) neutrinos through the process of coherent elastic neutrino-nucleus scattering (CENNS) in future ton scale detectors designed primarily for direct detection of dark matter is investigated. In particular, we focus on the possibility of distinguishing the various phases of the SN neutrino emission. The neutrino emission rates from the recent long-term Basel/Darmstadt simulations are used to calculate the expected event rates. The recent state-of-the-art SN simulations predict closer fluxes among different neutrino flavors and lower average energies compared to the earlier simulation models. The estimated total event rates are found to be typically a factor of 2 lower than those predicted using older simulation models. We find that future 1-ton class Xe detectors will be able to detect neutrinos from a SN at a distance of 10 kpc provided they have relatively low nuclear recoil energy thresholds of less than or similar to 1 keV. At the same time, with an optimistic threshold of similar to 1 keV, demarcating the neutrinos associated with the accretion phase of a SN at 10 kpc from the Earth will require 10-ton class Xe detectors, while distinguishing the neutrinos associated with the neutronization burst phase of the explosion would typically require several tens of ton detectors. We also comment on the possibility of studying the properties of nonelectron flavor neutrinos from the CENNS of SN neutrinos.

Sovan Chakraborty; Pijushpani Bhattacharjee; Kamales Kar

5.2.1.4 Isospin dependence of entrainment in superfluid neutron stars in a relativistic model

We study the entrainment effect between superfluid neutrons and charge neutral fluid (called the proton fluid) which is made of protons and electrons in a neutron star interior within the two-fluid formalism and using a relativistic model where baryon-baryon interaction is mediated by the exchange of σ , ω , and ρ mesons. This model of strong interaction also includes scalar self-interactions. The entrainment matrix and entrainment parameter are calculated using the parameter sets of Glendenning (GL) and another non-linear (NL3) interaction. The inclusion of rho mesons strongly influences the entrainment parameter ($\epsilon(\text{mom})$) in a superfluid neutron star. The entrainment parameter is constant at the core and drops rapidly at the surface. It takes values within the physical range.

Apurba Khetoo; Debades Bandyopadhyay

5.2.1.5 Generalizing thawing dark energy models: the standard vis-a-vis model independent diagnostics

We propose a two-parameter generalization for the dark energy equation of state (EOS) w_X for thawing dark energy models which include PNGB, CPL and Algebraic thawing models as limiting cases and confront our model with the latest observational data namely Type Ia supernovae, observational Hubble data, cosmic microwave background, Baryon Oscillation Spectroscopic Survey data. Our analysis reveals that the phantom type of thawing dark energy is favoured up to 2σ confidence level (CL). These results also show that thawing dark energy EOS is not unique from observational point of view. Though different thawing dark energy models are not distinguishable from each other from best-fitting values (up to 2σ CLs) of matter density parameter (Ω_m^0) and hubble parameter (H_0) at the present epoch, best-fitting plots of linear growth of matter perturbation

(f) and average deceleration parameter (q_{av}); the difference indeed reflects in best-fitting variations of thawing dark energy EOS, model-independent geometrical diagnostics like the statefinder pair r, s and $Om3$ parameter. We are thus led to the conclusion that unlike the standard observables (Ω_m^0, H_0, f and q_{av}), the model-independent parameters (r, s and $Om3$) and the variations of EOS (in terms of $w(X)-w'_X$ plots) serve as model discriminators for thawing dark energy models.

Debabrata Adak; Debasish Majumdar; Supratik Pal

5.2.1.6 MULTIWAVELENGTH OBSERVATIONS OF THE TeV BINARY LS I+61° 303 WITH VERITAS, Fermi-LAT, AND Swift/XRT DURING A TeV OUTBURST

We present the results of a multiwavelength observational campaign on the TeV binary system LS I+61°303 with the VERITAS telescope array (>200 GeV), Fermi-LAT (0.3-300 GeV), and Swift/XRT (2-10 keV). The data were taken from 2011 December through 2012 January and show a strong detection in all three wavebands. During this period VERITAS obtained 24.9 hr of quality selected livetime data in which LS I+61°303 was detected at a statistical significance of 11.9σ . These TeV observations show evidence for nightly variability in the TeV regime at a post-trial significance of 3.6σ . The combination of the simultaneously obtained TeV and X-ray fluxes do not demonstrate any evidence for a correlation between emission in the two bands. For the first time since the launch of the Fermi satellite in 2008, this TeV detection allows the construction of a detailed MeV-TeV spectral energy distribution from LS I+61°303. This spectrum shows a distinct cutoff in emission near 4 GeV, with emission seen by the VERITAS observations following a simple power-law above 200 GeV. This feature in the spectrum of LS I+61°303, obtained from overlapping observations with Fermi-LAT and VERITAS, may indicate that there are two distinct populations of accelerated particles producing the GeV and TeV emission.

E Aliu†; S Archambault†; B Behera†...P Majumdar; et al

5.2.1.7 Two component dark matter: a possible explanation of 130 GeV gamma-ray line from the galactic centre

Recently there has been a hint of a gamma-ray line at 130 GeV originated from the galactic centre after the analysis of the Fermi-LAT satellite data. Being monochromatic in nature, it rules out the possibility of having its astrophysical origin and there has been a speculation that this line could be originated from dark matter annihilation. In this work, we propose a two component dark matter scenario where an extension of the Standard Model by an inert Higgs doublet and a gauge singlet scalar concocted with $Z_2 \times Z'_2$ symmetry, is considered. We find that our scenario can not only explain the 130 GeV gamma-ray line through dark matter annihilation but also produce the correct dark matter relic density. We have used the Standard Model Higgs mass around 125 GeV as intimated by the LHC data.

Anirban Biswas; Debasish Majumdar; Arunansu Sil†; Pijushpani Bhattacharjee

5.2.1.8 Study of low frequency acoustic signals from superheated droplet detector

The bubble nucleation process in superheated droplet detector (SDD) is associated with the emission of an acoustic pulse that can be detected by an acoustic sensor. We have studied the neutron and gamma-ray induced nucleation events in a SDD with the active liquid R-12 (CCl_2F_2 , b.p. -29.8°C) using a condenser microphone sensor. A comparative study in the low frequency region ($\sim 0\text{--}10\text{ kHz}$) for the neutron and gamma-ray induced nucleation is presented here. From the analysis of the waveforms we observe a significant difference between the neutron and gamma-ray induced acoustic events.

Prasanna Kumar Mondal; Susnata Seth; Mala Das; Pijushpani Bhattacharjee

5.2.1.9 Masses, mixing angles and phases of general Majorana neutrino mass matrix

General Majorana neutrino mass matrix is complex symmetric and for three generations of neutrinos it contains 12 real parameters. We diagonalize this general neutrino mass matrix and express the three neutrino masses, three mixing angles, one Dirac CP phase and two Majorana phases (removing three unphysical phases) in terms of the neutrino mass matrix elements. We apply the results in the context of a neutrino mass matrix derived from a broken cyclic symmetry invoking type-I seesaw mechanism. Phenomenological study of the above mass matrix allows enough parameter space to satisfy the neutrino oscillation data with only 10% breaking of this symmetry. In this model only normal mass hierarchy is allowed. In addition, the Dirac CP phase and the Majorana phases are numerically estimated. Σm_i and $|m_{\nu ee}|$ are also calculated.

Biswajit Adhikary; Mainak Chakraborty; Ambar Ghosal

5.2.1.10 $\theta_{13}, \mu\tau$ SYMMETRY BREAKING AND NEUTRINO YUKAWA TEXTURES

Within the type-I seesaw and in the basis where charged lepton and heavy neutrino mass matrices are real and diagonal, $\mu\tau$ symmetric four and three zero neutrino Yukawa textures are perturbed by lowest order $\mu\tau$ symmetry breaking terms. These perturbations are taken to be the most general ones for those textures. For quite small values of those symmetry breaking parameters, permitting a lowest order analysis, current best-fit ranges of neutrino mass squared differences and mixing angles are shown to be accommodable, including a value of θ_{13} in the observed range, provided all the light neutrinos have an inverted mass ordering.

Biswajit Adhikary; Ambar Ghosal; Probir Roy

5.2.1.11 MULTIWAVELENGTH OBSERVATIONS AND MODELING OF 1ES 1959+650 IN A LOW FLUX STATE

We report on the VERITAS observations of the high-frequency peaked BL Lac object 1ES 1959+650 in the period 2007–2011. This source is detected at TeV energies by VERITAS at 16.4 standard deviation (σ) significance in 7.6 hr of observation in a low flux state. A multiwavelength spectral energy distribution (SED) is constructed from contemporaneous data from VERITAS, Fermi-LAT,

RXTE PCA, and Swift UVOT. Swift XRT data is not included in the SED due to a lack of simultaneous observations with VERITAS. In contrast to the orphan γ -ray flare exhibited by this source in 2002, the X-ray flux of the source is found to vary by an order of magnitude, while other energy regimes exhibit less variable emission. A quasi-equilibrium synchrotron self-Compton model with an additional external radiation field is used to describe three SEDs corresponding to the lowest, highest, and average X-ray states. The variation in the X-ray spectrum is modeled by changing the electron injection spectral index, with minor adjustments of the kinetic luminosity in electrons. This scenario produces small-scale flux variability of the order of $\lesssim 2$ in the high energy ($E > 1\text{MeV}$) and very high energy ($E > 100\text{GeV}$) γ -ray regimes, which is corroborated by the Fermi-LAT, VERITAS, and Whipple 10 m telescope light curves.

E Aliu†; S Archambault†; T Arlen†...P Majumdar; et al

5.2.1.12 Lense-Thirring precession in Plebanski-Demianski Spacetimes

An exact expression of Lense-Thirring precession rate is derived for non-extremal and extremal Plebanski-Demianski spacetimes. This formula is used to find the exact Lense-Thirring precession rate in various axisymmetric spacetimes i.e., Kerr-Newman, Kerr-de Sitter etc. We also show that if the Kerr parameter vanishes in the Plebanski-Demianski spacetime, the Lense-Thirring precession does not vanish due to the existence of NUT charge. To derive the Lense-Thirring precession rate in the extremal Plebanski-Demianski spacetime, we first derive the general extremal condition for Plebanski-Demianski spacetimes. This general result could be applied to obtain the extremal limit in any stationary and axisymmetric spacetimes.

Chandrachur Chakraborty; Partha Pratim Pradhan

5.2.1.13 Thermodynamics of quantum isolated horizons with model Hamiltonians

Following a recent proposal, we consider the most general structure possible for the Hamiltonian operator associated with the quantum isolated horizon (QIH) with explanations of the underlying physical motivations. After a brief overview of the microcanonical ensemble results, thermodynamic analysis with this model Hamiltonian is presented considering the usual canonical energy ensemble for a fixed number of punctures. It is shown that for a quantum spacetime admitting a thermodynamically stable QIH as its internal boundary, there must exist a specific bound on the Barbero-Immirzi parameter if the entropy of the QIH obeys the Bekenstein-Hawking area law. Arguing that the known classical results must follow in the correspondence limit, the model is fixed, yielding the energy spectrum of the QIH.

Abhishek Majhi

5.2.1.14 Late-time acceleration in a slow-moving Galileon field

In this paper, we examine the cosmological viability of a slow-moving Galileon field in a potential. The Lagrangian $L = -1/2 g^{\mu\nu}\pi_{;\mu}\pi_{;\nu} + G\mu\nu/2M^2\pi_{;\mu}\pi_{;\nu}$ respects the Galileon symmetry in curved spacetime. We carry out detailed investigations of the underlying dynamics of this Lagrangian with an Einstein-Hilbert term and a potential. We demonstrate that the model can give rise to a viable

ghost-free late-time acceleration of the universe. Furthermore, we study the cosmological perturbation of the model and see that the model gives different big bang nucleosynthesis constraints at early times. We also carry out the observational analysis of the model and use observational data from growth, type Ia supernovae data, baryon acoustic oscillations, and the cosmic microwave background to constrain the parameters of the theory.

Debabrata Adak; Amna Ali; Debasish Majumdar

5.2.1.15 Gamma ray and neutrino flux from the annihilation of neutralino dark matter at the Galactic halo region in the mAMSB model

We consider the lightest supersymmetric particle, the neutralino, in a minimal anomaly mediated supersymmetry breaking model to be a possible candidate for weakly interacting massive particles (WIMP) or cold dark matter, and we investigate its direct and indirect detections. The theoretically allowed supersymmetric parametric space for such a model, along with the recent bounds from the LHC, is constrained by the WMAP results for relic densities. The spin-independent and spin-dependent scattering cross sections for dark matter off nucleons are thus constrained from the WMAP results. They are found to be within the allowed regions of different ongoing direct detection experiments. The annihilation of such dark-matter candidates at the Galactic centre produces different standard model particles such as gamma-rays and neutrinos. In this work, we calculate the possible fluxes of these gamma-rays and neutrinos coming from the direction of the Galactic centre (and its neighbourhood) at terrestrial or satellite-borne detectors. The calculated gamma-ray flux is compared with the observational results of the HESS experiment. The neutrino fluxes of different flavours from the Galactic centre and at different locations away from the Galactic centre produced by WIMP annihilation in this model are also obtained for four types of Galactic dark-matter halo profiles. The detection prospects of such $\nu(\mu)$ coming from the direction of the Galactic centre at the ANTARES under-sea detector are discussed in terms of the muon signal yield from these muon neutrinos. Both the gamma-ray and neutrino signals are estimated for four different dark-matter halo profiles.

Kamakshya Prasad Modak; Debasish Majumdar

5.2.1.16 DISCOVERY OF TeV GAMMA-RAY EMISSION TOWARD SUPERNOVA REMNANT SNR G78.2+2.1

We report the discovery of an unidentified, extended source of very-high-energy gamma-ray emission, VER J2019+407, within the radio shell of the supernova remnant SNR G78.2+2.1, using 21.4 hr of data taken by the VERITAS gamma-ray observatory in 2009. These data confirm the preliminary indications of gamma-ray emission previously seen in a two-year (2007–2009) blind survey of the Cygnus region by VERITAS. VER J2019+407, which is detected at a post-trials significance of 7.5 standard deviations in the 2009 data, is localized to the northwestern rim of the remnant in a region of enhanced radio and X-ray emission. It has an intrinsic extent of $0.23^{\circ} \pm 0.03_{stat}^{\circ} + 0.02_{sys}^{\circ}$ and its spectrum is well-characterized by a differential power law ($dN/dE = N-0 \times (E/\text{TeV})^{\Gamma}$) with a photon index of $\Gamma = 2.37 \pm 0.14_{stat} \pm 0.20_{sys}$ and a flux normalization of $N-0 = 1.5 \pm 0.2_{stat} \pm 0.4_{sys} \times 10^{-12}$ photon $\text{TeV}^{-1} \text{cm}^{-2} \text{s}^{-1}$. This yields an integral flux of $5.2 \pm 0.8_{stat} \pm 1.4_{sys} \times 10^{-12}$ photon $\text{cm}^{-2} \text{s}^{-1}$ above 320 GeV, corresponding to 3.7% of the Crab Nebula flux. We consider the relationship of the TeV gamma-ray emission with the GeV gamma-ray emission seen from SNR

G78.2+2.1 as well as that seen from a nearby cocoon of freshly accelerated cosmic rays. Multiple scenarios are considered as possible origins for the TeV gamma-ray emission, including hadronic particle acceleration at the SNR shock.

E Aliu†; S Archambault†; T Arlen†...P Majumdar; et al

5.2.1.17 Searching for universal behaviour in superheated droplet detector with effective recoil nuclei

Energy calibration of superheated droplet detector is discussed in terms of the effective recoil nucleus threshold energy and the reduced superheat. This provides a universal energy calibration curve valid for different liquids used in this type of detector. Two widely used liquids, R114 and C₄F₁₀, one for neutron detection and the other for weakly interacting massive particles (WIMPs) dark matter search experiment, have been compared. Liquid having recoil nuclei with larger values of linear energy transfer (LET) provides better neutron- γ discrimination. Gamma (γ) response of C₄F₁₀ has also been studied and the results are discussed. Behaviour of nucleation parameter with the effective recoil nucleus threshold energy and the reduced superheat have been explored.

Mala Das; Susnata Seth

5.2.1.18 The nucleation parameter for heavy-ion induced bubble nucleation in superheated emulsion detector

The values of the nucleation parameter, k , for bubble nucleation induced by high energy heavy ions ¹²C (180 MeV/u), ²⁰Ne (400 MeV/u) and ²⁸Si (350 MeV/u) in superheated emulsion detector are determined by comparing the experimentally obtained normalized count rates with those obtained from simulations done using the GEANT3.21 simulation code. The results show that the nucleation parameter depends on the mass number of the incident heavy ions, and decreases with increasing mass number.

S Seth; M Das; S Bhattacharya; P Bhattacharjee; S Saha

5.2.1.19 Deriving the velocity distribution of Galactic dark matter particles from the rotation curve data

The velocity distribution function (VDF) of the hypothetical weakly interacting massive particles (WIMPs), currently the most favored candidate for the dark matter in the Galaxy, is determined directly from the circular speed ("rotation") curve data of the Galaxy assuming isotropic VDF. This is done by "inverting"-using Eddington's method-the Navarro-Frenk-White universal density profile of the dark matter halo of the Galaxy, the parameters of which are determined by using the Markov chain Monte Carlo technique from a recently compiled set of observational data on the Galaxy's rotation curve extended to distances well beyond the visible edge of the disk of the Galaxy. The derived most-likely local isotropic VDF strongly differs from the Maxwellian form assumed in the "standard halo model" customarily used in the analysis of the results of WIMP direct-detection experiments. A parametrized (non-Maxwellian) form of the derived most-likely local VDF is given. The astrophysical "g factor" that determines the effect of the WIMP VDF on

the expected event rate in a direct-detection experiment can be lower for the derived most-likely VDF than that for the best Maxwellian fit to it by as much as 2 orders of magnitude at the lowest WIMP mass threshold of a typical experiment.

Pijushpani Bhattacharjee; Soumini Chaudhury; Susmita Kundu; et al

5.2.1.20 Pointing of HAGAR telescope mirrors

An array of seven atmospheric Cherenkov telescopes was commissioned at a high altitude site in Hanle in the Ladakh region of the Himalayas. The array called HAGAR has been designed to observe celestial γ -rays of energy > 100 GeV. Each telescope is altitude-azimuth mounted and carries seven parabolic mirrors whose optic axes are co-aligned with the telescope axis. The telescopes point and track a celestial source using a PC-based drive control system. Two important issues in positioning of each HAGAR telescope are pointing accuracy of telescope axis and co-alignment of mirrors' optic axes with the telescope axis. We have adopted a three pronged strategy to address these issues, namely use of pointing models to improve pointing accuracy of the telescopes, RA-DEC scan technique to measure the pointing offsets of the mirrors and mechanical fine-tuning of off-axis mirrors by sighting a distant stationary light source. This paper discusses our efforts in this regard as well as the current status of pointing and monitoring of HAGAR telescopes.

KS Gothei†; TP Prabhu†; PR Vishwanath†...RJ Britto...L Saha; et al

5.2.1.21 OBSERVATIONS OF THE UNIDENTIFIED GAMMA-RAY SOURCE TeV J2032+4130 BY VERITAS

TeV J2032+4130 was the first unidentified source discovered at very high energies (VHEs; $E > 100$ GeV), with no obvious counterpart in any other wavelength. It is also the first extended source to be observed in VHE gamma rays. Following its discovery, intensive observational campaigns have been carried out in all wavelengths in order to understand the nature of the object, which have met with limited success. We report here on a deep observation of TeV J2032+4130 based on 48.2 hr of data taken from 2009 to 2012 by the Very Energetic Radiation Imaging Telescope Array System experiment. The source is detected at 8.7 standard deviations (σ) and is found to be extended and asymmetric with a width of 9.5 ± 1.2 along the major axis and 4.0 ± 0.5 along the minor axis. The spectrum is well described by a differential power law with an index of $2.10 \pm 0.14_{stat} \pm 0.21_{sys}$ and a normalization of $(9.5 \pm 1.6_{stat} \pm 2.2_{sys} \times 10^{-13} \text{ TeV}^{-1} \text{ cm}^{-2}) \text{ s}^{-1}$ at 1 TeV. We interpret these results in the context of multiwavelength scenarios which particularly favor the pulsar wind nebula interpretation.

E Aliu†; T Aune†; B Behera†...P Majumdar; et al

5.2.1.22 Origin of gamma-ray emission in the shell of Cassiopeia A

Non-thermal X-ray emission from the shell of Cassiopeia A (Cas A) has been an interesting subject of study, as it provides information about relativistic electrons and their acceleration mechanisms in shocks. The Chandra X-ray observatory revealed the detailed spectral and spatial structure of this supernova remnant in X-rays. The spectral analysis of the Chandra X-ray data of Cas A shows

unequal flux levels for different regions of the shell, which can be attributed to different magnetic fields in those regions. Additionally, the GeV gamma-ray emission observed by the Large Area Telescope on board the Fermi Gamma-Ray Space Telescope showed that the hadronic processes are dominating in Cas A, which is a clear signature of acceleration of protons.

Aims. The aim of this study is to locate the origin of gamma-rays based on the X-ray data of the shell of Cas A. We also aim to explain the GeV-TeV gamma-ray data in the context of both leptonic and hadronic scenarios.

Methods. We modelled the multi-wavelength spectrum of Cas A. We use a synchrotron emission process to explain the observed non-thermal X-ray fluxes from different regions of the shell. This results in estimates of the model parameters which are then used to explain TeV gamma-ray emission spectrum. We also use a hadronic scenario to explain both GeV and TeV fluxes simultaneously.

Results. Based on this analysis, it has been shown that the southern part of the remnant is bright in TeV gamma-rays. We also show that the leptonic model alone cannot explain the GeV-TeV data. Therefore, we need to invoke a hadronic model to explain the observed GeV-TeV fluxes. We found that the lepto-hadronic model provides the best fit to the data although the pure hadronic model is able to explain the GeV-TeV data.

L Saha; T Ergin; P Majumdar; et al

5.2.2 Theory

5.2.2.1 Minimal supersymmetry confronts R_b , A_{FB}^b and m_h

We study the impact of the measurements of three sets of observables on the parameter space of the constrained minimal supersymmetric standard model (cMSSM), its slightly general variant, the non-universal scalar model (NUSM), and some selected benchmark points of the 19-parameter phenomenological MSSM (pMSSM): (i) the direct measurement of the Higgs boson mass m_h approximate to 125 GeV at the CERN Large Hadron Collider (LHC); (ii) Z-boson decay width in the $b\bar{b}$ channel normalized to its hadronic width (R_b), and the forward-backward asymmetry on the Z-peak in the same channel (A_{FB}^b); and (iii) several B-physics observables, along with (g-2) of muon. In addition, there are constraints from non-observation of superparticles from direct searches at the LHC. In view of the recently re-estimated standard model (SM) value of R_b with improved higher order corrections, the measured value of R_b has a 1.2 σ discrepancy with its SM value, while the corresponding discrepancy in A_{FB}^b is 2.5 σ . MSSM contributions from light superpartners improve the agreement of R_b but worsen that of A_{FB}^b . We project this ($R_b - A_{FB}^b$) tension vis-a-vis the constraints arising from other observables in the parameter space of cMSSM and NUSM. We also consider a few well-motivated pMSSM benchmark points and show that pMSSM does not fare any better than the SM.

Gautam Bhattacharyya; Anirban Kundu†; Tirtha Sankar Ray†

5.2.2.2 Drell-Yan, ZZ, W^+W^- production in SM & ADD model to NLO+PS accuracy at the LHC

In this paper, we present the next-to-leading order QCD corrections for di-lepton, di-electroweak boson (ZZ, W^+W^-) production in both the SM and the ADD model, matched to the HERWIG parton shower using the aMC@NLO framework. A selection of results at the 8 TeV LHC, which

exhibit deviations from the SM as a result of the large extra-dimension scenario, are presented.

R Frederix†; MK Mandal†; P Mathews...S Seth

5.2.2.3 The consequences of SU (3) color singletness, Polyakov Loop and Z (3) symmetry on a quark-gluon gas

Based on quantum statistical mechanics, we show that the SU(3) color singlet ensemble of a quark-gluon gas exhibits a Z(3) symmetry through the normalized character in fundamental representation and also becomes equivalent, within a stationary point approximation, to the ensemble given by Polyakov Loop. In addition, a Polyakov Loop gauge potential is obtained by considering spatial gluons along with the invariant Haar measure at each space point. The probability of the normalized character in SU(3) vis-a-vis a Polyakov Loop is found to be maximum at a particular value, exhibiting a strong color correlation. This clearly indicates a transition from a color correlated to an uncorrelated phase, or vice versa. When quarks are included in the gauge fields, a metastable state appears in the temperature range $145 \leq T \text{ (MeV)} \leq 170$ due to the explicit Z(3) symmetry breaking in the quark-gluon system. Beyond $T \geq 170 \text{ MeV}$, the metastable state disappears and stable domains appear. At low temperatures, a dynamical recombination of ionized Z(3) color charges to a color singlet Z(3) confined phase is evident, along with a confining background that originates due to the circulation of two virtual spatial gluons, but with conjugate Z(3) phases in a closed loop. We also discuss other possible consequences of the center domains in the color deconfined phase at high temperatures.

Aminul Chowdhury Islam; Raktim Abir; Munshi G Mustafa; et al

5.2.2.4 Number of fermion generations from a novel grand unified model

Electroweak interactions based on the gauge group $\mathbf{SU(3)}_L \times \mathbf{U(1)}_X$, coupled to the QCD gauge group $\mathbf{SU(3)}_c$, can predict the number of generations to be multiples of three. We first try to unify these models within $\mathbf{SU(N)}$ groups, using antisymmetric tensor representations only. After examining why these attempts fail, we continue to search for an $\mathbf{SU(N)}$ GUT that can explain the number of fermion generations. We show that such a model can be found for $\mathbf{N} = \mathbf{9}$, with fermions in antisymmetric rank-1 and rank-3 representations only, and we examine the constraints on various masses in the model coming from the requirement of unification.

Pritibhajan Byakti; David Emmanuel-Costa†; Arindam Mazumdar; Palash B Pal

5.2.2.5 Entropy from near-horizon geometries of Killing horizons

We "derive" the Bekenstein-Hawking entropy for black holes based on the near-horizon symmetries of black hole space-times. To find out these symmetries we make use of an (R, T) plane close to a Killing horizon. We identify a set of vector fields that preserves this plane and forms a Witt algebra. The corresponding algebra of Hamiltonians is shown to have a nontrivial central extension. Using the Cardy formula and the central charge we obtain the Bekenstein-Hawking entropy.

Olaf Dreyer†; Amit Ghosh; Avirup Ghosh

5.2.2.6 On transverse spin sum rules

In this work we show that (i) both the form factors A_i and \bar{C}_i contribute to the matrix element of the energy-momentum tensor T_i^{+-} in a transversely polarized state, (ii) there is no relative suppression factor between these two contributions and (iii) the contribution to the matrix element of the Pauli-Lubanski operator $W_i \perp$ from that of T_i^{++} contains only the form factor B_i and not the form factor A_i . These results support our criticism and the conclusions as stated in Ref. [13]. Comparing and contrasting the spin sum rules in two different approaches, one advocated by us and the one proposed by Jaffe and Manohar, we point out that the physical content of the sum rules is very transparent in our approach, whereas, in the second approach details of the dynamics remain hidden and the separation into orbital and intrinsic spin parts is not visible.

A Harindranath; Rajen Kundu†; Asmita Mukherjee†

5.2.2.7 WESS-ZUMINO-WITTEN MODEL FOR GALILEAN CONFORMAL ALGEBRA

In this note, we construct a Wess-Zumino-Witten model based on the Galilean conformal algebra in two-spacetime dimensions, which is a nonrelativistic analogue of the relativistic conformal algebra. We obtain exact background corresponding to a-models in six dimensions (the dimension of the group manifold) and a central charge $c = 6$. We carry out a Sugawara type construction to verify the conformal invariance of the model. Further, we discuss the feasibility of the background obtained as a physical spacetime metric.

Somdeb Chakraborty; Parijat Dey

5.2.2.8 From AdS to Schrödinger/Lifshitz dual space-times without or with hyperscaling violation

It is observed that the (intersecting) branes of M/string theory, which are known to give AdS geometry (directly or upto a conformal transformation) in the near horizon limit, do also lead to Schrödinger/Lifshitz dual space-times (without or with hyperscaling violation) upon using appropriate solution generating transformation and dimensional reduction. We show that the dynamical exponents of the Schrödinger and the Lifshitz space-times obtained in this way always add upto 2. We illustrate this by several examples. including M2-, M5-branes of M-theory and $D(p + 1)$ -branes ($p \neq 4$, since in this case the near horizon limit does not give AdS geometry) of string theory as well as many of their intersecting solutions. The Schrödinger space-time can be obtained by the standard wave generating technique along one of the brane directions (for single brane) or one of the common brane directions (for intersecting branes) and then interchanging the light-cone coordinates by double Wick rotations, whereas, the Lifshitz space-time can be obtained by dimensionally reducing (for M-theory) along the wave direction or taking T-duality (for string theory) along the same direction. We thus obtain Schrödinger/Lifshitz dual spacetimes without or with hyperscaling violation from the same M/string theory solutions and they preserve some fraction of the supersymmetry.

Parijat Dey; Shibaji Roy

5.2.2.9 A framework for Higgs characterisation

We introduce a framework, based on an effective field theory approach, that allows one to perform characterisation studies of the boson recently discovered at the LHC, for all the relevant channels and in a consistent, systematic and accurate way. The production and decay of such a boson with various spin and parity assignments can be simulated by means of multi-parton, tree-level matrix elements and of next-to-leading order QCD calculations, both matched with parton showers. Several sample applications are presented which show, in particular, that beyond-leading-order effects in QCD have non-trivial phenomenological implications.

P Artoisenet†; P de Aquino†; F Demartin†; P Mathews; et al

5.2.2.10 Scalar sector properties of two-Higgs-doublet models with a global U(1) symmetry

We analyze the scalar sector properties of a general class of two-Higgs-doublet models which has a global U(1) symmetry in the quartic terms. We find constraints on the parameters of the potential from the considerations of unitarity of scattering amplitudes, the global stability of the potential and the rho-parameter. We concentrate on the spectrum of the non-standard scalar masses in the decoupling limit which is preferred by the Higgs data at the LHC. We exhibit charged-Higgs induced contributions to the diphoton decay width of the 125GeV Higgs boson and its correlation with the corresponding $Z\gamma$ width.

Gautam Bhattacharyya; Dipankar Das; Palash B Pal; et al

5.2.2.11 Gauge independence of the fermion pole mass

We study the question of complete gauge independence of the fermion pole mass by choosing a general class of gauge fixing, which interpolates between the covariant, the axial and the Coulomb gauges for different values of the gauge fixing parameters. We derive the Nielsen identity describing the gauge parameter variation of the fermion two point function in this general class of gauges. Furthermore, we relate the denominator of the fermion propagator to the two point function. This then allows us to study directly the gauge parameter dependence of the denominator of the propagator using the Nielsen identity for the two point function. This leads to a simple proof that, when infrared divergences and mass shell singularities are not present at the pole, the fermion pole mass is gauge independent, in the complete sense, to all orders in perturbation theory. Namely, the pole is not only independent of the gauge fixing parameters but also has the same value in both covariant and noncovariant gauges.

Ashok K Das; RR Francisco†; J Frenkel†

5.2.2.12 The pole of the fermion propagator in a general class of gauges

We study the behavior of the pole of the fermion propagator, in QED in n dimensions, in a general class of gauges which interpolate between the covariant, the axial and the Coulomb gauges. We use Nielsen identities, following from the BRST invariance of the theory, to determine the gauge variation of the fermion two point function in this general class of gauges. This allows us to show

directly and in a simple manner, to all orders in perturbation theory, that in the absence of infrared divergences and mass shell singularities, the fermion pole mass is gauge independent.

Ashok K Das; J Frenkel†

5.2.2.13 A natural scenario for heavy colored and light uncolored superpartners

Influenced by the current trend of experimental data, especially from the LHC, we construct a supersymmetric scenario where a natural dynamics makes the squarks and gluino super-heavy (order 10 TeV) while keeping the sleptons and the weak gauginos light (100-500 GeV). The dynamics relies on the interfusion of two underlying ideas: (i) gauge mediation of supersymmetry breaking with two messenger multiplets, one transforming as a triplet of weak SU(2) and the other as an octet of color SU(3); (ii) perturbative gauge coupling unification at the string scale even with these incomplete SU(5) multiplets. Interestingly, the relative magnitude of the triplet and octet messenger scales that ensures gauge unification at the two-loop level also helps to naturally keep the uncolored superpartners light while making the colored ones heavy.

Gautam Bhattacharyya; Biplob Bhattacharjee†; Tsutomu T Yanagida†; et al

5.2.2.14 Information content of the weak-charge form factor

Background: Parity-violating electron scattering provides a model-independent determination of the nuclear weak-charge form factor that has widespread implications across such diverse areas as fundamental symmetries, nuclear structure, heavy-ion collisions, and neutron-star structure. Purpose: We assess the impact of precise measurements of the weak-charge form factor of ^{48}Ca and ^{208}Pb on a variety of nuclear observables, such as the neutron skin and the electric-dipole polarizability. Methods: We use the nuclear density functional theory with several accurately calibrated nonrelativistic and relativistic energy density functionals. To assess the degree of correlation between nuclear observables and to explore systematic and statistical uncertainties on theoretical predictions, we employ the chi-square statistical covariance technique. Results: We find a strong correlation between the weak-charge form factor and the neutron radius, that allows for an accurate determination of the neutron skin of neutron-rich nuclei. We determine the optimal range of the momentum transfer q that maximizes the information content of the measured weak-charge form factor and quantify the uncertainties associated with the strange quark contribution. Moreover, we confirm the role of the electric-dipole polarizability as a strong isovector indicator. Conclusions: Accurate measurements of the weak-charge form factor of ^{48}Ca and ^{208}Pb will have a profound impact on many aspects of nuclear theory and hadronic measurements of neutron skins of exotic nuclei at radioactive-beam facilities.

P -G Reinhardt†; J Piekarewicz†; W Nazarewicz†; BK Agrawal; et al

5.2.2.15 Dissociation of quarkonium in an anisotropic hot QCD medium

We have studied the properties of quarkonium states in the presence of momentum anisotropy by correcting the full Cornell potential through the hard-loop resummed gluon propagator. The in-medium modification to the potential causes less screening, so quarkonium states become more

tightly bound than in isotropic medium. In addition, the anisotropy in the momentum space introduces a characteristic angular dependence in the potential and as a result the quark pairs aligned in the direction of anisotropy are bound stronger than those of perpendicular alignment. Since the weak anisotropy represents a perturbation to the (isotropic) spherical potential, we use the quantum mechanical perturbation theory to obtain the first-order correction due to the small anisotropic contribution to the energy eigenvalues of spherically symmetric potential.

Lata Thakur†; Najmul Haque; Uttam Kakade†; et al

5.2.2.16 Holographic quark-antiquark potential in hot, anisotropic Yang-Mills plasma

Using the gauge/gravity duality we calculate the heavy quark-antiquark potential in a hot, anisotropic and strongly coupled Yang Mills plasma in $(3 + 1)$ -dimensions. As the anisotropic medium we take a deformed version of $N = 4$ super Yang Mills theory at finite temperature following a recent work where the dual type JIB supergravity solution is also proposed. We turn on a small value of the anisotropy parameter, for which the gravity dual is known analytically (perturbatively), and compute the velocity-dependent quark-antiquark interaction potential when the pair is moving through the plasma with a velocity ϵ . By setting $\epsilon = 0$ we recover the static quark antiquark potential. We numerically study how the potential is modified in the presence of anisotropy. We further show numerically how the quark antiquark separation (both in the static and the velocity-dependent case) and hence, the screening length gets modified by anisotropy. We discuss various cases depending upon the direction of the dipole and the direction of its propagation and make a comparative study of these cases. We are also able to obtain an analytical expression for the screening length of the dipole moving in a hot, anisotropic plasma in a special case.

Somdeb Chakraborty; Najmul Haque

5.2.2.17 Ξ^- hyperon and hypernuclear production in the (K^-, K^+) reaction on nucleon and nuclei in a field theoretical model

We investigate the production of a cascade hyperon Ξ and bound Ξ hypernuclei in the (K^-, K^+) reaction on proton and nuclear targets, respectively, within a covariant effective Lagrangian model. The $K^+\Xi^-$ production vertex is described by excitation, propagation and decay of Λ and Σ resonance states in the initial collision of a K^- meson with a free or bound proton in the incident channel. The parameters of the resonance vertices are taken from previous studies and $SU(3)$ symmetry considerations. The model is able to provide a good description of the available data on total and differential cross sections for the $p(K^-, K^+), \Xi^-$ reaction. The same mechanism was used to describe the hypernuclear production reactions $^{12}\text{C}(K^-, K^+)_{\Xi^-}^{12}\text{Be}$ and $^{28}\text{Si}(K^-, K^+)_{\Xi^-}^{28}\text{mg}$ where Ξ bound state spinors calculated within a phenomenological model have been employed. Both the elementary and hypernuclear production cross sections are dominated by the contributions from the $\Lambda(1520)$ intermediate resonant state. The beam momentum dependence of the 0 degrees differential cross sections for the formation of the Ξ hypernuclei is found to be remarkably different from what has been observed previously in the impulse approximation model calculations.

R Shyam

5.2.2.18 Structure and Coulomb dissociation of O-23 within the quark-meson coupling model

We study the ground state structure of nuclei in the vicinity of the one-neutron drip line within the latest version of the quark-meson coupling (QMC) model with a particular emphasis on O-23. For this nucleus the model predicts a O-22(0(+)) circle times n2s(1/2) configuration for its ground state, with a one-neutron separation energy in close agreement with the corresponding experimental value. The wave function describing the valence neutron-core relative motion was then used to calculate the Coulomb dissociation of O-23 on a lead target at a beam energy of 422 MeV/nucleon. The experimental neutron-core relative energy spectrum and the total one-neutron removal cross sections are well described by the calculations. The widths of the longitudinal momentum distributions of the O-22 fragment are found to be broad, which do not support the formation of a neutron halo in this nucleus.

R Chatterjee†, R Shyam; K Tsushima†; et al

5.2.2.19 Production of the H dibaryon via the (K⁻, K⁺) reaction on a ¹²C target

We study the production of the stable six-quark H dibaryon via the (K⁻, K⁺) reaction on a ¹²C target within a covariant effective Lagrangian model. The calculations are performed within a factorization approximation, in which the full production amplitude is written as a product of the amplitudes for the K⁻ + p → K⁺ + Ξ⁻ and Ξ⁻ + p → H processes. The K⁺Ξ⁻ production vertex is described by excitation, propagation, and decay of Λ and Σ resonance states in the initial collision of a K⁻ meson with a target proton in the incident channel. The parameters of the resonance vertices are taken to be the same as those determined previously by describing the available data on total and differential cross sections for the p(Ki⁻, K⁺)Ξ⁻ reaction within a similar model. The Ξ⁽⁻⁾ + p → H fusion process is treated within a quark model where the H dibaryon is considered as a stable particle. For the K⁺ meson angle fixed at 0°, the H production cross section is found to be about 2.9 $\mu\text{b}/\text{sr}$ for H mass just below the Lambda Lambda threshold at a K⁻ beam momentum of 1.67 GeV/c. This is an order of magnitude larger than the value for this quantity reported earlier in calculations performed on a ³He target using a different model for the cascade hyperon production. We have also calculated the beam momentum dependence of the H production cross section and the energy spectrum of the emitted K⁺ meson.

R Shyam; O Scholten†; AW Thomas†

5.2.2.20 Zero sound in strange metals with hyperscaling violation from holography

Hyperscaling violating 'strange metal' phase of heavy fermion compounds can be described holographically by probe D-branes in the background of a Lifshitz space-time (dynamical exponent z and spatial dimensions d) with hyperscaling violation (corresponding exponent θ). Without the hyperscaling violation, strange metals are known to exhibit zero sound mode for $z < 2$ analogous to the Fermi liquids. In this paper, we study its fate in the presence of hyperscaling violation and find that in this case, the zero sound mode exists for $z < 2(1 + |\theta|/d)$, where the positivity of the specific heat and the null energy condition of the background dictate that $\theta < 0$ and $z \geq 1$. However, for $z \geq 2(1 + |\theta|/d)$, there is no well-defined quasiparticle for the zero sound. The systems behave like Fermi liquid for $2|\theta| = dz$ and like Bose liquid for $2|\theta| = qdz$ (where q is the number of

spatial dimensions along which D-branes are extended in the background space), but in general they behave as a new kind of quantum liquid. We also compute the ac conductivity of the systems and briefly comment on the results.

Parijat Dey; Shibaji Roy

5.2.2.21 Electric dipole polarizability in ^{208}Pb : Insights from the droplet model

We study the electric dipole polarizability α_D in ^{208}Pb based on the predictions of a large and representative set of relativistic and nonrelativistic nuclear mean-field models. We adopt the droplet model as a guide to better understand the correlations between α_D and other isovector observables. Insights from the droplet model suggest that the product of α_D and the nuclear symmetry energy at saturation density J is much better correlated with the neutron skin thickness Δr_{np} of ^{208}Pb than the polarizability alone. Correlations of $\alpha_D J$ with Δr_{np} and with the symmetry energy slope parameter L suggest that $\alpha_D J$ is a strong isovector indicator. Hence, we explore the possibility of constraining the isovector sector of the nuclear energy density functional by comparing our theoretical predictions against measurements of both α_D and the parity-violating asymmetry in ^{208}Pb . We find that the recent experimental determination of α_D in ^{208}Pb in combination with the range for the symmetry energy at saturation density $J = [31 \pm (2)_{est}]$ MeV suggests $\Delta r_{np} (^{208}\text{Pb}) = 0.165 \pm (0.009)_{expt} \pm (0.013)_{theor} \pm (0.021)_{est}$ fm and $L = 43 \pm (6)_{expt} \pm (8)_{theor} \pm (12)_{est}$ MeV.

X Roca-Maza†; M; Brenna†; G Colo†...BK Agrawal...et al

5.2.2.22 Lifshitz to AdS flow with interpolating p-brane solutions

In continuation with our studies of Lifshitz like Dp-brane solutions, we propose a class of 1/4 BPS supersymmetric interpolating solutions which interpolate between IR Lifshitz solutions and UV AdS solutions smoothly. We demonstrate properties of these classical solutions near the two fixed points. These interpolating solutions are then used to calculate the entanglement entropies of strip-like subsystems. With these bulk solutions the entropy functional also gets modified. We also make a curious observation about the electric-magnetic duality and the thermal entropy of the Hodge-dual Lifshitz Dp brane systems.

Harvendra Singh

5.2.2.23 Production of Ξ^- -Hypernuclei via the (K^-, K^+) Reaction in a Quark-Meson Coupling Model

We study the production of Ξ^- -hypernuclei, Be and Mg, via the (K^-, K^+) reaction within a covariant effective Lagrangian model, employing the bound Ξ^- and proton spinors calculated by the latest quark-meson coupling model. The present treatment yields the 0° differential cross sections for the formation of simple s-state Ξ^- particle-hole states peak at a beam momentum around 1.0 GeV/c with a value in excess of $1 \mu\text{b}$.

K Tsushima†; R Shyam; AW Thomas†

5.2.2.24 Quark number susceptibilities from two-loop hard thermal loop perturbation theory

We use the recently obtained two-loop hard thermal loop perturbation theory thermodynamics functions of a plasma of quarks and gluons to compute the diagonal second- and fourth-order quark number susceptibilities. The two-loop hard thermal loop perturbation theory thermodynamic functions used are reliable in the limit that the ratio of the quark chemical potential to temperature is small. Using this result, we are able to obtain (semi-)analytic expressions for the quark number susceptibilities at leading- and next-to-leading-order in hard thermal loop perturbation theory. We compare the hard thermal loop perturbation theory results with perturbative quantum chromodynamics calculations, a Polyakov-loop Nambu-Jona-Lasinio model calculation, and lattice quantum chromodynamics results.

Najmul Haque; Munshi G Mustafa; Michael Strickland†

5.2.2.25 Quasilocal first law for black hole thermodynamics

We first show that stationary black holes satisfy an extremely simple quasilocal form of the first law, $\delta E = \frac{R}{8\pi} \delta A$, where the (quasilocal) energy $E = \frac{A}{\ell} 8\pi\ell$ and (local) surface gravity $\bar{\kappa} = 1/\ell$, with A the horizon area and ℓ is a proper length characterizing the distance to the horizon of a preferred family of quasilocal observers suitable for thermodynamical considerations. Our construction is extended to the more general framework of isolated horizons. The local surface gravity is universal. This has important implications for semiclassical considerations of black hole physics as well as for the fundamental quantum description arising in the context of loop quantum gravity.

Ernesto Frodden†; Amit Ghosh; Alejandro Perez†

5.2.2.26 Clusters of bound particles in the derivative δ -function Bose gas

In this paper we discuss a novel procedure for constructing clusters of bound particles in the case of a quantum integrable derivative δ -function Bose gas in one dimension. It is shown that clusters of bound particles can be constructed for this Bose gas for some special values of the coupling constant, by taking the quasi-momenta associated with the corresponding Bethe state to be equidistant points on a single circle in the complex momentum plane. We also establish a connection between these special values of the coupling constant and some fractions belonging to the Farey sequences in number theory. This connection leads to a classification of the clusters of bound particles associated with the derivative δ -function Bose gas and allows us to study various properties of these clusters like their size and their stability under the variation of the coupling constant.

B Basu-Mallik; Tanaya Bhattacharyya†; Diptiman Sen†

5.2.2.27 Different realizations of kappa-momentum

We consider different realizations for the momentum sector of kappa-Poincare-Hopf algebra, which is associated with a curved momentum space. We show that the notion of the particle mass as introduced recently by Amelino-Camelia et al. in the context of relative locality is realization independent for a wide class of realizations, up to linear order in the deformation parameter l . On

the other hand, the time delay formula clearly shows a dependence on the choice of realization.

S Meljanac†; A Pachol†; A Samsarov†; Kumar S Gupta

5.2.2.28 Pion and nucleon in two flavour QCD with unimproved Wilson fermions

We calculate pion mass, pion decay constant, PCAC quark mass and nucleon mass in two flavour lattice QCD with unimproved Wilson fermion and gauge actions. Simulations are performed using DD-HMC algorithm at two lattice spacings and two volumes for several values of the quark mass. The cutoff effects in pion mass and nucleon mass for the explored region of parameter space are found to be negligible. We extract the average value of the up-down quark mass in the \overline{MS} scheme at 2 GeV, which is in good agreement with the world data. The chiral behaviours of pion mass, pion decay constant and quark condensate are found to be qualitatively consistent with NLO chiral perturbation theory. The extracted values of the pion decay constant and the chiral condensate are in reasonable agreement with the world data.

Abhishek Chowdhury; Asit K De; Sangita De Sarkar; A Harindranath; Jyotirmoy Maiti; Santanu Mondal; Anwesa Sarkar

5.2.2.29 Constraining the density dependence of the symmetry energy from nuclear masses

Empirically determined values of the nuclear volume and surface symmetry energy coefficients from nuclear masses are expressed in terms of density distributions of nucleons in heavy nuclei in the local density approximation. This is then used to extract the value of the symmetry energy slope parameter L . The density distributions in both spherical and well deformed nuclei calculated within microscopic framework with different energy density functionals give $L = 59.0 \pm 13.0$ MeV. Application of the method also helps in a precision determination of the neutron skin thickness of nuclei that are difficult to measure accurately.

BK Agrawal; JN De; SK Samaddar; et al

5.2.2.30 Two-loop hard thermal loop pressure at finite temperature and chemical potential

We calculate the two-loop pressure of a plasma of quarks and gluons at finite temperature and chemical potential using the hard thermal loop perturbation theory reorganization of finite temperature/density quantum chromodynamics. The computation utilizes a high temperature expansion through fourth order in the ratio of the chemical potential to temperature. This allows us to reliably access the region of high temperature and small chemical potential. We compare our final result for the leading-and next-to-leading-order hard thermal loop perturbation theory pressure at finite temperature and chemical potential with perturbative quantum chromodynamics calculations and available lattice quantum chromodynamics results.

Najmul Haque; Munshi G Mustafa; Michael Strickland†

5.2.2.31 Burgeoning the Higgs mass to 125 GeV through messenger-matter interactions in GMSB models

A 125 GeV Higgs renders the simpler GMSB models unnatural, essentially pushing the soft spectrum beyond the LHC reach. A direct coupling of the matter and messenger fields, that facilitates an enhanced mixing in the squark sector, is a way to ameliorate this deficiency. We construct all possible messenger-matter interaction terms considering the messenger multiplets in 1, 5 and 110 dimensional representations of the SU(5). A Froggatt-Nielsen like flavor framework connected with the origin of fermion mass hierarchy is utilized to control the interaction terms and suppress FCNC. We perform a detailed comparative study of the efficiency of such interaction terms to boost the Higgs mass keeping the soft spectrum light. We identify the more promising models and comment, on their status in present and future collider studies.

Pritibhajan Byakti; Tirtha Sankar Ray†

5.2.2.32 Exploring autocorrelations in two-flavor Wilson Lattice QCD using DD-HMC algorithm

We perform an extensive study of the autocorrelation of several observables in lattice QCD with two degenerate flavors of unimproved Wilson fermions and Wilson gauge action using the DD-HMC algorithm. We show that (1) at a given lattice spacing, autocorrelation of topological susceptibility and unsmeared plaquette show indication of a decrease with decreasing quark mass, (2) autocorrelation of topological susceptibility and topological charge density correlator increase with decreasing lattice spacing but the effect is milder in the latter case and (3) increasing the size and the smear level increase the autocorrelation of smeared Wilson loop.

Abhishek Chowdhury; Asit K De; Sangita De Sarkar; A Harindranath; Jyotirmoy Maiti; Santanu Mondal; Anwesha Sarkar

5.2.2.33 Hawking radiation from dynamical horizons

In completely local settings, we establish that a spherically symmetric, dynamically evolving black hole horizon can be assigned a Hawking temperature under a mild assumption. Moreover, we calculate the Hawking flux and show that the radius of the horizon shrinks in accordance with the amount of emitted flux.

Ayan Chatterjee†; Bhramar Chatterjee; Amit Ghosh

5.2.2.34 A Dirac-type variant of the xp-model and the Riemann zeros

We propose a Dirac-type modification of the xp-model to a $X \sigma \cdot p$ model on a semi-infinite cylinder. This model is inspired by recent work of Sierra et al. on the xp-model on the half-line. Our model realizes the Berry-Keating conjecture on the Riemann zeros. We indicate the connection of our model to that of gapped graphene with a supercritical Coulomb charge, which might provide a physical system for the study of the zeros of the Riemann Zeta function.

Kumar S Gupta; E Harikumar†; Amilcar R de Queiroz†

5.2.2.35 Symmetry energy of warm nuclear systems

The temperature dependence of the symmetry energy and symmetry free energy coefficients of infinite nuclear matter and of finite nuclei is investigated. For infinite matter, both these coefficients are found to have a weaker dependence on temperature at densities close to saturation; at low but homogeneous densities, the temperature dependence becomes stronger. For finite systems, different definitions of symmetry energy coefficients are encountered in the literature yielding different values. A resolution to this problem is suggested from a global liquid-drop-inspired fit of the energies and free energies of a host of nuclei covering the entire periodic table. The hot nucleus is modeled in a subtracted finite-temperature Thomas-Fermi framework, with dynamical surface phonon coupling to nucleonic motion plugged in. Contrary to infinite nuclear matter, a substantial change in the symmetry energy coefficients is observed for finite nuclei with temperature.

BK Agrawal; JN De; SK Samaddar; et al

5.2.2.36 Three-loop pressure and susceptibility at finite temperature and density from hard-thermal-loop perturbation theory

We present results of a three-loop hard-thermal-loop perturbation theory calculation of the thermodynamical potential of a finite temperature and baryon chemical potential system of quarks and gluons. We compare the resulting pressure and diagonal quark susceptibilities with available lattice data. We find reasonable agreement between our analytic results and lattice data at both zero and finite chemical potential.

Najmul Haque; Jens O Andersen; Munshi G Mustafa; et al

5.2.2.37 Quark and gluon spin-2 form factors to two-loops in QCD

We present complete two-loop radiative corrections to the graviton-quark- antiquark form factor $G^* \rightarrow q\bar{q}$ and graviton-gluon-gluon form factor $G^* \rightarrow gg$ in $SU(N)$ gauge theory with n_f light flavours using d -dimensional regularisation to all orders in $\epsilon = d - 4$. This is an important ingredient to next-to-next-to-leading order QCD corrections to hadronic scattering processes in models with large extra-dimensions where Kaluza-Klein graviton modes couple to Standard Model fields. We show that these form factors obey Sudakov integro-differential equation and the resulting cusp, collinear and soft anomalous dimensions coincide with those of electroweak vector boson and gluon form factors. We also find the universal behaviour of the infrared singularities in accordance with the proposal by Catani.

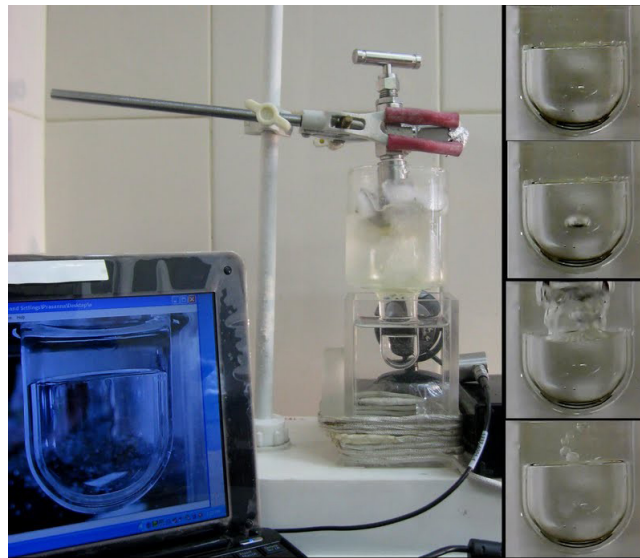
D de Florian; M Mahakhud; P Mathews; et al

5.3 Developmental Work

5.3.1 Astroparticle Physics and Cosmology

5.3.1.1 R & D of a single droplet module (SDM) for PICASSO dark matter search experiment

The R & D on the single droplet module system (SDM) for next generation PICASSO detector for dark matter search has been carried out at CAPP-lab. After studying several variations of the module, it has been observed that the bulk superheated liquid in a glass vessel, where possible nucleation sites are reduced using a surfactant, is the most stable one. The dead time of the device



and the temperature variation inside the module has been measured. The developed prototype detector with R114 ($C_2Cl_2F_4$, b.p $3.7^{\circ}C$) as the active liquid has been tested with and without a neutron source in the reduced superheat range of $0.14 - 0.30$

Prasanna K Mondal; Mala Das

5.4 Publications

5.4.1 Publications in Books/Monographs & Volumes Edited

Asit Kumar De, Einstein, Rabindranath o Sangeetprasanga, Rabindranath-Einstein: Ek Amimangsitto Sanglap, (SahityaSamsad, Kolkata, 2014, p. 267)

5.4.2 Publications in Journal

5.4.2.1 Astroparticle Physics and Cosmology

Chandrachur Chakraborty, Inner-most stable circular orbits in extremal and non-extremal Kerr-Taub-NUT spacetimes, European Physical Journal **C74** (2014)Art No: 2759

E Aliu†; S Archambault†; T Arlen†...P Majumdar; et al, A Three-Year Multi-Wavelength Study of the Very-High-Energy γ -Ray Blazar 1ES 0229+200, *Astrophysical Journal***782** (2014)Art No: 13

Sovan Chakraborty; Pijushpani Bhattacharjee; Kamales Kar, Observing supernova neutrino light curve in future dark matter detectors, *Physical Review* **D89** (2014)Art No: 013011

Apurba Kheto; Debades Bandyopadhyay, Isospin dependence of entrainment in superfluid neutron stars in a relativistic model, *Physical Review* **D89** (2014)Art No: 023007

VERITAS Collaboration; HESS Collaboration, LONG-TERM TeV AND X-RAY OBSERVATIONS OF THE GAMMA- RAY BINARY HESS J0632+057, *Astrophysical Journal***780** (2014)Art No: 168

Debabrata Adak; Debasish Majumdar; Supratik Pal, Generalizing thawing dark energy models: the standard vis-a-vis model independent diagnostics *Monthly Notices of the Royal Astronomical Society***437** (2014) 831

VERITAS Collaboration, Long Term Observations of B2 1215+30 with VERITAS, *Astrophysical Journal***779** (2013) Art No: 92

VERITAS Collaboration; Smithsonian Astrophys Observatory, VERITAS Observations of the MICROQUASAR CYGNUS X-3, *Astrophysical Journal***779** (2013)Art No: UNSP 150

E Aliu†; S Archambault†; B Behera†...P Majumdar; et al, Multiwavelength Observations of the TeV BINARY LS I+61° 303 WITH VERITAS, Fermi-LAT, AND Swift/XRT during A TeV Outburst, *Astrophysical Journal***779** (2013) Art No: UNSP 88

Anirban Biswas; Debasish Majumdar; Arunansu Sil†; Pijushpani Bhattacharjee, Two component dark matter: a possible explanation of 130 GeV gamma-ray line from the galactic centre, *Journal of Cosmology and Astroparticle Physics*, **Issue: 12** (2013) Art No: 049

Prasanna Kumar Mondal; Susnata Seth; Mala Das; Pijushpani Bhattacharjee, Study of low frequency acoustic signals from superheated droplet detector, *Nuclear Instruments & Methods in Physics Research* **A729** (2013)182

VERITAS Collaboration, Discovery of a New TeV GAMMA-Ray Source: VER J0521+211, *Astrophysical Journal***776** (2013)Art No: 69

Biswajit Adhikary; Mainak Chakraborty; Ambar Ghosal, Masses, mixing angles and phases of general Majorana neutrino mass matrix, *Journal of High Energy Physics*,**Issue: 10**(2013)Art No: 043

Biswajit Adhikary; Ambar Ghosal; Probir Roy, θ_{13} , $\mu\tau$ Symmetry Breaking and Neutrino YUKAWA TEXTURES, *International Journal of Modern Physics* **A28** (2013)Art No: UNSP 1350118

E Aliu†; S Archambault†; T Arlen†...P Majumdar; et al, Multiwavelength Observations and Modeling of 1ES 1959+650 in a Low Flux State, *Astrophysical Journal***775** (2013)Art No: 3

R3B Collaboration, Beyond the neutron drip line: The unbound oxygen isotopes O-25 and O-

26, Physical Review **C88** (2013) Art No: 034313

Chandrachur Chakraborty, Partha Pratim Pradhan, Lense-Thirring precession in Plebanski-Demianski Spacetimes, European Physical Journal **C73** (2013) Art No: 2536

Abhishek Majhi, Thermodynamics of quantum isolated horizons with model Hamiltonians, Physical Review **D88** (2013) Art No: 024010

Debabrata Adak; Amna Ali; Debasish Majumdar, Late-time acceleration in a slow-moving Galileon field, Physical Review **D88** (2013) Art No: 024007

Kamakshya Prasad Modak; Debasish Majumdar, Gamma ray and neutrino flux from the annihilation of neutralino dark matter at the Galactic halo region in the mAMSB model, Journal of Physics **G40** (2013) Art No: UNSP 075201

E Aliu†; S Archambault†; T Arlen†...P Majumdar; et al, Discovery of TeV GAMMA-Ray Emission Toward Supernova Remnant SNR G78.2+2.1, Astrophysical Journal **bf770** (2013) Art No: 93

Mala Das; Susnata Seth, Searching for universal behaviour in superheated droplet detector with effective recoil nuclei, Pramana-Journal of Physics **80** (2013) 983

S Seth; M Das; S Bhattacharya; et al, The nucleation parameter for heavy-ion induced bubble nucleation in superheated emulsion detector, Journal of Instrumentation **8** (2013) Art No: P05001

Pijushpani Bhattacharjee; Soumini Chaudhury; Susmita Kundu; et al, Deriving the velocity distribution of Galactic dark matter particles from the rotation curve data, Physical Review **D87** (2013) Art No: 083525

KS Gothe†; TP Prabhu†; PR Vishwanath†...RJ Britto...L Saha; et al, Pointing of HAGAR telescope mirrors, Experimental Astronomy **35** (2013) 489

E Aliu†; T Aune†; B Behera†...P Majumdar; et al, Observations of the Unidentified GAMMA-Ray Source TeV J2032+4130 by VERITAS, Astrophysical Journal **783** (2014) Art No: 16

L Saha; T Ergin; P Majumdar; et al, Origin of gamma-ray emission in the shell of Cassiopeia A, Astronomy & Astrophysics **563** (2014) Art No: A88

5.4.2.2 Theory

Gautam Bhattacharyya; Anirban Kundu†, Tirtha Sankar Ray†, Minimal supersymmetry confronts R_b , A_{FB}^b and m_h , Journal of Physics **G41** (2014) Art No: 035002

R Frederix†; MK Mandal†; P Mathews;...S Seth, Drell-Yan, ZZ, W^+W^- production in SM & ADD model to NLO+PS accuracy at the LHC, European Physical Journal **C74** (2014) Art No: 2745

Aminul Chowdhury Islam; Raktim Abir; Munshi G Mustafa; et al, The consequences of SU (3) color singletness, Polyakov Loop and Z (3) symmetry on a quark-gluon gas, *Journal of Physics* **G41** (2014) Art No: 025001

Pritibhajan Byakti; David Emmanuel-Costa†; Arindam Mazumdar; Palash B Pal, Number of fermion generations from a novel grand unified model, *European Physical Journal* **C74** (2014) Art No: 2730

Olaf Dreyer†; Amit Ghosh; Avirup Ghosh, Entropy from near-horizon geometries of Killing horizons, *Physical Review* **D89** (2014) Art No: 024035

A Harindranath; Rajen Kundu†; Asmita Mukherjee†, On transverse spin sum rules, *Physics Letters* **B728** (2014) 63

Somdeb Chakraborty; Parijat Dey, WESS-ZUMINO-WITTEN MODEL FOR GALILEAN CONFORMAL ALGEBRA, *Modern Physics Letters* **A28** (2013) Art No: 1350176

Parijat Dey; Shibaji Roy, From AdS to Schrödinger/Lifshitz dual space-times without or with hyperscaling violation, *Journal of High Energy Physics*, **Issue: 11** 92013) Art No: 113

P Artoisenet†; P de Aquino†; F Demartin†; P Mathews; et al, A framework for Higgs characterisation, *Journal of High Energy Physics*, **Issue: 11** (2013) Art No: 043

Gautam Bhattacharyya; Dipankar Das; Palash B Pal; et al, Scalar sector properties of two-Higgs-doublet models with a global U(1) symmetry, *Journal of High Energy Physics*, **Issue: 10** (2013) Art No: 081

Ashok K Das; RR Francisco†; J Frenkel†, Gauge independence of the fermion pole mass, *Physical Review* **D88** (2013) Art No: 085012

Ashok K Das; J Frenkel†, The pole of the fermion propagator in a general class of gauges, *Physics Letters* **B726** (2013) 493

Gautam Bhattacharyya; Biplob Bhattacharjee†; Tsutomu T Yanagida†; et al, A natural scenario for heavy colored and light uncolored superpartners, *Physics Letters* **B725** (2013) 339

P -G Reinhard†; J Piekarewicz†; W Nazarewicz†; BK Agrawal; et al, Information content of the weak-charge form factor, *Physical Review* **C88** (2013) Art No: 034325

Lata Thakur†; Najmul Haque; Uttam Kakade†; et al, Dissociation of quarkonium in an anisotropic hot QCD medium, *Physical Review* **D88** (2013) Art No: 054022

Somdeb Chakraborty; Najmul Haque, Holographic quark-antiquark potential in hot, anisotropic Yang-Mills plasma, *Nuclear Physics* **B874** (2013) 821

R Shyam, Ξ^- hyperon and hypernuclear production in the (K^- , K^+) reaction on nucleon and nuclei in a field theoretical model, *Nuclear Physics* **A914** (2013) 79

R Chatterjee†, R Shyam; K Tsushima†; et al, Structure and Coulomb dissociation of O-23 within the quark-meson coupling model, Nuclear Physics **A913** (2013) 116

R Shyam; O Scholten†; AW Thomas†, Production of the H dibaryon via the (K^- , K^+) reaction on a ^{12}C target, Physical Review **C88** (2013) Art No: 025209

Parijat Dey; Shibaji Roy, Zero sound in strange metals with hyperscaling violation from holography, Physical Review **D88** (2013) Art No: 046010

X Roca-Maza†; M Brenna†; G Colo†...BK Agrawal; et al, Electric dipole polarizability in ^{208}Pb : Insights from the droplet model, Physical Review **C88** (2013) Art No: 024316

Harvendra Singh, Lifshitz to AdS flow with interpolating p-brane solutions, Journal of High Energy Physics, **Issue: 8** (2013) Art No: 097

K Tsushima†; R Shyam; AW Thomas†, Production of Ξ^- -Hypernuclei via the (K^- , K^+) Reaction in a Quark-Meson Coupling Model, Few-Body Systems **54** (2013) 1271

A Harindranath; Rajen Kundu†; Asmita Mukherjee†; et al, Comment on "Proton Spin Structure from Measurable Parton Distributions", Physical Review Letters **111** (2013) Art No: 039102

Najmul Haque; Munshi G Mustafa; Michael Strickland†, Quark number susceptibilities from two-loop hard thermal loop perturbation theory, Journal of High Energy Physics, **Issue: 7** (2013) Art No: 184

Ernesto Frodden†; Amit Ghosh; Alejandro Perez†, Quasilocal first law for black hole thermodynamics, Physical Review **D87** (2013) Art No: 121503

B Basu-Mallick; Tanaya Bhattacharyya†; Diptiman Sen†, Clusters of bound particles in the derivative δ -function Bose gas, Nuclear Physics **B871** (2013) 362

S Meljanac†; A Pachol†; A Samsarov†; Kumar S Gupta, Different realizations of kappa-momentum, Physical Review **D87** (2013) Art No: 125009

Abhishek Chowdhury; Asit K De; Sangita De Sarkar; A Harindranath; Jyotirmoy Maiti; Santanu Mondal; Anwesa Sarkar, Pion and nucleon in two flavour QCD with unimproved Wilson fermions, Nuclear Physics **B871** (2013) 82

BK Agrawal; JN De; SK Samaddar; et al, Constraining the density dependence of the symmetry energy from nuclear masses, Physical Review **C87** (2013) Art No: 051306

Najmul Haque; Munshi G Mustafa; Michael Strickland†, Two-loop hard thermal loop pressure at finite temperature and chemical potential, Physical Review **D87** (2013) Art No: 105007

Pritibhajan Byakti; Tirtha Sankar Ray†, Burgeoning the Higgs mass to 125 GeV through messenger-matter interactions in GMSB models, Journal of High Energy Physics, **Issue: 5** (2013) Art No: 055

Abhishek Chowdhury; Asit K De; Sangita De Sarkar; A Harindranath; Jyotirmoy Maiti; San-

tanu Mondal; Anwesha Sarkar, Exploring autocorrelations in two-flavor Wilson Lattice QCD using DD-HMC algorithm, *Computer Physics Communications* **184** (2013) 1439

Ayan Chatterjee†; Bhramar Chatterjee; Amit Ghosh, Hawking radiation from dynamical horizons, *Physical Review* **D87** (2013) Art No: 084051

Kumar S Gupta; E Harikumar†; Amilcar R de Queiroz†, A Dirac-type variant of the xp-model and the Riemann zeros, *EPL* **102** (2013) Art No: 10006

Najmul Haque; Jens O Andersen; Munshi G Mustafa; et al, Three-loop pressure and susceptibility at finite temperature and density from hard-thermal-loop perturbation theory, *Phys Rev* **D89** (2014) 061701

D de Florian; M Mahakhud; P Mathews; et al, Quark and gluon spin-2 form factors to two-loops in QCD, *JHEP* **1402** (2014) 035

Anjan Kundu, Novel Hierarchies & Hidden Dimensions in Integrable Field Models: Theory & Application, *J Phys: Conference Series* **482** (2014) 012022

P Banerjee; B Basu-Mallick, Asymptotic form of level density distributions for a class of inhomogeneous 1D vertex models, *Journal of Physics: Conference Series* **411** (2013) 012005

BK Agrawal; JN De; SK Samaddar; et al, Symmetry energy of warm nuclear systems, *European Physical Journal* **A50** (2014) Art no.19

5.5 Ph D Awarded

Santanu Mondal [A Harindranath], Chiral Properties of Wilson Fermion in Lattice Quantum Chromodynamics, University of Calcutta, 2013

Raktim Abir [Munshi Golam Mustafa], Phenomenological Consequences of QCD Bremstrahlung Processes in RHIC and LHC, HBNI, Jan 27, 2014

Srijit Bhattacharjee [Parthasarathi Majumdar], Quantum Infrared Instabilities of gauge and gravity coupled Higgs Fields, University: HBNI, 14 March, 2014

5.6 Seminars/Lectures given in Conference/Symposium/Schools

Anjan Kundu

- i. Novel Hierarchies and hidden dimensions in integrable field models: Nonlinear Schroedinger equation, in International Workshop on Mathematics & Physics of Nonlinear Phenomena, Gallipoli, Italy, Jun 22-Jul 1, 2013
- ii. Hidden possibility of constructing two and higher-dimensional quantum integrable models in

Workshop on Quantum Integrable Systems, SN Bose Centre, Kolkata, Dec 2-6, 2013

iii. Construction of higher dimensional classical and quantum integrable models, by unravelling hidden dimensions, Workshop on Nonlinear Integrable Systems & their Applications, Trichy, Feb 24-Mar 1, 2014

iv. Non-circular symmetric Skyrmions in helimagnets in Workshop on Integrable and Nonintegrable Dynamical Systems, SN Bose Centre, Kolkata, Mar 21, 2014

v. Modelling rogue waves through exact dynamical lump soliton controlled by ocean currents, Indian Institute of Geomagnetism, IIG, Mumbai, Mar 24-26, 2013

vi. Novel Hierarchies & Hidden Dimensions in Integrable Field Models, TIFR (Theory Group), Mumbai, Mar 27- Apr 1, 2013

Palash B Pal

i. Discovering particles, 1-day conference on "Recent advances in Physics" organized by Bidhanagar College, Sep 15, 2013

ii. Wave-particle duality, Seminar at the Institute of Engineering and Management, Calcutta, Dec 17, 2013

iii. The world of neutrinos, the Outreach Program for the Indian Neutrino Observatory, Science City Auditorium, Calcutta, Nov 8, 2013

iv. Moulou kona (Elementary particles), "Cultivision" festival organized by the Research Scholars' Association of the Indian Institute of Cultivation of Science, Apr 18, 2013

Gautam Bhattacharyya

Geometrical CP violation and nonstandard Higgs decay:

i. Helsinki Institute of Physics, Finland, Oct 2013

ii. Dept. of Physics, University of Perugia, Italy, Nov 2013

iii. Conference 'Electroweak Symmetry Breaking and Flavour Physics, IIT Guwahati, Feb 2014

iv. Conference 'Current Trends in Particle Physics Research (CTPPR2014), Kalyani University, Mar 2014

v. The so-called God Particle: An incredible journey of mankind, National Science Day Celebration Lecture, National Institute of Cholera & Enteric Diseases, Kolkata, 28 Feb, 2014

Bireswar Basu-Mallick

Bound states of a quantum many-body system and number theory, Theoretical Physics Department, Universidad Complutense, Madrid, Spain, June 19, 2013

Asit Kumar De

Many Faces of Quantum Field Theories on Lattice, CHEP, IISc, Bangalore, May 31, 2013

BK Agrawal

i. Density content of symmetry energy from neutron-skin, nuclear masses and giant resonances, DAE Symposium on Nuclear Physics, BARC, Mumbai Dec 2-6, 2013

ii. Nuclear symmetry energy from nuclear observables, RIKEN Nishina Center for Accelerator based Science, Japan, Mar 25, 2014

Prakash Mathews

i. Diphoton production in the ADD model to NLO+parton shower accuracy at the LHC, 11th International Symposium on Radiative Corrections (Applications of Quantum Field Theory to Phenomenology), Durham, UK, Sept 2013

- ii. Higgs characterisation, Discussion Meeting on EWSB and Flavours in the light of LHC, IIT Guwahati, India, Feb 20-22, 2014

Munshi G Mustafa

- i. A set of seven lectures on Quantum Field Theory at Finite Temperature and density at FAIR Physics Compressed Baryonic Matter at FAIR, Bose Institute, Darjeeling, India, Jan 20-24, 2014
- ii. Equation of state of hot and dense matter, ANPhAS-2014, VECC, Kolkata, Feb 19-21, 2014
- iii. International Conference on Matter at Extreme Conditions -Then and Now, Jan 15-17, 2014, Bose Institute, Calcutta, India
- iv. FAIR Physics Compressed Baryonic Matter at FAIR, Jan 20-24, 2014, Bose Institute, Darjeeling, India
- v. 6th Asian Nuclear Physics Association Symposium (ANPhAS-2014), Feb 19-21, 2014, VECC, Calcutta, India

Koushik Dutta

- i. Inflation after PLANCK: An Issue, AAPCOS-2013 - Shimla
- ii. Inflation after PLANCK: An Issue, Rencontres du Vietnam on "Windows on the Universe", Vietnam
- iii. Open Inflation after BICEP, Cosmology Workshop, International Centre for Theoretical Science (ICTS), Bangalore
- iv. Cosmology with pNGBs, Aspects of Cosmology, Indian Institute of Astrophysics, Bangalore
- v. Before Big Bang, Max Planck Society, Science City, Kolkata

Pijushpani Bhattacharjee

- i. Direct detection of Dark Matter, International Conference on Advances in Astroparticle Physics & Cosmology (AAPCOS-2013), Shimla, India, Jun 14-17, 2013
- ii. Phase space distribution of dark matter particles in the Galaxy: Implications for direct and indirect detection, "SUSY-DM" Workshop, Centre for High Energy physics (CHEP), IISc, Bangalore, Oct 3-5, 2013
- iii. Dark Matter in the Galaxy: Direct detection of WIMPs, Workshop on Contemporary Trends in High Energy Physics & Experimentation, Punjab University, Chandigarh, Mar 10-11, 2014
- iv. Direct detection of WIMP Dark Matter, Current Trends in Particle Physics Research, (CTPPR2014), Kalyani University, Mar 13-15, 2014
- v. Dark Matter in the Galaxy: Rotation curve and the phase space distribution of Milky Ways dark matter particles, Seminar at the Mitchell Institute for Fundamental Physics, Texas A&M University, College Station, Texas, USA, Sep 19, 2013
- vi. Rotation curve and the velocity distribution of the Milky Ways dark matter particles, seminar at the McDonnell Center for the Space Sciences, Washington University, St Louis, MO, USA, Nov 1, 2013
- vii. Astroparticle Physics Dark Matter and its detection A set of three invited pedagogical lectures at the Instructional Workshop SANGAM@HRI-2014, Harish-Chandra Research Institute (HRI), Allahabad, Mar 24-29, 2014

Debades Bandyopadhyay

- i. Exploring many facets of core collapse supernovae and neutron stars, Sixth Asian Nuclear Physics Association Symposium, Variable Energy Cyclotron Centre, Kolkata, Feb 19-21, 2014
- ii. Role of magnetised crust on torsional shear mode oscillations, workshop on Neutron rich matter and neutron stars, ECT*, Trento, Italy, Oct 3, 2013

- ii. Role of magnetised crust on torsional shear mode oscillations, workshop on Neutron rich matter and neutron stars, ECT*, Trento, Italy, Oct 3, 2013
- iii. Nuclei in Neutron Star Crusts, conference on Nuclear Physics: Presence and Future, Boppard, Germany, Jun 4, 2013

Debasish Majumdar

- i. Two Component Dark Matter, an explanation of 130 GeV gamma line from galactic Centre, Centre for Theoretical Physics, Jamia Millia Islamia, New Delhi, India, Apr 2013
- ii. Neutrinos and Gamma Rays from the annihilation of neutralino Dark Matter from the Galactic centre in AMSB model, National Conference on Double Beta Decay and Neutrinos, IIT, Ropar and Panjab University, Chandigarh, Apr 2013
- iii. Dark Matter: evidence and detection, Department of Physics, Panjab University, Chandigarh, May 2013
- iv. Dark Matter Department of Physics, Kashmir University, Srinagar, May 2013
- v. Current Trends in Particle Physics Research, Department of Physics, University of Kalyani, Feb 2014

Mala Das

- i. Conference on double beta decay (DBD-2013), IIT Ropar & Panjab University, Chandigarh, Apr 20-21, 2013
- ii. Advances in Astroparticle Physics & Cosmology (APPCOS -2013) at IAS, Shimla, Jun 14-17, 2013
- iii. Laurentian University, Sudbury, Canada, Aug 27, 2013

Pratik Majumdar

- i. Status of Monte Carlo Production at SINP, CTA Consortium meeting, Chicago, May 2013
 - ii. Exploring the Universe with Very High Energy Particles and Photons, Workshop, Recent Advances in Particle Physics, Astrophysics and Cosmology, Department of Physics, Calcutta University, Aug 2013
 - iii. Calibration System for the Prototype Large Size Telescope in CTA, LST General Meeting, Institute of Cosmic Ray Research (ICRR), Kashiwa, Japan, Jan 2014
 - iv. Modelling of Supernova Remnants in Fermi and IACT Era and predictions for CTA), LST General Meeting, Institute of Cosmic Ray Research (ICRR), Kashiwa, Japan, Jan 2014
- Convenor** of Int workshop on Advances in Astroparticle Physics and Cosmology (AAPCOS 2013), Indian Institute of Advanced Studies (IIAS), Shimla, Jun 2013

5.7 Honours and Distinctions

Anjan Kundu

Selected as Fellow of the Indian National Science Academy (INSA, New Delhi) (January, 2014)

Gautam Bhattacharyya

Fellow of the National Academy of Sciences, India (NASI), Allahabad (2013)

5.8 Teaching elsewhere

Munshi G Mustafa

Electromagnetic Theory: Integrated MSc Ph D, First Semester, Bose Institute, Kolkata, Aug-Nov, 2013

5.9 Miscellany

RAD-2013



National Workshop on Exploring Radiation in many Splendors, RAD-2013, SINP, Sponsored by SINP (CSD, APC, ANP) and BRNS, Nov 23-24, 2013

Pijushpani Bhattacharjee

Currently serving as a member of the Scientific Management Board of the India-based Neutrino Observatory (INO) constituted by the Department of Atomic Energy, Govt of India

Debades Bandyopadhyay

Organised One day symposium in Astroparticle Physics and Cosmology held at Saha Institute of Nuclear Physics, Kolkata, Jan 3, 2014

Anjan Kundu

Member of the Editorial Board of the Proceedings of the Royal Society: Series A

Asit Kumar De

Organized as Convener the School on Quantum Field Theories on Lattice at SINP during 2-6 December 2013

The School had 3 world experts giving 5 lectures each on their areas of expertise (chiral perturbation theory, non-perturbative renormalization and algorithms). Most Indian lattice gauge theorists and people working in related areas including students and post-docs attended. The school was so



successful that several requests have been received for continuation of such schools periodically in future.

The lectures are available for downloads in our Institute website:

<http://www.saha.ac.in/theory/lattice.school/slides.html> The School website (where all other details are available):

<http://www.saha.ac.in/theory/lattice.school/index.html>

Bireswar Basu Mallick

Senior Associateship award of Abdus Salam ICTP, Trieste, Italy (2008-2013)

Koushik Dutta

Organizer, Topical Conference on Gravity and Cosmology, SINP, 9th December, 2013

Chapter 6
**Research Fellows/Visiting
Fellows/Research Associates**

Chapter 6

Research Fellows/Visiting Fellows/Research Associates

6.1 Visiting Fellows/Research Associates and Research Fellows

6.1.1 Research Fellows

ANP

- 1 Smt Purba Bhattacharya: SRF
- 2 Sri Hitesh Vijay Rahangdale: SRF
- 3 Sri Rajani Raman: SRF
- 4 Smt Ajanta Kundu: SRF

APC

- 1 Smt Soumini Chaudhury: SRF
- 2 Smt Susnata Seth: SRF
- 3 Sri Lab Saha: SRF
- 4 Smt Susmita Kundu: SRF
- 5 Sri Mainak Chakraborty: SRF
- 6 Sri Abhishek Majhi: SRF
- 7 Sri Anirban Biswas: SRF
- 8 Sri Debabrata Adak: SRF
- 9 Sri Chandrachur Chakraborty: SRF
- 10 Sri Kamakshya Prasad Modak: SRF
- 11 Sri Amit Dutta Banik: SRF
- 12 Sri Apurba Kheto: JRF
- 13 Sri Prasanta Char: JRF
- 14 Sri Anshu Chatterjee: JRF

B&SG

- 1 Smt Saptaparni Ghosh: SRF
- 2 Smt Amrita Banerjee: SRF
- 3 Smt Pritha Bhattacharjee: SRF
- 4 Sri Manindra Bera: SRF
- 5 Smt Nandini Pal Basak: SRF
- 6 Smt Kasturi Roy SRF:
- 7 Smt Suchismita Halder: SRF

- 8 Sri Shounak Baksi: SRF
- 9 Smt Madhurima Mitra: SRF
- 10 Smt Shilpita Karmakar: SRF
- 11 Sri Srijan Haldar: SRF
- 12 Smt Debashree Das: SRF
- 13 Smt Devika Srivastava: SRF
- 14 Sm Rukmini Mukherjee: SRF
- 15 Sri Avik Basu: SRF
- 16 Sri Sabyasachi Sen: JRF
- 17 Smt Zenia Kaul: JRF
- 18 Smt Isha Sengupta: JRF
- 19 Smt Piyali Majumder: JRF

Computetional Science

- 1 Smt Sanchita Mukherjee: SRF
- 2 Sri Manas Mondal: SRF
- 3 Smt Angana Ray: SRF
- 4 Debasish Mukherjee: J.R.F

CSD

- 1 Smt Moupriya Nag: SRF
- 2 Sm Chaitrali Sengupta: JRF
- 3 Sm Nidhi Agnihotri: JRF
- 4 Sm Sathi Goswami: JRF
- 5 Smt Sreeja Chakraborty: SRF
- 6 Sri Ajoy Mandal: SRF
- 7 Sri Sourav Ghoshal: JRF
- 8 Sri Tapas Paul: JRF

C&MB

- 1 Smt Jayeeta Ghosh: SRF

- 2 Smt Eashita Das: SRF
 3 Smt Kasturi Sengupta (Guha): SRF
 4 Sri Sourav Roy: SRF
 5 Smt Barnali Waugh: SRF
 6 Smt Seema Nath: SRF
 7 Sri Mahan Ray: SRF
 8 Smt Arpita Saha: SRF
 9 Sri Supratim Ghatak: SRF
 10 Sm Sanghati Roy Choudhuri: SRF
 11 Sm Soumita Mukherjee: SRF
 12 Sri Srijit Das: SRF
 13 Smt Malti Yadav: JRF
 14 Sri Kamalendu Pal: JRF

CMP

- 1 Sri Nazir Khan: SRF
 2 Sri Arindam Midya: SRF
 3 Sri Sudipta Mandal: SRF
 4 Smt Susmita Dhara: SRF
 5 Smt Moumita Nandi: SRF
 6 Smt Rajeswari Roy Chowdhury: SRF
 7 Sri Tapas Paramanik: SRF
 8 Sri Santanu Pakhira: SRF
 9 Sri Rakesh Chatterjee: SRF
 10 Sri Asim Ghosh: SRF
 11 Sri Debarshee Bagchi: SRF
 12 Smt Mahashweta Basu: SRF
 13 Smt Paramita Dutta: SRF
 14 Sri Niladri Sarkar: SRF
 15 Smt Moumita Dey: SRF
 16 Smt Srilekha Saha: SRF
 17 Sri Soumyajyoti Biswas: SRF
 18 Sourish Bandyopadhyay: SRF
 19 Sri Amit Dey: SRF
 20 Sri Atanu Rajak: SRF
 21 Sri Arijit Chatterjee: SRF
 22 Sri Gourab Majumder: SRF
 23 Sri Sabyasachi Nag: SRF
 24 Sri Sourav Kundu: SRF
 25 Smt Amrita Ghosh: JRF
 26 Smt Binita Mandal: JRF
 27 Smt Mily Kundu: JRF
 28 Sri Sanjib Banik: JRF
 29 Smt Sanjukta Pal: JRF
 30 Sri Sudip Mukherjee: JRF
 31 Sri Tirthankar Banerjee: JRF

HENPPD

- 1 Smt Sreemoyee Sarkar: SRF
 2 Sri Mahatsab Mandal: SRF

- 3 Ms Debarati Roy: SRF
 4 Ms Swagata Mukherjee: SRF
 5 Ms Sandhya Jain: SRF
 6 Shilpi Jain: SRF
 7 Sri Sourav Dey: SRF
 8 Sri Atanu Modak: SRF
 9 Sri Ashim Roy: JRF
 10 Sri Kuntal Mondal: JRF
 11 Sri Suvankar Roy Chowdhury: JRF
 12 Kalyanmoy Chatterjee: SRF

NPD

- 1 Sri Santosh Chakraborty: SRF
 2 Md Anisur Rahaman: SRF

PPD

- 1 Smt Anwesa Sarkar: SRF
 2 Sri Chandan Maity: SRF
 3 Sri Sudip Garai: SRF
 4 Sri Abhijit Ghosh: SRF
 5 Mr Alpha Michael: SRF
 6 Sri Sourav Pramanik: SRF
 7 Sri Abhik Mukherjee: SRF
 8 Sri Debajyoti Saha: JRF
 9 Sri Pankaj Kumar Shaw: JRF
 10 Sri Sabuj Ghosh: JRF
 11 Sri Satyajit Chowdhury: JRF

SP&MS

- 1 Smt Sayanee Jana: JRF
 2 Sri Abhisakh Sarma: SRF
 3 Smt Paramita Chatterjee: SRF
 4 Sri Safiul Alam Mollick: SRF
 5 Smt Tanusree Samanta: SRF
 6 Smt Manjula Sharma: SRF
 7 Sri Amaresh Metya: SRF
 8 Sri Santanu Maiti: SRF
 9 Sri Jayanta Das: SRF
 10 Sri Shyamal Mondal: SRF
 11 Smt Ishani Roy: SRF
 12 Sri Suvankar Chakraborty: SRF
 13 Sri Bishnudas Ghosh: SRF
 14 Sri Kousik Bagani: SRF
 15 Smt Mala Mukhopadhyay: SRF
 16 Sri Tanmay Ghosh: SRF
 17 Smt Debashree Chowdhury: SRF
 18 Sri Arka Bikash Dey: SRF
 19 Sri Asish Kumar Kundu: SRF
 20 Sri Kaustabh Dan: SRF
 21 Sri Debaleen Biswas: SRF
 22 Sri Rajendra Prasad Giri: SRF

23 Sk Abdul Kader Md Faruque: SRF
 24 Sri Achyut Maity: JRF
 25 Sri Arpan Maiti: JRF
 26 Smt Barnamala Saha: JRF
 27 Sri Gouranga Manna: JRF
 28 Smt Sruti Dutta: JRF
 29 Sri Sukanta Barman: JRF
 30 Sultsna Tajmili Hasnahena: JRF
 31 Sri Tapash Ghosh: JRF

Theory

1 Md Najmul Haque: SRF
 2 Smt Baishali Chakraborty: SRF
 3 Sri Arindam Mazumdar: SRF
 4 Sri Somdeb Chakraborty: SRF

5 Sri Pratyay Banerjee: SRF
 6 Sri Avirup Ghosh: SRF
 7 Sri Abhishek Chowdhury: SRF
 8 Sri Dipankar Das: SRF
 9 Sri Goutam Das: SRF
 10 Sri Satyajit Seth: SRF
 11 Sri Aritra Bandyopadhyay: JRF
 12 SriChiranjib Mandal: JRF
 13 Smt Chitrlekha Datta: JRF
 14 Sri Kumar Das: JRF
 15 Sri Kuntal Nayek: JRF
 16 Noasad Alam: JRF

6.1.2 SRF(EX), PDF, RA, VS, VF**APC**

1 Amna Ali: PDF

BSG

1 Moumita Gangopadhyay: RA-3
 2 Anita Roy: PDF

C&MB

1 Dr Nirmalya Dey: PDF
 2 Kamalika Roy Chowdhury: PDF

CSD

1 Mr Arnab Basu: RA-2
 2 Arpita Dutta: RA-1
 3 Dr Kausturi Sanyal: RA-1
 4 Munmun Bardhan: RA-3
 5 Binita Dutta: PDF
 6 Mousumi Banerjee: PDF

CMP

1 Biswanath Samantaray: RA-1
 2 Mayukh Majumder: SRF(Extended)
 3 Deep Talukdar: RA-1
 4 Satyaki Kar: RA-3
 5 Rima paul: RA-1

6 Dilip Kumar Bhoi: PDF

7 Dr Papri Dasgupta: RA-3

HENPP

1 Ms Payal Mohanti: RA-1

NPD

1 Dr Mukhesh Kumar Pradhan: PDF
 2 Shinjinee Dasgupta: PDF

SP&MS

1 Sourav Kanti Jana: PDF
 2 Rupali kundu: SRF(Extended)
 3 Sayan Bayan: RA-1
 4 Pabitra Das: RA

SGD

1 Biswa Pathik Pahari: PDF

Theory

1 Bhramar Chatterjee: SRF(Extended)
 2 Sarbani Majumdar: RA-1

PPD

1 Subir Biswas: SRF(Extended)
 2 Debabrata Banerjee: PDF

Chapter 7
Facilities

Chapter 7

Facilities

7.1 Centre for Advanced Research & Education

The Centre for Advanced Research and Education (CARE) was established as a centre of the Saha Institute of Nuclear Physics during the Xth Plan period, solely funded by a HRD project of DAE, with the purpose of inspiring motivated and talented students of physics and the biophysical sciences to advanced research. Its detailed objectives are as follows:

Nation's earliest fifty years' old Post-M.Sc. training programme in SINP, aimed at bridging the gap between M.Sc.-level courses and the frontiers of research, needs continuous and substantial improvement. The CARE committee monitors and executes these improvements through the CARE project. The quite successful undergraduate associateship (UGA) programme of SINP regularly invites some bright undergraduate students in physics, chemistry and biology to the Institute during their vacation periods and encourage them to take part in advanced level courses, doing some research projects, etc. CARE project also plans to cater the growing needs of various types of outreach programmes in different aspects of science to young students and science teachers across the country.

The activities of CARE also include the maintenance of the Prof. M.N. Saha Archive and a museum to showcase old equipments that are either made in-house or custom fabricated in SINP and are of some historic values.

The Centre aims to enrich the local scientific atmosphere in the state and outside, through organizing advanced level schools and workshops in active research areas both for students as well as for teachers employed in purely teaching institutions. For scientifically inclined people in the city at large, the Centre has also been organizing popular lectures on the history and culture of science in India.

The SINP Auditorium Complex is mainly used for holding various programmes, seminars, symposium, conferences national and international stature etc.

The Annual Report is published by CARE in every year which contains activities of Saha Institute of Nuclear Physics.

Activities:

1. Post M.Sc. Teaching Program
2. Publications and Documentations
3. Maintaining and managing the Auditorium complex and its Science Gallery
4. The Meghnad Saha Archive
5. Outreach Programmes
6. Undergraduate Associateship Programme
7. Summer Students' Programme
8. Schools/Workshop/Symposiums/Colloquiums/Conferences and CARE Seminars
9. Science Day Celebration with Visits to/of Undergraduate Colleges, High Schools

Some of the programs organized by the CARE in 2013-14

School/Seminar/Workshop

Brain Storming Session in Experimental Nonlinear Dynamics. April 9-10, 2013

Sponsored by CARE

Special Colloquia on Neutron Scattering- Probing Structure and Dynamics. Aug. 7, 2013. Speakers: Prof. Robert Mcgreevy and Prof. Sean Langridge (ISIS Neutron and Muon Facility, Rutherford Appleton Laboratory, UK) (Sponsored by CARE)

CARE Seminar on Role of AcSIR in Contemporary India : Some Thoughts and Perspectives. Speaker: Prof. Amit Chattopadhyay. Sept. 4, 2013

CMS Data Analysis School. Nov.7-11, 2013

National Workshop on Exploring Radiation in Many Splendors. Nov. 23-24, 2013. Theme: Application of Radiation and related modes of detection. Speakers : Sunanda Banerjee(SINP), Alokmay Datta(SINP), Marco Durante(GSI), Asimananda Goswami(SINP), A.J. Noble(Queens University) Eligibility M.Sc. and Junior Research Fellows

7th School on Genomics and Proteomics for Clinicians, Feb 24-28, 2014

13 Doctors from local hospitals/medical colleges participated in this program. CARE and the Structural Genomics Laboratory jointly organized this program, giving the participants hands-on training on state-of-the-art genomics and proteomics experiments

Outreach Programme Participated by CARE

17th National Exhibition on the theme of India Advancing towards a world power Sept 21-25, 2013, Ramkrishna Mission Vidyamandira Ground, Belur Math, Howrah. Organized by Central Calcutta Science and Culture Organization for Youth

10th Jatiya Sanhati Utsav-O-Bharat Mela, 2013. Dec. 11-17, 2013. Gobinda Nagar High School Ground, Canning, South 24 Parganas

Sundarban Kristi Mela O Loko Sanskriti Utsab, Dec. 20-29, 2013. Kultali Milon Tirtha Society, Kultali, P.S. Basanti, South 24 parganas

Outreach in Bnakura Ramananda College, Januray 8-9, 2014 (Debashis Mukhopadhyay and Montu Hazra, 500 participants)

Sundarban Lokopriya Utsav, Jan 23-30, 2014 by Sundarban Unnayan Niketan at Sonakhali Bazar, Vill & P.O. Sonakhali, P.S.Basanti. South 24 parganas

Acharya Satyendranath Basu Samarak Bijnan O Prajukti Mela, Jan 29 Feb 2, 2014 at Hedua Park (in front of Scottish Church College)

Outreach Programme Organised by CARE

CARE Science Education Meet on Aug 20, 2013

Discussion Meeting on Post High School Science Teaching in Educational and Research Institutions of India:

Speakers: Profs. Milan Kr. Sanyal (Director, SINP), Chitra Natarajan (Mumbai), L. S. Shashidhara (Pune), Pushpendu K. Das (Bengaluru), Rupamanjari Ghosh (Delhi), Sugata Marjit (Kolkata), Satyaki Bhattacharya, (SINP, Kolkata)

Pannel Discussion: Profs. Abhijit Chakrabarti (Co-ordinator. SINP), Arup Mitra (St. Xavier, Kolkata), Prof. Amit Ghosh (SINP, Kolkata)

Institute Laboratory Visited by the Students of Other Institute/University

5 students from Nagaland University undertook their B. Tech projects at SINP in Biotechnology from 4th Feb, 2013 to 3rd Apr, 2013

30 Physics undergraduate students from Mizoram University visited SINP on November 8, 2013 (Prof. Alokmay Datta and Debashis Mukhopadhyay have presented some work done in SINP before them)



Prof Abhijit Chakrabarti, meeting undergraduate students from Mizoram University, November 8, 2013

16 students and 3 teachers from St. Anthonys College, Dept. of Physics, Shillong, visited various Labs in SINP on Dec 11, 2013. (Talks were given by Prof. Alokmay Datta and Satyaki Bhattacharya)

A team of 22 students and teachers from Srikishan Sarda College, Hailakandi, Assam visited SINP on Feb 10, 2014

400 students and teachers of Delhi Public School, Ruby Park, Kolkata, visited SINP on Feb 13, 2014

Publication

CARE publication on Science Education beyond High School, Jan 11, 2014

7.1.1 The Post-M Sc Associateship Course

60th Post-M Sc Course, Session 2012-13

PHYSICS:

THIRD TERM : Student, Review Title (Supervisor)

1. Achyut Maity, Application of finite difference time domain (fdtd) numerical approach to understand the electron beam induced optical response of metal nanoparticles. (Prof Tapas Kumar Chini)-SPD
2. Amrita Ghosh, Supersolidity (Prof Sudhakar Yarlagadda) TCMP
3. Anshu Chatterjee, Search for gev-tev gamma-ray emission from 3c391 supernovae remnant using one year fermi-lat data (Prof Pratik Majumdar) APC
4. Aritra Bandyopadhyay, Study of leading order thermodynamics of quark gluon gas in hard thermal loop resummation (Prof Munshi G Mustafa) Theory
5. Arpan Maiti, Studies on localized surface plasmon resonance of chemically synthesized gold nanoparticles using electron beam spectroscopy and imaging. (Prof Tapas Kumar Chini)-SPD
6. Ashim Roy, Studies on electromagnetic and hadronic showers in a sampling calorimeter. (Prof Sunanda Banerjee, Prof Satyaki Bhattacharya & Prof Subir Sarkar) HENPP
7. Barnamala Saha, Nanomaterial based chemical and biosensors. (Prof Sangam Banerjee) SPD
8. Binita Mondal, Thermoelectric properties of nonheusler alloys. (Prof RR Ranganathan, & Prof Chandan Majumdar) ECMP
9. Chiranjib Mandal, Observation of dipole band(s) in weakly deformed nucleus ^{143}Sm lying near $n=82$ shell closure. (Prof Asimananda Goswami) NPD
10. Chitralekha Datta, Conserved quantities of some classical and quantum integrable models. (Prof Bireswar Basu Mallik) Theory
11. Debajyoti Saha, Investigation of complexity dynamics of the fluctuations in the glow discharge plasma and some preliminary results from sinp tokamak. (Prof AN Sekhar Ienger & Prof MS Janaki) Plasma Physics
12. Gouranga Manna, X-ray scattering from buried interfaces (Prof Milan Kumar Sanyal) SPD
13. Kumar Das, A study on the entropy-area relationship of a scalar field in a schwarzschild black hole. (Prof Parthasarathi Mitra) Theory
14. Kuntal Mondal, Cp violation in neutral kaon system. (Prof Palash Baran Pal) Theory
15. Kuntal Nayek, A review on the branes and solitons in string theory. (Prof Shibaji Roy) Theory
16. Mily Kundu, Polar intermetallic compounds-current status. (Prof RR Ranganathan & Prof Chandan Majumdar) ECMP
17. Naosad Alam, Study of the neutron and proto-neutron stars. (Prof Bijay Kumar Agarwal) Theory
18. Pankaj Kumar Shaw, Nonlinear dynamics experiments and theoretical modeling of ion cyclotron oscillation. (Prof AN Sekhar Ienger & Prof MS Janaki) Plasma Physics
19. Sabuj Ghosh, Experiments and theoretical modelling of intermittence chaos in a glow discharge plasma. (Prof AN Sekhar Ienger & Prof MS Janaki) Plasma Physics

20. Sanjib Banik, Magnetoelectricity in bi-layer thin films and in core shell nanoparticles. (Prof Indronil Das) ECMP
21. Sanjukta Paul, Manganite heterostructure. (Prof Y Sudhakar) TCMP
22. Satyajit Chowdhury, Study of lasing characteristics of zno nanowires by photoluminescence technique. (Prof Satyaban Bhunia) SPD
23. Sayanee Jana, Surfactant-templated mesoporous silica films to grow metal-nanoobjects. (Prof Satyajit Hazra)- SPD
24. Sruti Datta, Formation of organic-coated metal nanoparticles in a single-step method and possible mechanism. (Prof Satyajit Hazra)- SPD
25. Sudip Mukherjee, Classical and quantum annealing to optimization problems. (Prof BK Chakraborti & Prof Somnath Tewari) TCMP
26. Sukanta Barman, Magnetodielectric effect in multiferroic zircon type dycro4. (Prof. Probbhat Mandal) ECMP
27. Sultana Tajmili Hasnahena, The dielectric properties of some biopolymers with nanocomposites. (Prof Madhusudan Roy) AMS
28. Suvankar Roy Chowdhury, Proton identification with the compact muon solenoid (Prof Sunanda Banerjee, Prof Satyaki Bhattacharyay & Prof Subir Sarkar) HENPP
29. Tapash Ghosh, Synthesis of gold nanorod and characterization using analytical transmission electron microscopy. (Prof Biswarup Satpati) SPD
30. Tirthankar Banerjee, Kinetic phenomena in many body models of transport and markets. (Prof Abhik Basu & Bikash Chakraborty) - TCMP

The following 30 (Thirty) students have successfully completed the course.

1. Achyut Maity, 2. Amrita Ghosh, 3. Anshu Chatterjee, 4. Aritra bandyopadhyay, 5. Arpan Maiti, 6. Ashim Roy, 7. Barnamala Saha. 8. Binita Mandal, 9. Chiranjib Mandal, 10. Chitralkha Datta. 11. Debajyoti Saha, 12. Gouranga Manna, 13. Kumar Das, 14. Kuntal Mondal, 15. Kuntal Nayek, 16. Mily Kundu, 17. Naosad Alam, 18. Pankaj Kumar Shaw, 19. Sabuj Ghosh, 20. Sanjib Banik, 21. Sanjukta Paul, 22. Satyajit Chowdhury, 23. Sayanee Jana, 24. Sruti Datta, 25. Sudip Mukherjee, 26. Sukanta Barman, 27. Sultana Tajmili Hasnahena, 28. Suvankar Roy Chowdhury, 29. Tapash Ghosh, 30. Tirthankar Banerjee

Following three physics students have received best students awards for the session 2012-13 1. Mr Sudeep Mukherjee, 2. Ms Amrita Ghosh & 3. Mr Kuntal Nayek

Mr. Sudeep Mukherjee have been awarded the AP Patra Memorial Prize

61th Post-M Sc Course, Session 2013-14

The following (Physics) students have joined on 1st August 2013 for the session 2013-14 1. Amit Kumar Chatterjee, 2. Arnab Purohit, 3. Arnab Singh, 4. Arnab Kumar Pariari, 5. Biswajit Banerjee, 6. Biswarup Das, 7. Mithun Karmakar, 8. Mugdha Sarkar, 9. Rajarshi Bhattacharya, 10. Rohit Mishra, 11. Rome Samanta, 12. Santanu Adhikary, 13. Saswati Nandan, 14. Shamik Ghosh, 15. Sourav Karar, 16. Sourav Kumar Dey, 17. Souvik Mondal, 18. subhrajyoti Adhya, 19. Susmita Roy, 20. Srimanta Banerjee, 21. Dibya Chakravorty, 22. Roopam Sinha, 23. Nilmadhab Hati, 24. Ranajoy Banerji, 25. Sukannya Bhattacharya

First Term : (August to November)

Courses Teachers

Quantum Mechanics Prof Asit De (Theory)

Statistical Mechanics - Prof Pradeep Kr Mohanti (CMP)

Mathematical Methods- Prof Palash Baran Pal (Theory)

Computational & Numerical Methods- Prof. Subir Sarkar (HENPP), Prof. Supratik Mukherjee (ANP), Prof. Nayana Majumdar(ANP), Prof. Satyaki Bhattacharya(HENPP)

Second Term: (December to March)

1. Physics of nano-materials (Alokmay Datta) 2. Statistical Mechanics & its Applications (Bikas Kanti Chakrabarti) 3. Quantum field theory -1 4. Advanced topics in theoretical Physics (Kumar Sankar Gupta) 5. Nuclear structure, experimental and theoretical approaches I (Maitreyee Saha Sarkar) 6. Advanced theoretical course in Plasma Physics (Nikhil Chakrabarti) 7. Particle physics (Prakash Mathews) 8. Production and propagation of High Energy particles and Radiation (Pratik Majumdar)

BIOPHYSICAL SCIENCES

Session 2012-13

Third Term

REVIEW: Students, Review Title (Supervisor)

1. Debashis Mukherjee, Structural Databases and their use in Bioinformatics Applications. (Dhananjay Bhattacharyya)
2. Zenia Kaul, Programmed cell death (PCD) in late-onset neurodegeneration : Interplay between Type I (apoptosis), Type II (autophagic cell death) and Type III (programmed necrosis). (Oishee Chakrabarti)
3. Piyali Majumder, Is Alzheimer's Disease synonymous to Type III Diabetes ? (Debashis Mukhopadhyay)
4. Archisman Ghosh, Mode of recognition of hemoglobin molecules by the hemoglobin degrading proteases : Systematic studies with special emphasis on cysteine proteases. (Sampa Biswas)
5. Sabyasachi Sen, Transcription Factor 19 (TCF19) binding to chromatin: a biophysical and cell biological approach. (Chandrima Das)
6. Isha Sengupta, Chromatin dynamics of Sp110, a nuclear body protein. (Chandrima Das)
7. Tapas Pal, Single molecule FRET: A tool for exploring the dynamic mechanism of biomolecules. (Padmaja Mishra)
8. Saurav Ghoshal, Conventional Infrared Spectroscopic Methods and Limitations towards the Detections of Small Molecules and their Clusters. (Montu Hazra)
9. Malti Yadav, Role of DNA methylation in Epigenetic Inheritance. (Udayaditya Sen)
10. Kamalendu Pal, Structural aspects of Securin in DNA repair and regulation of the p53 pathway. (Udayaditya Sen)

The following 10 (Ten) students have successfully completed the Post-M.Sc. Biophysical Sciences course in the 2012-2013 session.

1. Archisman Ghosh, 2. Debasish Mukherjee, 3. Isha Sengupta, 4. Kamalendu Pal, 5. Malti Yadav, 6. Piyali Majumder, 7. Sabyasachi Sen, 8. Sourav Ghoshal, 9. Tapas Paul, 10. Zenia Kaul

Following student have been awarded for session 2012-13 in the Biophysical sciences course.

1. Ms Isha Sengupta

The following (Biophysical sciences) students have joined on 1st August 2013 for the session 2013-14

1. Abhishek Sau, 2. Aradhita Bhattacharjee, 3. Benazir Alam, 4. Debdatto Mookherjee, 5. Maireyee Bhattacharya, 6. Monalisa Kundu. 7. Sayantan Ganguly. 8. Shramana Chatterjee, 9. Sudeshna Das Chakraborty

Basic Courses : (Compulsory)

1. Macromolecular structure, Biochemistry & Chemical Biology (40 lectures by Munna Sarkar, Rahul Banerjee and Dhananjay Bhattacharya, Dipak Dasgupta and Abhijit Chakrabarti) : Biomembrane: Structure & dynamics, biomembrane transport. External and internal coordinate system, non-covalent interactions stabilizing biomolecules, Proteins, amino acids, peptide, secondary tertiary, quaternary structure of protein. Nucleic acids, Watson-Crick and non-Watson Crick basepair, DNA double helical and multistranded structures, RNA structural features. Basic Biochemistry Biomolecules in water, protein and carbohydrate (complex) solutions, pH, pK, shifts in pK, self assembly, protein structure & folding, conformation, binding and enzymes, purification & characterization of proteins, vitamins & co-enzymes, glycolysis, ATP cycle, TCA cycle, oxidative phosphorylation, biosynthesis / degradation of amino acids & proteins, biosynthesis of lipids and carbohydrates, hormone and growth factors. What is Chemical Biology?, Definition of life from a current perspective, Role of water in the chemistry of life, Biomolecular Recognition and its basics - an integral componet of chemical biology, Chemical equilibrium and kinetic (including enzyme kinetics) aspects, and its basic application in chemical biology, Chemical biology and its current trends.

2. Molecular & Cell Biology (40 lectures by Partha Saha and Kaushik Sengupta, Oishee Chakrabarti & Subrata Banerjee):

Biological Processes: Replication, Transcription, Translation, and related topics. Technique in molecular biology: DNA detection, RNA detection, Protein detection, cloning, PCR, and related methods. Cell as unit, identification, characterisation, function of cellular organelles, Golgi, ER, lysozome, mitochondria, cell-membrane, cell-cell communication, cell-signalling, basic of immune system.

3. Spectroscopy & X-ray crystallography (25 lectures by Samita Basu, Padmaja P Mishra, Montu Hazra & Dulal Senapati and 15 lectures by Udayaditya Sen and Sampa Biswas):

Spectroscopy: absorption, emission, excited state properties, acidity, basicity, polarization, anisotropy, solvent relaxation, quenching, energy transfer, electron transfer, Circular dichroism, Infrared spectroscopy, FTIR, Raman spectroscopy, Nanoscience. Basics of Crystallography : Crystals, lattice, symmetry, Braggs law, Reciprocal lattice, Ewald sphere; Structure factors: Atomic scattering factor, temperature factor, structure factor calculation; Data collection: Technique & strategy, data processing, extinctions & space group determination; Phase problem and electron density calculation: phasing techniques like MR, MIR, MAD, etc; Fiber Diffraction & Virus Crystallography and Model building & refinement.

4. Computer Programming & Bioinformatics (40 lectures by Pulak Kumar Ray and Gautam Garai)

Algorithm and flow-chart, FORTRAN programming, molecular modelling software, basic statistics, regression and curve-fitting. Brief introduction to Bioinformatics, Brief introduction to Biological databases, Sequence Alignment (Pairwise and Multiple), Database similarity searching by available tools like FASTA, BLAST etc., Some probability and statistical methods (such as Measures of central tendency, probability, probability distributions, Binomial distribution, Normal distribution, Poisson distribution, calculation of errors etc.

5. RadioChemistry & Radiation Physics (12 lectures by Susanto Lahiri & 8 lectures by Maitreyee Nandi)

Recapitulation about radioactivity- classification of the nuclides, natural decay chain; Radioactive decay modes- secular and transient equilibrium; Introduction to Nuclear Reactions- Q-values, threshold energy, cross section, excitation functions; Different types of detectors, Nuclear Activation and its applications; Clinical and other applications of radionuclide, radiotracer technique. Interaction of electromagnetic radiation with matter Cross-sections Attenuation and mass energy absorption coefficients Interaction of charged particles with matter Classical Theory of inelastic collisions with atomic electrons Bremsstrahlung Passage of heavy charged particles through matter Range energy relation Stopping power Bethe-Bloch formula — Interaction of neutrons with matter Capture Neutron, charged particle and photon induced nuclear reactions and their applications. Radiation quantities and units Particle & Energy flux and fluence flux and fluence Interaction of Radiation with Cells, LET Biological Effects of Radiation, Dosimetry Energy imparted Absorbed dose Kerma-Exposure Dose equivalent Charged particle equilibrium (CPE) Ambient and directional dose equivalents [$H^*(d)$ and $H(d)$] Radiation Protection Standards, Principles of Monitoring and Protection.

6. Molecular Genetics (20 lectures by Nitai P Bhattacharyya, Debashis Mukhopadhyay and Chandrima Das):

Fundamentals of Human Genetics : Molecular basis of heritable diseases; various markers used for diseased gene identification for monogenic diseases; complex traits. Chromatin and Epigenetics (CD): Chromosome, Chromatin, Nucleosomes, Histones, Histone Variants, Histone Chaperones, Chromatin remodelers, Euchromatin vs. Heterochromatin, DNA Methylation, Histone modification, Modifying enzymes (HATs, HDACs, HMTase, Demethylase), Chip, Chip-Seq, Chromatin readers and Histone code, Epigenetics and Cancer. Development of Molecular Genetics (DM): The legacy of classical genetics; the birth of microbial genetics; DNA as the genetic material; mutation; genetic fine structure.

Advance course

Each student has to select four (4) courses out of this list. No course would be offered for a single student. Time slot to each course would be given independently, so that any student can chose any combination of courses. When a student does not have any class, he/she has to go to his/her respective lab where he/she has been allotted to do lab-rotation.

Topics in Cell Biology : (Kaushik Sengupta & Oishee Chakrabarti)

Cytoskeletal components-cellular dynamics-cargo transport in cell-cell adhesion & migration-experimental set ups for cytoskeletal structure-function analysis- Nucleoskeletal components-

structure & function of lamins- laminopathies- LINC (Linker of Nucleoskeleton & Cytoskeleton) complexes. Protein translocation, protein trafficking (endocytosis, exocytosis, transcytosis), de novo organeller biogenesis, protein quality control (role of internal vesicles), lysosomal biogenesis and degradation.

Cell Signaling, Cell Cycle & Stem Cell Biology (Partha Saha & Subrata Banerjee)

Receptors-different forms and their mode of action-G-protein coupled receptors, tyrosine kinase receptors etc., Second messengers-cAMP, inositol phosphates, calcium ions etc., Protein-protein interaction in message transmission, Hormonal and growth factor signaling protein kinases, transcription factors, gene expression, Survival and death signaling apoptotic pathways and anti-apoptotic (survival) pathways. Apoptosis, necrosis and autophagy.

Phases of cell cycle, Regulation of cell cycle by cyclin-Cdk, Regulation of Initiation of eukaryotic DNA replication, Replication Licensing, Cell cycle checkpoints, Protein degradation by ubiquitination. Stem Cells: Pluripotency; Adult & Embryonic stem cells Hematopoietic stem cells, neuronal stem cells, mesenchymal stem cells; Reprogramming/Induced Pluripotency; Stem Cell niche and Mechanism of Self Renewal; Cancer Stem Cells; Regenerative medicine; Ethics in Stem Cell Research.

Chemical Biology of Chromatin & Epigenetics (Dipak Dasgupta & Chandrima Das)

Nucleus of prokaryotes and eukaryotes, Chromatin structure, composition and assembly from macromolecular perspective, Methods to study chromatin structure, Chromatin dynamics and remodeling with the role in control of gene expression, chromatin as drug target. Eukaryotic genome packing and higher order chromatin structure, Epigenetics and gene regulation, Nucleography, Detection of histone modifications, Protein-Protein interaction through reader domains, Chromatin dynamics and diseases.

Neurobiology (Debashis Mukhopadhyay and Nitaipada Bhattacharya)

Paring Back, Critical Periods, SENSATION AND PERCEPTION: Vision, Hearing, Taste and Smell, Touch and Pain, LEARNING AND MEMORY, MOVEMENT, SLEEP: The Stuff of Sleep, Sleep Disorders, How is Sleep Regulated? STRESS: The Immediate Response, Chronic Stress, AGING: Aging Neurons, Intellectual Capacity, CHALLENGES & ADVANCES: Pain, Epilepsy, Major Depression, Manic-Depressive Illness, Addiction, Learning Disorders, Stroke, Neurological Trauma, Anxiety Disorders, Neurological AIDS, Spinal Cord Injury.

Protein Folding (Soumen Basak)

Non-covalent forces in proteins; The Protein Folding problem; Concept of folding funnel and folding pathways; Folding schemes; Intermediate states; 2-state and 3-state folding; Molten globules; Mechanism of action of denaturants; Kinetic studies and Chevron Plots; Misfolding and aggregation; Intrinsically Disordered proteins.

Membrane Biophysics (Abhijit Chakrabarti)

Aminophospholipids, membrane proteins & cell surface glycoconjugates (2 lectures). Membrane Dynamics : Edidin & Frye experiment, heterocaryons, membrane diffusions, membrane domains, membrane asymmetry and lipid polymorphism (4 lectures) Membrane skeleton, Endocytosis, Protein translocation (4 lectures)

Macromolecular Crystallography (Udayaditya Sen and Sampa Biswas)

Structure factors: Atomic scattering factors, temperature factors, structure factor calculation (4

lectures). Phase problem and electron density calculation, phasing by MR and MIR, advanced phasing techniques, such as MAD/SAD, model building and refinement (4 lectures). Fiber diffraction (2 lectures). High throughput crystallography, cryo-crystallography and its application in trapping reaction intermediates; X-ray crystallography to elucidate structure-function relationship for some important biological pathways; crystallography of large macromolecular assembly.

Biomolecular simulation (Dhananjay Bhattacharyya & Pulak Ray)

Macromolecular modeling, Force-field, energy minimization, Monte-Carlo simulation, Genetic Algorithm, Molecular Dynamics simulation. Numerical Analysis : Solution of equation: Successive Bisection, Newton-Raphson Method, Numerical Integration: Trapezoid rule, Simpsons rule, Gauss 3-point rule, Differential Equation: Runge-Kutta method, Solution of Simultaneous equations, Curve fitting. Matrices, Some Statistical Calculations.

Drug discovery: a modern day approach (Munna Sarkar)

Pre 20th century drug discovery. Drug discovery pipeline, drug targets and target validation. Methods of lead identification and optimization. Early prediction of ADMET (Absorption, Distribution, Metabolism Excretion and Toxicity) . QSAR (Quantitative Structure Activity Relationship) predictions. Lipinski rule of 5. Polar surface area. Blood brain barrier crossing model. Predicting toxicity. Introduction to drug docking.

Advanced Imaging Techniques (Padmaja Mishra & Pulak Ray)

The purpose of this course is to investigate the variety of image transforms that are possible using the light microscope. Students shall be introduced with the technical details and applications of the advanced imaging techniques s.a. Multiphoton microscopy, Structured Illumination Microscopy (SIM), super resolution microscopy, Spinning Disk Microscopy , fluorescence correlation and cross-correlation spectroscopy, etc in biophysical research. Details of the Optical System, Detector requirements, data acquisition and analysis techniques will also be discussed. Transmission & Scanning Electron Microscopy, Atomic Force and Scanning Tunneling Microscopy.

Modern Spectroscopic Methods and Applications : (Samita Basu and Montu K Hazra)

Nanosecond to Femtosecond Laser Spectroscopic Techniques and their application to the various prototype and diverse bio-molecules of different sizes related to Biophysical Sciences. The spectroscopic methods we will cover are the following: (i) Time Resolved Fluorescence and Absorption (ii) Circular Dichroism (iii) Fourier Transform Infrared Spectroscopy (iv) Laser Induced Fluorescence Excitation and Dispersed Fluorescence Spectroscopy in Supersonic Jet (v) Resonant Enhanced Multi-Photon Ionization Spectroscopy (vi) Fluorescence and Time of Flight Mass Spectroscopic Detections (vii) Laser Photoacoustic Spectroscopy (viii) Cavity Ring-down Spectroscopy (ix) Raman Spectroscopy (x) Multiple Colors IR-UV double, IR-UV-UV triple and UV-UV double resonance spectroscopy (xi) One Color UV Photo-Dissociation and Multiple Colors Vibrational Mediated Photo-Dissociation Spectroscopy (xii) X-Ray Photoelectron Spectroscopy.

Polymer Chemistry (Amithabha De)

Conducting Polymers, Composites and Nanocomposites: Preparation, Characterization and Applications: i) Introduction (1 lecture) ii) Synthesis Techniques: Chemical and Electrochemical Polymerization (1 lectures) iii) Composites, Blends and Nanocomposites: Different types (2 lectures) iv) Characterization techniques of Polymers and Composites (1 lecture) v) Mechanism of Charge transport (2 lectures) vi) Potential application areas of conducting polymers (1 lecture) vii) Conducting polymers in Biosensors and Electrochemical Capacitors (2 lectures)

Advance Trace Analysis and Elements of Green Chemistry (Sushanta Lahiri)

Trace Analysis using nuclear techniques like neutron and charged particle activation analysis (ii) Accelerator Mass Spectrometry, etc (iii) Inductively coupled plasma optical emission spectrometry (iv) Inductively coupled plasma mass spectrometry (v) XRF, (v) Twelve principles of green chemistry (vi) Aqueous biphasic system.

7.2 Library

The Library of SINP is one of the major information resource centres within Eastern India in the field of Physical and Biophysical Sciences. It is our privilege to support the institutes march towards its vision- to be the pioneer research Institute of India. Through our well equipped and digitised library, the members of our institution and the other members associated with our research and development program are being benefited and this will assist towards scientific development of our Institute and the country at large.

The Library not only acquires, organizes and disseminates knowledge; it has put its foot ahead towards policies and procedures, systems and services. The details of our library are given below.

Collection: The library of SINP is one of the leading science-library within Eastern Region. In addition to huge collection of books and e-books on science and technology it also subscribe more than 264 leading journals in the field of physical, chemical and biophysical sciences. Library has a huge collection of books, e-books and non-book materials. The details are given below:

Books: 35772 (technical - 31699 + non-technical- 4073 [219 books are added in this year])

E- books: 1432 + (432 e-books of Oxford, CUP and World Scientific added in this year)

Bound volumes of journals: 51973

Current subscribed journals: 264 (Foreign 207 + Indian 57)

Online journals: 3000+

Reports: 26000+

Number of CD/DVD Rom: 1091

Thesis: 228

Major items/equipments available:

Library has two IBM servers where Libsys 4 (Rel 6.2 upgraded version) database is running.

30 Pcs are in the library out of 20 are for library user

One Hp Design jet plotter printer & one Canon plotter printer for poster printing

One Hp colour printer

Two Hp black & white printers

Four Xerox machines cum printers (black & white)

Three colour Xerox cum network printer (Sharp & Canon)

Three lamination machines

Two scanner & one spiral binding machine

Membership:

In addition to our 778 institute members (faculties, research fellows and non academic), library has the privilege to serve near about six hundred (572) external users coming from different scientific and educational institutes of Eastern India. The list of external users includes Calcutta University,

Jadavpur University, Viswa Bharati, IACS, IICB, ISI, Bengal Engineering and Science University, WBUT, CMERI, Guwahati University, North East Hilly University, Patna University etc. apart from numerous Under-Graduate/Post-Graduate colleges and project students.

Number of members & types of facilities are available for each category of members:

(A) SINP members (Total No. 778 academic 529, Non-academic 249)

- (1) Borrowing facility
- (2) Xerox facility
- (3) Inter-library-loan
- (4) Poster printing facility
- (5) Online searching & downloading

(B) VECC members (No. 107)

- (1) Borrowing facility
- (2) Online searching & downloading

(C) External members (No. 572)

- (1) Reading room facility for reference use
- (2) Xerox facility against payment
- (3) Online searching & downloading

(D) Institutional Members (No. 7)

- (1) Reading room facility for reference use
- (2) Borrowing facility
- (3) Online searching & downloading
- (4) Poster printing facility

Online facilities implemented through XI plan project:

Successfully our library has implemented the online and archival facilities of various journals of the following publishers from XI (LDER) and XII (LDRM) plan project grant. More than 3000 online journals as well as online archives (full-text pdf) available from our library website:

1. Institute of Physics, London
2. American Institute of Physics
3. American Physical Society
4. American Chemical Society
5. John Wiley online library
6. World Scientific
7. Springer
8. Taylor & Francis
9. Science Classic
10. Nature Publishing Group
11. Cambridge University Press
12. Royal Society of Chemistry
13. Royal Society of London
14. Oxford
15. IEEE

Library has the online e-books collection of Annual Reviews, Lecture Notes in Physics (volume 1 - 475) and 1000 e-books of T&F, CUP, Wiley, World Scientific and Oxford. Currently the library

is subscribing Web of Knowledge & Science Citation Index from 1945 to current, JSTOR (Mathematics & Statistics), Scopus from Elsevier and Springer protocols database.

With such enriched e-journal archives as well as e-books and e-serials. All the library users, both internal and external from Eastern India, can easily access their required information quickly for speed- up their research work and successfully reach their goal. This will also minimize the time of their achievement target. The impact of the mentioned implementation in the library is reflected in the below table which reveal the drastic increase in number of scientific paper with average Impact Factor published by our scientists and research scholars.

Publication of research papers (SINP) with average Impact Factor:

Year	Research papers actually published			Average Impact Factor		
Calendar year	Indian Journals	In Foreign Journals	In SCI Journals	For Publication in Indian Journals	For publication in foreign journals	For publication in SCI journals
2007	8	210	218	0.490	2.581	2.503
2008	11	261	269	0.267	2.844	2.679
2009	17	249	264	0.430	2.320	2.195
2010	13	209	220	0.397	2.553	2.426
2011	11	268	279	0.545	3.425	3.316
2012	14	370	384	0.782	3.878	3.743
2013	6	390	396	0.541	3.870	3.819

Chapter 8
Administration

Chapter 8

Administration

8.1 Governing Council

Chairman:

Dr. R. K. Sinha
Chairman, Atomic Energy Commission &
Secretary to the Government of India
Department of Atomic Energy
Anushakti Bhawan, C. S. M. Marg
Mumbai-400 001

Members:

Shri P. R. Baviskar, IAS
Joint Secretary(R&D)
Government of India
Department of Atomic Energy
Anushakti Bhawan, C. S. M. Marg
Mumbai-400 001

Smt. Meenaxi Rawat
Director (Finance)
Government of India
Department of Atomic Energy
Anushakti Bhawan, C. S. M. Marg
Mumbai-400 001

Prof. Dhiraj Bora
Director, Institute for Plasma Research
Near Indira Bridge, Bhat
Gandhinagar 382 242

Prof. Mustansir Barma
Director, Tata Institute of Fundamental Research
Homi Bhabha Road
Colaba, Mumbai-400 005

Prof. Amitava Raychaudhuri
Palit Professor of Physics
University of Calcutta
92, Acharya Prafulla Chandra Road
Kolkata-700 009

Shri Sukumar Ganai, IAS
Additional Secretary
Higher Education Department
Government of West Bengal
Bikash Bhaban, 5th floor
Salt Lake, Kolkata-700 091

Prof. Dhrubajyoti Chattopadhyay
Pro Vice-Chancellor (Academic)
University of Calcutta
Senate House
87/1, College Street
Kolkata-700 073

Prof. N. R. Das
Dean, FC for PG Studies in Technology
Department of Radiophysics & Electronics
University of Calcutta
92, Acharya Prafulla Chandra Road
Kolkata-700 009

Prof. Bikas K Chakrabarti
Director
Saha Institute of Nuclear Physics
Sector-1, Block-AF, Bidhannagar
Kolkata-700 064

8.2 Members of the Institute [As on March 31, 2014]

Prof Bikas Kanta Chakrabarti: Director

DIRECTOR'S OFFICE

- 1 Sri Jeevan Shaw: AAO(DO)
- 2 Sri Subhasish Ghoshal: Superintendent
- 3 Sri Goutam Mandal: Superintendent
- 4 Sri Manoj Biswas: Lower Division Clerk
- 5 Sri Ramesh Hari: Helper 'D'

REGISTRAR'S OFFICE

- Prof Nitai Pada Bhattacharyya: Prof-in-Charge
- 1 Sri Alok Mitra: AO(RO)
 - 2 Sri Bimlesh Kr Tripathi: Senior Hindi Translator
 - 3 Shri Bibekbijay Bandyopadhyay: Superintendent
 - 4 Shri Aditya Dhara: Lower Division Clerk
 - 5 Sri Rudal Prasad Ram: Technician 'D'
 - 6 Sri Mahadev Das: Caretaker

Academic Departments and Divisions

ASTROPARTICLE PHYSICS & COSMOLOGY (APC)

- 1 Prof Pijushpani Bhattacharjee: Sr Professor 'H+' & HOD
- 2 Prof Debades Bandyopadhyay: Sr Professor 'H'
- 3 Prof Debasish Majumdar: Professor 'G'
- 4 Prof Ambar Ghosal: Professor 'G'
- 5 Dr Mala Das: Associate Professor 'E'
- 6 Dr Pratik Majumder: Associate Professor 'E'
- 7 Shri Nilanjan Biswas: Scientific Assistant 'B'
- 8 Sri Bijay Kr Das: Superintendent

THEORY DIVISION

- 1 Prof Anjan Kundu: Sr Professor 'H+'
- 2 Prof Parthasarathi Mitra: Sr Professor 'H+'
- 3 Prof Avaroth Harindranath: Sr Professor 'H+'
- 4 Prof Palash B. Pal: Sr Professor 'H+'
- 5 Prof Asit Kr De: Sr Professor 'H' & HOD
- 6 Prof Kumar Sankar Gupta: Sr Professor 'H'
- 7 Prof Sibaji Roy: Sr Professor 'H'
- 8 Prof Gautam Bhattacharyya: Sr Professor 'H'
- 9 Prof Munshi Golem Mustafa: Sr Professor 'H'
- 10 Prof Bireswar Basu Mallick: Professor 'G'
- 11 Prof Prakash Mathews: Professor 'G'
- 12 Prof Harvendra Singh: Professor 'G'
- 13 Prof Bijay Kr. Agrawal: Professor 'G'
- 14 Prof Amit Ghosh: Professor 'G'
- 15 Prof Koushik Dutta: Associate Professor 'E'
- 16 Prof Arnab Kundu: Associate Professor 'E'
- 17 Smt Sangita Pande: Scientific Assistant 'B'
- 18 Sri Prodyut Kr Mitra: Technician 'E'
- 19 Sri Sudarshan Hazra: Technician 'B'
- 20 Sm Dola Mallick: AAO
- 21 Sri Arun Kr Bose: Caretaker

PLASMA PHYSICS DIVISION

- 1 Prof ANS Iyengar: "Sr Professor 'H'
- 2 Prof Mylavarapu Sita Janaki: Professor 'G' & HOD
- 3 Prof Nikhil Chakraborty: Professor 'G'
- 4 Sri Shantanu Chowdhury: Engineer 'F'
- 5 Sri Parthasarathi Bhattacharya: Scientific Officer 'D'
- 6 Sri Subhasis Basu: Scientific Officer 'D'
- 7 Sri Monobir Chattopadhyay: Scientific Officer 'C'
- 8 Sri Amalendu Bal: Scientific Assistant-F
- 9 Sri Abhijit Betal: Scientific Assistant-D

- 10 Sri Dulal Chatterjee: Superintendent
- 11 Sri Sib Sankar Sil: Technician 'E'
- 12 Sri Dipankar Das: Technician 'D'
- 13 Sri Ashok Kr Ram: Helper 'C'

SURFACE PHYSICS AND MATERIAL SCIENCE DIVISION

- 1 Prof Milan K Sanyal: Sr Professor 'J'
- 2 Prof Alokmay Datta: Sr Professor 'H' & HOD
- 3 Prof Purushottam Chakraborty: Sr Professor 'H+'
- 4 Prof Debabrata Ghosh: Sr Professor 'H+'
- 5 Prof SR Bhattacharyya: Professor 'G'
- 6 Prof Tapas Kr Chini: Professor 'G'
- 7 Prof Sangam Banerjee: Professor 'G'
- 8 Prof Manabendra Mukherjee: Professor 'G'
- 9 Prof Satyajit Hazra: Professor 'G'
- 10 Prof Srinanda Kundu: Professor 'F'
- 11 Prof Satyaban Bhunia: Professor 'F'
- 12 Prof Krishnakumar SR Menon: Professor 'F'
- 13 Dr Madhusudan Roy: Associate Professor 'F'
- 14 Dr Supratic Chakraborty: Associate Professor 'E'
- 15 Dr Mrinmay Kr Mukhopadhyay: Associate Professor 'E'
- 16 Dr Biswarup Satpati: Scientist 'E'
- 17 Sri Avijit Das: Scientific Officer 'D'
- 18 Sri Subir Roy: Scientific Officer 'D'
- 19 Sri Susanta Bandyopadhyay: Scientific Officer 'C'
- 20 Sri Souvik Banerjee: Scientific Assistant-C
- 21 Sri Goutam Sarkar: Scientific Assistant-C
- 22 Shri Debraj Dey: Scientific Assistant 'B'
- 23 Sri Ramkrishna Deb Das: Scientific Assistant 'B'
- 24 Sri Mukul Ch Das: AAO
- 25 Sri Subhasish Sanyal: Superintendent
- 26 Sri Shyama Prasad Mallick: Technician 'F'
- 27 Sri Harendra Nath Jana: Caretaker
- 28 Sri Provash Halder: Helper 'E'
- 29 Sri Gobardhan Jana: Helper 'C'

APPLIED ELECTRONICS SECTION (AES)

- 1 Sri Abhijit Sanyal: Engineer 'G', HOD
- 2 Sri Debasish Bandyopadhyay: Scientific Assistant-E
- 3 Sri Dwijendra Das: Scientific Assistant-C
- 4 Sri Singh Bahadur Thapa: Helper 'C'

NUCLEAR PHYSICS DIVISION

- 1 Prof Padmanava Basu: Professor 'G' & HOD
- 2 Prof Maitreyee Saha Sarkar: Professor 'G'
- 3 Prof Subinit Roy: Professor 'G'
- 4 Prof Ashimananda Goswami: Professor 'G'
- 5 Prof Ushasi Datta Pramanik: Professor 'G'
- 6 Prof Chinmay Basu: Professor 'F'
- 7 Prof (Smt) Anjali Mukherjee: Professor 'F'
- 8 Sri Sujib Ch Chattopadhyay: Scientific Officer 'C'
- 9 Sri Kaushik Chatterjee: Scientific Officer 'C'
- 10 Smt Jonaki Panja: Scientific Officer 'C'
- 11 Sri Ajoy Kr Mitra: Scientific Officer 'C'
- 12 Smt Rita Ghosh: Scientific Assistant-E
- 13 Sri Dilip Sil: Scientific Assistant-D
- 14 Smt Tultul Dutta: Superintendent
- 15 Sri Pradip Barua: Technician 'D'
- 16 Sri Sankar Prasad Singh: Technician 'C'
- 17 Sri Siladitya Chakraborty: Helper 'C'

HIGH ENERGY NUCLEAR AND PARTICLE PHYSICS DIVISION

- 1 Prof Sunanda Banerjee: Professor
- 2 Prof Sukalyan Chattopadhyay: Sr Professor 'H'
- 3 Prof Pradip Kr Roy: Professor 'G'
- 4 Prof Manoj K Sharan: Professor 'F'
- 5 Dr (Smt) Tinku Sinha: Scientist 'F'
- 6 Dr Satyaki Bhattacharya: Associate Professor 'F'
- 7 Dr Subir Sarkar: Associate Professor 'F'
- 8 Dr Suchandra Dutta: Associate Professor 'F'
- 9 Dr Debasish Das: Associate Professor 'E'
- 10 Sri Dipankar Das: Scientific Assistant-D
- 11 Smt Lipy Das Bose: Scientific Assistant-D
- 12 Sri Sanjib Kr Mondal: Superintendent
- 13 Sri Rakesh Kr Ram: Helper 'C'
- 14 Sri Sudam Bagdi: Helper 'C'

APPLIED NUCLEAR PHYSICS DIVISION

- 1 Prof Satyajit Saha: Sr Professor 'H' & HOD
- 2 Prof (Smt) Bichitra Ganguly: Professor 'G'
- 3 Prof PMG Nambissan: Professor 'G'
- 4 Prof Supratik Mukhopadhyay: Professor 'G'
- 5 Prof Chandi Charan Dey: Professor 'F'
- 6 Prof (Sm) Nayana Majumdar: Professor 'F'
- 7 Prof Sandip Sarkar: Professor 'F'
- 8 Dr Sankar De: Associate Professor 'E'
- 9 Sri Pradipta Kumar Das: Scientific Officer 'D'
- 10 Sri Saibal Saha: Scientific Officer 'D'
- 11 Sri Haradhan Dhar: Scientific Assistant-E
- 12 Sri Chandra Nath Marik: Scientific Assistant-D
- 13 Smt Soma Roy: Scientific Assistant-D
- 14 Sri Dilip Kr Sardar: Technician 'C'
- 15 Sri Kuntal Sarkhel: Helper 'C'
- 16 Sri Prabir Das: Helper 'C'

CONDENSED MATTER PHYSICS DIVISION

- 1 Prof Bikas Kanta Chakrabarti: Sr Professor 'I'
- 2 Prof R Ranganathan: Sr Professor 'H+' & HOD
- 3 Prof Atindra Nath Das: Sr Professor 'H'
- 4 Prof Sudhakar Yarlagadda: Professor 'G'
- 5 Prof Chandidas Mukherjee: Professor 'G'
- 6 Prof Indranil Das: Professor 'G'
- 7 Prof Prabhat Kr Mandal: Professor 'G'
- 8 Prof Chandan Mazumdar: Professor 'G'
- 9 Prof Pradeep Kr Mohanty: Professor 'G'

- 10 Prof Barnana Pal: Professor 'F'
- 11 Prof Asok Podder: Professor 'F'
- 12 Prof Bilwadal Bandyopadhyay: Professor 'G'
- 1 Prof Abhik Basu: Professor 'F'
- 3 Prof Arti Garg: Associate Professor 'E'
- 14 Prof Biswajit Karmakar: Associate Professor 'E'
- 15 Sri Tapan Kr Pyne: Scientific Officer 'D'
- 16 Smt Sankari Chakrabarti: Scientific Assistant-D
- 17 Sri Arindam Chakraborti: Scientific Assistant-C
- 18 Sri Dhrubajyoti Seth: Scientific Assistant-D
- 19 Smt Papia Mondal: Scientific Assistant-C
- 20 Sri Kausik Das: Scientific Assistant-D
- 21 Sri Tapan Kr Sarkar: Superintendent
- 22 Smt Suparna Das: Superintendent
- 23 Sri Arun Kumar Pal: Technician 'H'
- 24 Sri Anish Karmahapatra: Technician 'G'
- 25 Sri Sambu Hembrom: Technician 'D'
- 26 Sri Prabir Das: Technician 'B'
- 27 Sri Patit Paban Ranjit: Helper 'E'
- 28 Sri Jhantu Mallick: Helper 'C'
- 29 Shri Rajeshwar Dubey: Helper 'A'

CRYSTALLOGRAPHY & MOLECULAR BIOLOGY DIVISION

- 1 Prof Nitai Pada Bhattacharyya: Sr. Professor 'H+' & HOD
- 2 Prof Abhijit Chakrabarti: Sr. Professor 'H' & HOD
- 3 Prof Rahul Banerjee: Professor 'G'
- 4 Prof Udayaditya Sen: Professor 'G'
- 5 Prof Sampa Biswas: Professor 'F'
- 6 Prof Partha Saha: Professor 'F'
- 7 Sri Utpal Basu: Scientific Officer 'C'
- 8 Sri Abhijit Bhattacharya: Scientific Assistant-E
- 9 Sri Bikram Nath: Scientific Assistant-C
- 10 Sri Sushanta Debnath: Scientific Assistant-C
- 11 Sri Saikat Mukhopadhyay: Scientific Assistant-D
- 12 Sri Ashis Kumar Dutta: Scientific Assistant-D
- 13 Smt Durga Hazra: Superintendent
- 14 Sri Samir Kr Majumdar: Technician 'D'
- 15 Sri Chinmoy Chatterjee: Helper 'E'
- 16 Sri Sakal Dev Ram: Helper 'C'
- 17 Sri Bipin Bose: Helper 'C'

BIOPHYSICS AND STRUCTURAL GENOMICS DIVISION

- 1 Prof Subrata Banerjee: Professor 'G' & HOD
- 2 Prof Dipak Dasgupta: Sr Professor 'H+' & HOD
- 3 Prof Debashis Mukhopadhyay: Associate Professor 'F'
- 4 Dr (Smt.) Oishee Chakrabarti: Associate Professor 'E'
- 5 Dr Kaushik Sengupta: Associate Professor 'E'
- 6 Dr Chandrima Das: Associate Professor 'E'
- 7 Sri Shekhar Bhattacharya: Scientific Officer 'C'
- 8 Sri Arijit Pal: Scientific Assistant-D
- 9 Smt Mahuya Dutta: Lower Division Clerk
- 10 Sri Nirmal Das: Technician 'B'
- 11 Sri Raju Dutta: Technician 'C'
- 12 Sri Sanjay Shaw: Helper 'C'
- 13 Sri Shyamal Ch Digar: Helper 'C'
- 14 Shri Madhu Sudan Samal: Asstt Halwai-cum-Cook

CHEMICAL SCIENCES DIVISION

- 1 Prof Soumen Basak: Sr Professor 'H'
- 2 Prof Amitabha De: Professor 'G'
- 3 Prof Susanta Lahiri: Sr Professor 'H'
- 4 Prof Samita Basu: Sr Professor 'H' & HOD
- 5 Prof Maitreyee Nandy: Professor 'G'

- 6 Prof Munna Sarkar: Professor 'G'
- 7 Dr Padmaja Prasad Mishra: Associate Professor 'E'
- 8 Dr Montu K. Hazra: Associate Professor 'E'
- 9 Dr Dulal Senapati: Associate Professor 'E'
- 10 Sri Ajay Das: Scientific Assistant-E
- 11 Smt Chitra Raha: Scientific Assistant-E
- 12 Sri Avijit Shome: Scientific Assistant-C
- 13 Sri Subir Bandyopadhyay: Superintendent
- 14 Sri Bablu Ram: Technician 'D'
- 15 Sri Deepak Kr Ram: Technician 'A'
- 16 Sri Jitendra Nath Roy: Technician 'A'

COMPUTATIONAL SCIENCES DIVISION

- 1 Prof Dhananjay Bhattacharyya: Professor 'G' & HOD
- 2 Dr Gautam Garai: Scientist 'G'
- 3 Sri Deeptish Dey: Engineer 'F'
- 4 Sri Gautam Datta: Scientific Assistant-E
- 5 Sri Sumit Basu: Scientific Assistant-C
- 6 Sri Nanda Lal Sanpui: Technician 'C'
- 7 Sri Soumya Majumdar: Technician 'D'

Central Facilities

CENTRE FOR ADVANCED RESEARCH & EDUCATION

- 1 Prof Abhijit Chakrabarti: Sr. Professor 'H' & Head
- Smt Seema Bhattacharyya: Officer-In-Charge
- 1 Sri Amit Kumar Saha: Scientific Officer 'D'
- 2 Smt Dipa Dasgupta: Scientific Officer 'C'
- 3 Sri Sushanta Chakraborty: Scientific Assistant-E
- 4 Sri Jayant Kr Mukherjee: Scientific Assistant-D
- 5 Sri Pradip Das: Scientific Assistant-A
- 6 Sri Sudarshan Mondal: Superintendent
- 7 Sri Nirmal Ch Biswas: Technician 'B'
- 8 Sri Sanjib Kr Roy: Helper 'C'

ELECTRON MICROSCOPE

- 1 Sri Pulak Kumar Roy: Engineer 'G' & Head
- 2 Sri Ajoy Chakrabarty: Scientific Assistant-E

LIBRARY

- Prof R Ranganathan: Chairman
- 1 Sri Abhijit Kumar Malakar: Scientific Assistant-E
- 2 Sri Samit De: Scientific Assistant-E
- 3 Shri Mahesh Hembram: Scientific Assistant 'B'
- 4 Smt Manlunching: Scientific Assistant 'B'
- 5 Smt Anupama Saha: Technician 'C'
- 6 Sri Manoj Karmakar: Technician 'D'
- 7 Sri Kishori Lal Ram: Technician 'C'
- 8 Sri Kartick Ch Panigrahi: Helper 'C'

WORKSHOP

- Prof Sukalyan Chattopadhyay: Sr Professor 'H' & Chairman
- 1 Dr Jisnu Basu: Engineer 'F' & Officer-In-Charge
- 2 Sri Sadananda Dutta: Technician 'G'
- 3 Sri Ramen Jana: Technician 'G'
- 4 Sri Sudipta Barman: Scientific Assistant 'D' (Fitter)
- 5 Sri Narayan Chandra Dey: "Scientific Assistant-C (CNC Operator)"
- 6 Sri Debasish Sen: Technician 'G'
- 7 Sri Supriya Mondal: Technician 'G'
- 8 Sri Biplab Kr Dey: Technician 'E'
- 9 Sri Partha Sarathi Karmakar: Technician 'G' (Turner)
- 10 Sri Tarun Tapan Biswas: Technician 'E' (Fitter)
- 11 Sri Gopal Kr Chatterjee: Technician 'G' (Eng Stores)
- 12 Sri Ramkrishna Roy: Technician 'E' (Machinist)
- 13 Sri Bhairab Ch. Nath: Technician 'D' (Mil Fitter)
- 14 Sri Sunil Das: Technician 'D' (Mil Fitter)
- 15 Sri Durlav Tudu: Technician 'D' (Turner)

- 16 Sri Subrata Baidya: Technician 'D' (Machinist)
- 17 Sri Sadip Patra: Technician 'D' (Welder)
- 18 Sri Himadri Chakraborty: Technician 'D' (Machinist)
- 19 Sri Subal Ch Bindi: Technician 'D'
- 20 Shri C Palanivel: Technician 'C' (Glass Blower)
- 21 Sri Adhir Sarkar: Technician 'C'
- 22 Sri Santosh Kr Barman: Caretaker
- 23 Sri Deb Prasad Sardar: Helper 'E'
- 24 Sri Gopal Das: Helper 'C'

BUILDING MAINTENANCE (ELECTRICAL)

- Sri Abhijit Sanyal: Chairman, BM(Elec) Committee
- 1 Sri Debi Prasad Ghosh: Engineer 'G'
- 2 Sri Soumendra Pal: Engineer 'D', Engineer-in-Charge
- 3 Sri Swapan Kr Mandal: Scientific Assistant-E
- 4 Sri Somenath Ghosh: Scientific Assistant-D
- 5 Sri Saral Guha: Technician 'G'
- 6 Sri Kali Kanto Dey: Technician 'G'
- 7 Sri Madhusudan Kaity: Technician 'G'
- 8 Sri Asok Kr Majumdar: Technician 'E'
- 9 Sri Kalyan Paul Roy: Technician 'D'
- 10 Sri Gautam Kr Sabui: Technician 'C'
- 11 Sri Pratap Dhanuk: Technician 'D'
- 12 Sri Dilip Kr Chakraborty: Technician 'D'
- 13 Shri Jai Prakash Tiwari: Technician 'C'
- 14 Sri Jagannath Mondal: Technician 'C'
- 15 Sri Mahendra M Khapekar: Technician 'D'
- 16 Sri Dilip Ram: Caretaker
- 17 Sri Bijay Ram: Helper 'C'
- 18 Sri Sankar Adhikari: Helper 'C'

BUILDING MAINTENANCE (CIVIL)

- Prof Asimananda Goswami: Chairman, BM(Civil) Committee
- 1 Sri Rajkumar Sengupta: Engineer 'E'
- 2 Sri Siddhartha Saha: Engineer 'D'
- 3 Sri Subha Sankar Kundu: Technician 'H'
- 4 Sri Arup Polley: Technician 'H'
- 5 Sri Nil Kanta Sinha: Scientific Assistant-D
- 6 Sri Gobinda Pal: Scientific Assistant-D
- 7 Shri Sujoy Halder: Scientific Assistant 'B'
- 8 Sri Subir Modak: Superintendent
- 9 Sri Asok Kumar Das: Technician 'G'
- 10 Sri Sisir Kumar Mondal: Technician 'G' (Structural Draftsman)
- 11 Sri Sunil Murmu: Technician 'D'
- 12 Sri Samir Kr Chakraborty: Caretaker (Mali)
- 13 Sri Shyamal Kr Bose: Helper 'E'

Administrative Departments

ESTABLISHMENT

- 1 Sri Suchintya Kumar Gupta: Establishment Officer
- 2 Shri Biplab Kumar Ray: AAO(E-I)
- 3 Smt Chandana Basu: AAO
- 4 Sri Biswajit Dutta: Accountant
- 5 Shri Subhendu Naskar: Lower Division Clerk
- 6 Smt Paramita Pal: Lower Division Clerk
- 7 Sri Subhash Ch Gayen: Technician 'C'

DESPATCH

- 1 Smt Chandana Mitra: AAO
- 2 Sri Tarak Nath Bhattacharya: Technician 'C'
- 3 Sri Gouri Sankar Singh: Driver - V
- 4 Shri Pintu Ram: Helper 'C'

ACCOUNTS

- 1 Sri Niladri Sanyal: Dy Controller of Accounts
- 2 Shri Ved Prakash Mishra: Accounts Officer
- 3 Sri Swarup Kr Bose: AO(Accounts)
- 4 Sri Tapan Kr Bhattacharyya: AAO
- 5 Sri Goutam Ghosh: Superintendent
- 6 Shri Nand Kishor Gond: Lower Division Clerk
- 7 Shri Pourjok Majumder: Lower Division Clerk
- 8 Shri Manoj Lakra: Lower Division Clerk
- 9 Sri Biswanath Paul: Helper 'E'
- 10 Shri Pradip Ram: Asstt Halwai-cum-Cook
- 11 Sri Barun Kr Barua: Bearer-II

ACCOUNTS (BUDGET & AUDIT)

- 1 Sri Mrityunjay Dey: AO(Budget)
- 2 Sri Somnath Sarkar: AAO
- 3 Sri Pradip Dutta Sharma: Lower Division Clerk

ACCOUNTS (CASH)

- 1 Sri JS Raychaudhuri: AO(Accounts), Cash Section
- 2 Shri Raghunath Naskar: Superintendent
- 3 Smt Seethalakshmi Rath: Superintendent
- 4 Sri Avijit Saha: Superintendent
- 5 Sri Sanat Kumar Kotal: Technician 'B'

ACCOUNTS (SALARY)

- 1 Sri Rammohan Moitra: AAO(Salary)
- 2 Sri Debasish Das: AAO
- 3 Sm Nirupama Halder: Superintendent
- 4 Smt Monika Bhattacharya: Lower Division Clerk
- 5 Sri Madhu Bose: Helper 'E'

ACCOUNTS (PF & PENSION)

- 1 Sri Niranjan Sarkar: AAO(PF & Pension)
- 2 Sri Ranjit Dutta: AAO

PURCHASE

- 1 Smt Seema Bhattacharyya: AO-III & Off-In-Charge of Purchase Cell

Purchase (Domestic)

- 1 Sri Asit Ranjan Deb: AO(Purchase-Domestic)
- 2 Sri Gautam Das: Superintendent

- 3 Sri Ajoy Kumar Biswas: Superintendent
- 4 Sri Asim Halder: Superintendent
- 5 Ms Rekha Ram: Upper Division Clerk
- 6 Sri Soumyajit Karmakar: Lower Division Clerk
- 7 Sri Ashoke Kr Roy: Technician 'A'

Purchase (Foreign Cell)

- 1 Sri Sanjoy Chakraborty: AO(Purchase-Foreign)
- 2 Sri Sankar Nath Dewan: Sr Superintendent
- 3 Mr James Wilson Kerketta: Lower Division Clerk
- 4 Sri Gour Hari Das: Caretaker
- 5 Sri Ranjit Roy: Superintendent

STORE

- 1 Sri Shyamal Ch Biswas: Superintendent
- 2 Sri Asish Ram: Helper 'C'

MEDICAL UNIT

- 1 Prof Abhijit Chakrabarti: Chairman, MAC
- 2 Dr Sumalay Kar: Part-time Attending Physician
- 3 Dr Arup Kumar Sahu: Part-time Attending Physician
- 4 Sri Gobinda Chakraborty: AAO
- 5 Sri Dipak Kr Das: AAO
- 6 Smt Chandana Nayak: Lower Division Clerk
- 7 Shri Avishek Pal: Lower Division Clerk
- 8 Sri Nabin Kumar Halder: Technician 'B'

GUEST HOUSE & HOSTEL

- Prof Sukalyan Chattopadhyay: Prof-in-Charge, Guest House & Hostel, SINP Housing Com(MSA-II)
- Prof Chandni Das Mukherjee: Prof-In-Charge, Guest House & Hostel, Salt Lake Campus (MSA-I)
- 1 Shri Ramesh Singh: Helper 'C'
 - 2 Sri Somenath Das: Helper 'C'
 - 3 Smt Suro Mahato: Helper 'C'
 - 4 Sri Suresh Ch Das: Asstt. Halwai-cum-Cook
 - 5 Sri Sakti Pada Bisui: Asstt. Halwai-cum-Cook

CANTEEN

- Prof Debashis Mukhopadhyay: Chairperson, Canteen Committee
- 1 Sri Asok Kumar Roy: Asstt. Manager-cum-Storekeeper
 - 2 Sri Prabhat Maity: Halwai-cum-cook
 - 3 Sri Kartick Ch Maity: Asstt. Halwai-cum-Cook
 - 4 Sri Sujan Ch Mistri: Asstt. Halwai-cum-Cook
 - 5 Sri Shankar Andia: Asstt. Halwai-cum-Cook
 - 6 Sri Sailen Halder: Bearer-II
 - 7 Sri Nemai Ch Das: Bearer-II
 - 8 Sri Amar Das: Bearer-II
 - 9 Sri Subodh Kr Pradhan: Bearer-I
 - 10 Sri Sunil Ram: Bearer-II

TELEPHONE

- 1 Prof (Smt) Samita Basu: Prof & In-Charge
- 2 Smt Sunanda Chakraborty: Technician 'G'
- 3 Smt Bithi Biswas: Technician 'E'
- 4 Smt Pampa Bhattacharjee: Technician 'D'

SECURITY

- 1 Sri Supriya Gangopadhyay: Sr.Security Officer

2 Sri Ratan Kr Bose: Security Officer
 3 Sri Tapas Kr Dalal: Security Officer
 4 Sri Swaraj Nath Sarkar: Security Officer
 5 Sri Ashok Kr Singh: Security Officer
 6 Sri Ganesh Prasad Sharma: Security Supervisor 'B'
 7 Sri Tarak Chandra Nath: Security Supervisor 'B'
 8 Sri Gobinda Ch Roy: Lower Division Clerk
 9 Sri Balli Rana: Technician 'B'
 10 Sri Dukha Krishna Reddy: Technician 'A'
 11 Sri Subrata Kr Chowdhury: Technician 'B'
 12 Sri PB Thapa: Caretaker
 13 Sri Joyram Murmu: Helper 'E' (Watchman)
 14 Sri Madhusudan Bhakta: Helper 'E' (Watchman)
 15 Sri Sudhangsu Sekhar Mondal: Helper 'E' (Watchman)
 16 Sri Swapan Mukherjee: Helper 'E'
 17 Sri Mongol Oraon: Helper 'D' (Watchman)
 18 Sri Sibu Oraon: Helper 'D' (Watchman)
 19 Sri Tapan Kr Singha: Helper 'D' (Watchman)
 20 Sri Sudhir Kr Debnath: Helper 'C' (Watchman)
 21 Md Manayar Hasan Mondal: Technician 'B'
 22 Sri Ranjit Kr Roy: Helper 'C' (Watchman)
 23 Sri Arun Kumar Dutta: Helper 'B' (Watchman)
 24 Sri Pran Gopal Das: Helper 'C' (Watchman)
 25 Sri Gopal Chandra Saren: Helper 'C' (Watchman)

SECURITY (COSMETIC)

1 Sri Badal Hari: Helper 'E' (Sweeper)
 2 Sri Sakhi Chand Hari: Caretaker
 3 Sri Siblal Hari: Helper 'D' (Sweeper)
 4 Smt Anjali Hari: Helper 'D' (Sweeper)
 5 Sri Gobinda Ch Das: Helper 'D' (Sweeper)
 6 Sri Santosh Hari: Helper 'C' (Sweeper)
 7 Sri Ashok Mallick: Helper 'C'
 8 Sri Kala Chand Hela: Helper 'C' (Sweeper)

9 Sri Amit Hari: Helper 'A'

SECURITY (GARDENER)

1 Sri Gangadhar Maity: Technician 'E' (Supervisor Mali)
 2 Sri Sushil Kr De: Helper 'E' (Mali)
 3 Sri Santosh Kr Sarkar: Helper 'E' (Mali)
 4 Sri Santosh Kr Bachar: Helper 'E' (Mali)
 5 Sri Swapan Kr Mondal: Helper 'E' (Mali)
 6 Sk Mostakin: Helper 'C'

TRANSPORT

Prof Subrata Banerjee: Chairman, Transport Committee
 Sri Kaushik Chatterjee: Officer-in-Charge, Transport Sec
 1 Sri Dharmendra Prasad: Scientific Assistant-D
 2 Sri Aloke Kr Sarkar: Transport Supervisor
 3 Sri Swapan Kumar Mondal: Technician 'G'
 4 Sri Trinath Maharana: Technician 'G'(Vehi Mech)
 5 Sri Surai Mandi: Technician 'D'(Vehi Mech)
 6 Sri Kanai Lal Malakar: Technician 'D'
 7 Sri Tarak Nath Ghosh: Driver - IV
 8 Sri Dilip Baidya: Driver - IV
 9 Sri Madhusudan Mondal: Driver - IV
 10 Sri Gopal Ch Ghosh: Driver - III
 11 Sri Uttam Kr Roy: Driver - III
 12 Sri Kartick Ch Pal: Driver - III
 13 Sri Prabir Kr Mistri: Driver - III
 14 Sri Prabir Biswas: Driver - III
 15 Sri Asit Kr Mahapatra: Technician 'B'
 16 Sri Mongol Ch Mondal: Helper 'E'
 17 Sri Shankar Ram: Helper 'C'

List of Retirement: April 2013 to March 2014

- | | |
|--|--|
| 1 Smt Dipali Saha/ Adm 30.04.2013 | 13 Dr Arun Kr Pal/ Bio & SG 30.11.2013 |
| 2 Dr Polash Banerjee/ NPD 30.04.2013 | 14 Prof(Smt) Kajal Ghosh Ray/CMP 31.12.2013 |
| 3 Sri Pradip Kumar Das/ Adm 30.04.2013 | 15 Sri Tapan Chakraborty/ Adm 31.12.2013 |
| 4 Sri Ashok Maity/ Adm 30.05.2013(FN) | 16 Sri Banarashi Mallick/ BM(C) 31.12.2013 |
| 5 Smt Ratna Roychowdhury/ Library 30.06.2013 | 17 Sri Ashim Kumar Sarkar/ Adm 31.01.2014 |
| 6 Sri Ajoy Kr. Bhattacharya/ CMP 31.08.2013 | 18 Sri Prasanta Kumar Das/ Adm 31.01.2014 |
| 7 Sri Gautam Dutta/ Medical 30.09.2013 | 19 Dr SN Karmakar/ CMP 31.01.2014 |
| 8 Prof Pratap Bhattacharya/HENPP 31.10.2013 | 20 Dr (Smt) Srinanda Kundu/ SP & MS 31.03.2014 |
| 9 Sri V V Mallikarjuna Rao/ Adm 31.10.2013 | 21 Sri Gopal Chatterjee/ Workshop 31.03.2014 |
| 10 Sri Kamala Kanta Sarkar/ BM(C) 31.10.2013 | |
| 11 Sri Subrata Chowdhury/ Library 31.10.2013 | |
| 12 Sri Dulal Dey/ BM(C) 30.11.2013 | |

Voluntary Retirement List: April 2013 to March 2014

- 1 Sri Swadesh Ch Deb/ Adm 02.07.2013

List of Demise: April 01, 2013 to March 31, 2014

- 1 Prof Abhee kanti Dutt-Mazumder /HENPP 15.12.2013
2 Shri Babu Rajak /DO 07.03.2014

8.3 Audited Accounts

8.4 Balancesheet

SAHA INSTITUTE OF NUCLEAR PHYSICS

Balance Sheet as at 31st March, 2014

	<u>Schedule</u>	<u>2013-14</u>	<u>2012-13</u>
<u>CAPITAL FUND & LIABILITIES</u>			
CAPITAL FUND	1	554471208.49	708815201.33
CAPITAL RESERVE	2	0.00	7116996.30
EARMARKED FUNDS	3	8591225.00	10498421.00
CURRENT LIABILITIES AND PROVISIONS	4	2656560051.03	2798198561.07
TOTAL		<u>3219622484.52</u>	<u>3524629179.70</u>
<u>ASSETS</u>			
FIXED ASSETS			
Gross Block	5	3915601662.23	3703492767.23
Less : Accumulated Depreciation	5	<u>188599349.36</u>	<u>1617512127.35</u>
		2029602312.87	2085980639.88
INVESTMENT	6	638302004.00	63510000.00
CURRENT ASSETS, LOANS & ADVANCES	7	551718167.65	1375138539.82
TOTAL		<u>3219622484.52</u>	<u>3524629179.70</u>
SIGNIFICANT ACCOUNTING POLICES	15		
CONTINGENT LIABILITIES AND NOTES ON ACCOUNTS	16		

The Schedules referred to above form part of these Accounts


(V. P. Mishra)
Accounts Officer


(N. Sanyal)
Dy. Controller of Accounts


(Ravindra Singh)
Registrar

In terms of our attached Report of even date
For K. Sharma & Co
Chartered Accountants


(K. K. Sharma)
Partner

Membership No. 005313
1/B, Old Post Office Street, Room No.8, (First Floor),
Kolkata - 700 001
Dated :-19th September, 2014




(Bikas K. Chakrabarti)
Director

8.5 Income & Expenditure Account

SAHA INSTITUTE OF NUCLEAR PHYSICS

Income & Expenditure Account for the year ended 31st March, 2014

	<u>Schedule</u>	<u>2013-14</u>	<u>2012-13</u>
INCOME : -			
Income from Sales/Services	8	589665.00	347270.00
Grants	9	814362028.26	982922773.03
Interest Earned	10	10320901.00	23013196.00
Other Income	11	5609988.75	5766192.20
Excess of Expenditure over Income transferred to Capital Fund		378063884.14	
		<u>1208946467.15</u>	<u>1012049431.23</u>
EXPENDITURE : -			
Establishment Expenses	12	671304595.90	353321367.80
Administrative Expenses	13	268569062.70	270184179.51
Interest/Bank charges	14	80849.54	34844.25
Depreciation	5	268991959.01	278361821.69
Excess of Income over Expenditure transferred to Capital Fund			110147217.98
		<u>1208946467.15</u>	<u>1012049431.23</u>

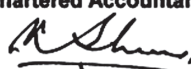
The Schedules referred to above form part of these Accounts


(V. P. Mishra)
Accounts Officer


(N. Sanyal)
Dy. Controller of Accounts


(Ravindra Singh)
Registrar

In terms of our attached Report of even date
For K. Sharma & Co
Chartered Accountants


(K. K. Sharma)
Partner

Membership No. 005313
1/B, Old Post Office Street, Room No.8, (First Floor),
Kolkata - 700 001
Dated :-19th September, 2014




(Bikas K. Chakrabarti)
Director

8.6 Receipts & Payments

SAHA INSTITUTE OF NUCLEAR PHYSICS

Receipts & Payments Account for the year ended 31st March, 2014		Payments	
Receipts	2012-13	2013-14	2013-14
Opening Balance b/f :-			
Cash in hand	68,284.00	7,764.00	57,79,63,916.90
Current Account Balances	65,21,90,811.03	72,72,85,064.68	26,07,96,533.70
Grant-in-aid received from DAE :-			
Recurring	61,12,00,000.00	65,93,93,000.00	21,21,08,895.00
Non-Recurring	32,50,00,000.00	14,31,11,000.00	32,74,83,944.64
Grant received from other agencies for on going projects	37,64,46,264.00	30,70,78,778.05	6,52,055.00
HBA & Other Advance recovery	29,76,262.00	25,60,503.00	57,47,90,752.00
Realisation of Margin Money Deposit	32,22,25,095.00	18,37,59,800.00	18,90,86,400.00
Realisation from other Deposit	1,73,14,200.00	38,552.00	1,47,200.00
Realisation of other advances	6,82,55,191.33	32,81,29,160.63	5,43,71,293.50
Interest Received	2,30,13,196.00	1,16,49,079.00	37,82,204.00
Income Receipts	61,13,462.20	61,99,653.75	
Current Liabilities			7,784.00
Pension Fund Receipts	5,50,486.00	1,04,59,325.60	17,84,89,162.43
	<u>2,40,53,53,251.56</u>	<u>2,37,97,53,206.71</u>	<u>2,40,53,53,251.56</u>
			<u>2,37,97,53,206.71</u>


(V. P. Mishra)
Accounts Officer



(N. Sanyal)
Dy. Controller of Accounts


(Ravindra Singh)
Registrar


(Bikas K. Chakrabarti)
Director



In terms of our attached Report of even date

For K. Sharma & Co
Chartered Accountants

(K. K. Sharma)
Partner

Membership No. 005313
1/B, Old Post Office Street, Room No.8, (First Floor),
Kolkata - 700 001
Dated :- 19th September, 2014

Chapter 9

External Collaborators

A Bhattacharjee, Visva Bharati Univ, Dept Phys, Santiniketan 731235, W Bengal, India

Abhitosh Kedia, Univ Delhi, Dept Phys & Astrophys, Delhi 110007, India

Achintya Singha, Bose Inst, Dept Phys, Kolkata 700009, India

Ajay K Sood, Department of Physics, Indian Institute of Science, Bangalore, Karnataka, India

AK Raychaudhuri, Department of Condensed Matter Physics and Material Sciences, S N Bose National Center for Basic Sciences, Kolkata 700098

AK Singh, Indian Inst Technol Kharagpur, Dept Phys & Meteorol, IN-721302 Kharagpur, W Bengal, India

Alejandro Perez, Univ Sud Toulon Var, Aix Marseille Univ, CNRS UMR 6207, Ctr Phys Theor, F-13288 Marseille 9, France

Ali Naji, School of Physics, Institute for Research in Fundamental Sciences (IPM), Tehran 19395-5531, Iran

Amílcar R de Queiroz, Univ Brasilia, Inst Fis, BR-70919970 Brasilia, DF, Brazil

Amitabh Ranjan, Laboratory of Transcription Biology, Center for DNA Fingerprinting and Diagnostics, Tuljaguda complex, 4-1-714 Mozamjahi Road, Nampally, Hyderabad 500 001, India

Amrit Krishna Mitra, Sch Trop Med, Dept Clin & Expt Pharmacol, Kolkata 700073, India

Aneeya K Samantara, CSIR Inst Minerals & Mat Technology, Bhubaneswar 751013, Orissa, India

Anirban Kar, Proteomics and Structural Biology

Unit, Institute of Genomics and Integrative Biology, CSIR, Room 307, Mall Road, Delhi 110007

Anirban Kundu, Univ Calcutta, Dept Phys, Kolkata 700009, India

Anis Biswas, Department of Physics, University of South Florida, Tampa, Florida 33620, USA

Ankita Bhattacharya, Indian Stat Inst, Div Biol Sci, Kolkata 700108, India

A Pachol, Univ Iceland, Inst Sci, IS-107 Reykjavik, Iceland

A Rooj, Visva Bharati Univ, Dept Phys, Santiniketan 731235, W Bengal, India

Arunansu Sil, Indian Inst Technol, Dept Phys, Gauhati 781039, India

A Samsarov, Rudjer Boskovic Inst, HR-10002 Zagreb, Croatia

Ashis Bhattacharjee, Visva Bharati Univ, Dept Phys, Santiniketan 731235, W Bengal, India

Asmita Mukherjee, Indian Inst Technol, Dept Phys, Bombay 400076, India

Atul V Thorat, Natl Univ Ireland Univ Coll Cork, Dept Chem, Mat Res Grp, Cork, Ireland

AV Thorat, Department of Chemistry and Tyn-dall National Institute, University College Cork, Cork, Ireland

AW Thomas, Univ Adelaide, Sch Chem & Phys, Special Res Ctr Subatom Struct Matter CSSM, Adelaide, SA 5005, Australia

Ayan Chatterjee, Tata Inst Fundamental Res, Bombay 400005, India

B Abelev, Lawrence Livermore Natl Lab, Livermore, CA 94550 USA

Balwinder Kaur, Indian Inst Technol Ropar,

Dept Chem, Rupnagar 140001, India

Bappaditya Roy, Univ Calcutta, Dept Biotechnol, Kolkata 700019, India

B Behera, DESY, D-15738 Zeuthen, Germany

B Erk, Deutsch Elektronen Synchrotron DESY, D-22607 Hamburg, Germany

B Ghosh, Dept of Physics, Jadavpur University, Kolkata-700 032

B Ghosh, Dept of Physics, NITMAS, South 24 Parganas, PIN-743368

Bidisha Sengupta, Department of Chemistry, Tougaloo College, Tougaloo, Mississippi, USA

Biplob Bhattacharjee, Univ Tokyo, TODIAS, Kavli IPMU, Kashiwa, Chiba 2778583, Japan

Bisnu Prasad Dash, Fakir Mohan Univ, PG Dept Biosci & Biotechnol, Mitrapur, Orissa, India

BK Chatterjee, Bose Institutue, Kolkata-700009

Bornali Sarma, VIT Univ, Dept Phys, Chennai 600048, Tamil Nadu, India

C Bostedt, SLAC Natl Accelerator Lab, Menlo Pk, CA 94025 USA

Chandan Saha, Sch Trop Med, Dept Clin & Expt Pharmacol, Kolkata 700073, India

Chiranjib Barman, Ctr Variable Energy Cyclotron, Kolkata, India

Chowdhury, Ujjal, CSIR Cent Glass & Ceram Res Inst, Nanostruct Mat Div, Kolkata 700032, India

D Adamova, Acad Sci Czech Republic, Inst Nucl Phys, CZ-25068 Rez, Czech Republic

Daniel Hurley, Complex and Adaptive Systems Laboratory, University College Dublin, Dublin, Ireland

D Anielski, CFEL, Max Planck Adv Study Grp, D-22607 Hamburg, Germany

David Emmanuel-Costa, Univ Lisbon, Dept Fis, P-1049001 Lisbon, Portugal

Debapriya De, MCKV Inst Engn, Dept Chem, Liluah 711204, Howrah, India

Debasis Banerjee, Department of Haematology, Ramkrishna Mission Seva Pratisthan, Kolkata, India

Dipanwita Majumdar, Bose Inst, Dept Phys, Kolkata 700009, India

Diptasikha Das, Univ Calcutta, Dept Phys, Kolkata 700009, India

Dipten Bhattacharya, CSIR Cent Glass & Ceram Res Inst, Nanostruct Mat Div, Kolkata 700032,

India

Diptiman Sen, Indian Inst Sci, Ctr High Energy Phys, Bangalore 560012, Karnataka, India

DM Rossi, GSI Helmholtzzentrum Schwerionenforsch GmbH, D-64291 Darmstadt, Germany

D Rolles, Deutsch Elektronen Synchrotron DESY, D-22607 Hamburg, Germany

E Aliu, Columbia Univ Barnard Coll, Dept Phys & Astron, New York, NY 10027 USA

E Amorini, INFN Lab Nazl Sud, Catania, Italy

E Harikumar, Univ Hyderabad Cent Univ, Sch Phys, Hyderabad 500046, India

Emilie Franceschini, Aix Marseille Univ, CNRS, UPR 7051, LMA, Marseille, France

Ernesto Frodden, Pontificia Univ Catolica Chile, Dept Fis, Santiago 22, Chile

F Aksouh, GSI Helmholtzzentrum Schwerionenforsch GmbH, D-64291 Darmstadt, Germany

F Demartin, Catholic Univ Louvain, Ctr Cosmol Particle Phys & Phenomenol CP3, B-1348 Louvain, Belgium

F Haas, Univ Fed Parana, Dept Fis, BR-81531990 Curitiba, Parana, Brazil

G (Mukherjee), Ctr Variable Energy Cyclotron, Kolkata 700064, India

Gobinda Gopal Khan, Univ Calcutta, Ctr Res Nanosci & Nanotechnol, Kolkata 700098, India

Goswami, Sudipta, CSIR Cent Glass & Ceram Res Inst, Nanostruct Mat Div, Kolkata 700032, India

Guy Cloutier, Univ Montreal Hosp Res Ctr CRCHUM, Lab Biorheol & Med Ultrason, Montreal, PQ, Canada

Hans Schamel, Theoretical Physics, University of Bayreuth, D-95440 Bayreuth, Germany

Haradhan Mandal, Visva Bharati Univ, Dept Phys, Santiniketan 731235, W Bengal, India

Heini Ruhanen, Complex and Adaptive Systems Laboratory, University College Dublin, Dublin, Ireland

Hirok Chaudhuri, Ctr Variable Energy Cyclotron, Kolkata, India

H Pai, Ctr Variable Energy Cyclotron, Kolkata 700064, India

HR Krishnamurthy, Indian Inst Sci, Dept Phys, Ctr Condensed Matter Theory, Bangalore 560012, India

Ian M Steele, Univ Chicago, Dept Geophys Sci,

Chicago, IL 60637 USA

I Sarkar, Deutsch Elekt Synchrotron, DESY Photon Sci, D-22603 Hamburg, Germany

I Znakovskaya, Max Planck Inst Quantum Opt, D-85748 Garching, Germany

J Adam, Czech Tech Univ, Fac Nucl Sci & Phys Engn, CR-11519 Prague, Czech Republic

Jaspal Singh, School of Basic and Applied Sciences, Guru Gobind Singh Indraprastha University, Dwarka, New Delhi 110078

Jayanta K Bhattacharjee, Harish Chandra Research Institute, Chhatnag Road, Jhansi, Allahabad 211019, India

Jens O Andersen, Department of Physics, Norwegian University of Science and Technology, N-7491 Trondheim, Norway

J Frenkel, Univ Sao Paulo, Inst Fis, BR-05508090 Sao Paulo, Brazil

Jincemon Cyriac, Mahatma Gandhi Univ, Sch Pure & Appl Phys, Kottayam 686560, Kerala, India

J Piekarewicz, Florida State Univ, Dept Phys, Tallahassee, FL 32306 USA

J Sethi, Tata Inst Fundamental Res, Bombay 400005, Maharashtra, India

Julio J Martinell, Univ Nacl Autonoma Mexico, Inst Ciencias Nucl, Mexico City 04510, DF, Mexico

Justin D Holmes, Natl Univ Ireland Univ Coll Cork, Dept Chem, Mat Res Grp, Cork, Ireland

Kamala Kanta Nanda, CSIR, Inst Minerals & Mat Technol, Colloids & Mat Chem Dept, Bhubaneswar 751013, Orissa, India

KANAGARAJ M, Centre for High Pressure Research, School of Physics, Bharathidasan University, Tiruchirappalli 620024

KB Modi, Department of Physics, Saurashtra University, Rajkot 360005, India

K Boretzky, GSI Helmholtzzentrum Schwerionenforsch GmbH, ExtreMe Matter Inst, EMMI, D-64291 Darmstadt, Germany

KK Iyer, Tata Inst Fundamental Res, Bombay 400005, Maharashtra, India

K Malik, K, Univ Calcutta, Dept Phys, Kolkata 700009, India

K Mandal, SN Bose Natl Ctr Basic Sci, Kolkata 700098, India

K Selvakumar; Indian Inst Technol Kharagpur,

Dept Phys & Meteorol, IN-721302 Kharagpur, W Bengal, India

KS Gothe, Tata Inst Fundamental Res, Mumbai 400005, Maharashtra, India

K Tsushima, Univ Adelaide, Special Res Ctr Subat Struct Matter CSSM, Sch Chem & Phys, Adelaide, SA 5005, Australia

L Acosta, INFN Lab Nazl Sud, Catania, Italy

L Auditore, Univ Messina, INFN Grpp Coll Messina, I-98100 Messina, Italy

Laura Blackmon, Department of Chemistry, Tougaloo College, Tougaloo, Mississippi, USA

Leonard S Kisslinger, Carnegie Mellon Univ, Dept Phys, Pittsburgh, PA 15213 USA

L Foucar, CFEL, Max Planck Adv Study Grp, D-22607 Hamburg, Germany

L Thakur, Indian Inst Technol Roorkee, Dept Phys, Roorkee 247667, Uttar Pradesh, India

Maitree Biswas, St Xaviers Coll, Dept Biotechnol, Kolkata, India

Malay Ghosh, Department of Haematology, NRS Medical College and Hospital, Kolkata, India

MA Morris, Department of Chemistry and Tyn-dall National Institute, University College Cork, Cork, Ireland

Manjistha Dutta, Jadavpur Univ, Dept Instrumentat Sci, Kolkata 700032, India

Manoranjana Khan, Jadavpur Univ, Dept Instrumentat Sci, Kolkata 700032, India

Michael Strickland, Kent State Univ, Dept Phys, Kent, OH 44242 USA

Mickael Blaise, Aarhus Univ, Dept Mol Biol & Genet, CARB Ctr, DK-8000 Aarhus, Denmark

M Kanagaraj, Bharathidasan Univ, Sch Phys, Ctr High Pressure Res, Tiruchchirappalli 620024, India

MK Mandal, Harish Chandra Res Inst, Reg Ctr Accelerator Based Particle Phys, Allahabad 211019, India

Mohit Randeria, Ohio State Univ, Dept Phys, Columbus, OH 43210 USA

M Sardar, Material Science Division, Indira Gandhi Center for Atomic Research, Kalpakkam 603 102, India

M Souheib Chebil, Univ Maine, LUNAM Univ, Fac Sci, IMMM,UMR CNRS 6283, F-72000 Le Mans 9, France

M Spanner, Natl Res Council Canada, Steacie Inst Mol Sci, Ottawa, ON K1A 0R6, Canada

MU Anu Prathap, Indian Inst Technol Ropar, Dept Chem, Rupnagar 140001, India

Muthu S Esakki, Centre for High Pressure Research, School of Physics, Bharathidasan Univ, Tiruchirappalli 620024

Neenu Varghese, Jawaharlal Nehru Ctr Adv Sci Res, Bangalore 560064, Karnataka, India

Neha Bhardwaj, School of Basic and Applied Sciences, Guru Gobind Singh Indraprastha University, Dwarka, New Delhi 110078

Nicolas Delorme, Univ Maine, LUNAM Univ, Fac Sci, IMMM,UMR CNRS 6283, F-72000 Le Mans 9, France

Nihar R Jana, Division of Cellular and Molecular Neuroscience, National Brain Research Centre, Manesar, Haryana, India

Nitai Debnath, Indian Stat Inst, Div Biol Sci, Kolkata 700108, W Bengal, India

Olaf Dreyer, Univ Roma La Sapienza, Dipartimento Fis, I-00185 Rome, Italy

O Mondal, Department of Physics, University of Burdwan, Burdwan 713104, India

O Scholten, Univ Groningen, Kernfys Versneller Inst, NL-9747 Groningen, Netherlands

Padma Kant Shukla, Ruhr Univ Bochum, Fac Phys & Astron, Int Ctr Adv Studies Phys Sci, Bochum, Germany

P Adrich, GSI Helmholtzzentrum Schwerionenforsch GmbH, D-64291 Darmstadt, Germany

Pandian Senthil Kumar, Univ Delhi, Dept Phys & Astrophys, Delhi 110007, India

Paramita Kar Choudhury, Indian Inst Sci, Dept Phys, Bangalore 560012, Karnataka, India

Paramjit Singh, Guru Gobind Singh Indraprastha Univ, Univ Sch Basic & Appl Sci, New Delhi 110078, India

P Artoisenet, Nikhef Theory Grp, NL-1098 XG Amsterdam, Netherlands

Patrick D Shipman, Department of Mathematics, Colorado State University, Fort Collins, Colorado 80523, USA

P Choudhury, CG&CRI, 196, Raja S C Mullick Road, Kolkata-700 032

P de Aquino, Vrije Univ Brussel, B-1050 Brussels, Belgium

P -G Reinhard, Univ Erlangen Nurnberg, Inst

Theoret Phys 2, D-91058 Erlangen, Germany

PK Mukhopadhyay, SN Bose Natl Ctr Basic Sci, LCMP, Dept Condensed Matter Phys & Mat Sci, Kolkata 700098

P Mitra, Univ Burdwan, Dept Phys, Burdwan 713104, W Bengal, India

Prabir Kr Panda, Siliguri Inst Technol, Dept Chem, Darjeeling 734009, India

PR Vishwanath, Indian Inst Astrophys, Bangalore 560034, Karnataka, India

Punyabrata Pradhan, SN Bose National Centre for Basic Sciences, Salt Lake City, Kolkata-700 098

Purusattam Ray, Inst Math Sci, Madras 600113, Tamil Nadu, India

Rahul Pandit, Centre for Condensed Matter Theory, Department of Physics, Indian Institute of Science, Bangalore 560012, India

Rajat Saha, Jadavpur Univ, Dept Phys, Kolkata 700032, India

Rajendra Srivastava, Indian Inst Technol Ropar, Dept Chem, Rupnagar 140001, India

Rajen Kundu, RKMVC Coll, Dept Phys, Kolkata 700118, W Bengal, India

Rajesh Kumar, Guru Gobind Singh Indraprastha Univ, Univ Sch Basic & Appl Sci, New Delhi 110078, India

Rajib Nath, Department of Condensed Matter Physics and Material Sciences, S N Bose National Center for Basic Sciences, Kolkata 700098, India

Rajkumar Kore, Indian Inst Technol Ropar, Dept Chem, Rupnagar 140001, India

Rajkumar Roychoudhury, Indian Stat Inst, Kolkata 700108, India

Raka Dasgupta, SN Bose National Centre for Basic Sciences, 3/JD Bidhannagar, Kolkata-700098, India

R Boll, CFEL, Max Planck Adv Study Grp, D-22607 Hamburg, Germany

R Chatterjee, Indian Inst Technol, Dept Phys, Roorkee, Uttar Pradesh, India

Rema Krishnaswamy, Jawaharlal Nehru Centre for Advanced Scientific Research, Jakkur Campus, Bangalore, India

R Frederix, CERN, PH Dept, TH Unit, CH-1211 Geneva 23, Switzerland

RN Bhowmik, Department of Physics,

Pondicherry University, RV Nagar, Kalapet,
Pondicherry 605014, India

R Palit, Tata Inst Fundamental Res, Bombay
400005, Maharashtra, India

R Ramakumar, Department of Physics and As-
trophysics, University of Delhi, Delhi-110007,
India

R Rawat, UGC DAE Consortium Sci Res, Indore
452001, India

RR Francisco, Univ Sao Paulo, Inst Fis, BR-
05508090 Sao Paulo, Brazil

R Thiyagarajan, Centre for High Pressure Re-
search, School of Physics, Bharathidasan Uni-
versity, Tiruchirappalli-620024, India

Rutuparna Rath, NEHU, Shillong

Sakuntala Chatterjee, SN Bose National Centre
for Basic Sciences, Salt Lake City, Kolkata-700
098

Samiran Ghosh, Univ Calcutta, Dept Appl
Math, Kolkata 700009, India

Sandeep Agarwal, SN Bose Natl Ctr Basic Sci,
LCMP, Dept Condensed Matter Phys & Mat
Sci, Kolkata 700098

Sanhita Modak, Theoretical Physics Depart-
ment, Indian Association for the Cultivation
of Science, Kolkata-700032, India

Sanjay Dey, St Xaviers Coll, Dept Biotechnol,
Kolkata, India

Santanu K Maiti, Physics & Applied Mathemat-
ics Unit, ISI, 203 BT Road, Kolkata-700108

S Archambault, McGill Univ, Dept Phys, Mon-
treal, PQ, Canada

S Arumugam, Centre for High Pressure Re-
search, School of Physics, Bharathidasan Uni-
versity, Tiruchirappalli, India

Satyendra K Das, Bhabha Atom Res Ctr, Ctr
Variable Energy Cyclotron, Kolkata 700064, In-
dia

Savita Sharma, Laboratory of Transcription Bi-
ology, Center for DNA Fingerprinting and Diag-
nostics, Tuljaguda complex, 4-1-714 Mozamjahi
Road, Nampally, Hyderabad 500 001, India

Sayan Chandra, Department of Physics, Uni-
versity of South Florida, Tampa, Florida 33620,
USA

S Bandyopadhyay, Univ Calcutta, Dept Phys,
Kolkata 700009, India

S Bhattacharya, Ctr Variable Energy Cyclotron,

Kolkata 700064, India

S Chakraborty, Indian Inst Technol, Ctr Mat Sci,
Kharagpur 721302, W Bengal, India

S Chakraborty, Department of Physics, Univer-
sity of Burdwan, Burdwan 713104, India

S Dey, Dept of Physics, Jadavpur University,
Kolkata-700 032

S Esakki Muthu, Bharathidasan Univ, Sch
Phys, Ctr High Pressure Res, Tiruchchirappalli
620024, India

S Ghosh, SN Bose Natl Ctr Basic Sci, Kolkata
700098, India

S Ghosh, Univ Calcutta, Dept Appl Math,
Kolkata 700009, India

Shantanu Chowdhury, Proteomics and Struc-
tural Biology Unit, Institute of Genomics and In-
tegrative Biology, CSIR, Room 307, Mall Road,
Delhi 110007, India

Shyamaprosad Goswami, Department of Chem-
istry, Bengal Engineering and Science University,
Shibpur, Howrah 711103, India

Sini Kuriakose, School of Basic and Applied
Sciences, Guru Gobind Singh Indraprastha Uni-
versity, Dwarka, New Delhi 110078, India

SK Giri, Indian Inst Technol, Dept Phys & Me-
teorol, Kharagpur 721302, W Bengal, India

SK Pradhan, Univ Burdwan, Dept Phys, Div
Mat Sci, Burdwan 713104, W Bengal, India

SK Srivastava, Indian Inst Technol, Dept Phys
& Meteorol, Kharagpur 721302, W Bengal, In-
dia

S Lala, Univ Burdwan, Dept Phys, Div Mat Sci,
Burdwan 713104, W Bengal, India

S Meljanac, Rudjer Boskovic Inst, HR-10002 Za-
greb, Croatia

S Mondal, Univ Burdwan, Dept Phys, Burdwan
713104, W Bengal, India

Smrutirekha Swain, CSIR, Inst Minerals &
Mat Technol, Colloids & Mat Chem Dept,
Bhubaneswar 751013, Orissa, India

S Mukherjee, Department of Physics, The Uni-
versity of Burdwan, Golapbag, Burdwan, West
Bengal, India

S Nannarone, INFN CNR, Lab Nazl TASC, I-
34012 Trieste, Italy

Somen Goswami, Jadavpur Univ, Dept Phys,
Kolkata 700032, India

Somnath Nag, Indian Inst Technol, Kharagpur

721302, W Bengal, India

Sourabh S Chauhan, Natl Inst Sci Educ & Res, Bhubaneswar 751005, Orissa, India

S Ramaprabhu, Indian Inst Technol, Dept Phys, Madras 600036, Tamil Nadu, India

Sreekantha Sil, Dept of Physics, Visva-Bharati, Santiniketan, PIN-731235

Srutarshi Pradhan, Sintef Petroleum Research, N-7465 Torndheim, Norway

S Saha, Tata Inst Fundamental Res, Bombay 400005, Maharashtra, India

S Sarkar, Bengal Engn & Sci Univ, Sibpur 711103, Howrah, India

Subash Chandra Sahu, CSIR Inst Minerals & Mat Technology, Bhubaneswar 751013, Orissa, India

Subhashri Das; Indian Inst Technol Kharagpur, Dept Phys & Meteorol, IN-721302 Kharagpur, W Bengal, India

Suchandra Chakraborty, Sch Trop Med, Dept Clin & Expt Pharmacol, Kolkata 700073, India

Sudipa Chakravarty, Inst Genet Engn, Kolkata, India

Sudip Malik, Indian Assoc Cultivat Sci, Polymer Sci Unit, Kolkata 700032, India

Sujay Ghosh, Sch Trop Med, Dept Clin & Expt Pharmacol, Kolkata 700073, India

Sumistha Das, Indian Stat Inst, Div Biol Sci, Kolkata 700108, W Bengal, India

Sutapa Ray, Univ Calcutta, Dept Biotechnol, Kolkata 700019, India

Tanaya Bhattacharyya, St Xavier Coll, Dept Phys, Kolkata 700016, India

Tandra Ghoshal, Natl Univ Ireland Univ Coll Cork, Dept Chem, Mat Res Grp, Cork, Ireland

Tanusri Saha-Dasgupta, SN Bose Natl Ctr Basic Sci, Kolkata 700098, India

T Arlen, Univ Calif Los Angeles, Dept Phys & Astron, Los Angeles, CA 90095 USA

T Aumann, GSI Helmholtzzentrum Schwerionenforsch GmbH, ExtreMe Matter Inst, EMMI, D-64291 Darmstadt, Germany

T Aune, Univ Calif Los Angeles, Dept Phys & Astron, Los Angeles, CA 90095 USA

T Ergin, TUBITAK Space Technol Res Inst, TR-06531 Ankara, Turkey

T Ghoshal, Department of Chemistry and Tyn-

dall National Institute, University College Cork, Cork, Ireland

Thangarasu Pandiyan, Univ Nacl Autonoma Mexico, Fac Chem, Mexico City, DF, Mexico

Tilman Butz, Univ Leipzig, Fak Phys & Geowissensch, Inst Expt Phys 2, D-04103 Leipzig, Germany

Tirtha Sankar Ray, Univ Melbourne, Sch Phys, ARC Ctr Excellence Particle Phys Terascale, Melbourne, Vic 3010

T Kar, Indian Assoc Cultivat Sci, Dept Mat Sci, Kolkata 700032, India

TP Prabhu, Indian Inst Astrophys, Bangalore 560034, Karnataka, India

Tsutomu T Yanagida, Univ Tokyo, TODIAS, Kavli IPMU, Kashiwa, Chiba 2778583, Japan

Tuhin Malik, ISM, Dhanbad

U Devarajan, Centre for High Pressure Research, School of Physics, Bharathidasan University, Tiruchirappalli, India

UK Bhaskar, Sreegopal Banerjee Coll, Dept Phys, Magra 712148, Hooghly, India

Uttiyoarnab Saha, BESU, Shibpur

Utpal Rana, Indian Assoc Cultivat Sci, Polymer Sci Unit, Kolkata 700032, India

Uttam Kakade, Indian Inst Technol Roorkee, Dept Phys, Roorkee 247667, Uttar Pradesh, India

V Anuraj, Indian Inst Technol Ropar, Dept Chem, Rupnagar 140001, India

Vikram Rathee, Department of Physics, Indian Institute of Science, Bangalore, Karnataka, India

VK Lakhani, Department of Physics, Saurashtra University, Rajkot 360005, India

V Vasanthi, Pondicherry Univ, Dept Phys, Pondicherry 605014, India

W Nazarewicz, Univ Tennessee, Dept Phys & Astron, Knoxville, TN 37996 USA

Ya M Mukovskii, National Research Technological University, (MISIS), Leninskii prospekt 4, Moscow, 119049, Russia

Yu Aksyutina, GSI Helmholtzzentrum Schwerionenforsch GmbH, ExtreMe Matter Inst, EMMI, D-64291 Darmstadt, Germany

Chapter 10

Index

Index

- Abbaneo, D, 129, 130
Abbrescia, M, 129, 130
Abelev†, B, 120, 129
Abir, Raktim, 166, 180, 182
Adak, Debabrata, 159, 162, 178, 179
Adam†, J, 120, 129
Adamova†, D, 120, 129
Adhikary, Biswajit, 160, 178
Adhya, SP, 120, 129
Adrich†, P, 122, 136
Agarwal†, Sandeep, 88, 105
Agnihotri, Nidhi, 35, 41, 49, 50
Agrawal, BK, 169, 172, 174, 176, 180–183
Ahlskog, M, 89
Akl, M Abi, 129, 130
Aksouh†, F, 122, 136
Aksyutina†, Yu, 123, 125, 136, 137
Ali, Amna, 162, 179
ALICE Collaboration, 130, 131
Aliu†, E, 157, 159, 161, 163, 164, 178, 179
Alleno, E, 72, 102
Andersen, Jens O, 176, 182
Anielski†, D, 117, 128
Anuraj†, V, 83, 104
Archambault†, S, 157, 159, 161, 163, 178, 179
Arlen†, T, 157, 161, 163, 178, 179
Artoisenet†, P, 168, 180
Arumugam†, S, 91, 106
Aumann†, T, 123, 125, 136, 137
Aume†, T, 164, 179
- Bagani, K, 79, 87, 101, 103
Bagchi, Debarshee, 65, 100
Baksi, Shounak, 24, 46
Bandyopadhyay, Debades, 158, 178, 184, 186
Bandyopadhyay†, S, 65, 100
Bandyopadhyay†, T, 42, 50
Banerjee, Amrita, 26, 27, 47
Banerjee, Avinanda, 23, 27, 46, 47
Banerjee, D, 142, 145, 149
Banerjee, Debabrata, 150
Banerjee, Debashis, 47
Banerjee, Debasis, 24, 46
Banerjee, Mousumi, 42, 43, 50, 51
Banerjee, P, 182
Banerjee, R, 48
Banerjee, Rahul, 31, 48
Banerjee, Ramanuj, 30, 32, 48
Banerjee, S, 78, 79, 82, 84, 87, 88, 95, 101, 103–106
Banerjee, Subrata, 22, 24, 25, 28, 46, 47
Banerjee, Sunanda, 139
Banerjee†, Debasis, 24, 46
Banerjee†, M, 117, 128
Banerji†, P, 86, 105
Bansal†, Manju, 43, 51
Bardhan, Munmun, 51, 98
Barma, Mustansir, 207
Barman, C, 146, 149
Barman, SR, 78, 91, 103, 106
Barman†, Chiranjib, 145, 149
Basak, Soumen, 34, 36, 41, 49, 50
Basu, Abhik, 62, 67, 68, 70, 100, 101
Basu, Avik, 24, 46
Basu, Chinmoy, 138, 140
Basu, Debjyoti, 144, 147, 149, 150
Basu, J, 127
Basu, M, 75, 102
Basu, Mahashweta, 63, 72, 100, 102
Basu, P, 123, 127, 136
Basu, S, 45
Basu, Samita, 34, 36, 40, 42, 43, 45, 49–52, 55
Basu, Soumalee, 36, 49
Basu, Sumanta, 47
Basu, U, 75, 102
Basu-Mallick, B, 173, 181–183
Basu†, S, 117, 128
Baviskar, RR, 207
Bayana, Sayan, 97, 107
Behera†, B, 159, 164, 178, 179
Bera, Kallol, 34, 41, 49, 50
Bhardwaj†, Neha, 83, 104
Bhaskar†, UK, 94, 106
Bhattacharjee, A, 96, 107
Bhattacharjee, Ashis, 105
Bhattacharjee, P, 163
Bhattacharjee, Pijushpani, 158–160, 164, 178, 179, 184, 186
Bhattacharjee, Pritha, 23, 27, 46, 47
Bhattacharjee, Srijit, 182
Bhattacharjee†, Ashis, 88
Bhattacharjee†, Jayanta K, 67, 101
Bhattacharya, A, 79, 103
Bhattacharya, Ankita, 106
Bhattacharya, Dipankar, 23, 46
Bhattacharya, Paramita, 38, 50
Bhattacharya, Purba, 116, 128
Bhattacharya, Rangana, 73, 102
Bhattacharya, S, 163, 179

- Bhattacharya, Satyaki, 139
 Bhattacharya, Sudeb, 116, 128
 Bhattacharya†, Ankita, 92
 Bhattacharya†, Dipten, 66, 101
 Bhattacharya†, S, 123, 136
 Bhattacharyya, Dhananjay, 43, 44, 51, 52
 Bhattacharyya, Gautam, 165, 168, 169, 179, 180, 183, 185
 Bhattacharyya, Nitai P, 24, 29, 46, 48, 63, 72, 100, 102
 Bhattacharyya, SR, 77, 94, 96, 103, 106
 Bhattacharyya†, Tanaya, 173, 181
 Bhattacharjee†, Biplob, 169, 180
 Bhattacharyya, Satyaranjan, 99
 Bhoi, D, 70, 74, 101, 102
 Bhoi, Dilip, 62, 100
 Bhowmik, RK, 137
 Bhowmik†, RN, 61, 66, 100
 Bhunia, Satyaban, 96
 Bisoi, Abhijit, 122, 124, 136
 Biswas, Anirban, 159, 178
 Biswas, Sampa, 32, 43, 48, 50
 Biswas, Soumyajyoti, 68, 69, 76, 101, 103
 Biswas, Subhanip, 36, 49
 Biswas, Subir, 144, 149
 Biswas†, Anis, 75, 102
 Biswas†, Maitree, 32, 48
 Blackmon, Laura, 27, 47
 Blaise, Mickael, 21, 46
 Boll†, R, 117, 128
 Bondyopadhyay, Sourish, 64, 100
 Bora, Dhiraj, 207
 Boretzky†, K, 123, 125, 136, 137
 Bose†, Adity, 34, 49
 Bose†, Madhuparna, 33, 48
 Bostedt†, C, 117, 128
 Botha, AJ, 84, 104
 Brenna†, M, 172, 181
 Britto, RJ, 164, 179
 Butz†, Tilman, 118, 128
 Byakti, Pritibhajan, 166, 175, 180, 181

 Caesar, C, 137
 Chakrabarti Abhijit, 23, 46
 Chakrabarti, A, 47
 Chakrabarti, Abhijit, 24, 42, 46, 47, 50, 51, 53
 Chakrabarti, Arunabha, 21, 46, 51
 Chakrabarti, Bikas K, 67–69, 71, 76, 101–103, 207
 Chakrabarti, Kuntal, 115, 128
 Chakrabarti, N, 142, 148–150
 Chakrabarti, Nikhil, 143–145, 147–151
 Chakrabarti, O, 21, 46
 Chakrabarti, Oishee, 22, 46
 Chakrabarty, S, 129
 Chakraborty, A, 137
 Chakraborty, Chandrachur, 157, 161, 177, 179
 Chakraborty, Madhumita, 23, 46
 Chakraborty, Mainak, 160, 178
 Chakraborty, P, 84, 104
 Chakraborty, Purushottam, 97, 107–109
 Chakraborty, S, 86, 105, 127, 137
 Chakraborty, Somdeb, 167, 170, 180
 Chakraborty, Sovan, 158, 178
 Chakraborty, Sreeja, 33, 48
 Chakraborty†, Sandipan, 36, 41, 49, 50
 Chakraborty†, Suchandra, 40, 51
 Chakravarty, Runu, 47
 Chakravarty, Sudipa, 24, 46, 47
 Chandra, Anjan Kumar, 71, 76, 102, 103
 Chandra†, Sayan, 75, 102
 Chatterjee, A, 47
 Chatterjee, Bhramar, 175, 182
 Chatterjee, Paramita, 97, 107
 Chatterjee, Rakesh, 61, 99
 Chatterjee, S, 127, 137
 Chatterjee, Sayani, 61, 100
 Chatterjee†, Raghunath, 50
 Chatterjee†, Ayan, 175, 182
 Chatterjee†, BK, 72, 102
 Chatterjee†, R, 171, 181
 Chatterjee†, Raghunath, 38
 Chatterjee†, Sakuntala, 61, 99
 Chattopadhyay, Dhruvajyoti, 207
 Chattopadhyay, P, 47
 Chattopadhyay, S, 120–122, 129, 130, 136
 Chattopadhyay, Sukalyan, 126
 Chaudhuri, H, 146, 149
 Chaudhuri, Sudip, 28, 47
 Chaudhuri†, Hirok, 145, 149
 Chaudhury, Soumini, 164, 179
 Chauhan†, Sourabh S, 143, 144, 149
 Chebil†, M Souheib, 92, 106
 Chini, Tapas Kumar, 87, 105
 Choudhury†, P, 74, 102
 Chowdhury Islam, Aminul, 180
 Chowdhury, Abhishek, 174, 175, 181
 Chowdhury, Ankan Dutta, 37, 49
 Chowdhury, Debasree, 81, 104, 107
 Chowdhury, S, 25, 47, 148
 Chowdhury†, Shantanu, 26, 47
 Chowdhury†, Ujjal, 66, 101
 Cloutier†, Guy, 85, 105
 CMS Collaboration, 131–136
 Colo†, G, 172, 181
 Cyriac†, Jincemon, 115, 127

 Das, AN, 68, 101
 Das, Anindita, 46
 Das, Ashok K, 168, 169, 180
 Das, Chandrima, 47, 53, 55
 Das, D, 120, 126, 129
 Das, Debasish, 120, 121, 126, 129, 130, 137
 Das, Dipankar, 168, 180
 Das, Dipanwita, 47
 Das, I, 75, 85, 102
 Das, K, 120, 129
 Das, Kalipada, 85, 105
 Das, L, 126
 Das, M, 163, 179
 Das, Mala, 160, 163, 177–179, 185

- Das, NR, 207
 Das, Pabitra, 87, 105
 Das, PK, 127
 Das, Puspendu K, 46
 Das, Samir, 51
 Das, Srijit, 29, 48
 Das, Subhashri, 124, 136
 Das, Sumistha, 106
 Das†, Anand Kant, 34, 49
 Das†, Avijit Kumar, 30, 48
 Das†, Diptasikha, 65, 100
 Das†, Satyendra K, 118, 128
 Das†, Sumistha, 92
 Dasgupta, D, 25, 47
 Dasgupta, Dipak, 26, 27, 47, 54, 88
 Dasgupta, P, 69, 101
 Dasgupta, Papri, 61, 63, 79, 100, 103
 Dasgupta†, Raka, 73, 102
 Dash, Bisnu Prasad, 24, 46, 47
 Datta Pramanik, U, 122–125, 127, 136–138
 Datta, Alokmay, 92
 Dattagupta, Jiban Kanti, 32, 48
 de Aquino†, P, 168, 180
 de Florian, D, 176, 182
 de Queiroz†, Amilcar R, 175, 182
 De Sarkar, Sangita, 174, 175, 181
 De, Amitabha, 35, 37, 41, 49, 50
 De, Asit K, 174, 175, 177, 181, 183, 186
 De, Debapriya, 106
 De, G, 137
 De, JN, 174, 176, 181, 182
 De, S, 114, 117, 127, 128
 De, Sankar, 119, 128, 137, 140
 De†, Debapriya, 96
 Deb Pal, Anindita, 25, 47
 Deb, Sanghamitra, 23, 46
 Debnath†, Nitai, 92, 106
 Delorme†, Nicolas, 92, 106
 Demartin†, F, 168, 180
 Devarajan†, U, 91, 106
 Dey, Amit, 60, 99
 Dey, CC, 115, 117, 118, 127, 128
 Dey, Chandi C, 118, 128
 Dey, Debraj, 99
 Dey, Moumita, 67, 101
 Dey, Parijat, 167, 172, 180, 181
 Dey, S, 69, 101
 Dey, SK, 69, 101
 Dey†, Sanjay, 32, 48
 Dreyer†, Olaf, 166, 180
 Dutt-Mazumder, Abhee K, 121, 129, 130
 Dutt-Mazumder, AK, 120, 129
 Dutta Chowdhury, Ankan, 35, 41, 49, 50
 Dutta Majumdar, AK, 120, 129
 Dutta, Binita, 35, 38, 49, 50
 Dutta, Koushik, 184, 187
 Dutta, Paramita, 70, 101
 Dutta, Sreetama, 129
 Dutta, Sruti, 32, 48
 Dutta, Suchandra, 139
 Dutta†, Manjistha, 143, 148–150
 Emmanuel-Costa†, David, 166, 180
 Ergin, T, 165, 179
 Erk†, B, 119, 128
 Foucar†, L, 119, 128
 Franceschini†, Emilie, 85, 105
 Francisco†, Joseph S, 38, 50
 Francisco†, RR, 168, 180
 Frederix†, R, 166, 179
 Frenkel†, J, 168, 169, 180
 Frodden†, Ernesto, 173, 181
 Gamot†, Tanesh D, 86, 105
 Ganai, Sukumar, 207
 Gangopadhyay, Rupali, 37, 49
 Garai, S, 142, 145, 149
 Garg, Arti, 60, 99
 Gayen, Sirshendu, 90, 105
 Ghosal, Ambar, 160, 178
 Ghose, D, 77, 103
 Ghose, Debabrata, 77, 79, 81, 87, 103–105, 107
 Ghosh, Abhijit, 148
 Ghosh, Ambarnil, 29, 48
 Ghosh, Amit, 166, 173, 175, 180–182
 Ghosh, Asim, 67, 101
 Ghosh, Avirup, 166, 180
 Ghosh, B, 69, 79, 84, 95, 101, 103, 104, 106
 Ghosh, Kaustab, 40, 42, 50
 Ghosh, M, 64, 100
 Ghosh, Rita, 125, 136
 Ghosh, Saptaparni, 21, 25, 26, 46, 47
 Ghosh, Sujay, 36, 40, 49–51
 Ghosh, Tanmay, 49, 51, 80, 95, 98, 104, 106
 Ghosh†, Arup K, 37, 49
 Ghosh†, Malay, 24, 46
 Ghosh†, S, 114, 119, 127, 128, 148, 150
 Ghosh†, Samiran, 143, 148–150
 Ghosh†, Sujay, 40
 Ghoshal, T, 129
 Ghoshal†, Tandra, 116, 128
 Ghoshray, A, 74, 102
 Ghoshray, Amitabha, 64, 100
 Ghoshray, K, 64, 74, 100, 102
 Giri†, SK, 63, 100
 Goswami, A, 122–124, 136
 Goswami, Alakananda, 31, 48
 Goswami, Somen, 79, 103
 Goswami†, Shyamaprosad, 30, 48
 Goswami†, Sudipta, 66, 101
 Gothe†, KS, 164, 179
 Goyal, Sneha Lata, 45
 Gupta, Dhruvajyoti, 125, 136
 Gupta, Kumar S, 174, 175, 181, 182
 Haas†, F, 148, 150
 Halder, Sukanya, 44, 51

- Haque, Najmul, 170, 173, 174, 176, 180–182
 Harikumar†, E, 175, 182
 Harindranath, A, 167, 174, 175, 180–182
 Hazra, Montu K, 38, 50
 Hazra, Satyajit, 97, 107
 Herranen, O, 89, 105
 HESS Collaboration, 178
 Holmes†, Justin D, 116, 128
 Hurley†, Daniel, 29, 48
- Islam, AKM Maidul, 93, 106
 Islam, Chowdhury Aminul, 166
 Iyengar, AN Sekar, 143–146, 149
 Iyer†, KK, 77, 103
- Jaman, AI, 73, 102
 Jana, S, 94, 106
 Jana, SK, 78, 103
 Jana†, Nihar R, 24, 46
 Janaki, MS, 142, 145, 146, 148–150
 Jilani†, S Mahaboob, 86, 105
- Kailasam†, Senthilkumar, 43, 51
 Kakade†, Uttam, 170, 180
 Kanagaraj†, M, 79, 103
 Kanjilal, Debasmita, 124, 136, 137
 Kar Choudhury†, Paramita, 82, 104
 Kar, Kamales, 158, 178
 Kar, Satyaki, 64, 100
 Kar†, Anirban, 25, 26, 47
 Kar†, T, 93, 106
 Karmakar, Shilpita, 24, 46
 Karmakar, SN, 70, 101
 Karmakar, Subhajit, 92, 106, 119, 128
 Kaur, J, 79, 103
 Kaur†, Balwinder, 86, 105
 Kedia†, Abhitosh, 87, 105
 Khamrui, Susmita, 32, 48
 Khan, N, 70, 74, 101, 102
 Khan, Nazir, 62, 100
 Khan, P, 120, 129
 Khan†, Gobinda Gopal, 114, 119, 127, 128
 Khan†, Manoranjan, 143, 149
 Kheto, Apurba, 158, 178
 Khurana, Raman, 139
 Kisslinger†, Leonard S, 120, 121, 129, 130
 Koley Seth, Banabithi, 50
 Kore†, Rajkumar, 82, 104
 Krishnamurthy†, HR, 60, 99
 Krishnaswamy†, Rema, 23, 46
 Kshetri, R, 122, 123, 136
 Kumar, Jishad, 63, 100
 Kumar†, Pandian Senthil, 87, 105
 Kumar†, Rajesh, 115, 127
 Kundu, Anjan, 182
 Kundu, S, 103
 Kundu, Susmita, 164, 179
 Kundu†, Anirban, 165, 179
 Kundu†, Rajen, 167, 180, 181
- Lahiri, Susanta, 35, 38, 40, 42, 49, 50
 Lahiry, Lakshmeshri, 24, 46
 Lakhani†, VK, 129
 Lala†, S, 93, 106
 Langer, C, 137
 Lepyoshkina, O, 137
- Mahakhud, M, 176, 182
 Maiti, Jyotirmoy, 174, 175, 181
 Maiti, Moumita, 40, 42, 50
 Maiti, Santanu, 88, 105
 Maiti†, Santanu K, 67, 70, 101
 Maity, Anup Kumar, 30, 48, 52
 Maity, Barun Kumar, 49
 Maity, Chandan, 143–145, 147–150
 Maity†, Annada C, 30, 48
 Maity†, Sibaprasad, 30, 48
 Majhi, Abhishek, 161, 179
 Majumdar, Debasish, 159, 162, 178, 179, 185
 Majumdar, Dipanwita, 106
 Majumdar, N, 129
 Majumdar, Nayana, 116, 128
 Majumdar, P, 157, 159, 161, 163–165, 178, 179
 Majumdar, Parthasarathi, 182
 Majumdar, Pratik, 185
 Majumdar, Sudip, 51
 Majumdar†, Dipanwita, 90
 Majumder, M, 64, 74, 100, 102
 Malherbe†, Johan B, 84, 104
 Malik†, K, 65, 100
 Malik†, Sudip, 115, 128
 Malik†, Tuhin, 125
 Mandal, Ajoy, 34, 49
 Mandal, Mahatsab, 120, 129
 Mandal, P, 65, 66, 70, 74, 76, 100–103
 Mandal, Prabhat, 62, 108
 Mandal, Swadesh, 34, 49
 Mandal†, Haradhan, 88, 105
 Mandal†, K, 114, 119, 127, 128
 Mandal†, MK, 166, 179
 Manikandan†, A, 39, 50
 Manna†, Abhishek, 30, 48
 Martinelli†, Julio J, 147, 150
 Mathews, P, 166, 168, 176, 179, 180, 182
 Mathews, Prakash, 183
 Mazumdar, Arindam, 166, 180
 Mazumdar, C, 72, 102
 Mazumdar, Chandan, 61, 100
 Meljanac†, S, 174, 181
 Metya, Amaresh, 77, 87, 103, 105
 Midya, A, 70, 74, 101, 102
 Midya, Arindam, 62, 66, 101
 Mishra, Sheo K, 97, 107
 Mitra, Ajoy Kumar, 125, 136
 Mitra, Madhurima, 47
 Mitra, Piyali, 43, 50
 Mitra†, Amrit Krishna, 40, 50, 51
 Mitra†, P, 96, 106
 Modak, Kamakshya Prasad, 162, 179

- Modak†, Sanhita, 73, 102
 Modi†, KB, 129
 Mohanty, PK, 61, 63, 75, 100, 102
 Mohanty, Pradeep K, 72, 102
 Mollick, SA, 77, 103
 Mollick, Safiul Alam, 79, 81, 103, 104, 107
 Mondal, Mojammel H, 80, 104
 Mondal, Mousumi, 36, 49
 Mondal, O, 129
 Mondal, PK, 72, 102
 Mondal, Prasanna K, 177
 Mondal, Prasanna Kumar, 90, 106, 160, 178
 Mondal, S, 94, 106
 Mondal, Santanu, 174, 175, 181, 182
 Mondal, Shyamal, 99
 Mondal†, S, 96
 Morris, MA, 129
 Mukherjee, A, 123, 124, 136
 Mukherjee, M, 41, 50, 80, 91–93, 104, 106
 Mukherjee, Manabendra, 85, 104
 Mukherjee, S, 106
 Mukherjee, Sanchita, 43, 44, 51
 Mukherjee†, A, 117, 128
 Mukherjee†, Asmita, 167, 180, 181
 Mukherjee†, G, 123, 136
 Mukherjee†, S, 61, 93, 100
 Mukhopadhyay, Chaitali, 47
 Mukhopadhyay, D, 47
 Mukhopadhyay, Debashis, 21, 22, 24, 46, 51, 53, 55, 56
 Mukhopadhyay, Debasish, 51
 Mukhopadhyay, PK, 105
 Mukhopadhyay, S, 129
 Mukhopadhyay, Supratik, 116, 128
 Mukhopadhyay†, PK, 88
 Mukovskii†, Ya M, 76, 103
 Mustafa, Munshi G, 166, 173, 174, 176, 180–182, 184, 186
 Muthu†, S Esakki, 78, 79, 91, 95, 102, 103, 106
- Nag, Moupnya, 34
 Nag, Moupriya, 41, 49, 50
 Nag†, Somnath, 122, 136
 Najif†, Ali, 62, 100
 Nambissan, PMG, 114–117, 119, 127–129, 138
 Nanda†, Kamala Kanta, 81, 104
 Nandi Ganguly, Bichitra, 129, 137, 140
 Nandi, Debabrata, 35, 49
 Nandi, Moumita, 62, 100
 Nandi, Susmita, 35, 49
 Nandi†, Debabrata, 37, 49
 Nandy, M, 39, 42, 50
 Nandy, Maitreyee, 45, 53, 55
 Nannarone†, S, 93, 106
 Nath, Seema, 30, 48
 Nath†, Rajib, 76, 103
 Nazarewicz†, W, 169, 180
- Pachol†, A, 174, 181
 Pahari, Biswa Pathik, 27, 28, 47
 Pai†, H, 123, 136
- Pal Basak, Nandini, 22, 28, 46, 47
 Pal, Barnana, 103, 108, 109
 Pal, Palash B, 166, 168, 180, 183
 Pal, Prasun K, 35, 49
 Pal, Rabindranath, 144, 147, 149, 150
 Pal, Supratik, 159, 178
 Palit†, R, 121, 129
 Panda†, Prabir Kr, 96, 106
 Pandit†, Rahul, 62, 100
 Pandiyan†, Thangarasu, 86, 105
 Pani, B, 48
 Panigrahi, Swati, 52
 Panjaa, J, 127
 Patra, Malay, 47
 Paul, B, 120, 129
 Paul†, Sima, 30, 48
 Perez†, Alejandro, 173, 181
 Piekarewicz†, J, 169, 180
 Poddar, A, 63, 69, 100, 101
 Poddar, Asok, 61, 66, 79, 100, 103
 Prabhu†, TP, 164, 179
 Pradhan, SK, 106
 Pradhan, MK, 123, 136
 Pradhan, Partha Pratim, 161, 179
 Pradhan, Punyabrata, 100
 Pradhan, Srutarshi, 71, 102
 Pradhan, Suman Kalyan, 25, 47
 Pradhan†, Punyabrata, 61, 99
 Pradhan†, SK, 94
 Pramanik, Sourav, 148, 150
 Prathap†, MU Anu, 82, 83, 89, 104, 105
- R3B Collaboration, 178
 Raha, Sanghamitra, 31, 48
 Rahaman, A, 127, 137
 Rahman, Atikur, 89, 90, 105
 Rai Chowdhury, A, 79, 103
 Rajbanshi, S, 122, 123, 136
 Ramakumar†, R, 68, 101
 Ramaprabhu†, S, 82, 104
 Rana†, Utpal, 115, 128
 Randeria†, Mohit, 60, 99
 Ranganathan, R, 61, 77, 100, 103
 Ranjan, A, 48
 Ranjan†, Amitabh, 32, 48
 Rao, VP, 78, 103
 Rath†, Rutuparna, 125
 Rathee†, Vikram, 23, 46
 Raut, R, 124, 136
 Rawat, Meenaxi, 207
 Rawat†, R, 85, 105
 Ray, Aurkie, 50
 Ray, I, 137
 Ray, J, 137
 Ray, Mayukh K, 87, 101
 Ray, Nihar Ranjan, 77, 103
 Ray, NR, 77, 103
 Ray, Pulak, 23, 46
 Ray, S, 122, 124, 136

- Ray, Sutapa, 21, 46
 Ray†, Purusattam, 69, 101
 Ray†, Tirtha Sankar, 165, 175, 179, 181
 Raychaudhuri, Amitava, 207
 Raychaudhuri, Mithu, 22, 46
 Raychaudhuri†, AK, 76, 103
 Reinhard†, P -G, 169, 180
 Reja, Sahinur, 107
 Roca-Maza†, X, 172, 181
 Rolles†, D, 119, 128
 Rooj, A, 96, 107
 Rossi†, DM, 122, 136
 Roy, Analabha, 71, 73, 102
 Roy, Anita, 22, 24, 28, 46, 47
 Roy, Bappaditya, 21, 46
 Roy, Kasturi, 21, 22, 46
 Roy, M, 96, 107
 Roy, Madhusudan, 88, 92, 96, 105, 106
 Roy, P, 120, 129
 Roy, PK, 120, 129
 Roy, Pradip, 120, 129
 Roy, Probir, 160, 178
 Roy, Santosh, 130
 Roy, Shibaji, 167, 172, 180, 181
 Roy, Subinit, 123, 125, 136
 Roy†, Partha Sarathi, 85, 104
 Roychoudhury†, Rajkumar, 148, 150
 Rozenberg†, Julian M, 38, 50
 Ruhanen†, Heini, 29, 48
- S Bhunia, 77, 103
 Saha Sarkar, M, 122, 123, 125, 136, 138
 Saha, Arpita, 50
 Saha, Biswajit, 107
 Saha, Chandan, 40
 Saha, L, 164, 165, 179
 Saha, Partha, 30, 48, 50, 52
 Saha, Rajat, 79, 103
 Saha, Ratan K, 85, 92, 105, 106
 Saha, S, 163
 Saha, Satyajit, 137
 Saha, Shaibal, 128
 Saha, Sutapa, 24, 46
 Saha-Dasgupta†, Tanusri, 64, 100
 Saha†, Chandan, 40, 50, 51
 Saha†, S, 121, 129
 Saha†, Uttiyoarnab, 125
 Sahu†, Subash Chandra, 98, 107
 Samaddar, SK, 174, 176, 181, 182
 Samanta, Anirban, 119, 128
 Samanta, Tapas, 75, 102
 Samanta†, Amalesh, 85, 104
 Samantara†, Aneeya K, 98, 107
 Samsarov†, A, 174, 181
 Sanyal, Milan K, 88–90, 105
 Sanyal, MK, 86, 105
 Saran, PK, 45
 Sarangi, MK, 45
 Sardar†, M, 84, 95, 104, 106
- Sarkar, Anwesa, 143, 147, 149, 150, 174, 175, 181, 182
 Sarkar, M Saha, 124, 136
 Sarkar, Munna, 33, 48, 55
 Sarkar, Neelakshi, 47
 Sarkar, Niladri, 67, 68, 70, 101
 Sarkar, PK, 45
 Sarkar, Sandip, 116, 119, 128
 Sarkar, Sourav, 129
 Sarkar, Sreemoyee, 121, 129, 130
 Sarkar, Subir, 139
 Sarkar†, B, 39, 50
 Sarkar†, I, 86, 105
 Sarkar†, S, 122, 124, 136
 Sarma, A, 86, 105
 Sarma†, Bornali, 143, 144, 149
 Satpati, B, 85, 93, 94, 105, 106
 Satpati, Biswarup, 49, 51, 80–83, 86, 88–90, 95, 98, 104–107
 Schamel†, Hans, 143, 144, 149
 Scholten†, O, 171, 181
 Selvakumar, K, 124, 136
 Sen, R, 48
 Sen, U, 48
 Sen, Udayaditya, 30, 32, 48, 51, 52
 Sen†, Diptiman, 173, 181
 Sen†, Pintu, 35, 41, 49, 50
 Senapati, Dulal, 49, 51, 80, 98, 104
 Sengupta Banerjee, Aditi, 25, 47
 Sengupta, Bidisha, 27, 28, 47
 Sengupta, Isha, 47
 Sengupta, K, 77, 103
 Sengupta, Kaushik, 23, 27, 46, 47
 Sengupta, MB, 47
 Sengupta, Pradeep K, 27, 28, 47
 Sengupta, Sudip, 145, 149
 Senyshyn†, A, 78, 103
 Seth, S, 163, 166, 179
 Seth, Susnata, 160, 163, 178, 179
 Sethi†, J, 121, 129
 Sharma†, Savita, 32, 48
 Shipman†, Patrick D, 79, 103
 Shukla†, Padma Kant, 147, 150
 Shyam, R, 170–172, 180, 181
 Sil, Arunansu†, 159, 178
 Sil†, Sreekantha, 67, 101
 Singh, AK, 124, 136
 Singh, Harvendra, 172, 181
 Singh, Jasdeep, 26, 47
 Singh, Sanjay, 78, 79, 91, 95, 102, 103, 106
 Singh†, Jaspal, 83, 104
 Singh†, Paramjit, 115, 127
 Singh†, RK, 87, 101
 Singha†, Achintya, 90, 106
 Sinha, RK, 207
 Sinha, Sumona, 91, 106
 Sinha, T, 120, 129
 Sinha, Tinku, 126
 Sinha†, Amitabha, 38, 50
 Sini†, Kuriakose, 83, 104

Smithsonian Astrophys Observatory, 178

Sood†, Ajay K, 46

Spanner†, M, 114, 127

Srihari, Velaga, 65, 100

Srijan, Haldar, 22, 46

Srivastava, D, 21, 46

Srivastava†, Rajendra, 82, 89, 104, 105

Srivastava†, SK, 117, 128

Steele, Ian M, 79, 103

Strickland†, Michael, 173, 174, 181

Sunil†, C, 42, 50

Swain†, Smrutirekha, 81, 104

Talukdar, D, 89, 105

Taylor, Jasmine, 28, 47

Thakur†, Lata, 170, 180

Thiyagarajan†, R, 95, 102

Thomas†, AW, 171, 172, 181

Thorat, T, 129

Thorat†, Atul V, 116, 128

Tomar†, BS, 35, 38, 49, 50

Tsushima†, K, 171, 172, 181

van der Berg†, NG, 84, 104

Varghese†, Neenu, 88, 105

Vasanthi†, V, 66, 100

VERITAS Collaboration, 178

Vishwanath†, PR, 164, 179

Wharton, AM, 143, 144, 146, 149

Yanagida†, Tsutomu T, 169, 180

Yarlagadda, Sudhakar, 60, 99, 107, 108

Yotprayoosak, P, 89, 105

Znakovskaya†, I, 114, 127

Annual Report 2013-2014 of Saha Institute of Nuclear Physics, Kolkata

CORRIGENDUM

In the Annual Report 2013-2014 of Saha Institute of Nuclear Physics, Kolkata the following additions/corrections may please be noted by all concerned .

(A) Page 209 under High Energy Nuclear and Particle Physics Division - Addition

2.a. Prof. Pratap Bhattacharya, Professor 'G' (* Court case relating to extension of service beyond retirement is subjudice)

(B) Page 213 under List of Retirement: April 2013 to March 2014 – Correction/ Addition

8. Prof. Pratap Bhattacharya/HENPP 31.10.2013 (**** Court case relating to extension of service beyond retirement is subjudice)***)



Registrar